



**Modeling paleosol formation on
the Chinese Loess Plateau during
the Quaternary interglacials**

Nirmani Ranathunga

To my Amma and Thaththa

Members of the examination committee

Prof. dr Marnik Vanclooster (chairman)

President, Earth and Life Institute, Faculty of Bioengineering, Université Catholique de Louvain, Louvain-la-Neuve, Belgium

Prof. dr. Veerle Vanacker

Earth and Life Institute, Georges Lemaître Centre for Earth and Climate Research, Faculty of Science, Université Catholique de Louvain, Louvain-la-Neuve, Belgium

Prof. dr. Sophie Opfergelt

Faculty of Bioengineers, Université Catholique de Louvain, Louvain-la-Neuve, Belgium

Prof. dr. ir Ann Verdoodt

Research group Soil Degradation and Soil Conservation, Department of Environment, Ghent University, Ghent, Belgium

Prof. dr. Qingzhen Hao

Key Laboratory of Cenozoic Geology and Environment, Institute of Geology and Geophysics, Chinese Academy of Sciences, China

Prof. dr. Daniela Sauer

Department Physical Geography, University of Göttingen, Göttingen, Germany

Prof. dr. Peter Finke (promoter)

Research Group Soil Genesis, Department of Environment, Faculty of Bioscience Engineering, Ghent University, Belgium

Prof. dr. Qiuzhen Yin (promoter)

Earth and Life Institute, Georges Lemaître Center for Earth and Climate Research, Faculty of Science, Université Catholique de Louvain, Louvain-la-Neuve, Belgium



Modeling paleosol formation on the Chinese Loess Plateau during the Quaternary interglacials

Doctoral dissertation presented by

Nirmani Ranathunga

IN PARTIAL FULFILLMENT OF THE REQUIREMENTS FOR THE
DEGREE OF
DOCTOR IN SCIENCES

GEORGES LEMAÎTRE CENTRE FOR EARTH AND CLIMATE
RESEARCH
EARTH AND LIFE INSTITUTE
FACULTY OF SCIENCE
UNIVERSITÉ CATHOLIQUE DE LOUVAIN



Modeling paleosol formation on the Chinese Loess Plateau during the Quaternary interglacials

Doctoral dissertation presented by

Nirmani Ranathunga

DISSERTATION SUBMITTED IN FULFILLMENT OF THE
REQUIREMENT FOR THE DEGREE OF DOCTOR IN BIOSCIENCE
ENGINEERING

DEPARTMENT OF ENVIRONMENT
FACULTY OF BIOSCIENCE ENGINEERING
GHENT UNIVERSITY

Promoters:

Ghent University

Prof. dr. Peter Finke, Department of Environment, Faculty of Bioscience
Engineering, Ghent University
Belgium

Université Catholique de Louvain

Prof. dr. Qiuzhen Yin
Earth and Life Institute, Georges Lemaitre Center for Earth and Climate
Research, Faculty of Science
Université Catholique de Louvain
Belgium

Dean of Université Catholique de Louvain

Prof. dr. Pascal Lambrechts

Dean of Ghent University

Prof. dr. Els Van Damme

Rector of Université Catholique de Louvain

Prof. dr. Vincent Blondel

Rector of Ghent University

Prof. dr.ir Rik Van de Walle

Dutch translation of the title: Modellering van de paleosolformatie op het Chinese Lössplateau tijdens de Quartaire interglacialen

French translation of the title: Modélisation de la formation des paléosols sur le plateau de Loess chinois pendant les interglaciaires du Quaternaire

Cover illustration: The Quaternary paleosols and loess formed in the Southern Chinese Loess Plateau, Baoji, China.

Copyright statement: All rights reserved. No part of this document may be reproduced or transmitted in any form or by any means, electronic, mechanical, photocopying, scanning, recording, or otherwise, without prior written permission of the author and/or dissertation promoter(s). A written permission of the author is also required to use the methods, products, schematics and programs described in this work for industrial or commercial use, and for submitting any part of this dissertation in scientific contests. Every other use is subjected to the copyright laws.

Acknowledgements

First, I am very grateful to my promoters Prof. dr. Peter Finke and Prof. dr. Qiuzhen Yin for their continuous guidance, motivation, expertise, kindness and knowledge given me throughout these four years. I consider myself extremely lucky to have carried out my PhD research under your wise guidance. Frankly, I am truly fortunate to work with you both. Because of my two great promoters, I finished this dissertation on time.

I would like to express my deep gratitude to Prof. Peter, for your inevitable support and knowledge during my PhD helped me become familiar with soil genesis modeling. You were always available whenever I needed your support to discuss my work and I appreciate everything you've taught me. I remember, when the Corona pandemic occurred, you not only helped me to run and monitor simulations remotely and send results but also gave me energy during the time I feel failure. You were always very kind to me, and your optimism, humor always made me relaxed, cool and energetic. I sincerely appreciate you and Mrs. Finke for ensuring my comfort during cold wintertime in Ghent. I would like to express my deep gratitude to Prof. Qiuzhen for hiring me for this project, believing me, and having the confidence placed on me for this work. All the time, your relentless support helped me to improve my knowledge of paleoclimates, interglacials, and explore those research areas efficiently that I was unfamiliar with. I especially thank Prof. Qiuzhen for arranging fieldwork in the Chinese Loess Plateau, where it was my very first visit to the plateau and an unforgettable journey in my research life. Your kind and loving words always encouraged me a lot. I remember once you wrote to me "I would love that all the students do so well like you, Nirmani", and Prof Peter wrote to me, super! 2 down 1 to go! , after the 2nd paper is published. I cannot count how many times I read this email. I also appreciate my promoters for their unceasing encouragements for participating conferences, taking some courses that improved me a lot as a young researcher. I would like to acknowledge the financial support I received from the F.R.S.-FNRS MIS (Incentive Grant for Scientific Research) program F.4529.18 entitled "Quantifying the relative contributions of temperature, precipitation and vegetation in the formation of the interglacial soils embedded in the Chinese loess (QuantLoess)". So, my heartfelt gratitude goes to Prof. Qiuzhen for granting the fellowship, I will never forget it in my life. The financial support enabled this research work and assisted me well during my stay in Belgium.

I would like to express my gratitude to the members of my examination committee: Prof. dr Marnik Vanclooster (chairman), Prof. dr. Veerle Vanacker, Prof. dr. Sophie Opfergelt, Prof. dr. ir Ann Verdoodt, Prof. dr. Qingzhen Hao, Prof. dr. Daniela Sauer for their appreciation on this dissertation. They have

thoroughly screened this thesis and their suggestions have highly improved the quality of this work.

All my simulations were carried out using the computer facilities in Soils Genesis research group at Ghent University. So, I would like to acknowledge our computers☺, Prof. Peter and ir. Rudi Hoeben for all the technical support throughout years.

I would like to say special thanks to all my colleagues: First, a big thank you to my friend Sastrika Anindita (and Arfah) for the kindness and help you gave me personally and in research work throughout my PhD. We spent time with computers, and had a good time at Coupure (Ghent) and enjoyed delicious Indo-SL meals☺. I am grateful to Tizita Endale and Wenjing Tian for the warmth of friendship, emotional support and encouragement received throughout this journey. You all were great friends in my life. I give special thanks to my officemates Nick Krekelbergh, Lotte Baert, Anja Derycke and to all the people and PhD fellows on the first floor- B block, Coupure at Ghent University, LinLin, Haichao, Oka, Ummehani, Orly, Hui, Junwei, Heleen, Qui, Lin Wang, Zenia, Desale, Astrid and all those unnamed ones. I would like to thank my Chinese friends from Université Catholique de Louvain. Especially to Zhipeng, my project colleague, I am truly grateful to you for all the assistance that I received from the first day I came to Louvain-la-Neuve in 2018 to the end of this journey. To Dr. Hao Lu, many thanks for your kind support whenever I asked help. Many thanks to both of you for assisting me during field work in China. Thank you very much QianQian Su, Anqi Lyu for all the support and warmth friendship. We had joyous times while we were in conferences together. I also thank Shaohua Tian, without you, it was impossible to find and gather data from Chinese literature. At this point, I would like to say special thanks to Prof. Yanyan Yu, Prof. Youbin Sun, Prof. Qingzhen Hao, Prof. Guoqiao Xiao and Prof. Peihong Shi for their immense support for sending some paleosol data to me.

Moreover, my special thank goes to Dr. Warshi Dandeniya and Prof. Udaya Vitharana for their support (e.g during visa process) and encouragement to fulfill this PhD. Moreover, to Dr. Priyantha Weerasinghe for being a great mentor at the beginning of my academic carrier.

Thanks to PLR (2015-2017), I have two lovely friends: Reshna Udas and Afroza Liza. Reshna, I will never forget your kind words and encouragement during some difficult times in the past. Liza, thank you for the great hospitality that you and Jakiul offered us during our visit to Germany. Thank you, Jeffery Lecoq, for facilitating wonderful and safe journeys. I will forever cherish the pleasant memories we all had together.

My special thank goes to Dilani Rathnayake and Gertrude Scynthya for their immense support both academically and personally throughout these years. We all had lovely times together here in Ghent with delicious SL foods. Moreover, my sincere thank goes to Sewwandi Alwis for all her generous support during the last six years. Furthermore, I am grateful to our close families and their support, Nimal ayya and Kumari Akka, Asanka Akka and Marlon ayya, Nirukshan ayya.

Finally, to my family and parents: most importantly, to my beloved husband, Amila Hemantha, I am sincerely grateful to my husband for encouraging me every day, listening to me and your patience, unconditional love and care throughout this study. Thanks for encouraging me to persuade higher studies when I want to find a job after my Bachelor's study. I sincerely thank my husband for all the support given to me in every step of my life. Thank you very much Amma and Thaththa for your unfailing love and affection and for the struggles that you suffered to see me through to this level. Especially Amma, you were always proud of me and encouraged me since childhood, and I am sure you will be satisfied with this achievement. Thank you my loving sister, Purnima Ranathunga, and my loving brother, Keerthimal Ranathunga. I am forever in debt to you two for taking care our parents while I have been away from home in the last six years and for your love, support, and taking care of me in every aspect of my life. Great thanks also go to my husband's family: I am so much grateful to Amma, Thaththa, Akka and Malli for their kind support, love and understanding throughout these years. I also express gratitude to my relatives: Nanda, Loku Amma, Aththamma, Mahappa, elder brothers (Susantha, Eranga), sisters (Gayani, Samankumari, Irosha, Mali) for their financial support and moral encouragement since my younger age.

TABLE OF CONTENTS

List of Tables.....	iv
List of Figures.....	v
List of Abbreviations.....	xi
Summary.....	xiii
Samenvatting.....	xvii
Résumé.....	xxi
CHAPTER 1. General introduction and objectives	1
1.1 The importance of studying interglacial soil development in the Quaternary.....	2
1.2 The Quaternary paleosols formed on loess.....	3
1.3 Study area - The Chinese Loess Plateau.....	6
1.3.1 Geography, climate and vegetation gradient.....	6
1.3.2 Quaternary loess-paleosol records in the Chinese Loess Plateau.....	8
1.3.3 Forcing factors of the Loess-paleosols sequences in China.....	13
1.4 Importance of linking climate evolution with paleosol development... ..	14
1.4.1 Inconsistencies between global climate and Chinese paleosol... ..	14
1.4.2 The necessity of combining soil-forming factors and dust addition in pedogenic processes in the CLP.....	16
1.5 Why modeling (paleo)soil evolution is important.....	17
1.5.1 Soil modeling and paleoclimate-paleosol relations.....	18
1.5.2. Soil modeling and soil-based ecosystem services.....	18
1.6 Research gaps and questions and research objectives.....	19
1.7 Structure of this thesis.....	21
CHAPTER 2. Methodology: interglacial paleosol simulation setup, and the SoilGen2, LOVECLIM1.3 models	23
2.1 Interglacial simulation periods used in the study.....	24
2.2 Research design.....	28
2.3 The SoilGen2 model.....	29
2.4 The LOVECLIM1.3 model.....	33
2.5 Bias correction and downscaling the climate model outputs to the soil model input scale.....	34
CHAPTER 3. Calibrating SoilGen2 for interglacial soil evolution in the Chinese Loess Plateau considering soil parameters and the effect of dust addition rhythm	39
3.1 Introduction.....	42

3.2 Materials and methods.....	44
3.2.1 Study locations and periods.....	44
3.2.2 The SoilGen2 model input data	45
3.2.3 Model calibration and parameters	47
3.3 Results and Discussion.....	54
3.3.1 Effect of dissolution constant of calcite and interception evaporation loss on decarbonatization	54
3.3.2 Assessment of clay migration related model parameters.....	56
3.3.3 Assessment of SOC related model parameters	58
3.3.4 Effect of dust deposition scenarios on the quality of the calibration result	61
3.4 Conclusions.....	66
CHAPTER 4. Driving factors of interglacial paleosol formation on the Chinese Loess Plateau and the effect of precession and ice sheets	69
4.1 Introduction	72
4.2 Material and methods	74
4.2.1 Locations and studied interglacials	74
4.2.2 Climate simulations.....	75
4.2.3 The SoilGen2 model and Input data	76
4.2.4 Research layout	77
4.3. Results and discussion	80
4.3.1 Analysis of the driving factors of the changes in paleosol development.....	80
4.3.2 Paleosol response to the astronomical forcing	87
4.3.3 Paleoclimate-paleosol response to NH ice sheets	96
4.3.4 Comparison of simulated and observed S4 and S5-1 paleosols in the southeast CLP	108
4.4. Conclusions.....	110
CHAPTER 5. Soil modeling for Soil Loss Tolerance estimations: Exploring natural baselines and long-term variations.....	113
5.1 Introduction	116
5.2 Materials and Methods.....	120
5.2.1 Study locations and study periods	120
5.2.2 The SoilGen2 model and input data	121
5.2.3 Climate simulations.....	123
5.2.4 Soil EB and SOC stocks, Ecosystems and scenario	124

5.3. Results and discussion	128
5.3.1. Spatio-temporal trends in simulated climate and vegetation	128
5.3.2 Soil EB and SOC stocks evolution and SLT	130
5.3.3 Soil ES evolution and SLT	142
5.3.4 Combining performance indices for ecosystem services	150
5.3.5 Concept of SLT under erosion/dust accumulation scenarios and semi-arid climate	152
5.4 Conclusions.....	154
CHAPTER 6. Conclusions	157
CHAPTER 7. Limitations, recommendations and perspectives	163
7.1 Paleosol evolution modeling - Scientific limitations	164
7.1.1 Input data	164
7.1.2 Climate and soil model limitations	165
7.1.3 Simulation limitations	171
7.2 Recommendations for future research	172
7.2.1 Future perspectives on model calibration and paleosol simulations	172
7.2.2 Future perspectives on soil-based ecosystem services	173
Appendix for chapter 2	174
Appendix for chapter 3.....	176
Appendix for chapter 4.....	198
Appendix for chapter 5.....	209
References.....	216
Curriculum Vitae.....	241

List of Tables

Table 2-1 Thickness and estimated Ages (ka) of paleosol units in the CLP (Sun et al., 2006b). Note that although all those age models are generated by orbital tuning method, different proxy indicators and tuning targets are employed in the chronological construction. Detailed descriptions of those age models are given in Sun et al. (2006b), Lu et al. (1999), Heslop et al. (2000), Ding et al. (2002) and Sun et al. (2006a).....	26
Table 2-2 Interglacial simulation duration used for paleosol simulations in the study.....	27
Table 3-1 Calibrated parameters, value range and number of simulations. 52	
Table 3-2 Calibrated SOC cycle parameters from other studies and in this study and default values.	59
Table 3-3 Impact of ten dust deposition rhythms on the quality of calibrations, expressed by standard deviations relative to the (scaled) dissimilarity of the calibration (Eq. 3-4).	62
Table 4-1 The sensitivity experiments, mean absolute errors, ranking and “gain” in MAE for calcite (top) and clay (bottom) in MIS 11 in Chang’an. Ex=Experiment; Joint=all boundary inputs by climate modeling and dust input reconstruction; Reference=all boundary inputs equal to Pre-Industrial Holocene time series; PP=precipitation; Evapo=potential evapotranspiration; Vege=vegetation; Temp=temperature.	82
Table 4-2 The sensitivity experiments, mean absolute errors, ranking and “gain” in MAE for calcite(top) and clay (bottom) in MIS 13 in Chang’an. Ex=Experiment; Joint=all boundary inputs by climate modelling and dust input reconstruction; Reference=all boundary inputs equal to pre-industrial Holocene time series; PP=precipitation; Evapo=potential evapotranspiration; Vege=vegetation; Temp=temperature	84
Table 5-1 Description of the soil erosion scenarios implemented in the event file in SoilGen2.	123
Table 5-2 SLT values for EB for four locations.....	138
Table 5-3 SLT values for SOC for four locations.....	142
Table 6-1 SoilGen2 calibrated process parameters and associated optimal values.....	159

List of Figures

- Figure 1-1** Photos of loess geomorphology from the Loess Plateau of China, (a). Lanzhou, northwestern CLP, (b) Baoji, southeastern CLP (photos by Ranathunga, KN, 2019).5
- Figure 1-2** Map of the Chinese Loess Plateau and its surroundings deserts in northern China and the arrows indicate the pathways of the monsoons atmospheric circulation system over China and dash arrow (red) indicates the westerly winds. (base map is from google satellite map in QGIS 3.24.1).8
- Figure 1-3** Schematic diagram for interglacial paleosol formation on loess. In A. (a) loess deposition during glacials. (b) Climate changes from glacial to interglacial and soil formation on both previously deposited loess and on new dust sediments during interglacial. (c) Dust addition increases again during glacial, and soil formation is weakened, burying soils. In B. the evolution of soil formation since initial loess deposition in a mid-latitude climate, showing increasing thickness, carbonate-rich (Bk) and clay-rich (Bt) horizons, A-horizon – black top part of the paleosols, Bw- weathering horizon (vertical lines) (after Stevens et al., 2007; Muhs, 2013). 10
- Figure 1-4** The alternating light colored loess and reddened paleosols, Baoji, southern Loess Plateau (photos by Ranathunga, KN, 2019). 10
- Figure 1-5** Loess-paleosol profiles on the Chinese loess plateau: (a) loess sediments in Lanzhou (western Loess Plateau), (b) Baoji (southern Loess Plateau) (photos by Ranathunga, KN) (c) Holocene soil (S0) and last glacial loess (L1) and (d) S5 paleosol, L6 loess and S6 paleosol at Weinan (southern Loess Plateau) (photos by Guoqiao Xiao). 11
- Figure 1-6** General and simplified correlation of the loess–paleosol succession on the Chinese Loess Plateau spanning the last 500 ka BP with the Marine Isotope Stages. The general correlation is based on the visual correlation of monsoon proxies (e.g. magnetic susceptibility) to the stacked benthic $\delta^{18}\text{O}$ Lisiecki and Raymo (2005) between each paleosol layer to an interglacial marine isotope stage. 12
- Figure 1-7** Chapter overview of thesis22
- Figure 2-1** The interglacial oxygen Marine Isotope Stages and corresponding paleosols in the CLP. Upper panel shows the records of Benthic $\delta^{18}\text{O}$ stack variation (Lisiecki and Raymo, 2005), lower panel shows magnetic susceptibility from the Chinese loess (Guo et al., 2009) over the last 500,000 years.28
- Figure 2-2** Summary of the research strategy used in the study.29
- Figure 2-3** Soil process sequence in the SoilGen2 model indicating input data at the upper boundary. Copied and adapted from Minasny et al. (2015). P, PE

and T stand for precipitation, potential evapotranspiration, temperature, respectively and CDE and CEC denote Convection Dispersion Equation and Cation Exchange Capacity accordingly. $h-\theta-K$ denotes the relations between hydraulic head, water content and hydraulic conductivity.32

Figure 2-4 A summary of soil process coverage of SoilGen2. SoilGen2 simulates soil forming processes (key processes as defined in Bockheim and Gennadiyev, 2000), and includes effects of erosion, deposition, weathering and bioturbation (the right-most five) (x-axis). The process coverage is presented in y-axis (1.0=full process coverage and <1.0=processes that are partially introduced).....33

Figure 2-5 Spatial downscaling of LOVECLIM1.3 output to the soil model input scale (monthly) (blue solid arrow); temporal scale of SoilGen2 processes at spatial scale (1*1 m²) and output (100 m²*100 m²=1ha) at yearly scale (black dash arrows) (after Finke et al., 2021b).37

Figure 2-6 Schematic representation of spatial downscaling of LOVECLIM1.3 output (climate and vegetation).....38

Figure 3-1 The locations of the soil profiles studied: black and red symbols represent the profiles used for S0 and for S5-1, respectively (modified after Hao and Guo (2005). The distribution of loess is indicated in yellow.45

Figure 3-2 Ten dust deposition rhythms applied in SoilGen2 (more information in Table A3-10).....54

Figure 3-3 Dissimilarity (%) as a function of (A).the calcite dissolution constant (log₁₀k_{so}) and (B). the interception evaporation loss (%) for grass/shrubs/agriculture in three profiles: Xifeng, Chenjiagou, Taoyu are denoted by open triangles, diamonds, squares, respectively. Green dots show profile averages.....56

Figure 3-4 Dissimilarity (%) as a function of (A). pressure head $h-\theta_{macro}$ (hPa), (B). filter coefficient n(-), (C). P_{Smax}-B combinations. Green bar shows the best average for five profiles. (D). ectorganic layer thickness (mm) in five profiles: symbols indicate Luochuan (open diamonds), Chang'an (solid triangles), Changwu (open squares), Wugong (open triangles), Weinan (solid circles). Green dots show profile averages.....58

Figure 3-5 Dissimilarity (%) for different values of (A). k_{HUM} , (B). k_{RPM} (C). f_{recto} in two profiles (D). the partitioning coefficient CO₂ / (BIO+HUM), in three profiles: Xifeng, Chenjiagou, Taoyu are denoted by triangles, diamonds, squares, respectively. Green dots show profile averages.61

Figure 3-6 Scaled dissimilarity (ranges from 1.2-6.8) between dust scenarios (rightmost) and calibrated three Holocene sites (fat dots) and during calibrations (leftmost) for calcite content.64

Figure 3-7 Scaled dissimilarity (ranges from 0.027-2.45) between dust scenarios (rightmost) and calibrated three Holocene sites (fat dots) and during calibrations (leftmost) for organic carbon.....64

Figure 3-8 Scaled dissimilarity (ranges from 0.01-0.14) between dust scenarios (rightmost) and three Holocene sites (fat dots) for simulated clay content.65

Figure 3-9 Scaled dissimilarity (ranges from 0.0005-0.019) between dust scenarios (rightmost) and calibrated three Holocene sites (fat dots) for simulated CEC.65

Figure 4-1 Map showing the Chinese Loess Plateau (yellow), locations of Jiuzhoutai, Xifeng, Chang’an loess sections in this study (solid red points) (Modified from Hao and Guo, 2005).75

Figure 4-2 Simulated depth distribution of calcite (kg/ha, left) and clay (Mg/ha, right) for MIS11 in Chang’an, for the Reference simulation, Joint simulation, reconstructed precipitation (PP), with added dust (PP+Dust) and potential evapotranspiration (PP+Dust+Evapo).83

Figure 4-3 Simulated depth distribution of calcite (kg/ha, left) and clay (Mg/ha, right) for MIS13 in Chang’an, for the Reference simulation, Joint simulation, reconstructed precipitation (PP), reconstructed Dust (Dust), with added dust (PP+Dust) and potential evapotranspiration (PP+Dust+Evapo).....85

Figure 4-4 Comparison between astronomical parameters with the simulated precipitation and paleosols during the five interglacials. (a) MIS 5; (b) MIS 7; (c) MIS 9; (d) MIS 11; (e) MIS 13 in Chang’an. In each panel, from top to bottom : astronomical parameters : (obliquity (red), precession (blue), eccentricity (black), mean annual precipitation simulated by LOVECLIM1.3, fraction of mass changed for calcite and for clay Ref Eq.[4-3]. The data are plotted in their own time scales and the 1000-year running mean of precipitation is plotted. The astronomical data are from Berger and Loutre (1991). Green dash arrows show the peaks of calcite and clay related to precipitation peaks and precession minimums mentioned in the text.91

Figure 4-5 Evolution of calcite mass at Chang’an during MIS 7. A relatively rapid dust deposition is depicted in the beginning of MIS 7 (as shown by red arrow). The boundary between the blue and white/gray areas in the paleosols demarcates the dust deposition rhythm during MIS 7. Blue stands for the atmosphere.92

Figure 4-6 Evolution of calcite mass at Chang’an during MIS 9 (top), and MIS5 (below). A very rapid dust deposition is depicted at the end of MIS 9 (as shown by red arrow) and of MIS 5 (yellow arrows).92

Figure 4-7 Comparison of the simulated paleoclimate in ice (OrbGHGIce) and no ice (OrbGHG) experiments with NH ice volume and astronomical

parameters in MIS 11 (left) and MIS 13 (right) in Chang'an. From top to bottom: (a, e) astronomical parameters (obliquity (red), precession (blue)), (b, f) NH ice volume difference relative to the simulated 0ka volume (Ganopolski and Calov, 2011), (c, g) the simulated annual mean precipitation and (d, h) temperature. The 1000-year running mean of precipitation and temperature is plotted. The astronomical data are from Berger and Loutre (1991).97

Figure 4-8 Evolution of calcite (top panel) and clay (bottom panel) in Chang'an during MIS 11 in ice (OrbGHGIce) and no ice (OrbGHG) experiments. In (a) and (b) orange arrows depict the formation of calcic horizons (Bk) and white arrow shows the calcite in the top soils in the first 12ka (a). Note that the Bk forms in the sub soils at (b) and the less visible Bk at (a). In (c) and (d), yellow arrows depict the formation of Bt horizons. Note that the two Bt forms at (d) and one Bt at (c).....98

Figure 4-9 Evolution of calcite (top panel) and clay (bottom panel) in Xifeng during MIS 11 in ice (OrbGHGIce) and no ice (OrbGHG) experiments. In (a) and (b) orange arrows depict the formation of calcic horizons (Bk) and white arrow shows the calcite in the top soils in the first 12ka (a). Note that a thick Bk forms in the sub soils at (b). In (c) and (d), yellow arrows depict the formation of Bt horizons. Note that the two Bt forms at (d) and one Bt at (c).99

Figure 4-10 Evolution of calcite (top panel) and clay (bottom panel) in Jiuzhoutai (JZT) during MIS 11 in ice (OrbGHGIce) and no ice (OrbGHG) experiments. In (a) and (b) orange arrows depict the formation of calcic horizons (Bk). Note that the Bk forms near the surface soils at (b) than in (a).101

Figure 4-11 Evolution of calcite (top panel) and clay (bottom panel) in Chang'an during MIS13 in ice (OrbGHGIce) and no ice (OrbGHG) experiments. Orange and yellow arrows depict the formation of calcic horizons (Bk) and illuvial horizons (Bt).103

Figure 4-12 Comparison of soil development between the ice scenario MIS 13 (OrbGHGIce) and the no ice scenario (OrbGHG) in Chang'an. In each panel, from top to bottom obliquity and precession, annual mean precipitation (a, e), annual mean temperature (b, f), fraction mass changed of calcite (c, g) and clay (d, h). Green dash arrows show the link from precession to precipitation and finally to clay peaks and to calcite peaks (orange dash arrows). Black dash arrows show the effect of temperature increase on clay peaks.....105

Figure 4-13 Evolution of calcite (top panel) and clay (bottom panel) in Xifeng during MIS13 in ice (OrbGHGIce) and no ice (OrbGHG) experiments. Orange arrows depict the formation of calcic horizons (Bk) and clay migration depths in red.106

Figure 4-14 Evolution of calcite (top panel) and clay (bottom panel) in Jiuzhoutai during MIS 13 in ice (OrbGHGIce) and no ice (OrbGHG) experiments.....107

Figure 4-15 The simulated S4 paleosol in Chang'an during MIS 11, evolution of (a) clay, (b) calcite. soil horizons: Bt- clay illuviation, Bk-calcic, Ah- organic mineral top soils.	109
Figure 4-16 The simulated S5-1 paleosol in Chang'an during MIS 13, evolution of (a) clay, (b) calcite. soil horizons: Bt- clay illuviation, Bk-calcic.	109
Figure 5-1 Geographic locations, from southeast to northwest Chang'an Luochuan, Xifeng, and Jingyuan in the CLP. Modified after Hao and Guo (2005).	121
Figure 5-2 A 1000-year moving average applied to the simulated climatic data for the MIS 5e (duration 22000 years, x axis) at the four locations: annual mean (a) precipitation (mm) and (b) temperature (°C). Green dotted line indicates the summer insolation during MIS 5e.	129
Figure 5-3 Effect of natural erosion rates on EB evolution, in erosion-only (a, b, c, d) and dust addition plus erosion scenario (e, f, g, h). X-axis is simulation year and y-axis is scaled to 1600 kmol+/ha. A blue dot at the y-axis represents initial EB value determined by the parent material at the start of simulation. Colored lines denote different rates of erosion.	133
Figure 5-4 Comparison of simulated exchangeable bases and calcite distribution for soils in Chang'an in erosion-only scenario.	134
Figure 5-5 Comparison of simulated exchangeable bases and calcite distribution for soils in Xifeng in erosion-only scenario.	135
Figure 5-6 Comparison of simulated calcite distribution between 1.5 and 2.0 Mg. ha ⁻¹ . yr ⁻¹ for soils in Jingyuan in erosion-only scenario.	136
Figure 5-7 Comparison of simulated exchangeable bases and calcite distribution for soils in Xifeng in dust addition plus erosion scenario.	136
Figure 5-8 Comparison of simulated calcite distribution between 1.5 and 2.0 Mg. ha ⁻¹ . yr ⁻¹ for soils in Jingyuan in dust addition plus erosion scenario.	137
Figure 5-9 Effect of natural erosion rates on SOC evolution, in erosion-only (a, b, c, d) and dust addition plus erosion scenario (e, f, g, h). X-axis is simulation year and y-axis is scaled to 140 Mg/ha. Colored lines denote different rates of erosion.	141
Figure 5-10 Effect of natural erosion rates on CSC evolution in erosion-only (a, b, c, d) and dust addition plus erosion scenario (e, f, g, h). X-axis is simulation year and y-axis is scaled to 100 Mg/ha. Colored lines denote different rates of erosion.	145

Figure 5-11 Evolution of organic carbon at 1.5 and 2.0 Mg. ha⁻¹. yr⁻¹ at Xifeng in only-erosion scenario. The calculated CSC differences at Xifeng is explained by these simulated OC at 1.5 and 2.0 Mg. ha⁻¹. yr⁻¹..... 146

Figure 5-12 The ratio of actual over potential evapotranspiration, Ω , in Chang'an and Jingyuan in erosion+ dust addition scenarion 147

Figure 5-13 Effect of natural erosion rates on WY evolution, in erosion-only (a, b, c, d) and dust addition plus erosion scenario (e, f, g, h). X-axis is simulation year and y-axis is scaled to 250 mm. Colored lines denote different rates of erosion. 149

Figure 5-14 Clay content evolution over last 5 ka of MIS 5e. Zero is the last year of simulation in x axis; y axis is soil profile depth. Formation of Bt and E horizons is depicted by yellow, in dust addition plus erosion (upper), and erosion only (lower) in Chang'an; A, B ; 1.0 Mg ha⁻¹ y⁻¹ and C, D ; 2.0 Mg ha⁻¹ y⁻¹. Note that the Bt forms near the surface at C and D. Gray scale ranges from 0 to 42 mass % of clay. Blue stands for the atmosphere. 150

Figure 5-15 Combined performance indices for three simulated ecosystem services (1-CSC, WY and Ω per scenario) (a) dust+erosion and (b) erosion-only and per erosion rate for the simulation locations. 152

List of Abbreviations

μm	Micrometer
B	Temperature change
BD	Bulk Density
BIO	Microbial biomass
BP	Before Present
C	Carbon
Ca^{+2}	Calcium ions
CaCO_3	Calcium carbonate
CEC	Cation Exchange Capacity
CLP	Chinese Loess Plateau
CO_2	Carbon dioxide
$\text{CO}_2 / (\text{BIO}+\text{HUM})$	Ratio of carbon mineralized (CO_2) over that still in the food web (microbial biomass and humus)
CSC	Carbon Sequestration Capacity
DIS	unscaled dissimilarity
DPM	Decomposable Plant Material
EAM	East Asian Monsoon
EASM	East Asian Summer Monsoon
EAWM	East Asian Winter Monsoon
EB	Exchangeable Bases
Ep	Potential Evapotranspiration
ES	Ecosystem Services
fr_{ecto}	Ratio of ectorganic/endorganic litter
h	hydraulic head
HUM	Humified Organic Matter
h- Θ macro	pressure head at which macropores empty
IOM	Inert Organic Matter
JS	Joint Simulation
K	hydraulic conductivity
ka	Thousand years
k_{HUM}	decay rate of humus
k_{RPM}	decay rate of resistant plant material
$\log_{10}k_{\text{SO}}$	calcium carbonate dissolution constant
LPS	Loess-Paleosol Sequences
Ma	Million years
MAE	Mean Absolute Error
MIS	Marine Isotope Stage
MS	Magnetic Susceptibility
n	Filter coefficient
NH	Northern Hemisphere
OSL	Optically-Stimulated Luminescence

P	Precipitation
PS _{max}	maximal splitting probability
RPM	Resistant Plant Material
SH	Siberian High
SLT	Soil Loss Tolerance
SOC	Soil Organic Carbon
T	Temperature
WY	Water Yield
Ω	ratio of actual over potential evapotranspiration

Summary

Soils of the past are paleosols. Once paleosols are draped by sediments (e.g. loess) those paleosols are transformed into buried paleosols (fossil soils). The Loess-paleosols sequences (LPS) in the Chinese Loess Plateau (CLP) are the most comprehensive terrestrial palaeoenvironmental records for paleoclimates, reflecting global scale climatic oscillations, namely glacial-interglacial phases. Environmental conditions over the Quaternary period have resulted in continuous loess deposits during glacials (cold-dry), which are nevertheless interrupted by paleosols during interglacials (warm-humid) in the CLP. In the context of paleosols, soil functions and their properties develop over long time scales under the influence of interglacial climatic conditions before young sediments bury these soils.

Paleosols in the CLP are not amply studied in terms of dynamical connection between climate and paleosols, for a given time duration that can only be approximated by soil modeling, and integrated soil genesis-climate models are important in assessing dynamical paleoclimate-paleosol relations. The overall theme of this research is to better understand the paleoclimate-paleosol relations in the CLP, particularly through quantitatively assessing paleosol responses to interglacial climates and ultimately to evaluate soil functioning in terms of soil-based ecosystem services. This knowledge of climate-soil relations (without human factor) is possibly essential in Anthropocene settings to serve as a reference. In this work, we combined two process models, LOVECLIM1.3 and SoilGen2, allowing simulation of paleosol formation over the past 500 ka years. For all the paleosol simulations, LOVECLIM1.3-simulated climate and vegetation were obtained for the extent of the interglacial period while dust addition rhythms and initial soil conditions (e.g. parent material properties) were defined in the soil model.

In the first step, in **chapter 2**, we discussed soil and climate models, the requirements (e.g. downscaling of climate output to the soil model input scale) and the interglacial period studied in the Loess Plateau. In **chapter 3**, the soil model was calibrated for various soil process parameters by confronting

simulated and measured soil properties for Holocene soils and MIS13 paleosols formed in the CLP. The calibration process involved optimizing process parameters of three main process formulations: decarbonatization, clay migration, and soil organic carbon cycling. The calibration results were in reasonable agreement with the range of literature values. After calibration, soil properties (contents of clay, calcite, organic carbon, and cation exchange capacity) show a strong response to ten reconstructed Holocene dust deposition scenarios reflecting the propagation of uncertainty in dust deposition. The conclusion was drawn that the calibrated soil model permits interglacial soil simulation in the CLP over long timescales; however, the simulated soil properties were sensitive to (uncertain) dust addition rhythms. In **chapter 4**, the calibrated SoilGen2 model was used to simulate paleosols in Marine Isotope Stages (MIS) 5, 7, 9, 11, and 13. We first tested the relative contributions of precipitation, temperature, potential evapotranspiration, vegetation and dust addition on paleosol development in MIS 11 and MIS 13 interglacials. Our results showed that precipitation, dust addition and potential evapotranspiration have the greatest impact on paleosols during MIS 11 and MIS13 interglacials, but their relative importance varies between soil properties (e.g. contents of clay and calcite) and between interglacials. As far as climate is concerned, Earth orbital parameters (precession, eccentricity, obliquity) and ice sheets in the Northern Hemisphere (NH) have been the two leading factors that govern the Earth's climate. The LPS in China have become very important for recognizing indirect influence of orbitally forced rhythms (precession, obliquity and eccentricity) during the Quaternary. However, studies focusing on successive changes from and also indirect influence from precession, over ice volume, to climate and finally to soil properties on the CLP are still rare and the response of these variations imprinted in paleosols is still unclear. For the first time, in **chapter 4**, we investigated paleosol response to these variations by visual comparison between contents of calcite and clay and precession variation. The link between precession variation and the simulated soil properties is indirect, through changes in climatic variables (e.g. precipitation). Our results demonstrated that a strong precession footprint was preserved in the

simulated S1 (MIS 5), S2 (MIS 7), S3 (MIS 9) and S5-1 (MIS 13) paleosols and a weak precession signal in the S4 paleosols (MIS 11) in the CLP. Furthermore, we hypothesized that understanding the indirect influence of ice-sheet changes on interglacial soil development by modeling might allow for a better interpretation of the paleosol development in the CLP. Therefore, two experiments with ice (OrbGHGIce) and without ice sheets (OrbGHG) were established to examine the paleosol response to ice sheet-induced climate changes in two interglacials, MIS 11 and MIS 13. Our results showed that, in response to ice sheets, precipitation and temperature evolve differently and led to strong carbonate leaching and clay migration in both interglacials. In addition, MIS 13 shows more carbonate leaching and clay migration than MIS 11.

As people become more conscious of the importance of sustainable soil use, soil ecosystem services are being put under close environmental scrutiny. Therefore, in **chapter 5**, the research was extended to modeling soil based ecosystem services using time series of climate and soil data. The study was conducted to test the response of soil stocks and soil ecosystem services on natural soil erosion rates (0, 0.5, 1.0, 1.5 and 2.0 Mg ha⁻¹ y⁻¹) and to assess threshold values that may not negatively affect soil functions. Thus, we tested the influence of natural erosion rates on long-term soil property changes and ecosystem services over long time scales (22000 years during MIS5e interglacial) using the soil formation model. Two scenarios of soil development were defined, namely (1) erosion plus dust addition and (2) only erosion. Two soil stocks (soil organic carbon, exchangeable bases) and a combined performance index reflecting the delivery of the ecosystem services: Carbon Sequestration Capacity (CSC), Water Yield (WY) and the ratio of actual over potential evapotranspiration (Ω) were evaluated under these defined rates of erosion. Results showed that soil stocks (soil organic carbon, exchangeable bases) and ecosystem services evolve and respond differently to increased erosion rates. The combined performance index for ecosystem services showed that soil ecosystem performance is worse at erosion rates above 1.0

Mg ha⁻¹ y⁻¹. This work demonstrated the necessity of choosing reference erosion rates (= soil loss tolerance rates) based on soil natural erosion rates.

General conclusions are summarized in **Chapter 6**. Overall, our work offered an integrated process model-based support for interpreting paleoclimate-paleosol interactions in the CLP. One of the greatest advantages of this study is that the two models combine quantitative climate and soil data at the comparable temporal scales and provide a quantitative outcome. The largest drawbacks are the broad range of data requirements of the soil model and the low resolution of the climate model in the CLP. We could conclude that LOVECLIM1.3-SoilGen2 is a feasible and valuable model combination for quantifying the effect of climatic forcings on the evolution of paleosols, and this combination can be the first attempt for future climate-soil modeling. However, both soil and climate models remain to be improved for precise quantifications, and therefore a number of challenges need to be addressed, which are described in **chapter 7**.

Samenvatting

Bodems gevormd in het verleden zijn paleosols. Zodra deze bodems zijn bedekt door sedimenten (bijvoorbeeld löss), worden het begraven paleosols (fossiele bodems). De Löss-paleosol-sequenties (LPS) op het Chinese Löss-plateau (CLP) zijn de meest uitgebreide terrestrische archieven voor paleoklimaten, en weerspiegelen klimaatschommelingen op wereldschaal weerspiegelen, met veelal glaciaal-interglaciale fasen. De omgevingsomstandigheden tijdens het Kwartair hebben geleid tot continue lössafzetting tijdens glacialen (koud-droog), welke worden afgewisseld door paleosols gevormd tijdens interglacialen (warm-vochtig) in de CLP. In de context van paleosols ontwikkelen bodemfuncties en hun eigenschappen zich over lange perioden onder invloed van interglaciale klimatologische omstandigheden voordat jonge sedimenten deze bodems begraven.

Paleosols in de CLP zijn niet uitgebreid bestudeerd in termen van de dynamische verbinding tussen klimaat en paleosols. Deze verbinding kan alleen worden benaderd door bodemmodellering, en geïntegreerde bodemgenese-klimaatmodellen zijn daarom belangrijk bij het beoordelen van dynamische paleoklimaat-paleosolrelaties. Het algemene thema van dit onderzoek is om de paleoklimaat-paleosolrelaties in de CLP beter te begrijpen, met name door de vorming van paleosols als reactie op interglaciale klimaten kwantitatief te beoordelen en uiteindelijk om het functioneren van de bodem te evalueren in termen van op de bodem gebaseerde ecosysteemdiensten. Deze kennis van klimaat-bodemrelaties (zonder de menselijke factor) is mogelijk essentieel in een Antropocene setting om als referentie te dienen. In dit werk hebben we twee procesmodellen gecombineerd, LOVECLIM1.3 en SoilGen2, waardoor de vorming van paleosols in de afgelopen 500 ka-jaren kan worden gesimuleerd. Voor alle paleosol-simulaties werden door LOVECLIM1.3 het gesimuleerd klimaat en vegetatie verkregen voor de omvang van de interglaciale periode, terwijl (eolische) stoftoevoegingsritmes en initiële bodemgesteldheid (bijv. moedermateriaalmateriaaleigenschappen) werden gedefinieerd in het bodemmodel.

In **hoofdstuk 2**, bespraken we bodem- en klimaatmodellen, de vereisten (bijv. neerschalen van de klimaatoutput naar de inputschaal van het bodemmodel) en de interglaciale periode die in het Lössplateau werd bestudeerd. In hoofdstuk 3 werd het bodemmodel gekalibreerd voor verschillende parameters van de belangrijkste bodemprocessen door gesimuleerde en gemeten bodemeigenschappen voor Holocene bodems en MIS13 paleosols gevormd in de CLP met elkaar te confronteren. Het kalibratieproces omvatte het optimaliseren van de procesparameters van drie belangrijke procesformuleringen: decarbonisatie, kleimigratie en de organische koolstofcycli in de bodem. De kalibratieresultaten kwamen redelijk overeen met het bereik van literatuurwaarden. Na kalibratie laten de bodemeigenschappen (gehalte aan klei, calcië, organische koolstof en kationenuitwisselingscapaciteit) een sterke respons zien op tien gereconstrueerde Holocene stofdepositiescenario's die de onzekerheid in stofdepositie weerspiegelen. De conclusie werd getrokken dat het gekalibreerde bodemmodel interglaciale bodemsimulatie in de CLP over lange tijdschalen mogelijk maakt; de gesimuleerde bodemeigenschappen waren echter gevoelig voor (onzekere) stoftoevoegingsritmes.

In **hoofdstuk 4** werd het gekalibreerde SoilGen2-model gebruikt om paleosols in Marine Isotope Stages (MIS) 5, 7, 9, 11 en 13 te simuleren. We hebben eerst de relatieve bijdragen van neerslag, temperatuur, potentiële verdamping, vegetatie en stoftoevoeging getest op paleosol-ontwikkeling in MIS 11 en MIS 13 interglacialen. Onze resultaten toonden aan dat neerslag, stoftoevoeging en potentiële verdamping de grootste impact hebben op paleosols tijdens MIS 11 en MIS13 interglacialen, maar hun relatieve belang varieert tussen bodemeigenschappen (bijv. gehalte aan klei en calcië) en tussen interglacialen. Wat het klimaat betreft, zijn de baanparameters van de aarde (precessie, excentriciteit, scheefstand) en ijskappen op het noordelijk halfrond (NH) de twee belangrijkste factoren die het klimaat op aarde bepalen. De LPS in China zijn erg belangrijk geworden voor het herkennen van indirecte invloed van orbitaal geforceerde ritmes (precessie, schuine stand en excentriciteit) tijdens het Kwartair. Studies die zich richten op opeenvolgende

veranderingen van (en ook indirecte invloed van) precessie, over ijsvolume, naar klimaat en uiteindelijk naar bodemeigenschappen op de CLP zijn echter nog steeds zeldzaam en de respons van deze variaties die in paleosols zijn vastgelegd, is nog steeds onduidelijk. In **hoofdstuk 4** hebben we voor het eerst de paleosol-respons op deze variaties onderzocht door visuele vergelijking tussen de inhoud van calciet en klei en precessievariatie. Het verband tussen precessievariatie en de gesimuleerde bodemeigenschappen is indirect, door veranderingen in klimaatvariabelen (bijvoorbeeld neerslag). Onze resultaten toonden aan dat een sterke precessievoetafdruk werd behouden in de gesimuleerde S1 (MIS 5), S2 (MIS 7), S3 (MIS 9) en S5-1 (MIS 13) paleosols en een zwak precessiesignaal in de S4 paleosols (MIS 11) in de CLP. Verder veronderstelden we dat het begrijpen van de indirecte invloed van ijskapveranderingen op interglaciale bodemontwikkeling door middel van modellering een betere interpretatie van de paleosol-ontwikkeling in de CLP mogelijk zou kunnen maken. Daarom werden twee experimenten met ijskappen (OrbGHG_{Ice}) en zonder ijskappen (OrbGHG) opgezet om de paleosol-respons op door ijskap veroorzaakte klimaatveranderingen in twee interglacialen, MIS 11 en MIS 13, te onderzoeken. Onze resultaten toonden aan dat, in reactie op ijskappen, neerslag en temperatuur verschillend evolueren en leiden tot sterke carbonaattuitlegging en kleimigratie in beide interglacialen. Bovendien vertoont MIS 13 meer carbonaattuitlegging en kleimigratie dan MIS 11.

Naarmate mensen zich meer bewust worden van het belang van duurzaam bodemgebruik, worden bodemecosysteemdiensten in toenemende mate onderzocht. Daarom werd het onderzoek in **hoofdstuk 5** uitgebreid tot het modelleren van op de bodem gebaseerde ecosysteemdiensten met behulp van tijdreeksen van klimaat- en bodemgegevens. De studie werd uitgevoerd om de respons van bodemvoorraden en bodemecosysteemdiensten op natuurlijke bodemerosiesnelheden (0, 0.5, 1.0, 1.5 en 2.0 Mg ha⁻¹ y⁻¹) te testen en om drempelwaarden te beoordelen die de bodemfuncties niet negatief mogen beïnvloeden. Daarom hebben we de invloed van natuurlijke erosiesnelheden op lange-termijn veranderingen in bodemeigendom en

ecosysteemdiensten over lange tijdschalen (22000 jaar tijdens MIS5e interglaciaal) getest met behulp van het bodemvormingsmodel. Er zijn twee scenario's van bodemontwikkeling gedefinieerd, namelijk (1) erosie plus stoftoevoeging en (2) alleen erosie. Twee bodemvoorraden (organische koolstof in de bodem, uitwisselbare basen) en een gecombineerde prestatie-index die de levering van de ecosysteemdiensten weerspiegelt: koolstofvastleggingscapaciteit (CSC), wateropbrengst (WY) en de verhouding tussen werkelijke en potentiële verdamping (Ω) werden geëvalueerd onder deze gedefinieerde erosiesnelheden. De resultaten toonden aan dat bodemvoorraden (organische koolstof in de bodem, uitwisselbare basen) en ecosysteemdiensten evolueren en verschillend reageren op verhoogde erosiesnelheden. De gecombineerde prestatie-index voor ecosysteemdiensten toonde aan dat de prestatie van het bodemecosysteem slechter is bij erosiesnelheden boven $1.0 \text{ Mg ha}^{-1} \text{ y}^{-1}$. Dit werk toonde de noodzaak aan om referentie-erosiesnelheden (= tolerantiepercentages voor bodemverlies) te kiezen op basis van natuurlijke bodemerosiesnelheden.

Algemene conclusies zijn samengevat in **hoofdstuk 6**. Over het algemeen bood ons werk een geïntegreerde procesmodel-gebaseerde ondersteuning voor het interpreteren van paleoklimaat-paleosol-interacties in de CLP. Een van de grootste voordelen van dit onderzoek is dat de twee modellen kwantitatieve klimaat- en bodemgegevens op vergelijkbare tijdschalen combineren en een kwantitatief resultaat opleveren. De grootste nadelen zijn het brede scala aan data-eisen van het bodemmodel en de lage resolutie van het klimaatmodel in het CLP. We zouden kunnen concluderen dat LOVECLIM1.3-SoilGen2 een haalbare en waardevolle modelcombinatie is voor het kwantificeren van het effect van klimaatforceringen op de evolutie van paleosols, en deze combinatie kan de eerste poging zijn voor toekomstige klimaat-bodemmodellering. Zowel bodem- als klimaatmodellen moeten echter nog worden verbeterd voor nauwkeurige kwantificering, en daarom moeten een aantal uitdagingen worden aangepakt, die worden beschreven in **hoofdstuk 7**.

Résumé

Les sols du passé sont des paléosols. Une fois que les paléosols sont recouverts de sédiments (par exemple le loess), ces paléosols sont transformés en paléosols enfouis (sols fossiles). Les séquences de loess-paléosols (LPS) du plateau de loess chinois (CLP) sont les enregistrements paléoenvironnementaux terrestres les plus complets pour les paléoclimats, reflétant les oscillations climatiques à l'échelle mondiale, les phases glaciaires-interglaciaires. Les conditions environnementales du Quaternaire ont entraîné des dépôts continus de loess lors des glaciaires (froid-sec), qui sont néanmoins interrompus par des paléosols lors des interglaciaires (chaud-humide) dans le CLP. Dans le contexte des paléosols, les fonctions des sols et leurs propriétés se développent sur de longues échelles de temps sous l'influence des conditions climatiques interglaciaires avant que les jeunes sédiments n'enfouissent les sols.

Les paléosols du CLP ne sont pas suffisamment étudiés en termes de connexion dynamique entre le climat et les paléosols. La formation et l'évolution des sols dans le temps ne peuvent être approchées que par la modélisation des sols, et les modèles intégrés genèse-climat des sols sont importants pour évaluer les relations dynamiques paléoclimat-paléosol. Le thème général de cette recherche est de mieux comprendre les relations paléoclimat-paléosol dans le CLP, notamment en évaluant quantitativement les réponses des paléosols aux climats interglaciaires et, in fine, d'évaluer le fonctionnement du sol en termes de services écosystémiques basés sur le sol. This knowledge of climate-soil relations (without human factor) is possibly essential in Anthropocene settings. In this work, we combined two process models, LOVECLIM1.3-SoilGen2, allowing simulation paleosols over the past 500 ka years. For all the paleosol simulations, LOVECLIM1.3-simulated climate and vegetation were obtained for the extent of the interglacial period while dust addition rhythms and initial soil conditions (e.g. parent material properties) were defined in the soil model.

Dans la première étape, au **chapitre 2**, nous avons discuté des modèles de sol et de climat, des exigences (par exemple, réduction d'échelle de la sortie climatique à l'échelle d'entrée du modèle de sol) et de la période interglaciaire étudiée dans le plateau de Loess. Dans le **chapitre 3**, le modèle de sol a été calibré pour divers paramètres de processus du sol en confrontant les propriétés du sol simulées et mesurées pour les sols de l'Holocène et les paléosols MIS13 formés dans le CLP. Le processus d'étalonnage impliquait l'optimisation des paramètres de processus de trois principales formulations de processus : la décalcification, la migration de l'argile et le cycle du carbone organique du sol. Les résultats de l'étalonnage étaient en accord raisonnable avec la plage de valeurs de la littérature. Après étalonnage, les propriétés du sol (teneur en argile, carbone organique de calcite et capacité d'échange cationique) montrent une forte réponse à dix scénarios de dépôt de poussière Holocène reconstruits reflétant la propagation de l'incertitude dans le dépôt de poussière. La conclusion a été tirée que le modèle de sol calibré permet la simulation du sol interglaciaire dans le CLP sur de longues échelles de temps ; cependant, les propriétés du sol simulées étaient sensibles aux rythmes (incertains) d'ajout de poussière.

Dans le **chapitre 4**, le modèle calibré SoilGen2 a été utilisé pour simuler les paléosols aux stades isotopiques marins (MIS) 5, 7, 9, 11 et 13. Nous avons d'abord testé les contributions relatives des précipitations, de la température, de l'évapotranspiration, de la végétation et de l'ajout de poussière sur le paléosol. développement dans les interglaciaires MIS11 et MIS13. Nos résultats ont montré que les précipitations, l'ajout de poussière et l'évapotranspiration ont le plus grand impact sur les paléosols pendant les interglaciaires MIS11 et MIS13, mais leur importance relative varie selon les propriétés du sol (par exemple, la teneur en argile et en calcite) et entre les interglaciaires. En ce qui concerne le climat, les paramètres orbitaux terrestres (précession, excentricité, obliquité) et les calottes glaciaires de l'hémisphère nord (NH) ont été les deux principaux facteurs qui régissent le climat terrestre. Les LPS en Chine sont devenus très importants pour reconnaître les rythmes orbitaux forcés (précession, obliquité et excentricité)

au cours du Quaternaire. Cependant, les études portant sur les changements successifs de la précession, du volume de glace au climat et enfin aux propriétés du sol sur le CLP sont encore rares et la réponse de ces variations imprimées dans les paléosols n'est toujours pas claire. Pour la première fois, dans le **chapitre 4**, nous avons étudié la réponse des paléosols à ces variations par comparaison visuelle entre les teneurs en calcite et en argile et la variation de précession. Nos résultats ont démontré qu'une forte empreinte de précession était conservée dans les paléosols simulés S1 (MIS 5), S2 (MIS 7), S3 (MIS 9) et S5-1 (MIS 13) et un faible signal de précession dans les paléosols S4 (MIS11) du CLP. De plus, nous avons émis l'hypothèse que la compréhension de l'influence des changements de la calotte glaciaire sur le développement des sols interglaciaires par la modélisation pourrait permettre une meilleure interprétation du développement des paléosols dans le CLP. Par conséquent, deux expériences avec glace (OrbGHGIce) et sans calottes glaciaires (OrbGHG) ont été mises en place pour examiner la réponse du paléosol aux changements climatiques induits par la calotte glaciaire dans deux interglaciaires, MIS 11 et MIS 13. Nos résultats ont montré qu'en réponse aux calottes glaciaires, les précipitations et la température évoluent différemment et conduisent à un fort lessivage des carbonates et à une migration des argiles dans les deux interglaciaires. De plus, MIS 13 montre plus de lessivage de carbonate et de migration d'argile que MIS 11.

Alors que les gens deviennent plus conscients de l'importance d'une utilisation durable des sols, les services écosystémiques des sols sont soumis à un examen environnemental approfondi. Par conséquent, dans le **chapitre 5**, la recherche a été étendue à la modélisation des services écosystémiques basés sur le sol en utilisant des séries chronologiques de données sur le climat et le sol. L'étude a été menée pour tester la réponse des stocks de sol et des services écosystémiques du sol sur les taux d'érosion naturelle du sol (0, 0.5, 1.0, 1.5 et 2.0 Mg ha⁻¹ y⁻¹) et pour évaluer les valeurs seuils qui peuvent ne pas affecter négativement les fonctions du sol. Ainsi, nous avons testé l'influence des taux d'érosion naturelle sur les changements à long terme des propriétés du sol et les services écosystémiques sur de longues échelles de

temps (22000 ans pendant l'interglaciaire MIS 5e) en utilisant le modèle de formation du sol. Deux scénarios de développement du sol ont été définis (1) érosion plus ajout de poussière et (2) érosion seule. Deux stocks de sol (carbone organique du sol, bases échangeables) et un indice pour les services écosystémiques combinés : la capacité de séquestration du carbone (CSC), le rendement en eau (WY) et le rapport entre l'évapotranspiration réelle et potentielle (Ω) ont été évalués sous ces taux d'érosion définis. Les résultats ont montré que les stocks (carbone organique du sol, bases échangeables) de sols et les services écosystémiques évoluent et réagissent différemment aux taux d'érosion accrus. L'indice de performance combiné pour les services écosystémiques a montré que la performance de l'écosystème du sol est pire à des taux d'érosion supérieurs à $1.0 \text{ Mg ha}^{-1} \text{ y}^{-1}$. Ce travail a démontré la nécessité de choisir des taux d'érosion de référence (= taux de tolérance à la perte de sol) basés sur les taux d'érosion naturelle du sol.

Les conclusions générales sont résumées au **chapitre 6**. Dans l'ensemble, notre travail a offert un support basé sur un modèle de processus intégré pour l'interprétation des interactions paléoclimat-paléosol dans le CLP. L'un des plus grands avantages de cette étude est que les deux modèles combinent des données quantitatives sur le climat et le sol à des échelles temporelles comparables et fournissent un résultat quantitatif. Les principaux inconvénients sont le large éventail d'exigences en matière de données du modèle de sol et la faible résolution du modèle climatique dans le CLP. Nous pourrions conclure que LOVECLIM1.3-SoilGen2 est une combinaison de modèles faisable et précieuse pour quantifier l'effet des forçages climatiques sur l'évolution des paléosols, et cette combinaison peut être la première tentative pour une future modélisation climat-sol. Cependant, les modèles de sol et de climat restent à améliorer pour des quantifications précises, et donc un certain nombre de défis doivent être relevés, qui sont décrits au **chapitre 7**.

CHAPTER 1. General introduction and objectives

1.1 The importance of studying interglacial soil development in the Quaternary

Soil is the thin outer skin of Earth, on which life relies. Soil temperature is one of the important factors that influence soil formation and plant growth. The amount of solar radiation from the Sun that reaches the Earth is the main driver influencing the soil temperature. Generally speaking, soil develops when soil temperature is above 5°C (as biological zero is defined in Soil Survey Staff, 2014) because it provides conditions that accelerate chemical, physical and biological processes by the action of water movement. However, in some regions, soil processes (cryoturbation) still occur at soil temperature below 5°C. Soil organic matter decompose maximally at optimum soil temperature between 21°C-38°C of (Broadbent, 2015) while stimulating microbial activities. Generally, vegetation growth increases when soil temperature is above 6°C (Ikawa and Kourouma, 1985).

Soil is a function of the combined effects of various factors: climate, vegetation, topography, parent material composition, parent material age, duration of soil formation. As soil is strongly linked to climate and given the global warming since the pre-industrial time, a big question is how soil reacts to this warming and what is its role in this warming. Some clues could be found from the soils that developed during the warm periods (interglacials) in the geological past. The Quaternary interglacials and associated soil formation have received much attention (Retallack, 2001; Holliday, 2004).

Interglacial soils are, once draped by young sediments (e.g loess, sand, volcanic ash), called buried paleosols (fossil soils), soils which formed in a past landscape under past external forcings (Ruhe, 1956; Retallack, 1998; 2001). Generally speaking, when the young sediment are sufficiently thick, soil changes after such fossilization are minimal (except rapidly changing soil properties such as organic matter decomposition, base saturation), and therefore Quaternary buried paleosols can be considered important paleo archives of climates, ecosystems, vegetation, parent materials and Aeolian sedimentation (Sheldon and Tabor, 2009; Schaetzl and Thompson, 2015; Tabor and Myers, 2015). The Quaternary paleosols (buried) are useful in

Quaternary stratigraphy, geomorphology, landscape evolution, archeology, paleoclimatology, and interpreting past climate or vegetation conditions (Muhs, 2013).

Particularly, paleosols are fundamental parts of Earth's paleo critical zones¹ (Amundson et al., 2007; Leopold et al., 2011; Nordt and Driese, 2013; Marin-Spiotta et al., 2014; Beverly et al., 2018). Therefore, paleosols are considered as memory of the past environment (Targulian and Goryachkin, 2004), in which some solid-phase properties can be renewed (e.g by organic matter decomposition), but part of its properties are well-preserved. Paleosols can be studied to disentangle the relative influence of various regional environmental conditions on soil formation and to reconstruct climate variations during the time of paleosol formation.

Paleosol formation is worth attention and a remarkable resource to understand pedogenesis. A thorough understanding of past soil variability, particularly in response to climate variability, would allow a robust projection of future soil ecosystems, leading to sustainable socio-economic development. Notably, the most extensive stratigraphic alternations between sediments and buried paleosols have been recorded in the loess landscapes of the world, mainly during the Quaternary loess-paleosol deposits.

1.2 The Quaternary paleosols formed on loess

1.2.1 Loess distribution and characteristics

Loess is one of the most extensive types of Quaternary deposits, occupying about 10 % of the total Earth surface. Loess deposits are spatially distributed mainly in arid to semi-arid regions in the mid-latitudes of the world (Pecsi, 1990). The major loess deposits are located in Central China, Central Asia, North America, South America, Central and Eastern Europe, and Argentina,

¹ Critical zone (CZ) is defined as "heterogeneous, near surface environment in which complex interactions involving rock, soil, water, air, and living organisms regulate the natural habitat and determine the availability of life-sustaining resources" (NRC, 2001). Paleo Critical Zones (PCZs) are originated from the concept of CZs, and are buried CZs that are isolated from modern processes (Ashley, 2020).

New Zealand (Muhs, 2013; Li et al., 2020). Soil developed from loess is very fertile and highly suitable for crop cultivation (Catt, 2001; Smalley et al., 2009).

Loess is the major type of wind-transported parent materials that comprise silt-sized, unconsolidated, yellow-brown color surficial additions (Pecsi, 1990). Loess typically has a silty texture (10-50 μm) of 40-70 % and weathers into a silty-clayey soil and 5-25% of clay and sand. A typical loess material consists of quartz (~40-80%, the dominant mineral), carbonates (1-20%), and lesser amounts of feldspars and dolomite. Clay minerals in loess are predominantly illite or montmorillonite and usually also contain smaller amounts of kaolinite, vermiculite, and chlorite (Pecsi, 1990; Smalley et al., 2011). However, the composition of loess varies depending on the source of the material and regions. The loess material properties are dependent on Aeolian transportation of dust, the dust mobility characteristics (e.g. dust source areas, aridity of source areas, transportation and deposition areas, accumulation on land as loess) that are purely regulated by climate (Ding et al., 2005; Maher et al., 2010; Újvári et al., 2016; Li et al., 2020).

1.2.2 Loess and paleosol sequences

Loess deposits are visible as distinctive sedimentary layers in the field. Loess was mostly deposited during glacial periods but this continued at low rates during interglacials, periods that favor soil formation. The Quaternary paleosols alternating with loess sediments reflect major Quaternary glacial-interglacials climatic fluctuations, as these loess-paleosols show fluctuations similar to those recorded in deep-sea sediments (Kukla, 1970; Evans and Heller, 2001).

Buried paleosols within Quaternary loess deposits can easily be separated visually (e.g. color), and analytically (e.g. texture) from loess deposits. So that, theoretically, paleosols are pedogenetically isolated from other paleosols by loess. Therefore, in many regions of the world, loess-paleosols formed in the Quaternary period are well-known as stratigraphic markers (e.g using color, grain size, mineralogy) and are used for paleoclimatic reconstructions (Muhs, 2013) by using climate imprints, so-called climate “proxy” data. Proxies can

be chemical (Magnetic Susceptibility (MS), stable isotopes, clay mineralogy, weathering ratios), biological zoological (molluscs, ostracods, chironomids, coleopterans) or botanical (pollen, diatoms, macrofossils, tree rings), which are transformed to the climatic parameter of interest (e.g. temperature) (Finke et al., 2021a).

Loess is widely distributed in Asia, particularly on the Chinese Loess Plateau (CLP) (**Figure 1-1**), which is the largest Quaternary loess accumulation in the world (Maher et al., 2010). The loess-paleosol sequences on the CLP are the most studied for paleoclimatic reconstructions resulting in a myriad of studies. Muhs (2013) stated that no geographic area received more attention for loess-paleosol studies than China. The Chinese loess is the longest complete and continuous terrestrial record and has attracted much attention from climatologists, paleopedologists, geographers, and geologists.

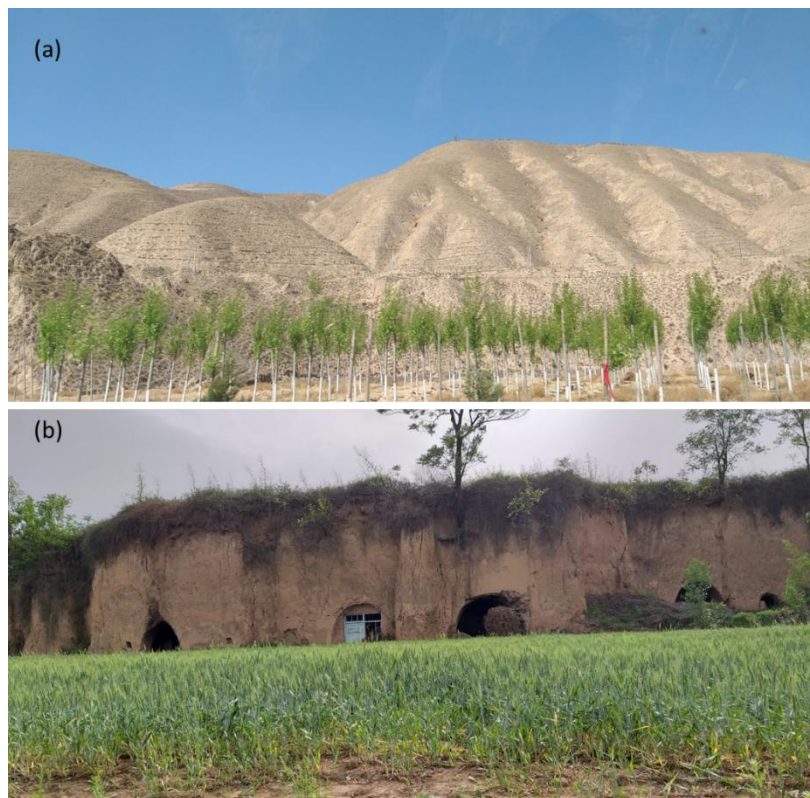


Figure 1-1 Photos of loess geomorphology from the Loess Plateau of China, (a). Lanzhou, northwestern CLP, (b) Baoji, southeastern CLP (photos by Ranathunga, KN, 2019).

1.3 Study area - The Chinese Loess Plateau

1.3.1 Geography, climate and vegetation gradient

The CLP in north central China, (**Figure 1-2**), is famous for its extensive loess landscapes and complete loess-paleosols records in the Quaternary, covering ~2.6 Ma (Zhang et al., 2013). It is located between 105-115 °E, 30-40 °N and has a total land area of ~6.4 x 10⁵ km² (Zhu et al., 2019). The depositional history dated back to more than 22 Ma ago preserving one of the longest terrestrial paleoclimate records in the world (Guo et al., 2002; Qiang et al., 2011).

Through time, the area of the CLP has been covered by thick, wind-blown sediments (loess); as a result, from northwest to southeast, the loess thickness ranges from ~350 m to 100 m. Dust addition decreases from northwest to southeast, which is further away from the dust source regions located in the north and northwest (Liu, 1985). The northwest loess units are found downwind and nearby the dust source areas (in the north and northwestern deserts) (Lu and Sun, 2000): Mongolian Gobi Desert, Gurbantuggut Desert, Taklimakan Desert, Qaidam Basin, Badain Juran Desert, Tengger Desert, Hobq Desert, Mu Us sandy land, Otindag sandy land, and Horqin sandy land (Sun et al., 2020). At present, during spring and winter, dust is entrained from the deserts and is accumulated on the Plateau (Roe, 2009; Maher et al., 2010).

The CLP is exposed to the continental monsoon climate that is characterized by the East Asian Monsoon (EAM), which is one of the most variable monsoon systems in the global climate system. The EAM has its two major components, the East Asian Winter Monsoon (EAWM) and the East Asian Summer Monsoon (EASM) that have exerted a direct influence on loess deposition and its soil formation of the loess plateau (An et al., 2014). Dust transportation over the region is closely coupled with the Siberian High (SH), also called Siberian anticyclone, a high atmospheric pressure cell centered over the Mongolia-Siberia region. During winter seasons, the SH pushes cold air masses over eastern and southern Asia, central China and these cold air flows

are known as the EAWM. These airflows passing over the northern deserts carry dust to the CLP. EAWM dominated during glacial periods and the changes of EAWM were primarily driven by changes in ice volume in the Northern Hemisphere (NH), which influenced the strength of the SH and the EAWM. The ice sheets in the NH enhance the cold surface conditions in the SH and a strong SH leads to a strong EAWM (Liu and Ding, 1998). The EAWM and Westerlies from the Asian continent deliver dust to the CLP (**Figure 1-2**) (Porter and An, 1995; Gong and Ho, 2002; Chang et al., 2006).

During interglacials, northern hemisphere EASM insolation slowly increases. Differential heating of the Asian continent and the surrounding oceans leads to a temperature contrast between the warmer land and the cooler oceans and causes a pressure gradient during summer months. The resulting pressure gradient between ocean and land produces airflows blowing from the South China Sea and equatorial Pacific Ocean resulting in heavy summer precipitation in the southern China, the EASM (Liu and Ding, 1998; An et al., 2014). Soil formation was triggered by summer precipitation and temperature during the EASM.

The CLP has a climate gradient from sub-humid (UNEP aridity index between 0.5 to < 0.65) in the southeast to arid (UNEP aridity index between 0.05 to < 0.20) climate in the northwest (Wen et al., 2018). As a result, from southeast to northwest, the average annual precipitation decreases from 800 mm to 300 mm (for the interval 1951–1990, and we assume annual precipitation and temperature over this period for all the locations in this study). The rain falls mainly during July, August and September, with more than 60% of the annual precipitation. The mean annual temperature decreases from 12-14 °C to 6-8 °C from southeast to northwest (Hao and Guo, 2005). The natural vegetation in the area responds to the climate gradients of precipitation, temperature and aridity gradient thus vegetation types grade from forest, forest-steppe, steppe

and desert steppe from the southeast to the northwest of the Loess Plateau (Feng et al., 2004a).

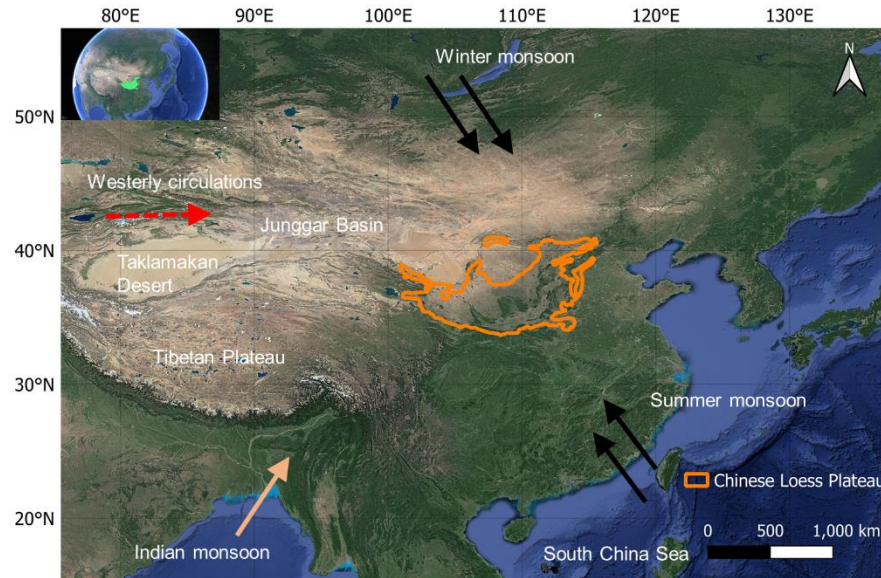


Figure 1-2 Map of the Chinese Loess Plateau and its surroundings deserts in northern China and the arrows indicate the pathways of the monsoons atmospheric circulation system over China and dash arrow (red) indicates the westerly winds. (base map is from google satellite map in QGIS 3.24.1).

1.3.2 Quaternary loess-paleosol records in the Chinese Loess Plateau

Loess-paleosol sequences (LPS) in China provide one of the most complete terrestrial records of interglacial–glacial cycles, which is strongly coupled with EAM variability in the region (Liu, 1985; An et al., 1990; Porter and An, 1995; Porter, 2001; Guo et al., 2002). The Quaternary LPS recorded at least 56 major soil-forming periods and paleosols (buried soils) which alternate with loess layers (Guo et al., 1996). In the CLP, dust addition continued during interglacials, at a low rate, adding parent materials at the top of the paleosols, and developing the soil surface in upward direction leading to the formation of the so-called accretionary paleosols (An et al., 1991b; Kemp, 2001). At the

same time, soil-forming processes extend into previously deposited loess. The two competing processes (soil formation and dust accumulation) and their variable rates determine paleosol expressions in the CLP (**Figure 1-3 A and B**).

Over glacial and interglacial time spans, the loess and paleosols have been developed as stacks (as continuous sequence of L and S) (**Figure 1-3 A**). These L and S denote loess layers and intervening paleosols, respectively, and starting from soil surface, L and S are numbered and increased downward. The youngest paleosol/loess are near the soil surface and the oldest paleosol/loess are in the bottom of the profile. This nomenclature produces the standard stratigraphy of S/L in the CLP: the Holocene soils (S0; below it is the L1 loess layer, underlain by the paleosol layer (S1). Likewise, the paleosol-loess stratigraphy alternates as, S0/L1, S1/L2, S2/L3, S3/L4, S4/L5, S5/L6, S6/L7.....L33/S33 (Kukla and An, 1989). In the CLP, loess layers are sufficiently thick to isolate one paleosol from another paleosol (**Figure 1-4** for example. For example, the thickness of L1 loess layer decreases southeastward from more than 30 m in the western Loess Plateau to less than 5 m in southeast Loess Plateau along the northwest-southeast transect. Therefore in this study, deep drainage and changes in recarbonatization and clay migration from upper paleosols to lower paleosols are assumed to be minimal. The alternating layers of yellowish-brown loess and reddish-brown paleosols (**Figures 1-4 and 1-5**) can be correlated with the Marine Isotope Stages (MIS), in which paleosols correlate with odd numbered MIS stages, the interglacials, and loess with even numbered MIS stages, the glacials (**Figure 1-6**) (Kukla, 1987). For example, Magnetic Susceptibility (MS) of the loess-paleosol deposits correlates closely with the marine oxygen isotope record of the deep-sea sediments (Kukla, 1987) illustrating that the LPS have fluctuated in response to glacial-interglacial conditions (An et al., 1990; Rutter et al., 1991; Ding et al., 1995; An, 2000; Porter, 2001). The coherence between the LPS and MIS stages suggests the oscillations of the EAM recorded in the loess–paleosol sequences were influenced predominantly by global ice volume (Kukla, 1987).

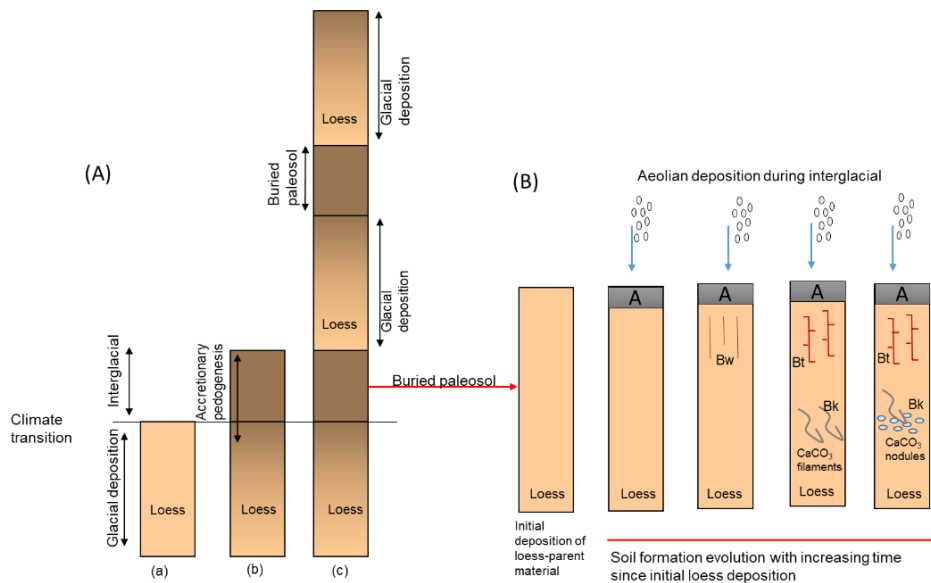


Figure 1-3 Schematic diagram for interglacial paleosol formation on loess. In A. (a) loess deposition during glacial. (b) Climate changes from glacial to interglacial and soil formation on both previously deposited loess and on new dust sediments during interglacial. (c) Dust addition increases again during glacial, and soil formation is weakened, burying soils. In B. the evolution of soil formation since initial loess deposition in a mid-latitude climate, showing increasing thickness, carbonate-rich (Bk) and clay-rich (Bt) horizons, A- horizon – black top part of the paleosols, Bw- weathering horizon (vertical lines) (after Stevens et al., 2007; Muhs, 2013).



Figure 1-4 The alternating light colored loess and reddened paleosols, Baoji, southern Loess Plateau (photos by Ranathunga, KN, 2019).

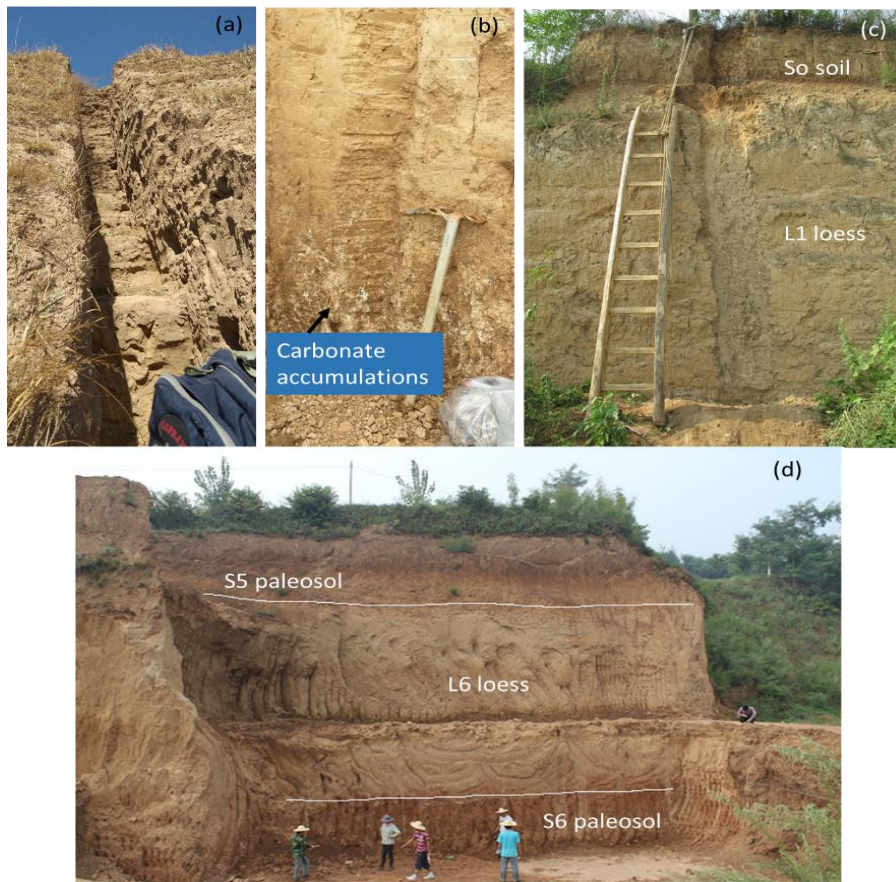


Figure 1-5 Loess-paleosol profiles on the Chinese loess plateau: (a) loess sediments in Lanzhou (western Loess Plateau), (b) Baoji (southern Loess Plateau) (photos by Ranathunga, KN) (c) Holocene soil (S0) and last glacial loess (L1) and (d) S5 paleosol, L6 loess and S6 paleosol at Weinan (southern Loess Plateau) (photos by Guoqiao Xiao).

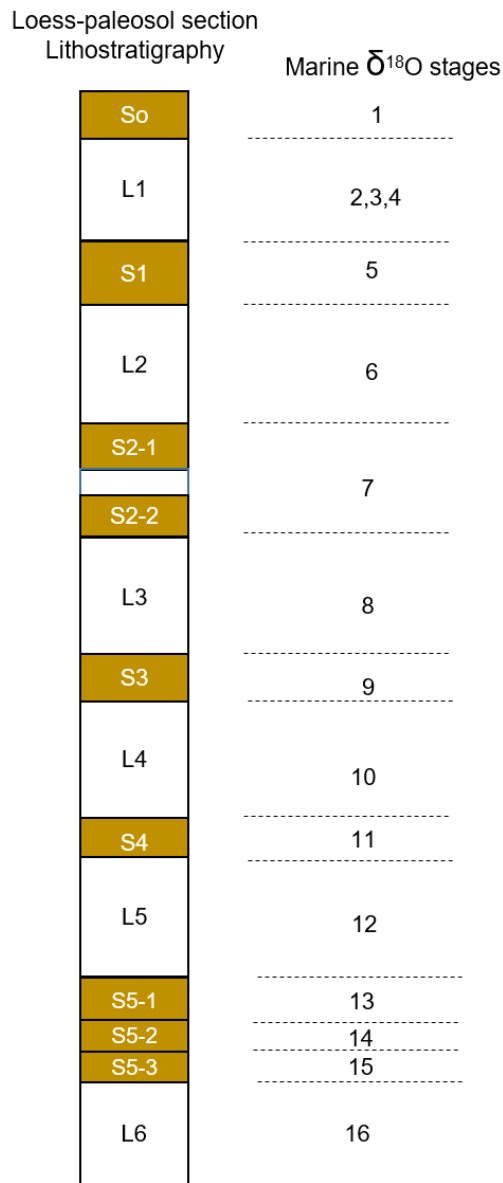


Figure 1-6 General and simplified correlation of the loess–paleosol succession on the Chinese Loess Plateau spanning the last 500 ka BP with the Marine Isotope Stages. The general correlation is based on the visual correlation of monsoon proxies (e.g. magnetic susceptibility) to the stacked benthic $\delta^{18}\text{O}$ Lisiecki and Raymo (2005) between each paleosol layer to an interglacial marine isotope stage.

1.3.3 Forcing factors of the Loess-paleosols sequences in China

Loess-paleosol sequences over the Quaternary glacial-interglacial periods are strongly controlled by climate changes that are driven by climate forcings such as global ice volume, insolation, sea-level change, atmospheric CO₂ as well as climate internal feedbacks (An et al., 1990; 1991a; 1991b; An, 2000). The periodicities of the three astronomical parameters, eccentricity (~100 ka), obliquity (~41 ka) and climatic precession (~21 ka), have been found in many proxies (e.g. magnetic susceptibility, grain size) in the LPS, indicating the important role of astronomically-driven insolation changes on the LPS (Ding et al., 2002). In agreement with the fact that precession is the main factor controlling the daily insolation variation at middle-low latitudes (Berger, 1978), where the CLP is located, modelling studies confirmed that the EASM is closely correlated with precession (Kutzbach et al., 2008; Yin et al., 2008; 2009; Lyu et al., 2021). Many authors have correlated loess-based proxies with the astronomical parameters to develop an orbitally tuned astronomical time scale for loess deposits in the CLP (Lu et al., 1999; Heslop et al., 2000; 2002; Ding et al., 2002; Sun et al., 2006a). In addition, the proxy records on the CLP also show a dominant ~100 ka ice volume cycle over the past ~800 ka that is linked to the glacial-interglacial cycles, implying an important impact of ice-sheets on the EAM evolution (Ding et al., 1995; Lu et al., 2003; Hao et al., 2012; Sun et al., 2015). As mentioned earlier, the large extent of NH ice sheets during glacials increases the strength of EAWM. During interglacials, changes of NH ice sheets are relatively small as compared to glacials, and their effect on the EASM is therefore reduced, with insolation playing a dominant role on the EASM (Yin et al., 2008; 2009; Shi et al., 2020).

1.4 Importance of linking climate evolution with paleosol development

1.4.1 Inconsistencies between global climate and Chinese paleosol

Although the LPS are highly correlated with the global MIS and climate, some of the observed paleosols in the CLP do not correlate well with the global climate.

For example, globally, MIS 13 interglacial was the coolest interglacial over the past 1 Ma. However, most studies in the Loess Plateau show that the S5-1 paleosol is the most intensively developed paleosol in the past 1.2 Ma and can be easily recognized by its thickness and dark red color (Ding et al., 2002; Hao and Guo, 2005; Yin and Guo, 2008, Guo et al., 2009). Paleosol properties that are associated with the intensity of pedogenesis show the climate on the Loess Plateau is anomalously warm and humid during MIS13, indicating a strengthened summer monsoon period (An, 2000; Guo et al., 2009; Hao et al., 2012).

Previous studies have shown that MIS 11 was an unusually warm interglacial in the last 1 Ma. (Droxler et al., 2003; Loutre and Berger, 2003). Geological records have revealed that many regions of the world were wetter during MIS 11, and it was somewhat colder than the present (Candy et al., 2014). However, this conclusion contradicts the S4 paleosols formed in the western Loess Plateau (Shi et al., 2016), where they received less rain during MIS 11 as reflected by CaCO₃ content and soil color. Wu et al. (2007) proposed that the climate was generally humid and warm and unstable, reflecting regional climate differences within the Loess Plateau during the S4 paleosol formation by using terrestrial mollusc assemblages in the Xifeng and Louchuan loess sections. However, conclusions obtained from other paleosol sections in the CLP are somewhat different. Several authors generally concluded that the S4 paleosol reflects the warmest period in the past 1.2 Ma (Guo et al., 1998; 2000) and is regarded as the marker paleosol in the past 2.6 Ma (Liu, 1985). On the contrary, according to Vidic et al. (2003), S4 is a moderately well-developed paleosol, in which the intensity of pedogenesis is less than S5-1

paleosol in the CLP, and MIS 11 does not provide evidence for an extremely warm climate. In the CLP, most of the S4 paleosol is a single paleosol, but differences still exist over the western and central parts of the CLP due to a mild warm and humid climate in the northwestern parts (Shi et al., 2013; 2016), whereas a strong warm-humid climate dominated in the southeastern parts (Hao and Guo, 2005). These distinct differences in climate have resulted in remarkable regional differences in soil development over the Loess Plateau during the MIS 11 interglacial. On the other hand, a weaker paleosol developed in the CLP (Jia et al., 2018) during the MIS9 strong interglacial.

These inconsistencies suggest that climate evolution and soil development during some interglacials do not reflect the globally defined climate conditions. The reason is understandable. Quantitative reconstruction of paleoclimate variation in the CLP is largely based on the proxies recorded in the loess-paleosol sequences. However, the evolution of paleoclimate changes is diverse based on different proxies, possibly due to their different sensitivities (e.g. seasonal changes) to climate change, (e.g. timing of local monsoon precipitation), to the EAM and also to the westerly and Indian monsoon and to dust addition rates. Climate change is a complicated process because of the complexity of the climate system. Therefore, it is plausible that different proxies show diverse climate information and may commonly present different paleoclimate and paleosol conditions. Soil formation is indeed determined by various factors (e.g. climate and associated vegetation, time). Importantly, terrestrial paleosols carry more local information and may or may not consistently respond to global-scale climate variability, suggesting local paleosol response to global-climate events is not always uniform. Therefore, studies focusing on the evolution of paleoclimate and paleosol development in the CLP at the same time scale are necessary.

1.4.2 The necessity of combining soil-forming factors and dust addition in pedogenic processes in the CLP

There have been extensive investigations of loess-paleosol properties for paleoclimatic interpretations, as paleosol analysis has been the common method for interpreting paleoclimate. However, the properties of loess-paleosols are a complex result of the impacts of the prevailed environmental conditions. Particularly, paleosol characteristics are dependent on soil forming conditions (the relative influence of climatic parameters combined with a low rate of deposition) and it is always difficult to distinguish and separate the different climate components and forcings on paleosol development. It is not straightforward to obtain precise climate information based entirely on the paleosol properties, because soil formation is driven by soil-forming factors, which change over the soil formation period. In addition, dust deposition is continuous during interglacials, at variable rates and the variability of dust influx can interfere with soil formation processes to some degree. It should be noted that these factors together should be taken into account when interpreting paleoclimate-paleosol linkages in the CLP.

For paleopedologists, it is always a great challenge to link paleoclimate evolution with paleosol development because paleosols reflect the integrated state of soils (the most recent phase of soils), which does not correspond to the particular paleoclimate in the past. The unequal temporal resolution of paleoclimate evolution and paleosol development hampered paleoclimate-paleosol interpretations. Hence, it is elusive to understand information recorded in the paleosol proxies because they show the time-integrated effects (records) of the entire climate period. Similarly, modeled climate and field observed soil cannot be directly compared because simulated climate data are confined to a defined period, but soil formation is slowly continuing. In addition, soil processes such as leaching, illuviation, bioturbation can change the relative position of soil materials resulting in chronological errors in paleosol profiles and difficulties in synchronization and/or correlation with other data curves from different proxies and mismatch between data-model

comparisons. Furthermore, the comparison between paleoclimatic conditions and paleosol properties can be controversial due to unequal spatial resolution. These difficulties lead to limitations in paleoclimate-paleosol interpretations and research. Thus, it is important to keep in mind that soil analysis does not deliver precise environmental information of the past and limits paleosol-paleoclimate research. Despite all these challenges, various proxies can at least deliver us major environmental variations and their impacts on the paleosol formation. However, one should be careful with the retrieval of information from paleosols.

In conclusion, there is an urgent need for an improved understanding of paleoclimate-paleosol relations in the CLP and the above mentioned limitations can only be achieved by combining process based models capable of simulating the complexity of the soil and climate system. The importance of using process based soil-climate models in (paleo)pedology research is presented in section 1.5.

1.5 Why modeling (paleo)soil evolution is important

Soil exhibits changing features and characteristics through time. Soil that we observe today, is a product of its long-term functioning in a soil forming environment with complex interactions with other systems (e.g. hydrosphere, atmosphere, lithosphere, and biosphere). Dokuchaev (1883) initially perceived and included soil formation in the state factor model (functional-factorial model); later, it was noticeably improved by (Jenny, 1941) in his book *Factors of soil formation*. The model defines soil genesis by,

Soil or Soil property = f (cl,o,r,p,t, ...)

where, cl is climate, o denotes organisms, r stands for relief, p is the parent material, t is time, and the three dots were included to define additional factors that may determine soil formation in a local context, such as dust influx in the Chinese loess region. To date, it is fundamental to the (quantitative) soil formation models and for the use of paleopedological research (Retallack, 1998).

A soil model is a simplified tool representing the complex soil-forming environment (Bethke, 2007). Thus, a soil model consists of simplified equations and mathematical concepts that can describe the impact of five factors of soil formation “CLORPT” (Jenny, 1941) and processes on soil formation to a fair degree.

1.5.1 Soil modeling and paleoclimate-paleosol relations

Soil models are important tools to simulate paleoclimate-paleosol relations because they can integrate soil-forming factors during (paleo)pedogenesis and converge paleoclimate evolution and paleosol development at the same temporal scale. Thus, the simulated paleosol is a direct reflection of simulated paleoclimate. In addition, the application of process-based soil models provides a quantitative expression of the (paleo)soil development for a given interglacial climate and its duration. It has been noted that quantitative expressions of the soil forming processes and evolving soil properties allow a better understanding of the soil system (Stockmann, 2011). Therefore, the application of process-based soil models on buried paleosols is a promising approach in paleopedology research.

1.5.2. Soil modeling and soil-based ecosystem services

Soil is the Earth's supporting system; soil functions support Earth's life through soil based ecosystem services. The relationship between soil and ecosystem services is well defined. Soil has been distinguished as soil natural capital or soil stocks (= soil properties), which are the basis for providing ecosystem goods and services (Daily et al., 1997; Dominati et al., 2010; 2014; Bouma, 2014). Soil processes support soil natural capital either positively (e.g. soil formation) or negatively (e.g. soil degradation), which subsequently affect delivering soil functions (soil ecosystem services).

As far as soil functions are considered, currently, as we live in a world with an increase in population, most of the soil functions are under threat (Montanarella et al., 2016). Soils are degrading worldwide due to human-induced soil erosion processes (Poesen, 2018), that decline soil resources

(Tan et al., 2005) being crucial for ensuring soil ecosystem services. For example, human-induced soil erosion, with rates much higher than natural soil erosion rates, affects soil degradation (Lal, 2001; Montgomery, 2007; Guerra et al., 2017; Poesen, 2018). Therefore, modeling of soil processes is key to quantifying soil ecosystem services, particularly considering soil as a natural capital. The application of soil models to quantify soil ecosystem services has been highlighted in the international soil-modeling consortium (Vereecken et al., 2014). Furthermore, process-based soil models (mechanistic soil models) are valuable tools to quantify the effect of pedogenetic factors on the soil forming processes (Minasny and McBratney, 2006; Godderis et al., 2010; Finke, 2012a). Such models are also necessary for the decision-making process of sustainable use and management of the soil resource (Lin, 2011) and are useful for different application studies, e.g. in archaeological land evaluation (Zwertvaegher et al., 2013), for global change studies (Keyvanshokouhi et al., 2016), and to reconstruct the present soils (Finke, 2012a).

Finally, as the best terrestrial record that equivalents marine sedimentary records, LPS in China are therefore crucial for the investigation of paleoclimate-paleosol relations.

1.6 Research gaps and questions and research objectives

The overall aim of this thesis is to identify and quantify paleoclimate-paleosol relations during interglacials in the past 500 ka. For that, I define the following research gaps, questions and objectives to be addressed.

There have been no attempts made so far to investigate the link between paleoclimate- paleosol with the use of mathematical models, in terms of relative contribution of soil forming factors on paleosol formation in the CLP. In addition, the indirect effects of ice sheets and insolation on climate and their contribution to interglacial soil development is still not well understood. Studies focusing on successive changes from astronomical forcing and ice volume over climate, and finally to soil properties on the CLP are still rare, and the

response of these variations imprinted in paleosols is still unclear. In this study, for the first time, the indirect links between the astronomical parameters, ice volume and soil properties are investigated through soil-climate model simulations. This thesis applies the two process models (SoilGen2-LOVECLIM1.3) for revealing the relation between paleoclimate and forcing factors on buried paleosol development in the CLP. Subsequently, the study extends to analyze soil-based ecosystem services as a function of climate change, as an application study on the paleoclimate-paleosol relations, in the last interglacial.

Regarding the modeling of soil functions that delivers as soil-based ecosystem services, separating human-induced and natural soil erosion impacts on soil ecosystem services is complex, without knowing the natural soil erosion rates that may or may not negatively affect soil functions. In order to separate the human-induced soil erosion, we must focus on soil development under natural soil erosion rates over longer time scales. Simulating the effect of natural soil erosion rates on soil development through process-based models provides the potential to understand soil ecosystem services in a natural environment. For these studies, therefore, applying longer time scales of combined climate and soil data under natural soil erosion rates is essential, as current methods (on an inventory basis) are not always sufficient to provide quantitative interpretations over time. Therefore, we apply soil-climate modeling to simulate the role of natural erosion rates on soil stocks and soil-based ecosystem services, as it offers to evaluate changes (variability) in ecosystem service delivery due to human pressure, relative to changes (variability) inherent to natural systems.

There are three main objectives to be pursued:

1. Calibrate the SoilGen2 soil formation model for studying paleosols in the CLP (**Chapter 3**)

- a. What soil processes must be calibrated in the SoilGen2 model to properly represent soil development in the loess plateau? And how well can soil properties be calibrated with process parameters?
- b. How can dust addition rates in the CLP affect soil processes and soil properties?

2. Simulate paleosol evolution in response to interglacial climate, vegetation and dust addition and to understand the link between precession and NH ice volume and paleosol in the CLP over the past 500 ka (**Chapter 4**)

- a. What are the dominant drivers of paleosol formation during interglacials?
- b. How do paleosols in the CLP respond to precession variability and NH ice volume forcings affecting interglacial climate?

3. Evaluate climate-paleosol relations towards sustainable soil functioning (**Chapter 5**)

- a. How do natural soil erosion rates influence long-term soil property changes and ecosystem services?
- b. What insights can be gathered from soil-climate modeling for Soil Loss Tolerance (SLT) estimation?

1.7 Structure of this thesis

This thesis has three research chapters (3, 4 and 5) covering the three main research objectives mentioned above. The research chapters have been published (Chapters 3 and 4) as peer-reviewed articles in international journals, and Chapter 5 is submitted. **Figure 1-7** gives the chapter overview. Supporting information for each chapter can be found in the Appendix.

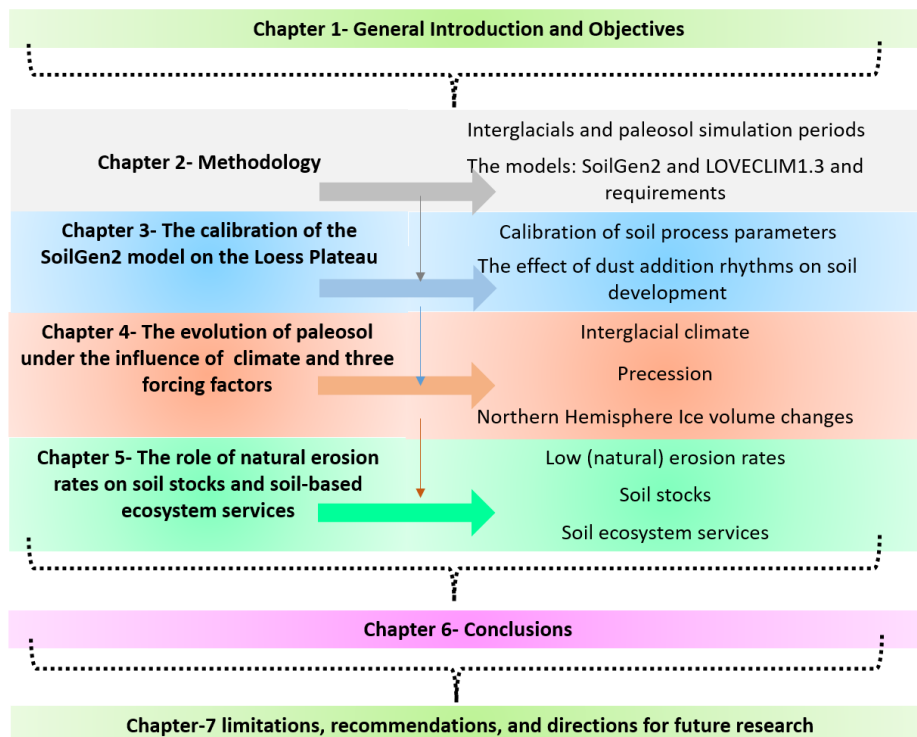


Figure 1-7 Chapter overview of thesis

Author contribution

This chapter was designed and written by KN Ranathunga. Peter Finke and Qiuzhen Yin had a significant contribution through commenting, reviewing and giving suggestions for improving this chapter.

**CHAPTER 2. Methodology: interglacial paleosol
simulation setup, and the SoilGen2,
LOVECLIM1.3 models**

2.1 Interglacial simulation periods used in the study

We focused on the interglacial periods from MIS 1 to MIS 13 to simulate paleosol development using SoilGen2. As mentioned in chapter 1, numerous studies have demonstrated a close correlation of the proxy variations within the Chinese loess sequences with the marine oxygen isotope records which are considered as a proxy of global continental ice volume. The paleosol layers in the loess were correlated to interglacial stages as defined in the marine oxygen isotope and loess layers to glacial stages.

The studied interglacials cover the major part of the odd MIS and the paleosol duration in the Chinese loess. There are few studies on the paleosol duration in the loess, as illustrated by (Sun et al., 2006b) (**Table 2-1**). The age of the paleosols corresponds in general to the odd MIS stages, but the start year and end year of paleosols could vary slightly between proxies and depends also on which marine $\delta^{18}\text{O}$ stack is used to compare with the loess proxies. Given this fact and also given the dating uncertainties in both the marine $\delta^{18}\text{O}$ and loess records, in this study, the definition of simulation periods for interglacial paleosols is also based on precession (Berger and Loutre, 1991). It means that the start year of the interglacial simulation is taken at the mid-point between a precession minimum and a precession maximum at the beginnings of the odd MIS stage and start year of the paleosol layers (the lower boundary of a paleosol layer). The purpose is to avoid an extreme precession condition for the start of the interglacial, which is usually considered the mid-point between a minimum and a maximum $\delta^{18}\text{O}$. The end year of the interglacial simulation is taken at the end of the odd MIS stages, which corresponds generally to the end year of paleosols development (the upper boundary of a paleosol layer) (**Table 2-1**). Based on these criteria, the simulation periods used in the thesis are given in **Table 2-2**. The estimated ages of different paleosols units in the CLP (**Table 2-1**) are different due to several reasons, which can be attributed to (1) selection of the insolation curves as tuning targets, (2) selection of the time controls and construction of an initial timescale, (3) orbital tuning by adjusting the age of each time control, (4) fine adjustment of the age of each data point by employing different methods and

(5) the use of different proxy indices (e.g., magnetic susceptibility, grain size ratio and bulk grain size) in establishing the timescales (Lu et al., 1999; Heslop et al., 2000; Ding et al., 2002). Therefore, indeed, the “differences” between different studies could be due to uncertainty on the age or time scales development based on orbital tuning.

The studies mentioned in the **Table 2-1** used different monsoon proxies which are sensitive to spatial differences across the region and can provide valuable insights into the East Asian summer and winter monsoons over glacial-interglacial timescales across the CLP (in the central and northwestern CLP) (Ding et al., 2002; Heslop et al., 2000). Therefore, our simulation periods (**Table 2-2**) correspond more or less to the paleosol boundary ages estimated in different studies in the CLP (Lu et al., 1999; Heslop et al., 2000; Ding et al., 2002; Sun et al., 2006a; 2006b).

In addition, we assumed soil formation period of 17 ka for the Holocene, because Zwertvaegher et al. (2013) showed that soil could develop before the typical Holocene epoch (the past ~12ka BP) in Europe. Even though Holocene soil formation periods in the CLP are not consistent with Europe, our simulation periods are slightly longer than the Holocene, and they are 17-0 ka for the Holocene. It was done solely to include the less intensive soil formation periods during SoilGen2 simulations. Our choice will not affect the degree of soil development because, if the climate is cold or dry, leaching will not occur and no decarbonatization, clay migration will be simulated either.

We simulated six paleosol units during past six interglacials, the corresponding MIS stages and paleosol units are illustrated in **Figure 2-1**.

Table 2-1 Thickness and estimated Ages (ka) of paleosol units in the CLP (Sun et al., 2006b). Note that although all those age models are generated by orbital tuning method, different proxy indicators and tuning targets are employed in the chronological construction. Detailed descriptions of those age models are given in Sun et al. (2006b), Lu et al. (1999), Heslop et al. (2000), Ding et al. (2002) and Sun et al. (2006a).

Paleosol unit	Depth (m)	Age	Age	Age	Age	Age
Locations	Jingyuan	Jingyuan	Luochuan	Baoji	Jingchuan, Lingtai, Puxian, Baoji, Pingling	Lingtai and Zhaojiachuan
S0 top	0	0			0	0
S0 base	1.7	11			11	11
S1 top	37.5	73	71	79	73	72
S1 base	45.6	129	129	129	128	128
S2 top	66.6	189	188	196	190	190
S2 base	76.7	244	254	250	245	245
S3 top	89.4	280	279	290	307	279
S3 base	96.5	335	334	342	336	336
S4 top	116.5	396	385	386	360	394
S4 base	119.9	424	428	417	412	426
S5SS1 top	139.6	473	471	503	479	473
S5SS1 base	142.4	506		556	531	506
S5SS2 top	147.8	567		568	549	558
S5SS3 base	153.1	624	576	625	622	622
S6 top	173.5	682	658	693	684	682
S6 base	175.5	710	670	713	710	712
Reference study	Sun et al. (2006b)	Sun et al. (2006b)	Lu et al. (1999)	Heslop et al. (2000)	Ding et al. (2002)	Sun et al. (2006a)

Proxy Indicator	magnetic susceptibility, mean grain size	magnetic susceptibility	magnetic susceptibility, mean grain size	Median grain size	magnetic susceptibility, mean grain size
Target curve	summer insolation at 65°N	Insolation values 65°N	summer insolation at 65°N	Insolation values 65°N	summer insolation at 65°N
Reference of target curve	Laskar (1990)	Berger and Loutre (1991)	Laskar (1990)	Berger and Loutre (1991)	Laskar (1990)

Table 2-2 Interglacial simulation duration used for paleosol simulations in the study.

Interglacial	Start (ka BP)	End (ka BP)	Duration (ka)
MIS1	17	0	17
MIS5	133	75	58
MIS7	247	192	55
MIS9	340	282	58
MIS11	424	382	42
MIS13	538	471	67

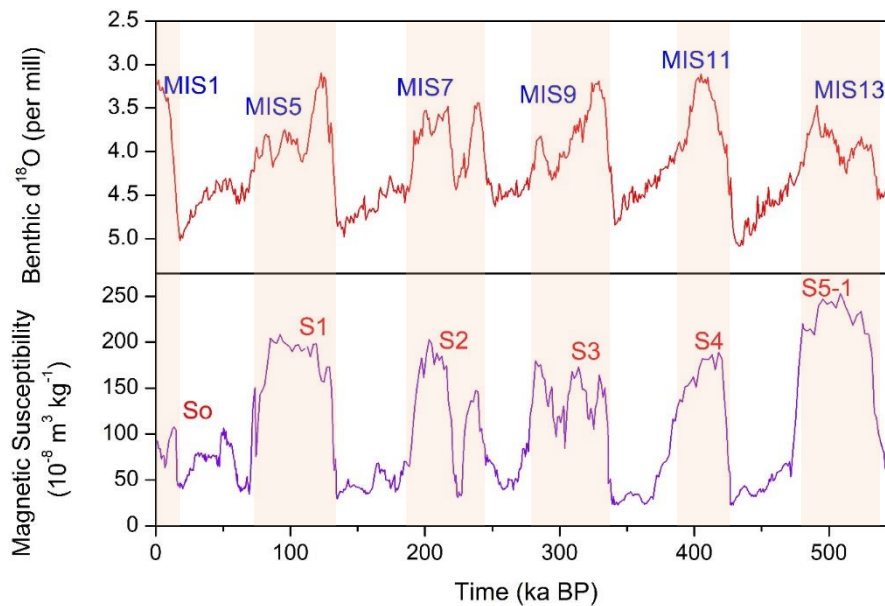


Figure 2-1 The interglacial oxygen Marine Isotope Stages and corresponding paleosols in the CLP. Upper panel shows the records of Benthic $\delta^{18}\text{O}$ stack variation (Lisiecki and Raymo, 2005), lower panel shows magnetic susceptibility from the Chinese loess (Guo et al., 2009) over the last 500,000 years.

2.2 Research design

In this study, the LOVECLIM1.3 and SoilGen2 models are used in combination for simulating interglacial climate and paleosol, respectively. However, the output (climate and vegetation data) of the climate model needs to be processed to be compatible with the SoilGen2 soil formation model. Furthermore, SoilGen2 must obtain input data for paleosol simulations from various sources. A detailed description of models and models requirements (e.g. bias correction and downscaling of climate output) are presented in the following sections. **Figure 2-2** gives an overview of the research design.

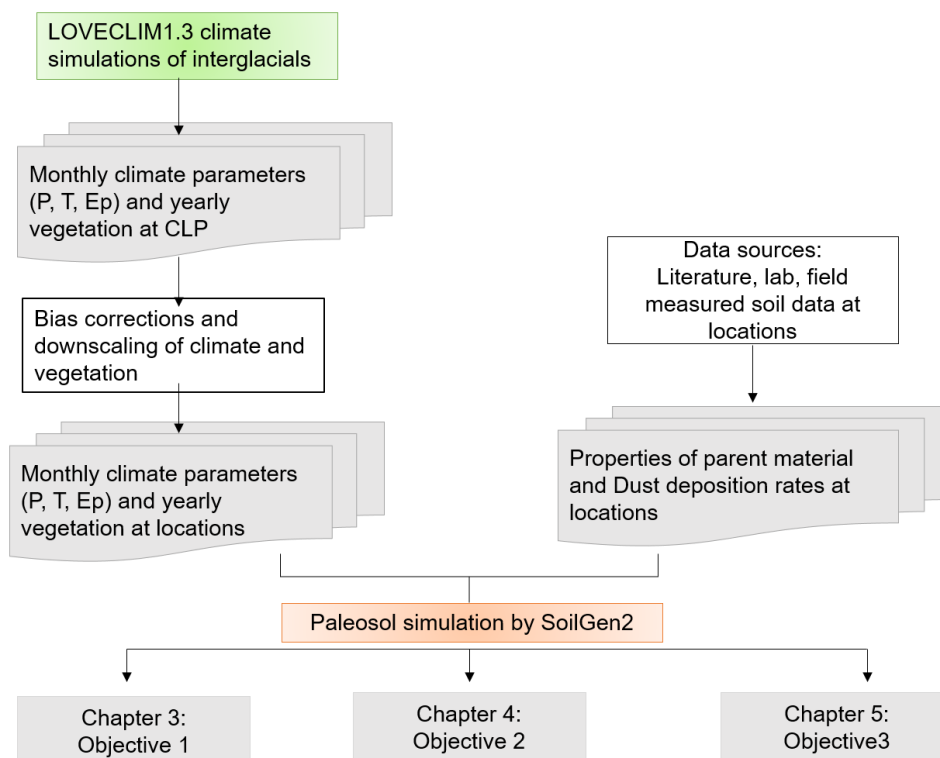


Figure 2-2 Summary of the research strategy used in the study.

2.3 The SoilGen2 model

The SoilGen2 model (Finke and Hutson, 2008; Finke, 2012a) is a one-dimensional (soil profile scale) model that can simulate vertical changes in soil properties over millennia as result of pedogenetic processes driven by external forcings such as climate, vegetation and events like dust deposition. Below, we summarize its main functionalities.

The model simulates transport of water, heat and solutes by solving partial differential equations with finite differencing methods using the scheme of the LEACHC-model (Hutson and Wagenet, 1992). Uptake of cations Ca, Mg, K, Na and Al by plants, decomposition of organic matter, fertilization, atmospheric deposition, erosion or sedimentation and precipitation, dissolution and adsorption of chemicals provide source and sink terms to these equations. Additionally, diffusive transport of CO₂ and vertical mass

transport caused by bioturbation and plowing are simulated. The soil development processes simulated by SoilGen2 include (de-)calcification and (de-)gypsification, physical weathering, chemical weathering of seventeen minerals, clay migration and the soil organic carbon (SOC) -cycle. Clay migration is simulated considering three main mechanisms: (i) splash detachment at the soil surface by raindrop impact, (ii) clay dispersion or flocculation in any soil compartment due to low or high ionic strength of rain or soil water, and (iii) filtering. Filtering is the sink term for transport models and estimates how much clay stays in certain point in a time due to roughness of surface areas, due to friction (Finke et al., 2015).

SoilGen2 simulates the five soil organic carbon pools of the RothC 26.3 (Coleman and Jenkinson, 2014) model for each soil compartment. Decomposable plant material (DPM), resistant plant material (RPM), humified organic matter (HUM) and microbial biomass (BIO) degrade according a first-order process with specific decay rate constants modified by temperature and soil moisture. Decayed BIO and HUM partially recombine to mimic a food web. Inert organic matter (IOM) refers to an inactive (non-decaying) soil carbon pool. Soil organic carbon cycling parameters are vegetation related. SoilGen2 distinguishes four vegetation types: grass/shrubland, deciduous and coniferous forest and agriculture. Each vegetation type has a maximal rooting depth, ion uptake forcing function, and parameters related to Soil organic carbon cycling (e.g. decomposition rates and the partitioning of plant litter to above and below ground).

The (1-D) model handles geomorphic processes such as erosion and deposition as events at the upper boundary by removing and adding soil layers. Agricultural practices are characterized by input fertilization, planting and harvesting dates and tillage. A simulated soil profile is discretized by multiple layers of equal thickness (e.g. 5 cm). The model simulation time steps vary with the simulated processes: for water and solute flow: seconds to hours, physical weathering and heat flow: every hour, SOC cycling and weathering: every day and bioturbation, erosion, and deposition: every year (**Figure 2-3**). Thus, soil properties are generated by dynamic interactions

between soil solid (mineral and organic matter), liquid and air phases. For detailed model description, reference is made to Finke and Hutson (2008), Finke (2012a), Finke et al. (2015), Opolot et al. (2015) and Finke (2020).

The model has been tested for the above mentioned soil processes in several case studies, including the CLP. Here we elaborate on these tests and their conclusions.

1. SOC cycling process in the SoilGen2 model was calibrated for both Belgian and Chinese loess soils (Yu et al., 2013). Results showed that the decomposition rates k_{HUM} of humus and k_{RPM} , of resistant plant material, and the fraction of litter that is ectorganic, fr_{ecto} , (leaf litter; (Kononova, 1975), were the most sensitive parameters. In addition, their calibration results were comparable to those obtained in previous studies. These results confirmed that the SoilGen2 carbon module can be applied to paleosols formed in the loess parent material.

2. The model has also been applied and tested for soil development in southern Norwegian soils (Sauer et al., 2012). These authors compared simulated soil properties with measured data from twelve soil profiles composing two soil chronosequences. Results showed that SoilGen2 simulated clay content and particle size distribution well, but underestimated soil properties such as CEC, organic carbon, base saturation and pH.

3. The clay migration module in the SoilGen2 model has been calibrated in French loess soils, by adapting six parameters (Finke et al., 2015). The calibrated model has been tested on a total of eighteen soil profiles, including both forest and agricultural soils. The results indicated that the $h-\theta_{macro}$ (the pressure head at which macropores empty) and the filter coefficient (n), were the most sensitive parameters.

4. A modeling study shows that SoilGen2 simulated soil properties are sensitive to reconstructed boundary and initial conditions (Keyvanshokouhi et al., 2016) and these authors have documented SoilGen2 as a soil development model suitable for global change studies. Several authors have

concluded on this point (Minasny et al., 2015; Kuzyakov and Zamanian, 2019). Moreover, Opolot et al. (2015) provide an extensive review of the SoilGen2 governing processes (**Figure 2-4**), integrating case studies mentioned. Therefore, the existing SoilGen2 model provides a fair opportunity for modeling soils and paleosols.

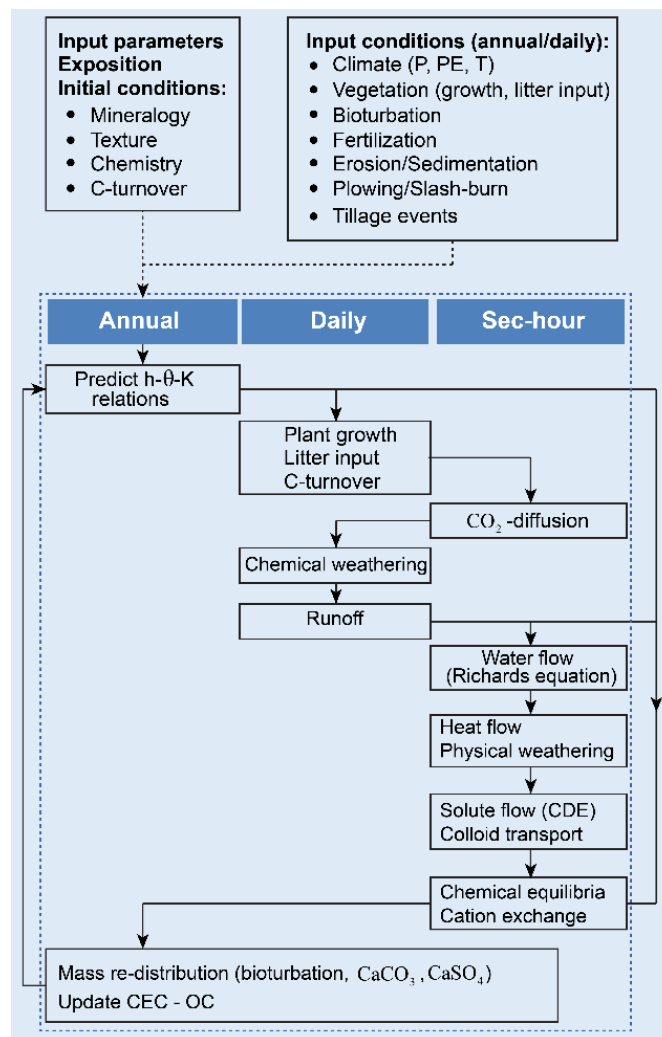


Figure 2-3 Soil process sequence in the SoilGen2 model indicating input data at the upper boundary. Copied and adapted from Minasny et al. (2015). P, PE and T stand for precipitation, potential evapotranspiration, temperature, respectively and CDE and CEC denote Convection Dispersion Equation and Cation Exchange Capacity accordingly. h- θ -K denotes the relations between hydraulic head, water content and hydraulic conductivity.

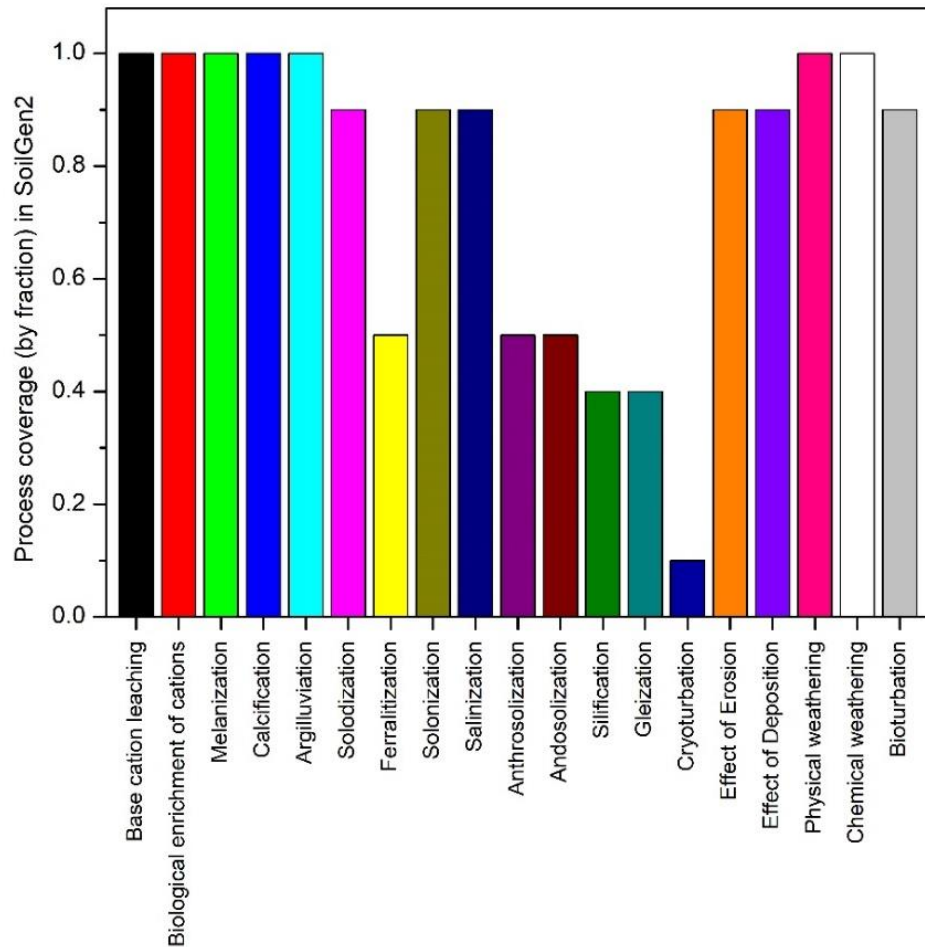


Figure 2-4 A summary of soil process coverage of SoilGen2. SoilGen2 simulates soil forming processes (key processes as defined in Bockheim and Gennadiyev, 2000), and includes effects of erosion, deposition, weathering and bioturbation (the right-most five) (x-axis). The process coverage is presented in y-axis (1.0=full process coverage and <1.0=processes that are partially introduced).

2.4 The LOVECLIM1.3 model

LOVECLIM1.3, “a three-dimensional Earth system model of intermediate complexity”, was used to provide climate simulations that are needed by the soil model. It takes into account the interactions between the atmosphere (ECBilt), the ocean and sea ice (CLIO), and the terrestrial biosphere (VECODE). ECBilt is a quasi-geostrophic atmospheric model with a horizontal

resolution of 5.6°x 5.6°. VECODE is a vegetation model that simulates the dynamics of three main terrestrial plant types, forest, grassland and desert (Goosse et al., 2010). The CLIO (3°x 3°) component is made up of an ocean general circulation model coupled to a comprehensive thermodynamic-dynamic sea-ice model. LOVECLIM has been used in many studies for past and future climate. It has been used to simulate the EASM during MIS 13 (Yin et al., 2009). Although LOVECLIM is a model of intermediate complexity, its results on the EASM response to orbital forcing and ice sheets have been previously confirmed by another more complex general circulation model HadCM3 (atmosphere-ocean general circulation model) (Muri et al., 2013). It has also been used to simulate the climate of the last nine interglacials over the last 800 ka (Yin and Berger, 2012; 2015) and to study the interglacial climate in China in response to changes of insolation, Greenhouse gases concentrations (GHG) and ice sheets (Yin et al., 2008; 2009).

Transient simulations² were performed for MIS 1, MIS 5, MIS 7, MIS 9, MIS 11 and MIS 13 interglacials for the durations as mentioned in section 2.1. First, the paleoclimates for all these interglacials were simulated without the influence of NH ice sheets (ORBHG) and second, paleoclimates for MIS 11 and MIS 13 were simulated with the influence of ice sheets (ORBHGIce).

2.5 Bias correction and downscaling the climate model outputs to the soil model input scale

The LOVECLIM1.3 outputs including monthly mean temperature (T), monthly total precipitation (P) and potential evapotranspiration (Ep) and areal fractions of vegetations in the LOVECLIM-grid cell are used as input for SoilGen2.

The simulated monthly climate data are corrected for bias by using the simulated and observed climates during 1971-2000. For correction of temperature, the difference between the simulated and observed climates is used, whereas the ratio between them is used for the correction for P and Ep. Bias-corrected climate data (monthly averages or sums) represent the whole Loess Plateau due to the spatial resolution of LOVECLIM1.3 (5.6° * 5.6°) and

² In transient simulation, climate forcing is varying in time like in reality.

still need correction for obtaining local values for individual sites. This is illustrated in **Figure 2-5**. Within the selected monthly temporal scale, we downscaled the monthly values by using today's detailed maps (spatial resolution 0.05°) based on observations of the annual mean temperature (Liao, 2007), annual mean precipitation (Hu, 2007) and aridity (Ep/P) (Feng et al., 2004a). The downscaling (Bierkens et al., 2000) used either a difference (temperature) or ratio (precipitation and potential evapotranspiration) for correction. During downscaling, we assumed that current spatial distribution in climatic conditions (P, Ep, T and aridity) across the Loess Plateau remained valid for the older interglacials, that was supported by the spatial differences of paleosol development during older interglacials (e.g. MIS 11), as mentioned in the introduction and by Hao and Guo (2005).

The annual mean precipitation (amp) for a given site is obtained by applying the downscaling rule as follows: (Hu, 2007):

$$\frac{amp_{i,t}}{AMP_{sim,CLP,t}} = \frac{amp_{i,obs,T}}{AMP_{obs,CLP,T}} \quad \text{Eq. [2-1]}$$

where, $amp_{i,t}$ is annual mean precipitation at location i and in year t (that is what we required), $amp_{i,obs,T}$ is annual mean precipitation at location i for today (Hu, 2007). $AMP_{sim,CLP,T}$ stands for the LOVECLIM1.3 simulated annual mean precipitation, after bias correction, for the whole CLP in year t and $AMP_{obs,CLP,T}$ is the annual mean average precipitation for whole CLP (today) from the map by Hu (2007). The same rule was applied for downscaling monthly precipitation and monthly potential evapotranspiration.

The annual mean temperature (amt) for a given site is obtained by applying the downscaling rule as follows (Liao, 2007):

$$amt_{i,t} - AMT_{sim,CLP,t} = amt_{i,obs,T} - AMT_{obs,CLP,T} \quad \text{Eq. [2-2]}$$

Where, $amt_{i,t}$ is annual mean temperature at location i and in year t (that is what we required), $amt_{i,obs,T}$ is annual mean temperature at location i for today (Liao, 2007). $AMT_{sim,CLP,t}$ stands for the LOVECLIM1.3 simulated annual mean temperature, after bias correction, for the whole CLP in year t and $AMT_{obs,CLP,T}$ is the annual mean average temperature for whole CLP (today) from the map by Liao (2007).

$obs_{CLP, T}$ is the annual mean average temperature for whole CLP (today) from the map by Liao (2007). The same rule was applied for downscaling monthly temperature.

LOVECLIM1.3 simulates time series of vegetation types for the entire CLP as areal % of grass, forest and desert. First, the LOVECLIM1.3 simulated vegetation fractions are corrected using bias-corrected temperature and precipitation before downscaling to the location of interest. The actual vegetation type per year (for SoilGen) in each site was obtained by downscaling using the aridity map (Feng et al., 2004a). For this, the area fractions are downscaled to local vegetation types (e.g. grasses, shrubs, deciduous forest) by assuming a relation between the aridity (the ratio between E_p and P , E_p/P) and the vegetation type.

For every simulation location, first, the number of gridcells (in the aridity map by Feng et al., 2004a) which have a higher aridity than an aridity of a location are counted. The resulting percentage, $X\%$ is the percentage of grid cells that have a higher aridity because many gridcells in the map are dryer, with higher aridity. For example, if $X=95\%$, 95% of the sites are more arid and thus only 5% is more moist, it is then a moist site and likely the vegetation is forest. The X is compared to the LOVECLIM1.3 simulated vegetation coverage fractions for the whole plateau for every year a percentage of desert (D), grass (G) and forest (F) as follows:

- If $X \leq D$ then vegetation is equal to desert for that year t and location i
- Else: If $X \leq (D+G)$ then vegetation is grassscrub for that year t and location i
- Else: If $X \leq (D+G+F)$ (the rest, since $D+G+F=100\%$) then vegetation is deciduous forest for that year t and location i

Figure 2-6, shows the Schematic representation of spatial downscaling of LOVECLIM1.3 output (climate and vegetation) as described above. Moreover, appendix for chapter 2 provides the latitude and longitude for all the studied paleosol sections.

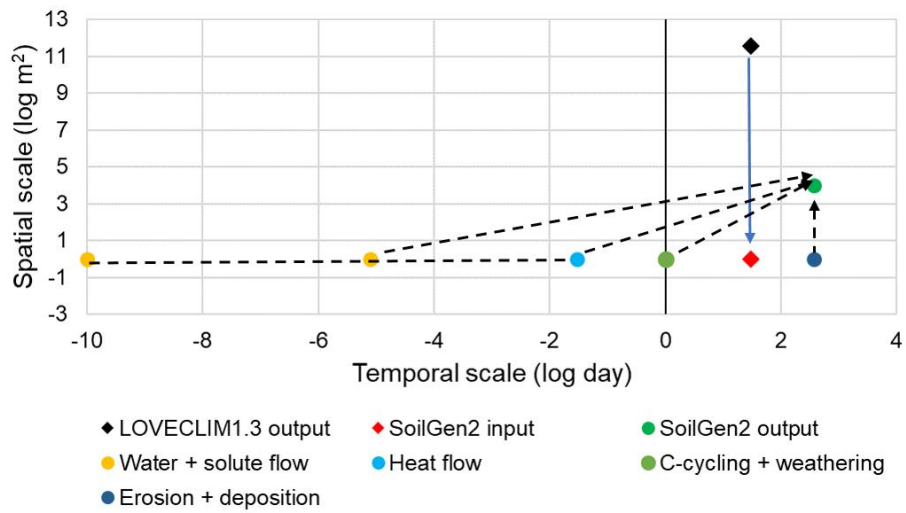


Figure 2-5 Spatial downscaling of LOVECLIM1.3 output to the soil model input scale (monthly) (blue solid arrow); temporal scale of SoilGen2 processes at spatial scale (1*1 m²) and output (100 m²*100 m²=1 ha) at yearly scale (black dash arrows) (after Finke et al., 2021b).

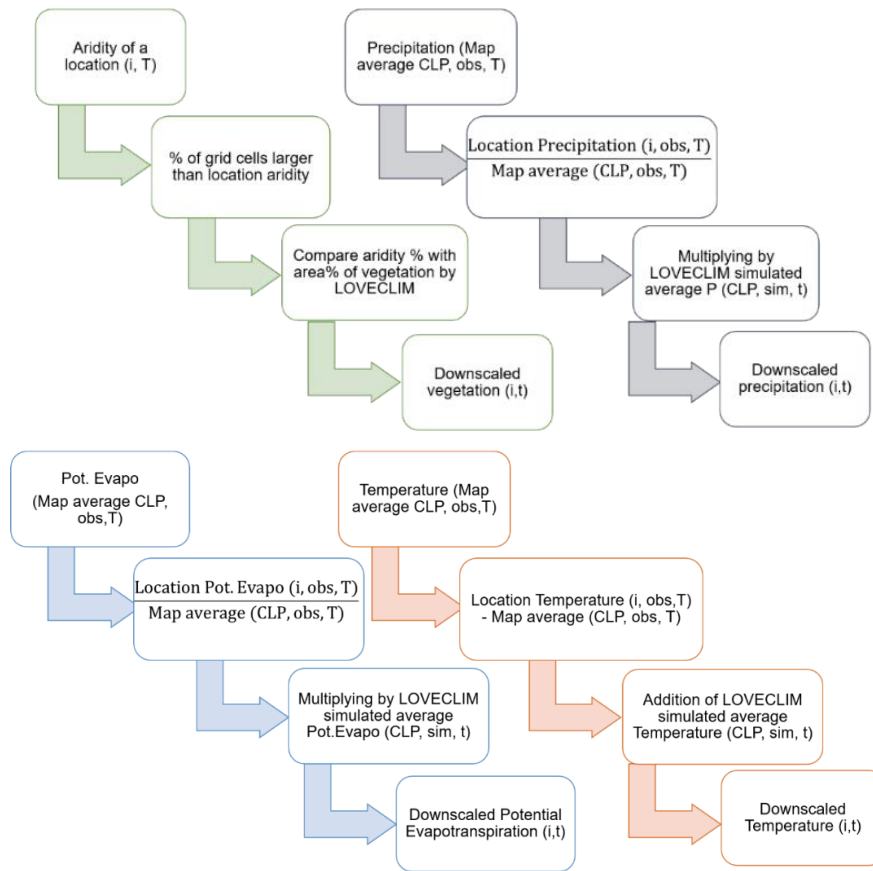


Figure 2-6 Schematic representation of spatial downscaling of LOVECLIM1.3 output (climate and vegetation).

Author contribution

This chapter was designed and written by KN Ranathunga. Peter Finke and Qiuzhen Yin had a significant contribution through commenting, reviewing and giving suggestions for improving this chapter.

CHAPTER 3. Calibrating SoilGen2 for interglacial soil evolution in the Chinese Loess Plateau considering soil parameters and the effect of dust addition rhythm

This chapter has been modified from published manuscript: Ranathunga, K. N., Finke, P. A., Yin, Q., & Yu, Y. (2022). Calibrating SoilGen2 for interglacial soil evolution in the Chinese Loess Plateau considering soil parameters and the effect of dust addition rhythm. Quaternary International, 607, 100-112. doi.org/10.1016/j.quaint.2021.08.019.

Abstract

To better understand interglacial paleosol development by quantifying the paleosol development processes on the Chinese Loess Plateau (CLP), we need a soil genesis model calibrated for long timescales. Here, we calibrate a process-based soil genesis model, SoilGen2, by confronting simulated and measured soil properties for the Holocene and MIS-13 paleosols formed in the CLP for various parameter settings. The calibration was made sequentially on three major soil process formulations, including decarbonatization, clay migration and soil organic carbon cycling, which are represented by various process parameters. The order of the tuned parameters was based on sensitivity analyses performed previously on the loess in Western Europe and the CLP. After the calibration of the intrinsic soil process parameters, the effect of uncertainty of dust deposition rate on calibration results was assessed. Our results show that the simulated soil properties are very sensitive to ten reconstructed dust deposition scenarios, reflecting the propagation of uncertainty of dust deposition in model simulations. Our results also show the equal importance of calibrating soil process parameters and defining correct external forcings in the future use of soil models. Our calibrated model allows interglacial soil simulation in the CLP over long timescales.

Keywords: SoilGen2 calibration; Soil parameters; Uncertainty; Dust deposition

3.1 Introduction

The Quaternary loess-paleosol sequences on the Chinese Loess Plateau (CLP) are remarkable terrestrial archives for understanding the interglacial paleosol formation over the past 2.6 million years (Ma). Despite numerous paleosol-paleoclimate studies, research focusing on quantifying interglacial pedogenic processes in the CLP is rare (Finke et al., 2021b). Quantitative expressions of the soil-forming processes and evolving soil properties allow a better understanding of the development of the soil (Stockmann, 2011). To explore and quantify paleosol-forming processes in the CLP, we need a soil development model calibrated for long time scales on the interglacial paleosols. Such model must consider changes in soil forming factors (Jenny, 1941) by using them as external forcing to modulate soil development processes, leading to simulate soil properties.

Process-based soil development models are useful tools to reconstruct or predict soil characteristics in the past and future over long-term spans. During soil development, texture, mineralogy, organic matter content and chemical properties change at different periods, such as annual, decadal, centennial and millennial. Therefore, if a model simulates for multi-millennium periods, soil properties such as soil texture, soil organic carbon content and associated soil characteristics like the relations between h (hydraulic head), Θ (volumetric water content) and K (hydraulic conductivity) as well as cation exchange capacity (CEC) cannot be regarded as constants. Therefore, soil processes such as clay production by physical weathering, clay migration and the organic carbon cycle must be dynamically simulated. Here, we use the SoilGen2 model (Finke, 2012a), as it is one of the few and most complete soil profile development models (Minasny et al., 2015).

To maximize the reliability of the model output, the model should be calibrated by adjusting process parameters to obtain an optimal match between measured and simulated soil data. The process parameters to be adjusted should first be identified in a preceding sensitivity analysis. For SoilGen2, sensitivity analyses were done using the Morris' method (Morris, 1991) for clay

migration in European soils (Finke et al., 2015) and for the SOC cycle in both Chinese and European soils (Yu et al., 2013) and decarbonization (Finke and Hutson, 2008). These analyses resulted in a calibration order based on decreasing sensitivities of the involved parameters.

Soil formation is controlled by external forcings (boundary conditions to the model, e.g. climate change, tillage history) and initial conditions (properties of parent materials) (Jenny, 1941), which, however, are often associated with uncertainty in paleosol study. Therefore, it is useful to check the calibrated model with respect to its sensitivity to possible realizations of external forcings. As mentioned in chapter 1, various studies have described the role of dust addition on the pedogenesis in the CLP (Liu, 1985; Kukla and An, 1989; An et al., 1991b; Porter, 2001; Guo et al., 2002; Stevens et al., 2006; Maher, 2016). Pang and Huang (2006) found that soil formation differences between two regions (middle and middle-lower reaches of the Yellow River) are due to continuous dust deposition onto soils. Another study by Li et al. (2019) also revealed the importance of influx of Aeolian input as (added) parent material of soils, which plays a vital role in pedogenesis. These studies proved that continuous dust addition makes soil profiles grow in two directions (upward and downward). Huang et al. (2003) stressed that there is a need to understand dust accumulation and rates in Holocene soil formation in the CLP. Dust addition was maximal during glacial periods, but continued during soil-forming intervals, albeit at a lower rate, and the deposited dust may have been modified by post-depositional processes (e.g. pedogenesis during warm periods), forming accretionary interglacial paleosols (Kemp, 2001; Sun et al., 2010). Kohfeld and Harrison (2003) have stated uncertainty in the dust addition reconstructions during glacial-interglacial cycles. Therefore, it is of relevance that we examine the influence of the uncertainty of dust addition reconstruction on the paleosol development in a modeling context.

Thus, the overarching goal of this study is to calibrate the SoilGen2 model (Finke, 2012a) a soil process-based soil development model, for the interglacial soils formed in the CLP. The specific research objectives of this study are (a) to calibrate three major soil process formulations, sequentially:

decarbonatization, clay migration and soil organic carbon cycling represented by various process parameters, and (b) to investigate the sensitivity of soil development to different dust deposition scenarios.

3.2 Materials and methods

3.2.1 Study locations and periods

Considering the spatial variation of climate on the CLP, three Holocene soil (S0) (the most recent soil profiles) were used for the CaCO₃ and Soil Organic Carbon (SOC) calibration, namely, Xifeng (mean annual precipitation 550 mm, mean annual temperature 8.7 °C), Taoyu in Qing'an county (507.3 mm, 10.4 °C) and Chenjiagou in Qishan county (623.8mm, 12 °C).

Holocene soils are influenced by ongoing and continuous dust addition with high amounts of calcium carbonate, limiting the clay migration in the soil. In general, the semi-arid climate in the area is not favorable for clay transport. In addition, compared with the MIS 13 paleosols, measurements indicate that the two Holocene soil profiles (Tables A3-1, A3-2 in appendix for chapter 3) have no depth variations of the clay fraction (<2µm), and in Xifeng (Table A3-5 in appendix for chapter 3) there are some significant changes of the clay fraction (ranging from 8 to 22 %). As clay migration during S0 is relatively weak, the S5-1 paleosol, formed during MIS 13 about 500,000 years ago, was used for the clay migration calibration as this paleosol shows strong eluviation and pedogenesis (An et al., 1987; Yin and Guo, 2008; Lu et al., 2018). The S5-1 paleosol from five profiles are used: Changwu (578 mm, 9.2 °C), Luochuan (600 mm, 9.2 °C), Weinan (645 mm, 13.6 °C), Chang'an (603 mm, 13.1 °C) and Wugong (650-750 mm, 12-14 °C) (**Figure 3-1**).

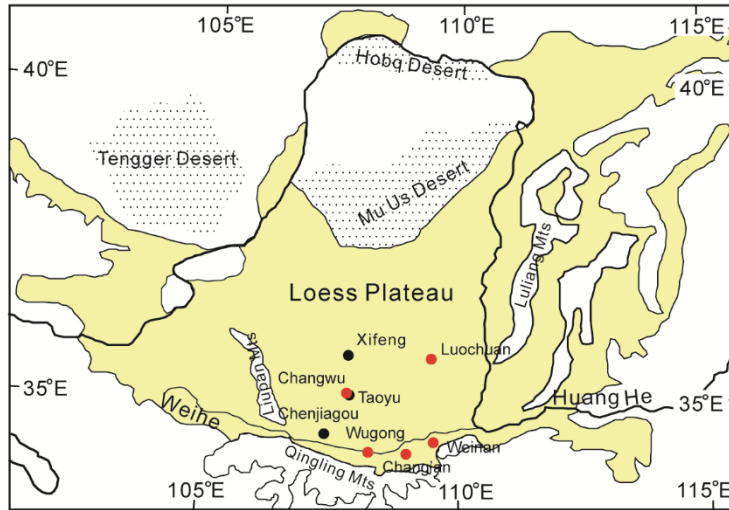


Figure 3-1 The locations of the soil profiles studied: black and red symbols represent the profiles used for S0 and for S5-1, respectively (modified after Hao and Guo (2005). The distribution of loess is indicated in yellow.

3.2.2 The SoilGen2 model input data

In the SoilGen2 model the input data of initial and boundary conditions represent the major soil-forming factors (Climate, Organisms, Relief, Parent material).

Climate is characterized by simulated time series of precipitation, potential evapotranspiration and temperature by the climate model LOVECLIM1.3 for the entire simulation period, which is essential for interglacial paleosol simulations (Yin and Berger, 2015). The climates of the last 17-0 ka and of the MIS-13 (511-481 ka) were simulated by the model LOVECLIM1.3. After bias correction and downscaling (details are provided in chapter 2), the simulated climatic data were used as inputs in the SoilGen2 model, representing the site level climate. The simulated precipitation, potential evapotranspiration and temperature greatly differ between MIS1 and MIS13 (Figure A3-1 in appendix for chapter 3). The most probable vegetation for every year is obtained by

downscaling the vegetation distribution over the CLP that was simulated by LOVECLIM1.3 to the location of interest. Starting date of agriculture for S0 is based on archeological data (Yu et al., 2016). We found agricultural practices (e.g. fertilization and plowing) only in Chenjiagou site. Fertilization was mimicked by applying ion concentrations (mol/m²) for Ca⁺², Mg⁺², Na⁺, K⁺, Cl⁻, SO₄⁻², HCO₃⁻ for the last 64 years during simulations. These ions are added into the soil solution phase, subsequently involves soil chemical equilibria. The plowing depth was 15 cm (soil depth of mixing between soil layers) with 50% of mixing intensity³ per year (default in SoilGen2) in the last 3000 years in the late Holocene. Bioturbation and plant litter input were based on vegetation type and climate. Bioturbation was related to the vegetation type: for the Holocene soils, 14.9 Mg ha⁻¹ yr⁻¹ upper 40 cm for grassland and 15.8 Mg ha⁻¹ yr⁻¹ upper 50 cm for agriculture (with plowing). For S5-1 soils, 8.4 Mg ha⁻¹ yr⁻¹ upper 40 cm depth for deciduous forest and 16.4 Mg ha⁻¹ yr⁻¹ upper 45 cm depth for grassland. These values are based on Gobat et al. (1998). Root depths were set to 100 cm for forests and 80 cm for grass shrub (50 cm in S5-1 soils) and 60 cm for agriculture. The depth of bioturbation is related to vegetation types and varies with vegetation per location. For each vegetation type (e.g. deciduous forest, grassland), the bioturbation depths are same in between sites. A relation between mean annual temperature and precipitation (Lieth, 1975) calculated the annual plant biomass input in SoilGen2.

For the three Holocene sites, dust deposition speeds were based on Magnetic Susceptibility (MS) data and Optically-Stimulated Luminescence (OSL) dating in Weinan loess section (Kang et al., 2013). MS in the dated section (Weinan) and the three sites were compared to set age control points. The deposition rate between any two age control points was calculated according to the depth and age while assuming 0 ka BP age at the top of the section. For S5-1 soils,

³ Mixing intensity is defined as the fraction of mass mixed vertically every 5 cm soil layer, over an (input) soil depth, e.g. the rooted depth. After this mixing, the same fraction of the mixed materials mixed horizontally (per layer) with the remaining mass fraction that is not vertically mixed in that soil layer. This results in a new amount of material in each soil layer including the effect of bioturbation. Each simulation year, the profile sum of bioturbation over depth is expressed as mass (Ton /ha. year).

the rhythm of dust addition in each location was based on Xifeng and Changwu loess sections (Guo et al., 2009) while applying site-specific dust deposition data (Lu and Sun, 2000).

For relief we assume a plateau position. The properties of the loess deposited in the preceding glacial period serve as initial conditions at the start of simulations, while the properties of the loess deposited during the interglacial are defined by those of the overlying loess. We assume that those loess properties (e.g. mineralogical and texture) remain the same for both under and -over lying loess. A detailed description of these inputs is presented in the appendix for chapter 3. The model was run by setting loss or increase of calcite and gypsum influence on all textural fractions (sand, silt, clay proportionally) because of the less-leaching environment. We assumed free drainage condition at lower boundary of soil.

3.2.3 Model calibration and parameters

3.2.3.1 Calibration layout

We aim to obtain one set of calibrated parameters that are suitable for interglacial paleosol simulations in the loess plateau. As already mentioned, the calibration of soil process parameters was done partly for Holocene soils (simulation period from 17ka to 0ka) and partly for the S5-1 paleosol (simulation period from 511 ka to 481 ka). The calibration was done per group of process parameters in a predefined order. The order of the tuned parameters was based on published sensitivity analyses and feedback mechanisms in the soil. For instance, since clay migration hardly occurs in calcareous soils, it is necessary to calibrate (de-)calcification first and thereafter clay migration. Lastly, SOC cycling parameters were calibrated, because changes in clay content and soil water content, soil temperature affect the organic matter decomposition rates. Therefore, these three main soil process formulations were calibrated representing various process parameters (**Table 3-1**) (see sections 3.2.3.2, 3.2.3.3 and 3.2.3.4).

The optimal value for a parameter was selected using the dissimilarity (Gower, 1971):

$$DIS_{Profile} = \frac{1}{K} \sum_{k=1}^K abs (X_{r,k} - X_{s,k}) \quad \text{Eq. [3-1]}$$

where X represents the soil property of interest, k is the number of soil compartments (55 in the present study); s refers to the value for the simulation and r for the reference (measurement). The measurements are in the Tables A3-1, A3-2, A3-3, A3-8, A3-9 in appendix for chapter 3. Figures A3-3 to A3-13 shows comparison between the simulated and measured soil profiles in the Holocene (for CaCO₃ and organic carbon content) and in MIS 13 (clay content) at the end of calibration.

Process parameters were calibrated stepwise in the predefined order (Table 3-1) and adjusted separately until the average value for DIS reached a minimum over the locations of interest. During the calibration process, only the calibrating process parameter was changed (in the value range) at a time, while the others (column two in Table 3-1) kept their average (initial) or previously calibrated values. As model runtime for simulations covering the Holocene or MIS13 are long run, advanced calibration methods (e.g. multi parameter analysis) involving many simulations were unfeasible.

3.2.3.2 Decarbonatization

Calcium carbonate (calcite) content is a major soil property, noticeably in the arid and semi-arid CLP, and it is one of the major minerals (10-20%) in the loess when deposited (Liu, 1985). Decarbonatization or, more general, calcite redistribution, is a major soil-forming process in the loess plateau. It influences various soil properties e.g. soil pH, bulk density, porosity, cations in soil solution and determines differences in water storage between loess/paleosol layers due to changes in soil physical properties. In the SoilGen2 model, calcite redistribution is determined by the solubility of calcite and the transport of the solute (leaching). The solubility is defined by the log₁₀k_{so} (calcium carbonate dissolution constant). Depending on the Ca⁺² and CO⁻²₃ ion concentration, pH in the soil solution, soil temperature, the dissolution constant varies over time, and the reference value (at 25 °C) was calibrated by analyzing results at eight equidistant values (**Table 3-1**) at their equilibrium.

To calibrate the degree of leaching in soils, we calibrated the interception evaporation fraction. Only the effective rainfall of the total precipitation reaches the soil, via stem flow and throughfall, and the remaining water in the foliage (e.g. leaves, twigs, small branches) evaporates to the atmosphere during and after rain, as the fraction of net precipitation (Savenije, 2004; Li et al., 2016a). Interception evaporation affects infiltration and thus solute transport into the deeper parts of the soil profile. The amount of intercepted water (vegetation dependent) was varied using seven equidistant values (ranging from 1% to 7%) for both grass/shrubs and agriculture (**Table 3-1**).

3.2.3.3 Clay migration

Clay migration indicates the strength of pedogenesis and is a profile formation process. Clay migration can form a distinct clay-enriched layer over thousands of years (Van Breemen and Burman, 2002). Clay migration was calibrated taking into account (1) splash detachment, (2) determination of the fraction of dispersible clay, (3) transport via macropores, (4) filtering and (5) production of clay by physical weathering. In the CLP, clay migration mainly starts after decarbonatization, when the double layer has lost (calcium) Ca^{+2} ions by leaching (Vidic and Lobnik, 1997). Clay particles ($<2\mu\text{m}$) may accumulate at depth as a consequence of filtering or of flocculation (e.g. on top of a calcic horizon where the Ca^{+2} ions are abundant, Schaetzl and Thompson, (2015). From an ecological point of view, the clay fraction is an important soil property for soil water retention and permeability characteristics in loess and paleosol sections. The parameters related to clay migration were calibrated after decarbonatization.

The clay migration process was calibrated by tuning 4 individual processes (iii, iv, v, and vi in **Table 3-1**). We first calibrate the ectorganic layer thickness (above ground leaf litter), as it reduces splash detachment of clay by limiting raindrops collisions with the mineral topsoil (see Eq. A-1 in appendix for chapter 3). The role of the surface litter layer thickness has long been studied under different vegetation types in the loess plateau of China concerning soil erosion control, runoff and sediment accumulation (Li and Shao, 2006; Geißler

et al., 2012; Zhou et al., 2016). After that, the pressure head (h) at which soil macropores empty was calibrated. This allows to assess during simulation, via h, the amount of clay in contact with soil macropores. This clay, if in dispersed state, can be transported (see Eq. A-2 in appendix for chapter 3).

During clay migration, some of the dispersed clay is filtered due to too low water flow velocities in macropores (Jarvis et al., 1999; DeNovio et al., 2004). The filter coefficient (n) was subjected to calibration (see Eq. A-3 in appendix for chapter 3).

Lastly, two parameters that describe the rate of physical weathering as a function of soil temperature change were calibrated. PS_{max} is the maximal probability that soil particles split by physical weathering, and B is the temperature change ($^{\circ}C\ h^{-1}$) at which the splitting probability becomes maximal. By updating the splitting probability as a function of temperature change, the model produces grains in the clay fraction. PS_{max} and B were calibrated concomitantly (16 pairs of values for B and PS_{max}) (see from Eq. A-4 to Eq.A-7 in appendix for chapter 3). The order of calibration of the clay migration parameters was based on a sensitivity analysis for West European loess soils, in a much moister climate than the CLP-climate (Finke et al., 2015).

3.2.3.4 Decomposition of soil organic matter

SOC influences various soil properties e.g. CEC, pH, porosity, bulk density; these also change during soil development. Variations in soil texture, temperature and moisture alter soil organic matter decomposition rates, which in turn can affect the SOC pools in soils.

Following the RothC 26.3 concepts, the turnover rate (decay rate) of organic matter added to the soil is described as follows; **Eq. [3-2]** depicts the amount of organic carbon (Y) that decomposes from active pools per month. **Eq. [3-2]** exponentially calculates the remainder of soil carbon at the end of each month.

$$Y = Y_0 (1 - e^{-abckt}) \quad \text{Eq. [3-2]}$$

Where, Y_0 is the starting amount of carbon from any active pool, a and b are the rate modifying factors for temperature and soil moisture respectively, c is the modifying factor for soil cover, k stands for decay rate constant for a particular pool, and t converts the annual decomposition rate constants into monthly values ($t=1/12$). Amongst these rate modifying factors, contributions per soil layer to the soil moisture deficit and temperature fluctuations vary over time and soil depth (in each 5 cm) in the model. Soil moisture deficit is, as in RothC, defined as effective precipitation minus potential evapotranspiration, which deficit is distributed over depth using the air-filled porosity (soil water content minus porosity).

We considered those parameters identified as sensitive by Yu et al. (2013), and added the slightly less sensitive partitioning coefficient $CO_2 / (BIO+HUM)$, describing the fate of the lost C from BIO and HUM during decomposition. This partitioning coefficient is a function of soil clay content **[Eq.3-3]**:

$$\frac{CO_2}{(BIO+HUM)} = 1.67 (1.85 + 1.60 e^{-0.0786 * \% Clay}) \quad \text{[Eq.3-3]}$$

Therefore, the order of SOC calibration was k_{HUM} (decomposition rate (yr^{-1}) of humus), fr_{ecto} (ratio of ectorganic/endorganic litter), k_{RPM} (decomposition rate of (yr^{-1}) of resistant plant material) and finally the partitioning coefficient $CO_2 / (BIO+HUM)$ (the ratio of carbon mineralized (CO_2) over that still in the food web (biomass and humus) during decomposition). For fr_{ecto} , only two Holocene sites were calibrated that had no agriculture.

Table 3-1 Calibrated parameters, value range and number of simulations.

Soil forming process	Order	Process parameter with units	Range of values	Simulations per parameter and total
decarbonatization	(i)	Dissolution constant of calcite ($\log_{10} k_{sd}$)	-9.2 to -7.8	8 and 24
	(ii)	Interception evaporation fraction (-) For grass/shrubs/agriculture	0.01-0.07	7 and 21
Clay migration	(iii)	Thickness of the ectorganic layer (mm)	0.5-3.5	7 and 35
	(iv)	Pressure head (hPa) at which macropores empty	-6 to -30	7 and 35
	(v)	Filter coefficient for clay (-)	0.2-0.8	7 and 35
Physical weathering	(vi)	Particle splitting probability (PS)	1.338×10^{-6} - 2.163×10^{-6}	16 and 80
		soil temperature change (B) °C / hour (4x4 combinations)	0.45-1.95	
Soil organic carbon cycling	(vii)	Decomposition rate (yr^{-1}) of humus	0.001-0.035	12 and 36
	(viii)	Ratio of ectorganic/endorganic litter (-)	0.35-0.7	11 and 22
	(ix)	Decomposition rate of (yr^{-1}) of resistant plant material	0.01-0.675	13 and 39
	(x)	Partitioning coefficient CO_2 / (BIO+HUM)	0.3-3.0	9 and 27

3.2.3.5 The uncertainty of dust deposition rhythms on soil development

Changing dust addition speed over time can influence the rates of soil processes. For instance, lower speed allows more time for calcite leaching, whereas higher speed rapidly re-carbonates the soil. Therefore, we explored the uncertainty of dust addition on the calibration results.

Hereto, ten Holocene dust deposition scenarios were applied to determine whether the calibrated results are persistent in this respect. Here, we solely considered the variation of the speed of dust addition over time (rhythm for short) while assuming that the mineralogical composition of the added dust as well as the total amount of added dust remain similar. Dust accumulation rhythms were reconstructed in various case studies (Table A3-10 in appendix

for chapter 3) using depth-age models. However, there were depositional hiatuses in the published dust records due to uncertainty of soil age. We recovered those distorted age points by linear interpolation between the more certain ages in the original series. Albani et al. (2015) reported that this method has uncertainties depending on the used age points. Dust addition was mimicked by adding compartments of 5 cm during soil development. Each year when the added dust thickness reaches a multifold of 5 cm was used to add 1 compartment. In general, the selected dust records exhibit higher dust addition during both the early and/or the late Holocene relative to the middle Holocene (**Figure 3-2**).

We analyzed the effect of ten reconstructed dust deposition scenarios on the simulated soil properties calcite, organic carbon, clay content and CEC. To compare the soil properties, we applied scaled dissimilarity, the ratio between the unscaled dissimilarity (DIS) (see **Eq. [3-1]**), and the difference of maximum and minimum measured value of the corresponding soil property in that particular profile. The scaled dissimilarity is dimensionless, and thus soil variables can be compared. We compared the scaled dissimilarity (DIS_{scaled}) of the best calibration (*cal*) with those of the dust scenarios (*i*), and compared the impact of these dust scenarios to the quality of the calibrations by calculating a standard deviation for each considered soil property:

$$sdDIS_{scaled} = \sqrt{\frac{1}{10} \sum_{i=1}^{10} (DIS_{scaled,i} - DIS_{scaled,cal})^2} \quad \text{Eq. [3-4]}$$

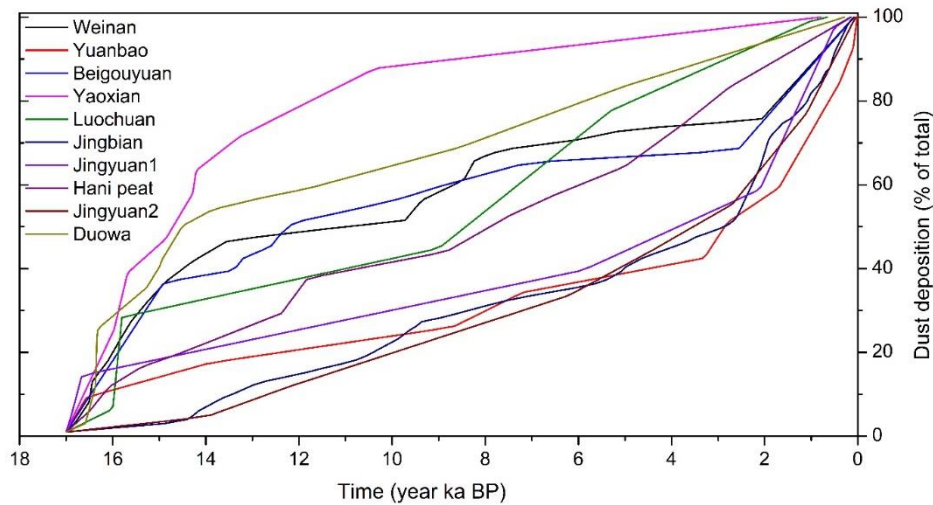


Figure 3-2 Ten dust deposition rhythms applied in SoilGen2 (more information in Table A3-10).

3.3 Results and Discussion

3.3.1 Effect of dissolution constant of calcite and interception evaporation loss on decarbonatization

The best-calibrated $\log_{10}k_{so}$ (lowest averaged dissimilarity) was -9.0 for the studied three profiles (**Figure 3-3A**). This result was in between the previous values for $\log_{10}k_{so}$: -9.2 (Zwertvaegher et al., 2013), -8.46 for Belgium and Hungary loess soils (Finke and Hutson, 2008) and -8.36 for Belgium loess soils (Finke, 2012a), which were typically derived for European loess soils, leaching climate, whereas CLP possesses a semi-arid climate. Laboratory experiments have found $\log_{10}k_{so}$ -8.48 at 25 °C (Jacobson and Langmuir, 1974). The $\log_{10}k_{so}$ of -9.0 indicates a low dissolution rate of calcite. This may be caused by (i) the temperature correction to the solubility constant (different temperature regimes in Europe and the CLP), (ii) the grain sizes of the calcite, and (iii) the lower leaching in the semi-arid CLP (Li et al., 2013; 2018).

The best-calibrated interception loss for grass/shrub and agriculture was 3% (**Figure 3-3B**). We assumed an equal amount of interception loss for all types

of vegetation dominating in the Holocene at the sites of interest: grass, shrubs and agricultural crops. This interception loss was much lower for shrublands than the literature reported (Table A3-11 in appendix for chapter 3). Ochoa-Sánchez et al. (2018) has reported interception values for grasses (in there table 2) from the global literature, where the grass interception loss is between maximum 100% - minimum 5% of the total precipitation. The calibrated interception loss approximately fits at the lower end of the literature findings, and for agricultural crops, it closes to the values reported by Wang et al. (2012) (Table A3-11). The interception loss varied between forest types: we assigned 14% for deciduous and 21% for coniferous. These values corresponded to 175% of the SoilGen2 model default (deciduous=8% and coniferous=12%). Varying these percentages did not affect decarbonatization, (therefore forest interception is not involved in the calibration), since Holocene soils were not covered by forests for long periods at the studied locations whereas grasses, shrubs and crops were the dominating vegetation types (Yu et al., 2016; Sun et al., 2017). The forest interception losses (14% and 21%) are well comparable to Su et al. (2016)'s findings (14.3% for broadleaved forests), and between 14.7%-31.8% (Wei et al., 2005) for major Chinese forests and within the range of 11.1% and 24% (Liu et al., 2003; Zhang et al., 2006a; Wang et al., 2012; Jian et al., 2015; Sheng and Cai, 2019) (Table A3-11 in appendix).

In general, calibrated canopy interception losses were consistent with other authors' findings and statements (e.g. Nisbet, 2005), who stated that forests intercept more than grasslands because grass/shrubs or crops have less canopy than forests. Thus, our results were not unexpected. Moreover, these results agree with values reported for forest canopy interception. This interception can take up an amount of 10-50% of total rainfall (Klaassen et al., 1998; Carlyle-Moses and Gash, 2011), in which coniferous takes 25-50%, and broadleaved occupies 10-35% (Rutter et al., 1975), and it is about 12-25% in semi-arid areas (Hörmann et al., 1996).

The high variation of interception found in literature can be attributed to various factors: Climate (rainfall variability, intensity and duration) as well as vegetation characteristics (species, canopy storage capacity, plant

morphological and biomass-related traits of species: e.g. tree density, leaf area index, leaf shape, canopy structure) (Hörmann et al., 1996; Crockford and Richardson, 2000) are not easily measured. Therefore, we assume that the calibrated interception losses are fair.

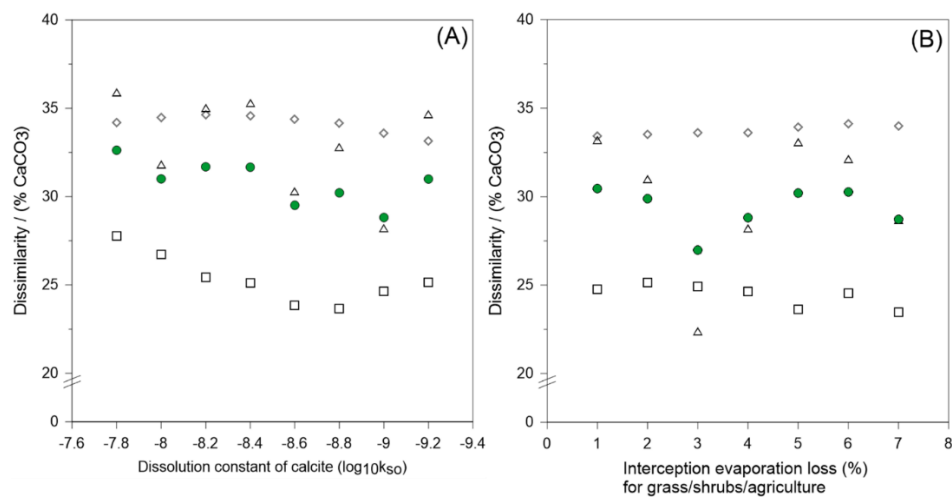


Figure 3-3 Dissimilarity (%) as a function of (A) the calcite dissolution constant ($\log_{10}k_{so}$) and (B) the interception evaporation loss (%) for grass/shrubs/agriculture in three profiles: Xifeng, Chenjiagou, Taoyu are denoted by open triangles, diamonds, squares, respectively. Green dots show profile averages.

3.3.2 Assessment of clay migration related model parameters

Results showed unexpected indifference of clay migration to the pressure head at which macropores empty ($h-\theta_{macro}$) (**Figure 3-4A**). We confirmed this result by evaluation of various additional $h-\theta_{macro}$. The reason for this may be the drier climate in semi-arid China, which causes most macropores to be air-filled and consequently macropore water flow velocity and associated clay transport will be less, which will increase filtering. DeNovio et al. (2004) also emphasized the importance of pore water velocity on clay migration. Until now, the pressure head $h-\theta_{macro}$ had been calibrated for leaching climates in Western Europe, e.g. -1hPa (Finke, 2012a) and -18.3hPa (Finke et al., 2015).

These studies have confirmed that the clay translocation depths of the soils are highly dependent on $h-\theta_{macro}$ and the filter coefficient (n). Thus, we conclude that the amount of precipitation is the critical and limiting climate variable that determines clay migration in arid and semi-arid Chinese loess regions. Therefore, the initial value of $-18hPa$ was kept in the following steps.

The filter coefficient (n) also determines the clay mobility in the soil. The best-calibrated “ n ” was 0.5 at the minimum dissimilarity (**Figure 3-4B**), which was comparable with previous calibrated results: 0.6607 (Finke, 2012a) for loess soils in Belgium, 0.51 (Finke et al., 2015) for loess-derived soil in northern France and 0.7 for silt-clay soils in Sweden (Jarvis et al., 1999).

Regarding physical weathering, optimal-calibrated values were found for PS_{max} at 2.163×10^{-6} and B at $0.95 \text{ }^\circ\text{C} / \text{hour}$ across five soil profiles (**Figure 3-4C**). Finke et al. (2015) found the PS_{max} and B at 1.338×10^{-6} and $1.95 \text{ }^\circ\text{C} / \text{hour}$ respectively in French soils, and Finke (2012a) obtained best-calibrated results at 3×10^{-6} for PS_{max} at $1^\circ \text{C} / \text{hour}$ soil temperature gradient. The calibrated PS_{max} in this study was in between the PS_{max} of these studies and is plausible.

Concerning the ectorganic layer thickness, the best-calibrated value was 0.5 mm (**Figure 3-4D**). We could not refer to literature because no studies refer to this parameter in the context of modeling. Finally, a check showed that the ectorganic layer thickness variations did not change the indifference to the pressure head $h-\theta_{macro}$.

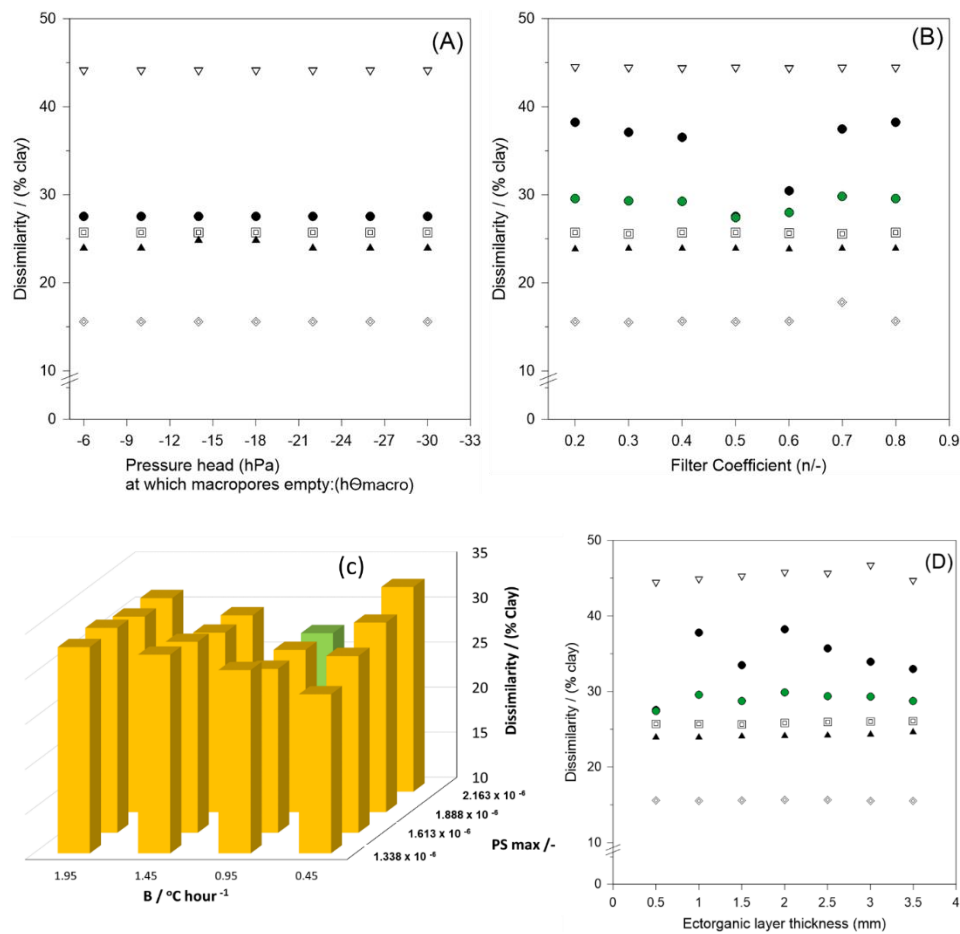


Figure 3-4 Dissimilarity (%) as a function of (A). pressure head $h-\Theta_{macro}$ (hPa), (B). filter coefficient $n(-)$, (C). PSmax-B combinations. Green bar shows the best average for five profiles. (D). ectorganic layer thickness (mm) in five profiles: symbols indicate Luochuan (open diamonds), Chang'an (solid triangles), Changwu (open squares), Wugong (open triangles), Weinan (solid circles). Green dots show profile averages.

3.3.3 Assessment of SOC related model parameters

Concerning SOC cycling parameters, the best-calibrated rate constants (k) were found at: $k_{HUM}=0.0025 \text{ yr}^{-1}$ (**Figure 3-5A**) and $k_{RPM}=0.02 \text{ yr}^{-1}$ (**Figure 3-5B**). The found k_{HUM} and k_{RPM} were lower than the values reported by Todorovic et al. (2010), Stamati et al. (2013), Yu et al. (2013), Finke et al. (2019), and the default RothC rates (**Table 3-2**), whereas k_{HUM} was within the

range reported by Shirato et al. (2004) for Andosols. The low k_{HUM} indicates a longer turnover period, and therefore soil can accumulate more soil organic matter. This is reasonable due to several reasons. In the CLP, the climate (arid to semi-humid) variables may be the most critical; low precipitation may reduce the organic matter decomposition rate. In contrast, it should be noted that the low precipitation could also limit vegetation growth and decrease plant litter supply. The found k_{HUM} may be a reasonable value for calcareous loess soils (Ca^{+2} rich, high pH) that can provide better protection to SOM. Several authors have found that soils rich in calcite can store more organic matter, thereby decreasing turnover rates (e.g. Rasmussen et al., 2018; Rowley et al., 2018). Via the low k_{HUM} , a SOM-protection process is mimicked and we assume that this k_{HUM} is reasonable for the soils of the CLP. Furthermore, silt-rich clayey fine-parent material can also provide better protection to SOM (e.g. Hassink, 1997; Stemmer et al., 2000), and dust deposition can bury fresh organic material, resulting in low SOM turnover rates. The low k_{RPM} suggests a relatively slow decomposition of RPM than that of the default RothC value (**Table 3-2**), which was originally established for agricultural soils.

Table 3-2 Calibrated SOC cycle parameters from other studies and in this study and default values.

Reference	k_{HUM}	k_{RPM}	fr_{ecto}	Vegetation and study area
Stamati et al. (2013)	0.27 0.0041	0.34 0.21		Grassland, Iowa, USA Shrubland, Crete, Greece
Yu et al. (2013)	0.016-0.019 0.0065- 0.0074	0.3 0.27	0.37- 0.43 0.30- 0.38	Forests, China Forests, Belgium
Todorovic et al.(2010)	0.009	0.6(fixed)		Cropland, Austria
Finke et al. (2019) (5 pool)	0.012	0.089		Grassland, California
Finke et al. (2019) (4 pool)	0.008	0.089		Grassland, California
In this study	0.0025	0.02	0.60	Grass/shrubs, forests, China
Default	0.02	0.3	0.58	

The calibrated f_{ecto} in the grass/shrubs litter was 0.60 (**Figure 3-5C**), which was approximately similar to the SoilGen2 model default (0.58) based on measured data by Kononova (1975). The found ratio of ectorganic/endorganic litter (60/40) was similar to the default ratio (58/42) in SoilGen2. The partitioning coefficient $\text{CO}_2 / (\text{BIO}+\text{HUM})$ (**Figure 3-5D**) was higher (2.1) than the RothC default value (1.67). Possible reasons for this are (i) that the actual ratio varied with clay contents different from the ones used to calibrate the RothC26.3 model, and (ii) clay contents in SoilGen2 vary over time.

However, the calibrated organic carbon cycling parameters are conditional to the plant litter inputs; these were based on LOVECLIM1.3 simulated mean annual precipitation and temperature. Neither SoilGen2 nor RothC does determine climate-dependent vegetation growth (biomass production) and organic carbon input into the soil. We assumed root litter distribution according to a root density function, where plant roots depths decrease with soil depths per vegetation type.

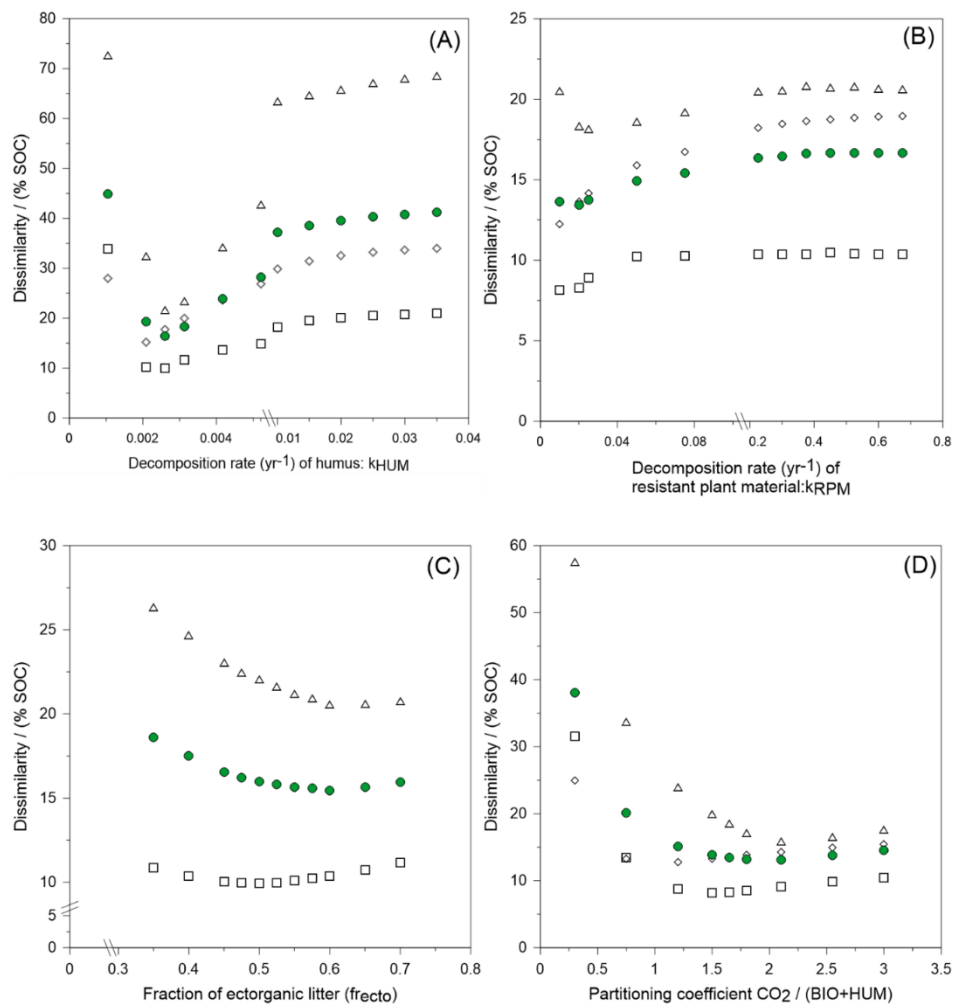


Figure 3-5 Dissimilarity (%) for different values of (A). k_{HUM} , (B). k_{RPM} (C). f_{recto} in two profiles (D). the partitioning coefficient $CO_2 / (BIO+HUM)$, in three profiles: Xifeng, Chenjiagou, Taoyu are denoted by triangles, diamonds, squares, respectively. Green dots show profile averages.

3.3.4 Effect of dust deposition scenarios on the quality of the calibration result

Certainly, due to longer time scales of paleosol formation, soil-forming boundary conditions can be heavily affected by uncertainty. Little is known about the degree of uncertainty with respect to the calibrated soil profiles. If

such boundary conditions are proven to be influential, this means that besides calibrating internal soil process parameters to simulate paleosol development, the uncertainty of model boundary conditions should also be considered. However, calibrating boundary conditions is unusual; it requires substantial computational effort as perturbations of time series of model boundary conditions must be evaluated (Minasny et al., 2015). The impact of ten reconstructed dust scenarios on the quality of the calibrations are shown in **Table 3-3** which gives the scaled dissimilarity results on a % scale.

Table 3-3 Impact of ten dust deposition rhythms on the quality of calibrations, expressed by standard deviations relative to the (scaled) dissimilarity of the calibration (Eq. 3-4).

Soil profiles	Soil variables			
	SOC	CEC	Calcite	Clay
Taoyu	0.71%	0.01%	61.63%	3.99%
Xifeng	22.09%	0.40%	116.43%	0.18%
Chenjiagou	2.75%	0.08%	42.70%	1.87%
Average	8.52%	0.16%	73.59%	2.01%

As shown in **Table 3-3**, the quality of simulated calcite contents responds strongly to the dust deposition scenarios, with an average standard deviation greater than 50%. It was to be expected that the highest uncertainty was obtained for calcite as the profile distribution of calcite is closely related to the input at the surface via dust and the interplay with subsequent leaching processes. In decreasing order of sensitivity to dust deposition rhythm, soil properties were ranked calcite> soil organic carbon>clay content>CEC. The CEC showed the smallest uncertainty, and clay content was also small because of lower clay migration in the Holocene soils.

Unexpectedly, the uncertainty of CEC is minute (**Table 3-3**), however in the present study, the simulated CEC was largely overestimated in the top soils while usually underestimated in the subsoils (see **Figure A3-2** in appendix for chapter 3). This may have been caused by combined (in) accuracies of simulated SOC and clay content during simulations, as a relation between SOC and clay content is used to calculate the CEC in the SoilGen2 model.

Thus, errors of SOC and clay content propagate into the CEC. Therefore, the (in) accuracy of simulated CEC can be affected partly by the dust deposition distribution over time and partly by inaccuracy of the assumed relation (Foth and Ellis (1996: p.57) between SOC, clay and CEC.

Figures 3-6, 3-7, 3-8 and 3-9 show the scaled dissimilarity variations compared to the final calibration results in each dust addition scenario for the above soil properties. Note that vertical axis-scales are different. In general, the comparison between the dust scenarios to the final calibrated results revealed that the calcite, organic carbon and CEC fluctuations were larger in Xifeng than in the other two sites (**Figures 3-6, 3-7 and 3-9**); these are located south of Xifeng. An opposite trend was observed for simulated clay content (**Figure 3-8**), where the fluctuations were relatively small in Xifeng. Note that clay content distribution was calibrated for MIS 13 because clay migration in the Holocene is minor. Fluctuations in simulation quality must therefore entirely be attributed to the sediment properties. Our findings suggest that the impact of uncertain dust input rhythms varies between sites. The impact is larger for faster soil development processes (calcite redistribution, SOC-accumulation) and less for slower processes such as clay migration. Moreover, it is important to note that the uncertainty caused by variants of dust addition is larger than that of the calibrations (**e.g. Figures 3-6 and 3-7**). It is worth mentioning that uncertainty of dust deposition rates can exist due to lack of dating of these Holocene soils and in paleosols. It has been emphasized that the different quantities of dust addition can contribute to uncertainty during formation of paleosols in the CLP (Meijer et al., 2020). However, it is impossible to assess the uncertainty of dust addition rates in the MIS13 paleosols in the present study since we only have two available geologic dust addition rhythms (Guo et al., 2009). In summary, the dust deposition scenarios strongly affected the quality of the calibration. Thus, accuracy of dust scenarios should be considered during interglacial paleosol simulations.

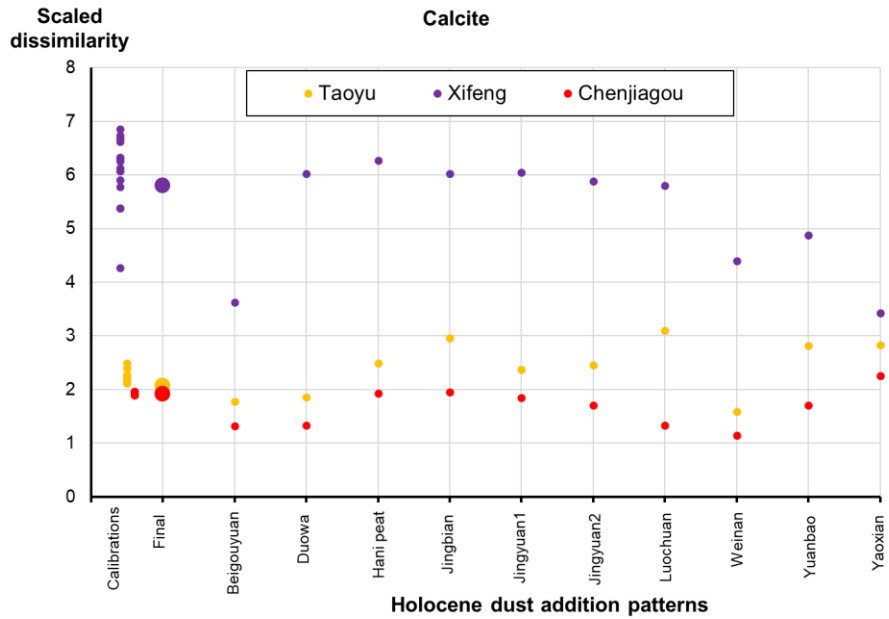


Figure 3-6 Scaled dissimilarity (ranges from 1.2-6.8) between dust scenarios (rightmost) and calibrated three Holocene sites (fat dots) and during calibrations (leftmost) for calcite content.

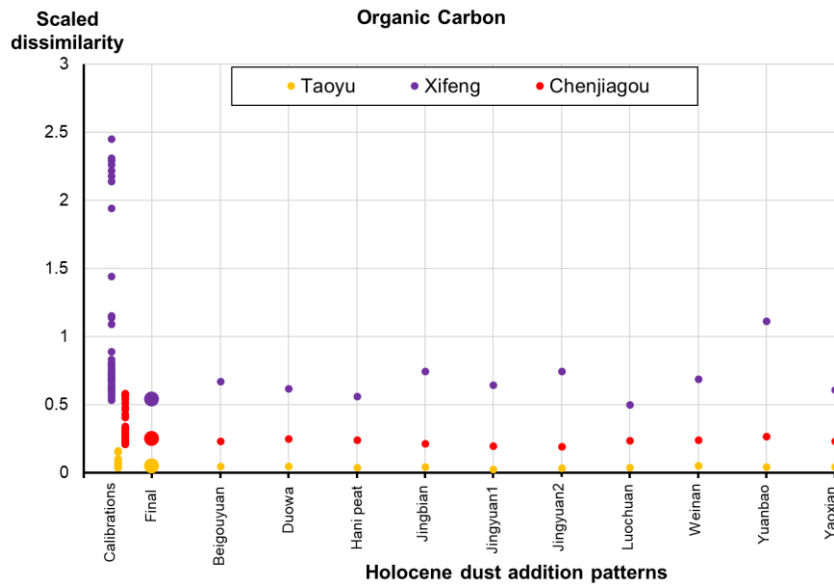


Figure 3-7 Scaled dissimilarity (ranges from 0.027-2.45) between dust scenarios (rightmost) and calibrated three Holocene sites (fat dots) and during calibrations (leftmost) for organic carbon.

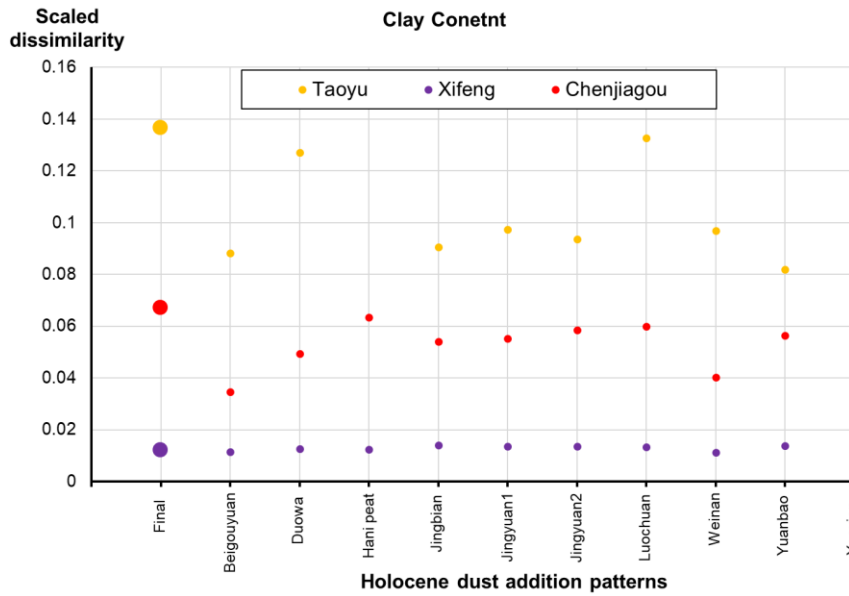


Figure 3-8 Scaled dissimilarity (ranges from 0.01-0.14) between dust scenarios (rightmost) and three Holocene sites (fat dots) for simulated clay content.

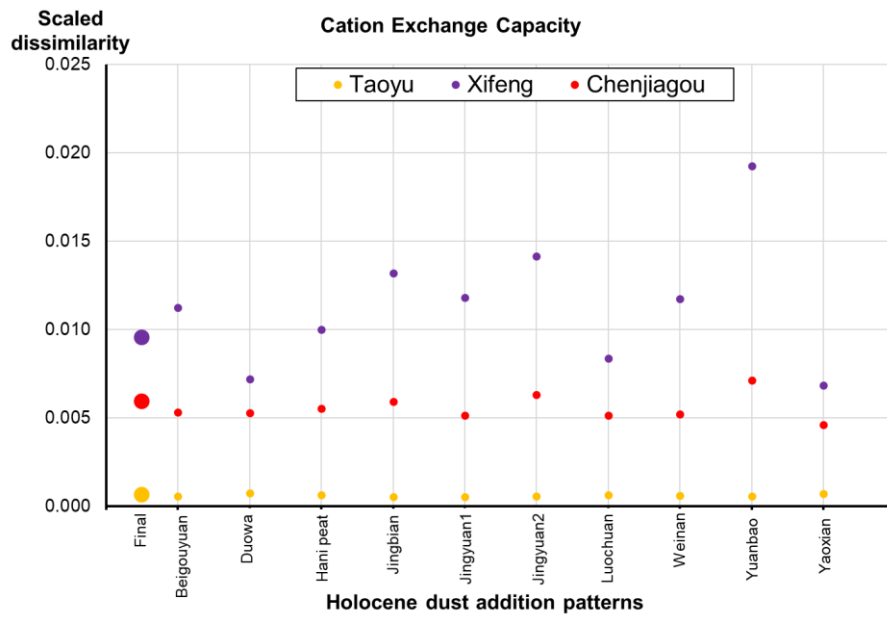


Figure 3-9 Scaled dissimilarity (ranges from 0.0005-0.019) between dust scenarios (rightmost) and calibrated three Holocene sites (fat dots) for simulated CEC.

3.4 Conclusions

The most sensitive soil-forming process parameters were calibrated in the SoilGen2 model for the CLP. An optimal value per parameter was found by confronting measurements to simulations and calculating the dissimilarity between both.

Our results show that: $\log_{10}k_{so}=-9.0$, the interception evaporation for grass/scrubs/agriculture= 3%, the filter coefficient (-) = 0.5, PS_{max} and $B=2.163 \times 10^{-6}$ and $0.95 \text{ } ^\circ\text{C} / \text{hour}$, respectively, the ectorganic layer thickness =0.5 mm, the decay rates: $k_{HUM}=0.0025 \text{ yr}^{-1}$, $k_{RPM}=0.02 \text{ yr}^{-1}$ and fraction of litter that is ectorganic=0.60 and partitioning coefficient $\text{CO}_2 / (\text{BIO}+\text{HUM})=2.1$. These values fall inside previously found ranges. As an exception, the pressure head ($h-\theta_{macro}$) at which macropores empty did not respond to the calibration, which was attributed to the semi-arid climate. This leads to the conclusion that sensitivity analyses done in one climate may not be fully applicable to another climate.

Our results also show that SoilGen2-simulated/calibrated soil properties were highly sensitive to alternative Holocene dust deposition rhythms. The sensitivity varied in the following order: Calcite>soil organic carbon>clay content>CEC by 73.59%, 8.52%, 2.01% and 0.16% respectively. The study shows that dust addition is an influential soil formation process in the CLP. Therefore, both the amount and rhythm of the dust deposition are important variables for quantifying paleosol development with process-based soil models in future studies.

Our results show that on the millennial time scale, uncertain model input and boundary conditions propagate through the model. As a result, even after calibrations, soil models are not free from these uncertainties. The uncertainty of process-based soil models with large run-time, like SoilGen2, would benefit from considering the accuracy of input data. In conclusion, our study emphasizes the equal importance of calibrating soil process parameters and defining correct external forcings in the future use of soil models.

Author contributions

The first author (KN. Ranathunga) performed the research by implementing the experimental setup, integrating data, visualizing and interpreting the results and writing the paper. Peter Finke had a significant contribution through conceptualizing the experiment, providing the software, reviewing and supervising the research. Qiuzhen Yin had a significant contribution through providing modeled climate data for soil simulations, funding, reviewing and supervising the research. Yanyan Yu contributed greatly to the paper through providing all the initial data for soil simulations and reviewing of this paper.

**CHAPTER 4. Driving factors of interglacial
paleosol formation on the Chinese Loess Plateau
and the effect of precession and ice sheets**

This chapter has been compiled from submitted manuscript in March 2022: “Ranathunga, K. N., Finke, P. A., Yin, Q., & Wu, Z. (2022). Driving factors of interglacial paleosol formation on the Chinese Loess Plateau and the effect of precession and ice sheets” to the journal of Quaternary Science Reviews.

Abstract

The loess-paleosol sequences in the Chinese Loess Plateau (CLP) are an important terrestrial paleoclimate record. However, quantitative understanding of the response of paleosol development to various climate and environmental factors remains poor. Based on simulations with combined soil-climate models (SoilGen2-LOVECLIM1.3), this study investigates the sensitivity of paleosol development to different factors as well as the influence of NH ice sheets and astronomical forcing during the interglacials of the past 500ka. Sensitivity analyses show that precipitation, dust addition and potential evapotranspiration are the dominant factors controlling the interglacial paleosol formation, but their relative importance varies between interglacials and for different soil properties such as calcite and clay contents. Our results show that the simulated S1, S2, S3, S5-1 paleosols, which correspond to MIS 5, 7, 9 and 13 respectively, exhibit strong but indirect relationship with precession through its control on precipitation, whereas the precession signal is weak in the simulated S4 paleosol, in line with the weak precession variation during MIS 11. The results also show variable length of lags between different soil properties and precession and also in different interglacials. The lag between the simulated calcite and precession is shorter than that of clay. Moreover, clay content also shows strong relation with temperature during MIS 5 and MIS 13. Large NH ice sheets in the early and late phases of the interglacials have substantial impact on both temperature and precipitation in the CLP and thus on carbonate leaching and clay migration. Therefore, the simulated paleosols result mainly from the joint effect of precession and NH ice sheets, and they show qualitative agreement with observations.

Key words: Interglacials, soil-climate modeling, Chinese Loess Plateau, paleosol formation, precession, NH ice sheets

4.1 Introduction

Soil formation is influenced by various environmental factors (e.g. dust input, climatic conditions and associated vegetation) usually coined the factors of soil formation (Jenny, 1941): climate, organisms, relief, parent material, and time. Ultimately, a (paleo-)soil is the integrated result of the variety of complex interactions between lithosphere, biosphere, hydrosphere, and atmosphere by soil-forming processes modulated by these environmental factors. Each interglacial period is characterized by climatic conditions regulated by external forcings. As concluded in chapter 3, dust deposition rates and composition exert a major control on paleosol characteristics and formation. In addition, the degree of pedogenesis is reported to be largely determined by the time (duration) of soil development (Sheldon and Tabor, 2009).

Due to complicated interactions of soil forming factors, it remains challenging to quantitatively estimate the relative contributions of paleoclimate factors, in terms of precipitation, temperature, potential evapotranspiration, vegetation and dust addition on paleosol development and this leads to uncertain interpretations. Interpretations are often weak because pedogenesis may have overwritten soil properties during later periods, so that the observed soil properties comprise the integral effect of varying paleoclimate factors over time. Therefore, it is not always feasible to differentiate and evaluate the influence of these factors by doing just analysis of bulk paleosol properties. In addition, the significance of the soil forming factors on paleosol formation is controversial (Kemp, 2001), and our understanding of these factors is still insufficient. This motivates us to quantitatively assess the relative contributions of precipitation, temperature, potential evapotranspiration, vegetation and dust addition on paleosol development. In order to evaluate which factor plays a key role, soil-climate process modeling is an interesting and valuable tool, and it shows how soil properties (as a result of pedogenesis) vary for a given paleoclimatic condition during an interglacial (soil forming interval). Therefore, modeling studies are helpful to quantitatively disentangle paleoclimatic factors responsible for paleosol development. A preliminary investigation of the past soil development in the CLP has been performed by

Finke et al. (2017) using model simulations, and they concluded that the number of months with precipitation surplus is the most important factor of soil development in the CLP. Here we make an in-depth analysis of paleoclimate change and soil development of the interglacials in the past 500 ka. We propose a sensitivity analysis, using the SoilGen2-LOVECLIM1.3 soil-climate process models to simulate the paleosol development in the CLP as a function of varying paleoclimatic factors to quantitatively assess the relative contributions of these factors on paleosol development.

As far as climate is concerned, the glacial-interglacial climatic variations on the CLP have been found to be closely linked with the variation of insolation which is determined by the Earth's orbital parameters (Berger and Loutre, 1991), and also with ice volume change at high latitudes. These have been the two dominant forcings on the Earth climate throughout the Quaternary, and their influence on the East Asian Summer Monsoon (EASM) is substantial (Ding et al., 1994; Yin et al., 2008; 2009; Sun et al., 2015; Lyu et al., 2021; Meng et al., 2021). Many proxy indexes in the LPS have recorded the major periodicities of the three astronomical parameters (precession, obliquity and eccentricity) and of the global ice volume changes, indicating the dominant influences of these factors on the climate and therefore on the paleosol formation in the CLP (Ding et al., 1994; Wu et al., 2001; Hao et al., 2012; Sun et al., 2015; Cheng et al., 2021). Due to their large size, ice sheets play an important role during glacial periods. Climate simulations show that, despite the smaller size, during interglacials, ice sheets also play a non-negligible role on the EASM (Yin et al., 2008; 2009; Shi et al., 2020). However, it is still not clear to which extent the ice sheet-induced climate change has affected the interglacial paleosol development. Moreover, although model simulations show a dominant effect of precession on the EASM and on the summer precipitation in northern China (Yin et al., 2008; 2009; Shi et al., 2020; Lyu et al., 2021), many proxy studies show a weak precession cycle in the LPS (Feng et al., 2004b; Sun et al., 2006b; 2015; 2019; 2021; Peterse et al., 2014; Thomas et al., 2016; Ma et al., 2017). Therefore, Precession signals are expected to leave strong footprints on proxy records of palaeoclimatic

variations in the CLP. Middle and Late Pleistocene loess-paleosols in the western CLP show high-resolution precessional footprints (suggesting potential precession dominated monsoon variations since Middle Pleistocene, compared to the central CLP (Sun et al., 2021). Unlike paleosols, loess layers such as L1, L2, L4, L5, and L6 show relatively clear precessional footprints (Sun et al., 2006a; 2006b; Hao et al., 2012). Glacials and interglacials show different climate statuses. In contrast to glacials, interglacials are influenced by variable climatic factors, deposition and soil formation processes (e.g. temperature, monsoon circulation, dust addition rates). Therefore, unsteady dust deposition and pedogenic processes during the interglacials may explain that the loess has a higher resolution of precession footprints than the paleosols, thereby masking the precession footprints (Lu et al., 2004). The relatively weak precession signal has been ascribed to uncertainties and complexities of proxy records and differences in pedogenesis and sedimentation rates in the CLP (Sun et al., 2021). Therefore, the question of whether or not the interglacial paleosols record precession signals at EASM variations remains to be investigated.

Therefore, it is hard to identify the relative role of precession and NH ice sheets on the paleosol formation by using only proxy analyses of the LPS, and process-based climate-soil models must be used. Therefore, the objectives of this study are (a) to find the most influential climate variables for interglacial paleosol development in the CLP, (b) to explore the impact of precession variation and the impact of NH ice sheets over climate and finally to paleosol development. For the first objective, the extent of NH ice sheets is fixed to the present-day configuration, and for the second objective, ice sheet changes in the Northern Hemisphere (NH) are included the climate simulations.

4.2 Material and methods

4.2.1 Locations and studied interglacials

From Northwest to Southeast, three sites with different climate are selected (**Figure 4-1**): Jiuzhoutai, Xifeng and Chang'an. Chang'an (mean annual temperature 13°C, mean annual precipitation 600-700 mm) is located about 5

km southeast of Xi'an City in the southern part of the loess plateau. Xifeng, (8.7 °C, 550 mm) is located in the central CLP. The Jiuzhoutai (10°C, 310 mm) loess section is located in Lanzhou city in the northwest of the CLP.

In our study, five paleosol units of the mid-late Pleistocene are studied, and these are S1, S2, S3, S4 and S5-1. The corresponding simulation periods and MIS are 133-75 ka BP (MIS 5), 247-192 ka BP (MIS 7), 340-282 ka BP (MIS 9), 424-382 ka BP (MIS 11) and 538-471 ka BP (MIS 13). **Figure 4-1** shows the major paleosol sections simulated in the study.

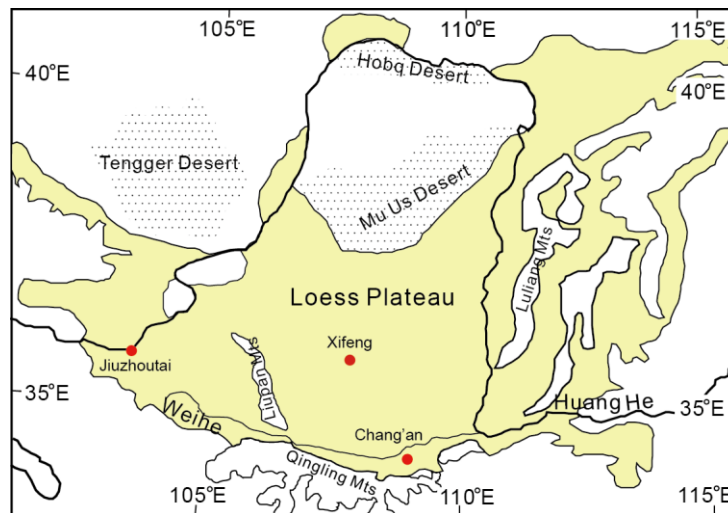


Figure 4-1 Map showing the Chinese Loess Plateau (yellow), locations of Jiuzhoutai, Xifeng, Chang'an loess sections in this study (solid red points) (Modified from Hao and Guo, 2005).

4.2.2 Climate simulations

Quantitative climate fields during the interglacials are obtained from interglacial climate simulations with the LOVECLIM1.3 model. Some results have been presented in Yin et al. (2021) and detailed model and experiment design can be found there. In our study, two sets of transient simulations are performed for each interglacial. In LOVECLIM1.3, the first set are driven by changes in insolation and Greenhouse gases concentrations, CO₂ concentration was between ~180 ppmv and ~300 ppmv, (OrbGHG

experiments), and in the second set of simulations, ice sheets changes in the NH (Ganopolski and Calov, 2011) are additionally considered (OrbGHGIce experiments).

4.2.3 The SoilGen2 model and Input data

In chapter 4, the calibrated SoilGen2 model (in chapter 3) was used to simulate paleosols during interglacials MIS5, MIS 7, MIS 9, MIS 11 and MIS13. SoilGen2 simultaneously simulates soil chemical, physical and biological processes at the pedon scale, contains quantitative expressions of the soil-forming processes and simulates evolving soil properties. Therefore, paleosol-paleoclimate responses can be quantified.

For each interglacial, the mineralogy of the loess and the added dust properties are specified. In addition, properties of added dust during one interglacial was set as initial loess properties for later interglacial paleosol. In our study, especially the dust composition (e.g. mineral, texture) in under and –overlying loess layers are averages of nearby loess layers (L) or nearby loess sections due to lack of dust composition for every loess layer beyond the L1 layer. In this study, to reconstruct the past dust deposition rhythms for paleosols (Chang'an and Xifeng) in the CLP, we have used two dust deposition rhythms published by Guo et al. (2009) and for Jiuzhoutai by (Chen et al., 2014). Moreover, as we applied a 1-D model, dust accumulation is an external input and is mimicked by adding soil layers (5 cm) at the top of the soil profile in a defined year. During simulations, hydrological conditions at the lower boundary was set as always free drainage and the model was run by setting loss or increase of calcite and gypsum influence on sand, silt, clay proportionally. For paleosol simulations, initial soil data were gathered from (un)published literature and/or from experts (loess data for above and below the paleosols are shown in Tables A4-5 to A4-8 in appendix for chapter 4).

4.2.4 Research layout

4.2.4.1 Sensitivity analysis to identify most influential climate variable for interglacial paleosol development

In order to investigate the relative contributions of precipitation (P), temperature (T), potential evapotranspiration (Ep), vegetation, and dust addition on paleosol development, a sensitivity experiment was done during the two interglacials MIS 11 and MIS 13 which have quite contrasting climate forcings (Wu et al., 2020). The experimental design is described below.

We perform five sensitivity experiments at each interglacial; in each experiment, one parameter is allowed to change at a time (e.g. precipitation, temperature, potential evapotranspiration, vegetation, dust accumulation), and others are kept constant (as in reference). Thus, we isolate the impact of the changes in the climatic factors and vegetation and dust deposition. The reference simulation is performed with the last 100-year average climatology of the Holocene simulation mimicking the Pre-Industrial climate. The reference simulation includes a constant dust deposition rhythm, which adds 10 cm over 210 years based on Kang et al. (2018). In our analysis, the soil simulation carried out with all the boundary conditions for a particular interglacial is defined as the joint simulation (hereafter JS), which shows the combined effect of all soil forming factors for that interglacial. An experiment that closely reproduces the soil properties of the JS indicates the most influencing variable for paleosol development. In other words, a close similarity between the JS and a particular sensitivity experiment suggests the most influencing parameter for that interglacial paleosol development.

Additional simulations were run for both the MIS 13 and MIS 11 interglacials by combining variables (e.g. P + Ep) to understand their combined influence. The Mean Absolute Error (MAE) was calculated between the joint simulation (JS, combined effect) and each of the experiments (Ex) separately (**Eq.4-1**) by comparing the soil property values for 5 cm depth intervals. Additionally, we calculate “gain” in MAE (%), which expresses the contributions (%) of each

variable or combination of variables relative to the MAE between the JS and the reference experiment (ref) (Eq.4-2).

$$MAE(JS - Ex) = \frac{1}{K} \sum_{k=1}^K abs(X_{j,k} - X_{s,k}) \quad \text{Eq. [4-1]}$$

$$Gain\ in\ MAE = \left(1 - \frac{MAE(JS-Ex)}{MAE(JS-ref)}\right) * 100 \quad \text{Eq. [4-2]}$$

where X represents the soil property of interest, k is the number of soil compartments; j refers to the value for the joint simulation and s to each experiment. The evaluated soil properties are: calcium carbonate mass and clay mass in each soil compartment. The process parameters related to decarbonatization and clay migration were calibrated in chapter 3 and these processes describe important aspects of soil development. Therefore we chose the variables carbonate mass and clay mass to pursue the research objectives of this study. As these metrics are based on equal-depth comparisons at 5 cm depth intervals, we additionally visually evaluate if there is a match (or not) in depth patterns of soil properties between experiments, the joint simulation and the reference experiment.

4.2.4.2 Assessing paleoclimate and paleosol response to the precession forcing

In order to evaluate the relation between the astronomical forcing, climate and paleosols, we focus on the precession cycle and the simulated climate and paleosols during MIS 5, MIS 7, MIS 9, MIS 11 and MIS 13. For this, paleosol simulations are performed at the moist Chang'an loess section in the southeast of CLP, where the relatively strong pedogenesis would allow to exhibit a strong response to the climate and astronomical forcing during these interglacials. In these simulations, NH ice sheets are fixed into their present values and the major climate forcing is insolation determined by precession, obliquity and eccentricity (Berger and Loutre, 1991).

To evaluate the impact of astronomical forcings on soil properties calcite and clay, we calculate, for each year of the interglacial, the fraction of mass change relative to the initial mass and average this fraction over the soil profile:

$$\textit{Fraction of mass change} = \frac{1}{K} \sum_{k=1}^K \textit{abs}\left(\frac{M_{sim,k} - M_{init,k}}{M_{init,k}}\right) \quad \text{Eq. [4-3]}$$

Where K=number of soil compartments, $M_{sim,k}$ =the simulated mass of a soil property in compartment k, $M_{init,k}$ =the initial mass in compartment k. $M_{init,k}$ can be either the amount in the parent loess or in the added dust, depending on the compartment.

4.2.4.3 Assessing impact of NH ice sheet variations on paleoclimates and paleosols

As we would like to investigate the impact of NH ice sheet changes on paleosol development (during interglacials), we performed two sets of soil simulations driven respectively by the two sets of climate simulations with (OrbGHGIce) and without ice sheets (OrbGHG). Soil Simulations are performed at all the three sites at Jiuzhoutai (in Lanzhou), Xifeng and Chang'an, and for the most contrasting interglacials, MIS 11 and MIS 13. In the two sets of soil simulations, the boundary conditions (precipitation, potential evapotranspiration, temperature and vegetation: and therefore, carbon input) are different due to impact of ice sheets. The initial conditions (parent materials) are similar. The comparison of soil properties between the two set of soil simulations allows to investigate the effect of NH ice sheets on paleosol development through their impact on climate and vegetation on the CLP.

4.3. Results and discussion

4.3.1 Analysis of the driving factors of the changes in paleosol development

In this section, we discuss the importance of the parameters, P, T, Ep, vegetation and dust addition on paleosol formation for MIS 11 and MIS 13. We use three measures: (i) the MAE (mass/ha) between each simulation and the reference scenario; (ii) the gain in quality (in %) relative to the reference scenario; (iii) a visual comparison of depth distributions. The two quantitative measures are used to rank the importance of reconstructed time series of boundary inputs, while the visual comparisons are used to identify if weak MAE and gains are caused by biases in depth patterns (e.g. by depth shift or by mass bias).

4.3.1.1 MIS11

The results of the sensitivity analysis for MIS11 are in **Table 4-1** and **Figure 4-2**. As shown in **Table 4-1** (top), in order of increasing MAE, the individual experiments are ranked precipitation < temperature < vegetation < potential evapotranspiration < dust deposition for calcite. Based on the MAE, precipitation is the best individual factor. For calcite, the largest gain in MAE relative to the reference scenario is obtained by using reconstructed (here it means precipitation simulated by LOVECLIM1.3) precipitation time series for MIS 11 instead of the reference time series. This gain is improved by adding reconstructed dust input as a second factor and further improved by adding reconstructed potential evapotranspiration as a third factor. The following mechanisms explain this ranking: precipitation-caused leaching fluxes are the main cause of redistribution of calcite in the soil, and dust is the main source of calcite during the interglacial. Reconstructed time series of Ep influence the depth of leaching and thus also contribute to the calcite depth distribution (**Figure 4-2, left**).

For clay, most individual factors do not appear to positively contribute to the MAE (**Table 4-1 bottom**, negative values of the gain), with the clear exception of reconstructed dust input. Nevertheless, visual inspection shows that the

clay depth distribution pattern is similar, but with bias, between the joint- and the precipitation-simulations and not so between the joint- and dust-simulations (**Figure 4-2, right**). Addition of reconstructed time series of precipitation strongly improves the gain, and a limited further gain is obtained by adding reconstructed potential evapotranspiration (**Table 4-1 bottom**). The mechanism that could explain the lack of a direct impact of only precipitation is that clay migration is limited as long as the topsoil is still calcareous. Dust input is the source of both new calcite and new clay and therefore has a dominant effect. The combined effect of dust and rain defines both the input of clay and calcite as well as their transport to deeper soil layers and therefore determines their depth distributions (**Figure 4-2**). Reconstructed potential evapotranspiration for MIS 11 adds little to the gain.

For both the calcite and the clay simulations, we find that the combined impacts of the precipitation, dust addition, and potential evapotranspiration are very similar to the JS, indicating that the impact from these factors is much stronger than when compared to other combinations of factors (Tables A4-1, A4-2 and Figure A4-1 in appendix for chapter 4). We did not perform simulations combined with vegetation changes, because these are a function of precipitation and temperature changes in LOVECLIM1.3.

Table 4-1 The sensitivity experiments, mean absolute errors, ranking and “gain” in MAE for calcite (top) and clay (bottom) in MIS 11 in Chang’an. Ex=Experiment; Joint=all boundary inputs by climate modeling and dust input reconstruction; Reference=all boundary inputs equal to Pre-Industrial Holocene time series; PP=precipitation; Evapo=potential evapotranspiration; Vege=vegetation; Temp=temperature.

MIS 11-calcite			
Experiment	Mean absolute error (kg/ha)	Gain (%)	Ranking
Joint-Reference	64157.3	0.0%	
Joint-Ex(Dust)	55143.4	14.0%	
Joint-Ex(Evapo)	51419.7	19.9%	
Joint-Ex(Vege)	48686.9	24.1%	
Joint-Ex(Temp)	38970.2	39.3%	
Joint-Ex(PP)	20060.4	68.7%	Best 1-factor
Joint-Ex(PP+Temp)	20190.0	68.5%	
Joint-Ex(PP+Evapo)	20137.0	68.6%	
Joint-Ex(PP+Dust)	7205.9	88.8%	Best 2-factor
Joint-Ex(PP+Dust+Evapo)	2825.9	95.6%	Best 3-factor

MIS 11-clay			
Experiment	Mean absolute error (Mg/ha)	Gain (%)	Ranking
Joint-Ex(PP)	21.5	-23.2%	
Joint-Ex(Vege)	17.9	-3.1%	
Joint-Ex(Temp)	17.6	-1.4%	
Joint- Ex(Evapo)	17.5	-0.5%	
Joint-Reference	17.4	0.0%	
Joint-Ex(Dust)	7.1	59.5%	Best 1-factor
Joint-Ex(PP+Evapo)	21.9	-26.0%	
Joint-Ex(PP+Temp)	21.4	-22.8%	
Joint-Ex(Dust+PP)	1.3	92.5%	Best 2-factor
Joint-Ex(Dust+PP+Evapo)	0.5	97.4%	Best 3-factor

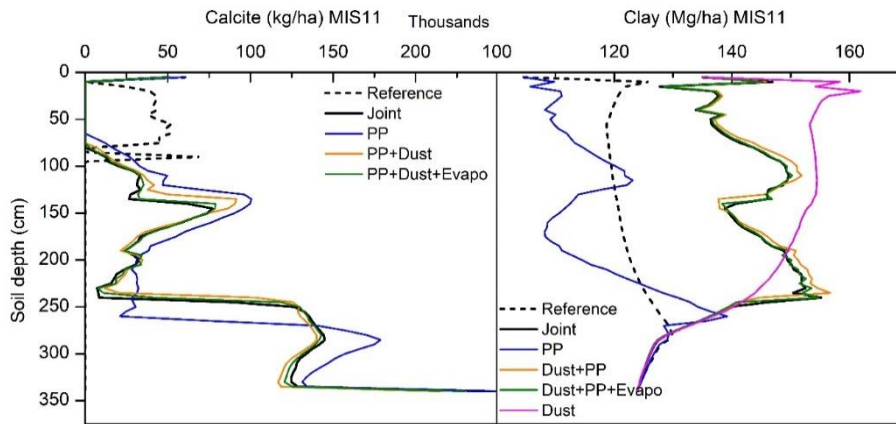


Figure 4-2 Simulated depth distribution of calcite (kg/ha, left) and clay (Mg/ha, right) for MIS11 in Chang'an, for the Reference simulation, Joint simulation, reconstructed precipitation (PP), with added dust (PP+Dust) and potential evapotranspiration (PP+Dust+Evapo).

4.3.1.2 MIS13

The results of the sensitivity analysis for MIS 13 are in **Table 4-2** and **Figure 4-3**.

For calcite, the largest gain in MAE relative to the reference scenario is again obtained by using reconstructed precipitation time series for MIS 13, and is improved by adding reconstructed dust input as a second factor and further improved by adding reconstructed potential evapotranspiration as a third factor (**Table 4-2 top**). These results are identical to those of MIS 11, but in general the gains relative to the Holocene reference scenario are less in MIS 13, which is due to the fact that boundary inputs for the reference scenario are closer to those of MIS 13 than to MIS 11. The gain by adding the third factor (potential evapotranspiration) is substantial, in contrast to that in the MIS 11 situation, in which the gain in MAE is quite small when adding potential evapotranspiration time series (6.83%), whereas it is 32.26% in MIS13. The result implies the importance of potential evapotranspiration during MIS 13 (**Table 4-2 top**). Apparently, in MIS 13 it is the precipitation deficit (PP-Evapotranspiration) rather than the precipitation that determines the leaching of calcite. A similar conclusion was drawn for MIS13 soils by Finke et al.

(2017). **Figure 4-3** shows depth patterns of the best performing and reference scenarios.

Table 4-2 The sensitivity experiments, mean absolute errors, ranking and “gain” in MAE for calcite(top) and clay (bottom) in MIS 13 in Chang’an. Ex=Experiment; Joint=all boundary inputs by climate modelling and dust input reconstruction; Reference=all boundary inputs equal to pre-industrial Holocene time series; PP=precipitation; Evapo=potential evapotranspiration; Vege=vegetation; Temp=temperature

MIS 13-calcite			
Experiment	Mean absolute error (kg/ha)	Gain (%)	Ranking
Joint-Ex(Dust)	43172.7	-0.8%	
Joint-Reference	42832.6	0.0%	
Joint-Ex(Vege)	38716.3	9.6%	
Joint-Ex(Evapo)	37900.4	11.5%	
Joint-Ex(Temp)	33965.3	20.7%	
Joint-Ex(PP)	26241.4	38.7%	Best 1-factor
Joint-Ex(PP+Temp)	27037.7	36.9%	
Joint-Ex(PP+Evapo)	26618.2	37.9%	
Joint-Ex(PP+Dust)	21337.5	50.2%	Best 2-factor
Joint-Ex(PP+Dust+Evapo)	7519.8	82.4%	Best 3-factor

MIS 13-clay			
Experiment	Mean absolute error (Mg/ha)	Gain (%)	Ranking
Joint-Ex(Dust)	16.2	-149.0%	
Joint-Ex(PP)	13.8	-112.9%	
Joint-Ex(Vege)	7.3	-13.0%	
Joint-Ex(Temp)	7.1	-9.0%	
Joint-Ex(Evapo)	6.7	-3.7%	
Joint-Reference	6.5	0.0%	Best 1-factor
Joint-Ex(PP+Evapo)	16.2	-149.4%	
Joint-Ex(PP+Temp)	14.6	-124.3%	
Joint-Ex(PP+Dust)	4.9	24.5%	Best 2-factor
Joint-Ex(PP+Dust+Evapo)	3.5	46.6%	Best 3-factor

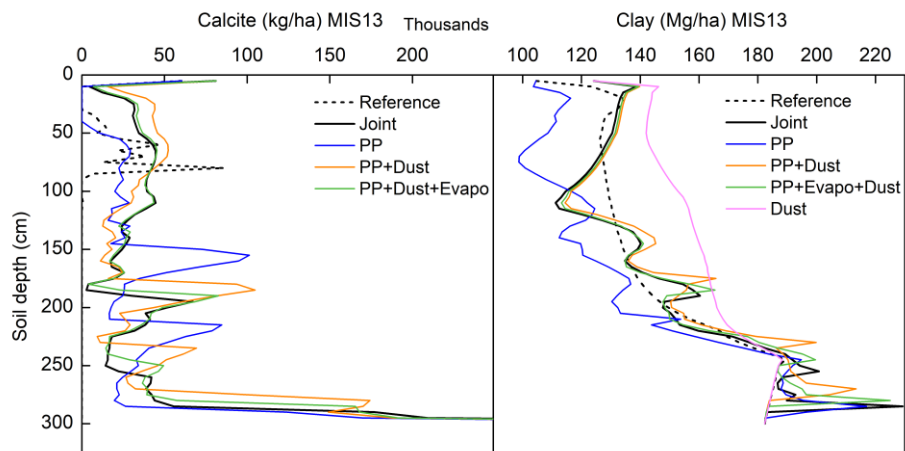


Figure 4-3 Simulated depth distribution of calcite (kg/ha, left) and clay (Mg/ha, right) for MIS13 in Chang'an, for the Reference simulation, Joint simulation, reconstructed precipitation (PP), reconstructed Dust (Dust), with added dust (PP+Dust) and potential evapotranspiration (PP+Dust+Evapo).

For clay, all individual factors show negative gains (**Table 4-2 bottom**), which indicates that no single factor can reproduce the clay depth patterns. Visual inspection (**Figure 4-3, right**) shows, that the clay depth distribution pattern is similar between precipitation-only and joint-simulation scenarios, but that a strong negative bias exists in the (lower) amount of clay in the precipitation-only scenario (PP) (**Figure 4-3, right**). This bias, now positive, also exists for the dust deposition-only scenario (Dust) (**Figure 4-3, right**). This explains why the combination of precipitation and dust scenario has a better (positive) gain than the other 2-factor combinations (Table A4-4 in appendix for chapter 4).

Addition of potential evapotranspiration further improves the gain. Like in the calcite mass depth distribution, the gains are less than in MIS 11, because the reference Holocene scenario is closer to the joint MIS 13 scenario, and again it is the precipitation deficit (PP-Evapotranspiration) rather than the precipitation that determines the leaching, of clay. The calculated months with precipitation surplus (P-Ep) are quite larger in MIS 13 (70998) than in MIS 11 (66940) only in the first 42 ka (length of MIS 11), affecting the stronger leaching in S5-1 paleosols. This could be a reason for the stronger calcite leaching during MIS 13 than in MIS 11 (there are two calcic horizons in 150

cm and 250 cm depths, see **Figure 4-3, left**). In addition, the longer the duration of MIS 13 (67 ka) enhances soil development. These results are in agreement with Finke et al. (2017).

It has been stated that the degree of paleosol formation in the CLP is controlled by summer monsoon precipitation (Liu, 1985). Strongly developed paleosols can be seen in the southern part of the CLP, where it receives abundant mean annual precipitation (600-700 mm). As a proxy indicator, calcite concentrations in paleosols and depths to calcic horizons have been extensively studied for understanding the summer precipitation and temperature history in the CLP (e.g. He et al., 2015). The depths of the CaCO₃ layer are primarily determined by the balance between potential evapotranspiration (temperature-dependent) and precipitation. The downward leaching of Ca⁺² and re-precipitation of CaCO₃ are controlled by precipitation and potential evapotranspiration, respectively.

Clay contents in Bt horizons are indicators of strong soil formation, and Bt formation is triggered by water movement within the soils. As earlier mentioned, clay migrates mainly after calcite is removed. Clay content in paleosols is greatly determined by the amount present in the parent material beneath paleosols and the dust addition during the interglacial. It has long been accepted that atmospheric dust deposition is a significant source of soils and sediments on the paleosol formation in the CLP (Liu, 1985; An et al., 1991a; Ding et al., 1999; Qiang et al., 2011; Sun et al., 2020). Overall, the sensitivity analysis revealed that the dust addition, precipitation, and potential evapotranspiration are the most sensitive factors for interglacial paleosol development. These combined factors explain more of the soil development in the CLP than when one of them acts alone, and therefore these should minimally be reconstructed (by proxies) when interglacial soil formation is to be simulated in the CLP (e.g. for MIS 5, MIS 7 and MIS 9).

4.3.2 Paleosol response to the astronomical forcing

In this section, we discuss the possible impact of precession variations on paleosol development in different interglacials, MIS 5, MIS 7, MIS 9, MIS 11, and MIS 13 in Chang'an. **Figure 4-4** shows a comparison between the astronomical parameters, the LOVECLIM1.3-simulated climate, and the simulated calcite and clay in each interglacial. The mass of the clay and calcite is averaged over the total thickness of the simulated paleosol, accounting for the amount of clay and calcite originally present in the loess and in the dust added during the interglacial. These averages illustrate how much clay or calcite has moved within the paleosol profile. When the simulated calcite or clay does not move within the profile, and dust deposition is large, the profile average decreases and vice versa **Eq. [4-3]**. In addition, the simulated paleosol profiles develop (soil thickens) from the left (start) to the right (end) of each interglacial period (x-axis).

Figure 4-4 shows an indirect link between simulated soil properties and precession through its control on precipitation in each interglacial. Interestingly, the indirect relationship between precession and the simulated soil properties shows that precipitation maximum and precession minimum are in phase, linking the simulated calcite and clay peaks with the precession minimum. This is the first time that the indirect effect of precession on the paleosol properties is demonstrated by soil modeling study, confirming the findings from proxy analyses (e.g. Sun et al., 2019). The paleosol development in response to precession during each individual interglacial is discussed here under.

During MIS 5, there are three precession minima (precession minimum corresponds to NH summer insolation maximum) which occur at 127, 106 and 83 ka BP (**Figure 4-4a**). The amplitude of variation in precession decreases gradually from 133 ka BP to 75 ka BP due to reduced eccentricity, which modulates the amplitude of variation of precession (Berger and Loutre, 1991). The three precession minima have nearly in-phase relationships with the precipitation maxima and the calcite maxima (**Figure 4-4a**). The calcite peaks

roughly match the peaks of precession and precipitation. The clay peaks also match but to a less extent and with a lag of ~4000, 5000 and 6000 years. The lag is due to the fact that clay migration can happen only after calcite is leached from soils. Therefore, the clay peaks generally occur ~ 5000 years later than the calcite peaks during MIS 5. Moreover, **Figure 4-4a** shows that there are more peaks in clay than in calcite. **Figure A4-3a (in appendix for chapter 4)** shows that actually the clay peaks are also correlated well with the annual mean temperature peaks, because clay production is also strongly controlled by temperature. These results show that the simulated clay is more influenced by the annual mean temperature, whereas the calcite peaks correspond well to annual mean precipitation and precession minima during MIS 5.

During MIS 7, there are three precession minima at 242, 220 and 198 ka BP, which correlate well to three precipitation maxima. Clay and calcite peaks are approximately in phase with the precipitation and the precession peaks, especially in the middle and the end of MIS 7 (at 220 and 198 ka BP) (**Figure 4-4b**). The calcite peaks lag the precession peaks by only 2000-3000 years and the clay peaks, which lags the precession minimum by 3000-4000 years. The indirect relation between the simulated paleosol properties and precession is hardly noticed in the initial stages of MIS 7 (247-234 ka BP) (**Figure 4-4b**); a possible reason could be due to the effect of other controls on paleosol development e.g relatively rapid dust addition (**Figure 4-5**) plus high precipitation during the initial stages. In general, the clay peaks lags the calcite peaks only by 1000 years. Unlike the varying lags between the calcite and clay peaks in other interglacials (e.g. MIS 5, MIS 9 and MIS 13, see next section), the time lag between the calcite and clay peaks is shorter during MIS 7, this may be due to high precipitation at all the three precession minima. Moreover, **Figure 4-4b** shows that there are more peaks in clay than in calcite. In addition, **Figure A4-3b (in appendix for chapter 4)** shows that the clay peaks are also well correlated with the annual mean temperature peaks in the initial stages of MIS 7 (247-225 ka BP), but shows a poor relation after 220 ka BP.

During MIS 9, there are three precession minima at 335, 313, 291 ka BP, which correlate well to precipitation peaks and then roughly to the calcite and clay peaks (**Figure 4-4c**). The indirect relation between the simulated clay, calcite, and the precession is distinct at the start (at 335 ka BP) and the middle (at 313 ka BP) of MIS 9, whereas the precession footprint in the simulated paleosol is relatively weak at 291 ka BP (**Figure 4-4c**). This may relate to the dust addition variability, which is very rapid at the end of MIS 9 interglacial (**Figure 4-6**), resulting in less time to leach calcite in the soils. The delay of the calcite peaks is about 3000-4000 years to the precession peaks. However, the clay peaks lag the precession peaks by around ~5000-6000 years. Compared to MIS 5, the delay between the calcite and clay peaks is shorter (around ~ 2000 years) during MIS 9. This may be due to the differences between dust addition patterns during the two interglacials. Most field-observation studies in the CLP have shown intervening loess layers in the S1 paleosol profiles during the last interglacial, whereas no such intervening loess layers are found in the S3 paleosols during MIS 9. These dust addition rhythms are well incorporated during SoilGen2 simulations (**Figure 4-6**). The differences of time lags to precession during MIS 5 and MIS 9 are because calcareous dust impedes the clay migration process by several thousand years more in MIS 5 than in MIS 9. As shown in **Figure A4-3c (in appendix for chapter 4)**, the clay peaks show no relation to annual mean temperature peaks during MIS 9.

MIS 11 is different from the other interglacials; two precession minima are observed at 409 and 389 ka BP (**Figure 4-4d**). During MIS 11, the amplitude of variation of precession is low when compared to other interglacials due to its small eccentricity, and therefore the intensity of precipitation peaks is small (**Figure 4-4d**). In MIS 11 simulations, two calcite peaks are found during MIS 11 although the precession signal is weak during MIS 11, with a larger peak at 409 ka and a smaller one at 389 ka through the control of precipitation during MIS 11. Hence, calcite peaks slightly respond and lag the two precession peaks by ~2000-3000 years, and are less prominent than in the other interglacials. Nevertheless, clay peaks do not relate to the precession

peaks during MIS 11. This is because clay migration is a slow process and it could respond weakly to the small variation of precipitation due to small variation of precession during MIS 11, likewise, there is no distinct relationship between the clay peaks and the annual mean temperature peaks during MIS 11 (**Figure A4-3d in appendix for chapter 4**).

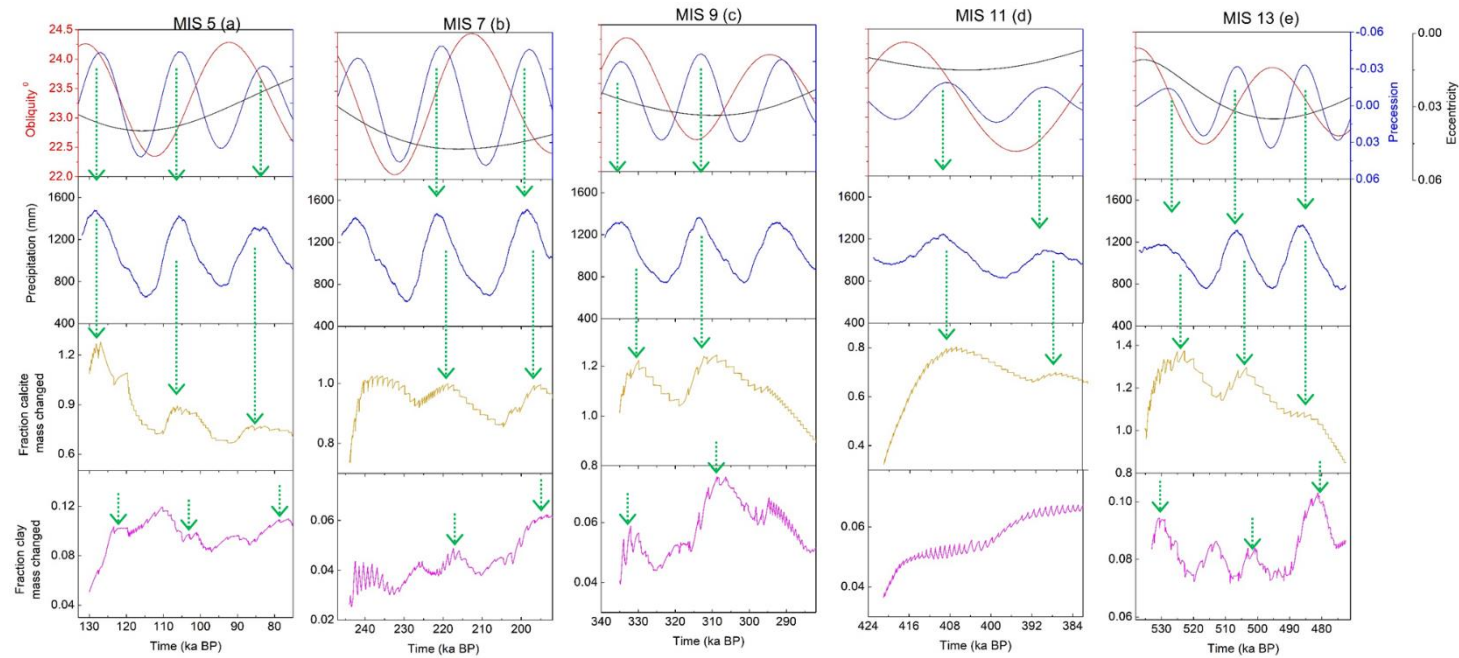


Figure 4-4 Comparison between astronomical parameters with the simulated precipitation and paleosols during the five interglacials. (a) MIS 5; (b) MIS 7; (c) MIS 9; (d) MIS 11; (e) MIS 13 in Chang'an. In each panel, from top to bottom : astronomical parameters : (obliquity (red), precession (blue), eccentricity (black), mean annual precipitation simulated by LOVECLIM1.3, fraction of mass changed for calcite and for clay Ref Eq.[4-3]. The data are plotted in their own time scales and the 1000-year running mean of precipitation is plotted. The astronomical data are from Berger and Loutre (1991). Green dash arrows show the peaks of calcite and clay related to precipitation peaks and precession minimums mentioned in the text.

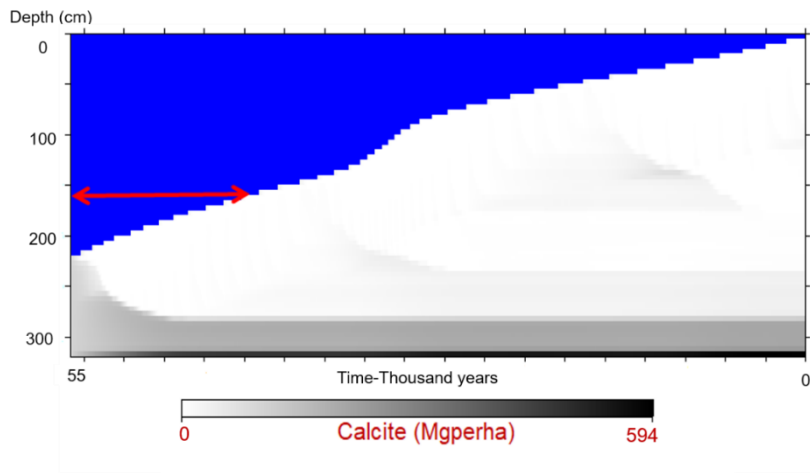


Figure 4-5 Evolution of calcite mass at Chang'an during MIS 7. A relatively rapid dust deposition is depicted in the beginning of MIS 7 (as shown by red arrow). The boundary between the blue and white/gray areas in the paleosols demarcates the dust deposition rhythm during MIS 7. Blue stands for the atmosphere.

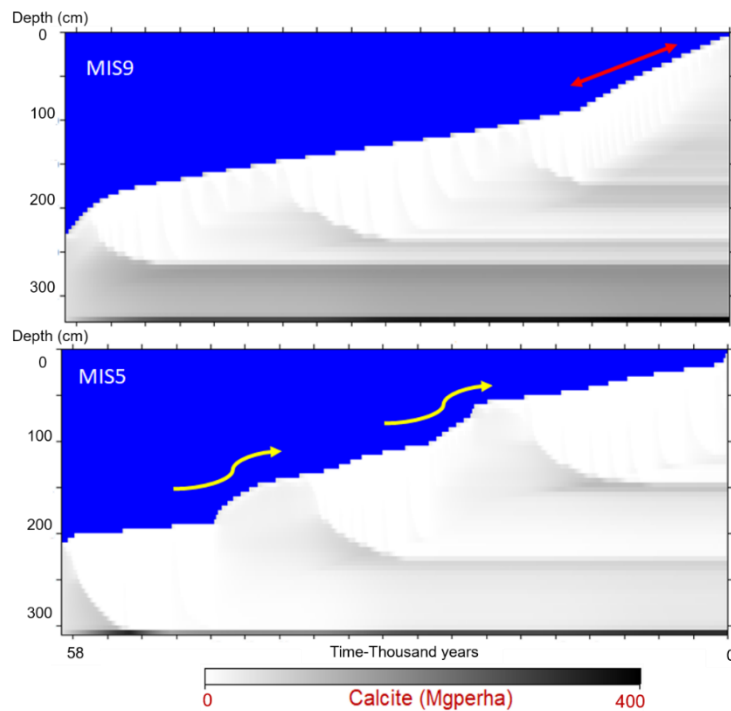


Figure 4-6 Evolution of calcite mass at Chang'an during MIS 9 (top), and MIS 5 (below). A very rapid dust deposition is depicted at the end of MIS 9 (as shown by red arrow) and of MIS 5 (yellow arrows).

MIS 13 has long been considered as a controversial interglacial (Yin and Guo, 2008; Guo et al., 2009), because it was a relatively cool interglacial globally speaking but the paleosol S5-1 on the CLP that was formed during MIS 13 is the strongest over the past 1 Ma. During MIS 13, there are three precession minima at 528, 506, 485 ka BP, which correlates well with precipitation maxima and the calcite peaks and to a less extent with clay peaks (**Figure 4-4e**). The calcite peaks generally lag the precession peaks by ~ 4000 years. The clay peaks lag behind the precession peaks by about 6000 years.

The first clay peak in MIS 13 corresponds well to the first precipitation peak and both precede the precession minimum at 528 ka BP by 1000-2000 years (**Figure 4-4e**). This is probably modulated by the large obliquity maximum, which precedes the precession minimum by a few thousand years. At the same time, calcite continuously leaches and accumulates in soils (**Figure 4-11b**) and, the calcite peak occurs 4000 years later than precession minimum at 528 ka BP. At 506 ka BP, both the calcite and clay peaks approximately correlate with the precession minima and the precipitation maxima; calcite and clay lag precession by ~3000 and ~6000 years, respectively, and the clay peak lags the calcite peak by 3000 years. At 485 ka BP, a weak and stable calcite peak is observed, which lags precession only by 1000 years (**Figure 4-4e**). However, the clay peak is quite strong and lags precession by 5000 years, and the clay peak lags the calcite peak by 4000 years (**Figure 4-4e**). In addition, one more clay peak occurs at 513 ka BP, which does not correspond to precession minima, but is strongly related to the annual mean temperature peak (**Figure A4-3e in appendix for chapter 4**). Moreover, it seems that the delay between the indirect impact of precession to precipitation and to the clay peak at 506 ka BP is due to the effect of annual mean temperature, where the clay peak follows the pattern of temperature. Overall, the two clay peaks in the middle of MIS 13 are more strongly modulated by annual mean temperature than by the indirect influence of precession through its control on precipitation. Therefore, in response to precipitation, temperature and calcite leaching, we observe four clay peaks during MIS13.

For all the five interglacials, the simulated precipitation is indirectly linked with precession and therefore the precession has indirect influence on the paleosol development. The LOVECLIM1.3 simulated precipitation has nearly 20-ka cycle corresponding to the precession cycle, which has been found in the pedogenic MS-flux index of the loess records and is suggested to be consistent with the EASM variability over the CLP (Beck et al., 2018; Kong et al., 2020; Cheng et al., 2021). When precession is minimum, NH summer occurs at perihelion and the NH summer insolation is high, resulting in increased summer monsoon precipitation. In addition, on orbital scale, annual summer precipitation is dominated by precession over the East Asia, but annual mean temperature by ice volume and CO₂ (Lyu et al., 2021). Therefore, the major controlling factors of temperature and precipitation are not necessarily the same on orbital scale and therefore we see a significant offset in between the simulated precipitation and temperature.

In summary, our analyses show that although the simulated calcite and clay lag precession, the simulated paleosol preserves clear but, indirect precession footprints during MIS 5, MIS 7, MIS 9 and MIS 13. During MIS 11, there is a weak precession (indirect) footprint in the simulated calcite but no clear precessional footprint in the clay. This is probably due to the smaller amplitude of precession variation during MIS 11 related to its small eccentricity, which in turn causes smaller variation in precipitation. This finally leads to a single S4 layer in most areas of the Loess Plateau (despite the distinct regional differences of the S4 paleosol across the CLP). This is supported by the findings of Guo et al. (1998) and Shi et al. (2013).

In general, there is a roughly good relationship between precession and calcite, and a less good but approximately visible relationship between precession and clay. Moreover, besides precipitation, temperature also has a clear influence on the simulated clay content during MIS 5, MIS 7 and MIS 13. The calcite and clay peaks of the five interglacials are lagged differently to the indirect precession forcing through precipitation, perhaps because the amplitudes of precession peaks are slightly different between the interglacials. We suggest that this lagged pattern results from nonlinear response of climate

to astronomical forcing. Our results also suggest that different strategies should be applied on different time periods and on different loess properties when orbital tuning is used to establish the chronology of the LPS.

Although there are some differences, our results can at least be partly comparable with loess records. In the CLP, different monsoon related proxies show the existence of weak precession signals within the paleosols, but strong precession footprint has been discovered in high-resolution loess records in the northwestern CLP (e.g. Ma et al., 2017; Sun et al., 2019). It is easier to compare the number of precession peaks in our simulated paleosols with that in the loess records from the northwestern Loess Plateau, because dust accumulation rate is high and pedogenesis is weak there. It is noteworthy that precession footprint could be faded from the paleosols of the southern CLP due to low deposition rates and a strong pedogenesis accompanied by warm and wet climatic conditions (Sun et al., 2015; 2021; Ma et al., 2017; Meng et al., 2021).

Recently, Zhang et al. (2021) found three distinct precession peaks within the S1 paleosol in the Huanxian section (100 km north of the Xifeng loess section). Ma et al. (2017) investigated the precession signals in 18 S1 paleosol profiles over the entire CLP, and they found significant spatial difference (presence or absence) of the three precession peaks within the S1 paleosol due to changes in deposition rates and pedogenesis. In good agreement with these observations, we also found three peaks in the simulated clay and calcite within the S1 paleosol. Recently, Sun et al. (2021) stated that most paleosols in the western CLP show three precessional peaks in the magnetic susceptibility records. For both MIS 5, MIS 7, MIS 9, there are three peaks in our simulated paleosols, which roughly correspond to the three precession minima. The MIS 13 paleosols also show three clay peaks related to precession in response to NH ice sheets (**see section 4.3.3**).

4.3.3 Paleoclimate-paleosol response to NH ice sheets

In this section, we discuss paleoclimate and paleosol development differences between the two sets of simulations with (OrbGHGIce) and without (OrbGHG) ice sheets using MIS 11 and MIS 13. The LOVECLIM1.3-simulated climate is different between with and without ice sheets scenarios. Similarly, we noticed paleosol development differences at three loess sections along the steepest climatic gradient in the Loess Plateau: Jiuzhoutai (in Lanzhou), Xifeng and Chang'an in response to indirect effects of NH ice sheets through its control on the simulated precipitation in the CLP.

4.3.3.1 Climate and soil response to NH ice sheets during MIS 11

Figure 4-7c shows that, in the first several thousand years of MIS 11, the simulated annual mean precipitation is substantially reduced in response to larger ice sheets (**Figure 4-7b**), and it is reduced by up to ~200 mm in Chang'an (**Figure 4-7c**) and Xifeng (**Figure A4-4a in appendix for chapter 4**) and by up to ~100 mm in Jiuzhoutai (**Figure A4-4b**). In OrbGHGIce and OrbGHG experiments, the precipitation reaches its maximum during ~410-406 ka BP because change of ice volume is small during this period. Interestingly, during ~403-386 ka BP, precipitation increases by ~300-200 mm in response to ice sheet and shows more oscillations at Chang'an (**Figure 4-7c**) and Xifeng (**Figure A4-4a**) and it increases by ~150 mm in Jiuzhoutai (**Figure A4-4b**). After about ~386 ka BP, the precipitation change is very small. Based on climate model results, Yin et al (2008, 2009) show that the response of precipitation in East Asia to ice sheets is nonlinear and it depends on the background insolation, on the size, shape and location of the ice sheets. They show that large ice sheets reduce the precipitation when summer insolation is low (precession is high) and that small ice sheets could reinforce the precipitation whatever for a precession minimum or a precession maximum. This could explain the precipitation decrease between 424-410ka BP and the precipitation increase between 403-386ka BP, both in response to ice volume increase (**Figure 4-7b**). As quite expected, the simulated annual mean temperature is strongly reduced in response to the large ice sheets at the beginning of MIS11 (**Figure 4-7d**, and **Figure A4-4 c, d**). It remains

unchanged or even increases between ~410 ka BP and 394 ka BP during which the change of the NH ice sheets is small or the ice sheets even melted at the peak of MIS 11 (**Figure 4-7b**).

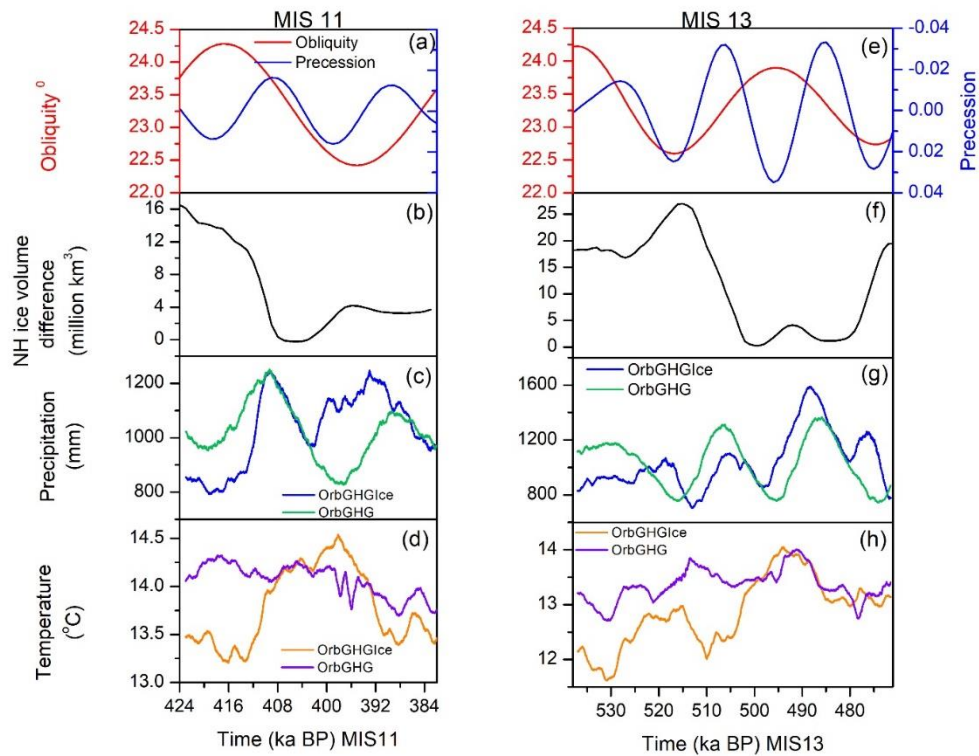


Figure 4-7 Comparison of the simulated paleoclimate in ice (OrbGHGIce) and no ice (OrbGHG) experiments with NH ice volume and astronomical parameters in MIS 11 (left) and MIS 13 (right) in Chang’an. From top to bottom: (a, e) astronomical parameters (obliquity (red), precession (blue)), (b, f) NH ice volume difference relative to the simulated 0ka volume (Ganopolski and Calov, 2011), (c, g) the simulated annual mean precipitation and (d, h) temperature. The 1000-year running mean of precipitation and temperature is plotted. The astronomical data are from Berger and Loutre (1991).

In Chang’an, most of the simulated calcite in the top soils remains in the first 12000 years from the start of the interglacial in the ice scenario (**Figure 4-8a**), and dissolves shortly after the precipitation peak. In the no ice scenario, a second calcic layer (Bk) begins to form toward the end of MIS 11 (**Figure 4-8b**), whereas it is less noticeable in the ice scenario in the sub soils (**Figure**

4-8a). This may be due to the increased precipitation in the second half of the MIS 11 interglacial in the ice scenario (**Figure 4-7c, blue line**). In both cases, two major calcic horizons are present at two depths. In the ice scenario (**Figure 4-8a**), calcite accumulation is thicker at the bottom of the paleosol than in the no ice scenario (**Figure 4-8b**). The evolution of clay content is dissimilar between the two scenarios; two clay-rich illuvial horizons (Bt) become more developed through time in the no ice scenario (**Figure 4-8d**), whereas only one and a strong Bt horizon develops in the ice scenario (**Figure 4-8c**) which may have been formed by joining two clay peaks. Similar to calcite, clay migration occurs after the first 12000 years in the ice scenario (**Figure 4-8c**).

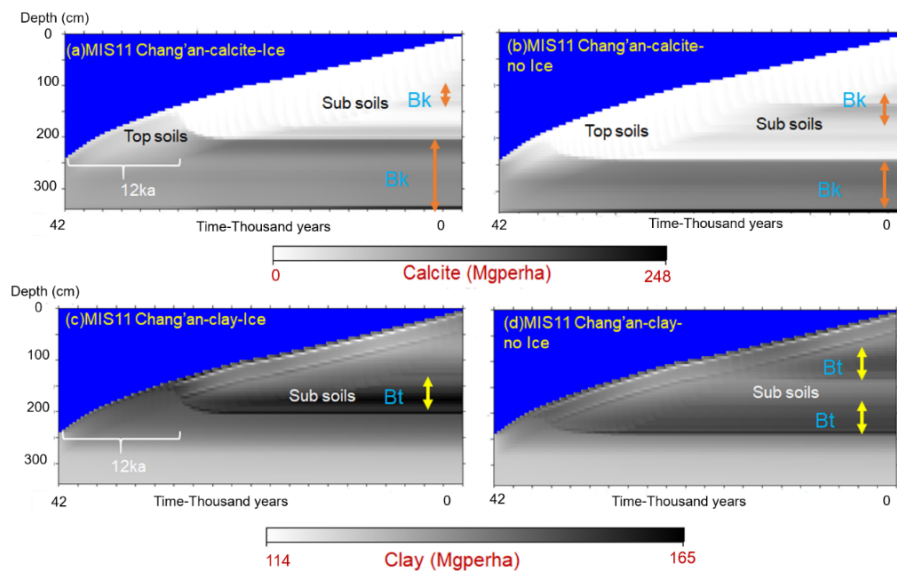


Figure 4-8 Evolution of calcite (top panel) and clay (bottom panel) in Chang'an during MIS 11 in ice (OrbGHGIce) and no ice (OrbGHG) experiments. In (a) and (b) orange arrows depict the formation of calcic horizons (Bk) and white arrow shows the calcite in the top soils in the first 12ka (a). Note that the Bk forms in the sub soils at (b) and the less visible Bk at (a). In (c) and (d), yellow arrows depict the formation of Bt horizons. Note that the two Bt forms at (d) and one Bt at (c).

In Xifeng, the evolution of both calcite and clay in the simulated S4 paleosol is similar to Chang'an. Calcite in the top soils is removed by the increased

precipitation in the second half of MIS 11, in the ice scenario (**Figure 4-9a**), causing a thick Bk horizon at the bottom of the profile, whereas most of the calcite remains in the sub soils in the no ice scenario (**Figure 4-9b**). Therefore, in both scenarios, the calcic horizons form at different depths. Ice sheet scenario (**Figure 4-9a**) shows that the thickness of the deepest Bk is more prominent than in no ice sheet scenario (**Figure 4-9b**). In Xifeng, two Bt horizons develop in the no ice sheet scenario (**Figure 4-9d**), while it is one (thick and strong) in the ice scenario (**Figure 4-9c**).

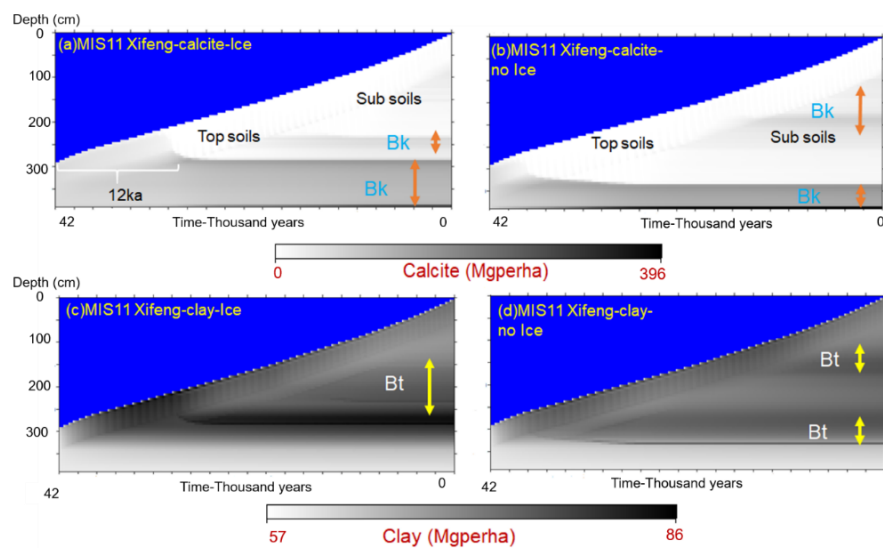


Figure 4-9 Evolution of calcite (top panel) and clay (bottom panel) in Xifeng during MIS 11 in ice (OrbGHGIce) and no ice (OrbGHG) experiments. In (a) and (b) orange arrows depict the formation of calcic horizons (Bk) and white arrow shows the calcite in the top soils in the first 12ka (a). Note that a thick Bk forms in the sub soils at (b). In (c) and (d), yellow arrows depict the formation of Bt horizons. Note that the two Bt forms at (d) and one Bt at (c).

In Jiuzhoutai (northwestern (NW) Loess Plateau), the evolution of calcite in the S4 paleosol is approximately similar between the two scenarios. In both cases, it shows less decalcification (darker areas) in the top soil and the formation of calcic horizons (Bk) at two different depths (**Figure 4-10a and b, orange arrows**). A mild precipitation increase in the second half of the MIS11

interglacial intensifies calcite leaching and accumulation and the formation of Bk in the sub soils in the ice scenario (**Figure 4-10a**). Therefore, at the end of MIS 11, the gap between the two calcic horizons in the ice sheet scenario (**Figure 4-10a**) is much smaller than in the no ice scenario (**Figure 4-10b**). In general, calcite accumulates near the bottom of the paleosol profiles in Chang'an and Xifeng, whereas it remains in the sub soils in Jiuzhoutai. This is because Jiuzhoutai in the NW receives low annual precipitation. In both scenarios, soil expressions are almost similar for clay (**Figure 4-10c and d**); the evolution of the simulated clay distribution patterns in depths are identical between the two scenarios. This suggests weak soil development in the northwestern CLP. Denote that the contrast in clay content between subsoil and topsoil is caused by differences in initial clay content of underlying loess and added dust.

The simulated differences of the S4 paleosol development in the ice scenario are in agreement with the loess records (a single S4 paleosol in the central and in most areas in the CLP, Hao and Guo, 2005). For example, there are regional differences of the S4 paleosol formation along the NE-SE climate gradient in the CLP, as supported by spatial variations of the S4 paleosol during MIS 11 due to stronger gradients in mean annual temperature and precipitation (Guo et al., 1998; Hao and Guo, 2005). In addition, the evolution of clay and calcite profile averages confirms that the simulated S4 paleosol is similar to the loess records in the CLP, in response to precession and NH ice sheets, when compared to no ice scenario (**Figure A4-5 in appendix for chapter 4**).

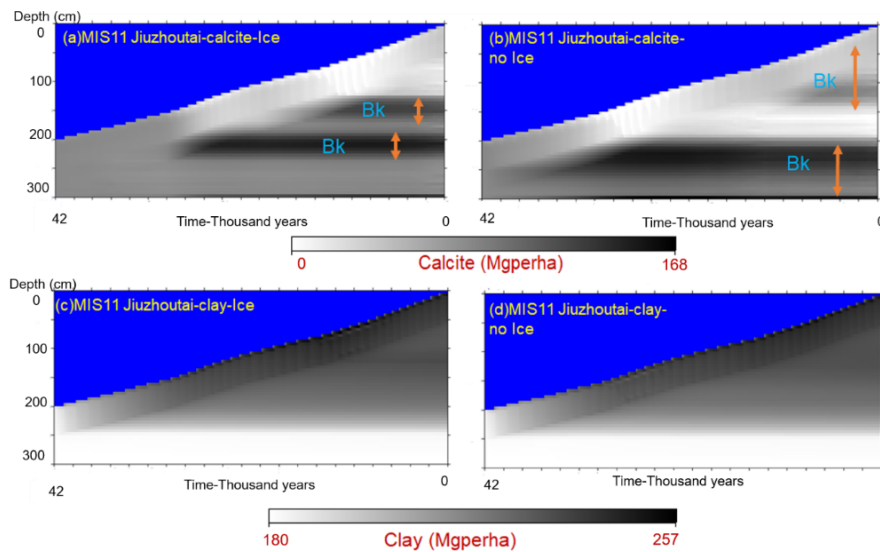


Figure 4-10 Evolution of calcite (top panel) and clay (bottom panel) in Jiuzhoutai (JZT) during MIS 11 in ice (OrbGHGIce) and no ice (OrbGHG) experiments. In (a) and (b) orange arrows depict the formation of calcic horizons (Bk). Note that the Bk forms near the surface soils at (b) than in (a).

4.3.3.2 Climate and soil response to NH ice sheets during MIS13

Figure 4-7g shows that in the first several thousand years of MIS13 the simulated annual mean precipitation is substantially reduced in response to larger ice sheets (**Figure 4-7f**), and it is reduced by up to ~300 mm in Chang'an (**Figure 4-7g**), and ~200mm in Xifeng (**Figure A4-6p in appendix**) and by up to ~150 mm in Jiuzhoutai (**Figure A4-6q**). In OrbGHGIce experiment, the precipitation drops at the peak of ice volume and increases during 514 -503 ka BP in response to greater insolation (at precession minima) and decreasing ice volume. In OrbGHGIce and OrbGHG experiments, the precipitation reaches its maximum during ~491-483 ka BP because ice volume change is small and precession is minimum (**Figure 4-7e**) during this period. Only in the OrbGHGIce experiment, the precipitation reaches a second small peak at 476 ka BP with the precipitation increasing by ~400 mm in response to relatively small ice sheet (**Figure 4-7f**) and Xifeng

(**Figure A4-6p**), and it increases by ~150 mm in Jiuzhoutai (**Figure A4-6q**). However, after 476 ka BP, the precipitation continues to decrease.

The simulated annual mean temperature (**Figure 4-7h**) is strongly reduced and fluctuated in response to large ice sheets at the beginning of MIS13, and is less until 503 ka BP (**Figure 4-7 h, orange line and Figure A4-6 r, s**). After 503 ka BP, the simulated annual mean temperature reaches its maximum between ~499 and 487 ka BP, where the ice volume change is very small. After 487 ka BP, the temperature difference is very small.

In Chang'an, the evolution of calcite and clay content in the S5-1 paleosol is highly sensitive to the simulated evolution of precipitation over the whole period. Due to the higher precipitation, calcite in the top soils dissolves in the first 39,000 years from the beginning of MIS13 (during 538-499 ka BP) in the no ice scenario (**Figure 4-11b**). At the same period, calcite remains in the surface and (sub) soils in the ice scenario (**Figure 4-11a**, gray areas). In the last 28,000 years of MIS 13 (after 499 ka BP), decarbonatization is fast in the ice scenario due to precipitation increase (**Figure 4-11a**, whiter areas), which in turn leads to the formation of a thick Bk horizon at the bottom of the profile. In both scenarios, these differences cause the formation of calcic horizons at different depths (sub soils and the bottommost of the profile).

The evolution of clay content is dissimilar between the two scenarios. Three illuvial horizons (Bt) become more developed through time in the no ice scenario (**Figure 4-11d**), whereas only one Bt is simulated in the ice scenario (**Figure 4-11c**). Clay migration noticeably starts 24,000 years before the end of MIS 13, and causes a uniform distribution (Bt) in the sub soils (between 100 cm - 250 cm) (**Figure 4-11c**).

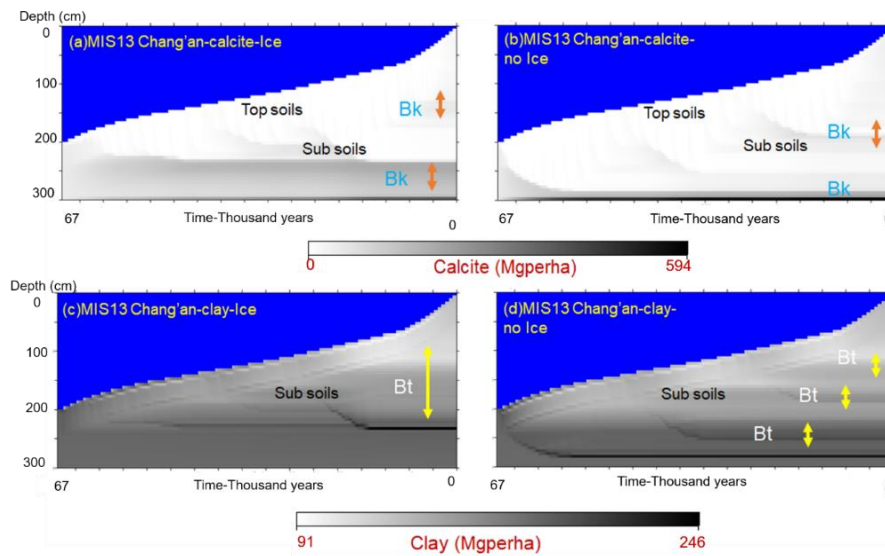


Figure 4-11 Evolution of calcite (top panel) and clay (bottom panel) in Chang'an during MIS13 in ice (OrbGHGIce) and no ice (OrbGHG) experiments. Orange and yellow arrows depict the formation of calcic horizons (Bk) and illuvial horizons (Bt).

In addition, we notice that paleosol response to precession is different in the ice scenario (OrbGHGIce) during MIS 13 (e.g Chang'an) as compared to the no ice scenario. In OrbGHGIce, we note that the first clay peak corresponds well to the first precipitation peak and appears just ~2000 years after the precession peak at 528 ka BP, in response to the increasing annual mean temperature (**Figure 4-12b**), whereas the first clay peak precedes precession in OrbGHG experiment (**Figure 4-12h**). A clay peak at 506 ka BP in the OrbGHGIce experiment is more or less in-phase with precipitation and with precession, whereas it lags precession by 6000 years in the no ice (OrbGHG) experiment (**Figure 4-12h**). In addition, there is an additional clay peak at 497 ka BP (**Figure 4-12d**), which is strongly corresponded to the annual mean temperature peak (**Figure 4-12b**), when both precession and obliquity are at maximum (**Figure 4-12**). Moreover, the two clay peaks (at 506 and 497 ka BP) are more or less joined (**Figure 4-12d**), due to increasing temperature during period 510-490 ka BP (**Figure 4-12b**). Therefore, it may represent one

clay peak corresponding to precession minima at 506 ka BP through its indirect control on interglacial precipitation and temperature.

In both OrbGHGIce and OrbGHG, clay peak approximately correlates with precession minima at 485 ka BP but with a few thousand years lag (**Figure 4-12d and h**). Therefore, it is evident that MIS 13 paleosols may exhibit three precession peaks in the ice experiment, when both precipitation and temperature are determined by the indirect influence of NH ice sheet-induced changes (**Figure 4-12, left**). As mentioned, the results are similar to the loess records in the CLP.

In the meantime, calcite shows an indirect and a very weak response to precession minima at 528 ka BP (**Figure 4-12c**) because calcite remains in soils in the first 8000 years of MIS 13 in the ice simulation (**Figure 4-11a**) as compared to the no ice simulation (**Figure 4-11b**). In both OrbGHGIce and OrbGHG, the delay of the calcite peak to precession is more or less the same at 506 ka BP (about 3000-4000 years) (**Figure 4-12c and g**). At 485 ka BP, the precession signal in the simulated calcite is noticeable in the ice simulation (**Figure 4-12c**), whereas a very weak peak is found in the no ice simulation (**Figure 4-12g**).

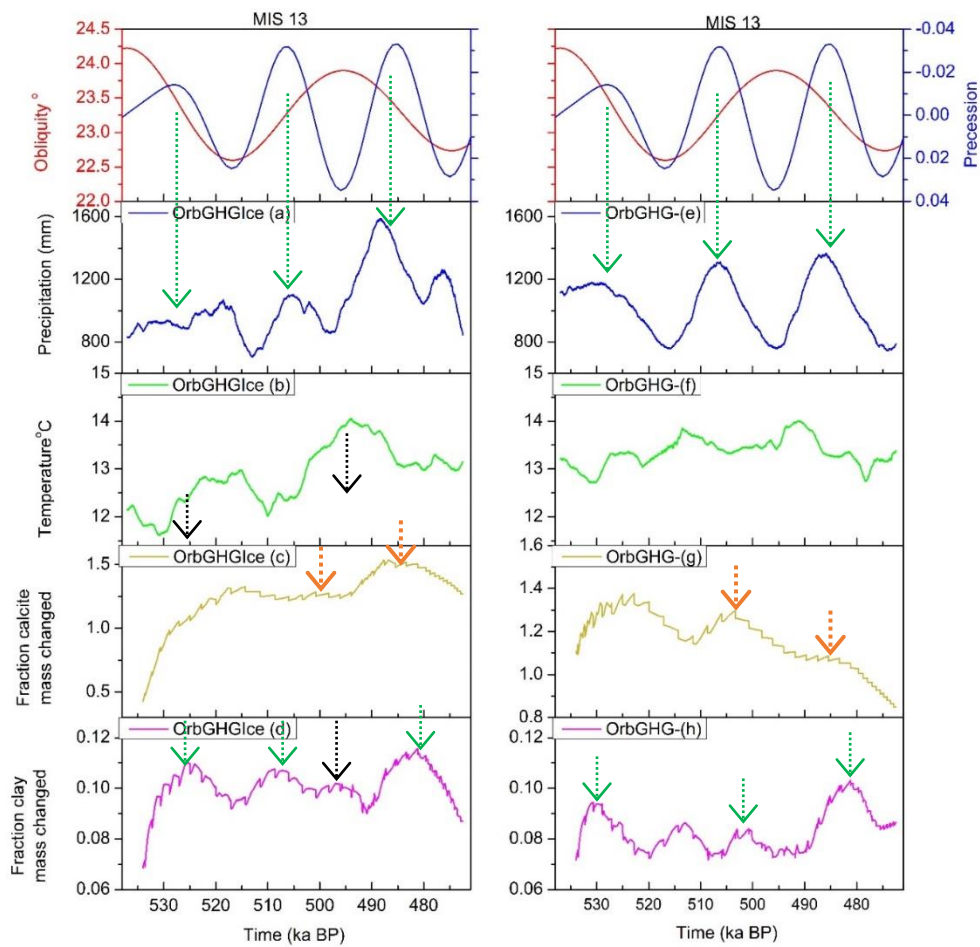


Figure 4-12 Comparison of soil development between the ice scenario MIS 13 (OrbGHGlce) and the no ice scenario (OrbGHG) in Chang'an. In each panel, from top to bottom obliquity and precession, annual mean precipitation (a, e), annual mean temperature (b, f), fraction mass changed of calcite (c, g) and clay (d, h). Green dash arrows show the link from precession to precipitation and finally to clay peaks and to calcite peaks (orange dash arrows). Black dash arrows show the effect of temperature increase on clay peaks.

In Xifeng, decarbonatization is evident over the whole duration of MIS 13 (whiter areas in the subsoils and top soils) in the no ice scenario (**Figure 4-13b**), whereas it is mainly visible in the last 24,000 years before the end of MIS 13 in the ice scenario (**Figure 4-13a**). Compared to no ice scenario (**Figure 4-13b**), in ice scenario (**Figure 4-13a**), most of the calcite are at the

bottom of the profile, as similar to calcite in Chang'an. The evolution of clay distribution at the end of MIS 13 in the S5-1 paleosol is mostly similar between the scenarios (**Figure 4-13c, d**). Compared to the no ice scenario (**Figure 4-13d**), clay content in the top soils is relatively larger in the ice scenario (**Figure 4-13c**, darker areas in the top soils) in the first 39,000 years of MIS 13: this may be due to the low precipitation, which lessens the intensity of clay migration during that period. However, clay migrates just below 200 cm depths (red arrow) when the precipitation increases in the last 24,000 years before the end of MIS 13 (**Figure 4-13c**).

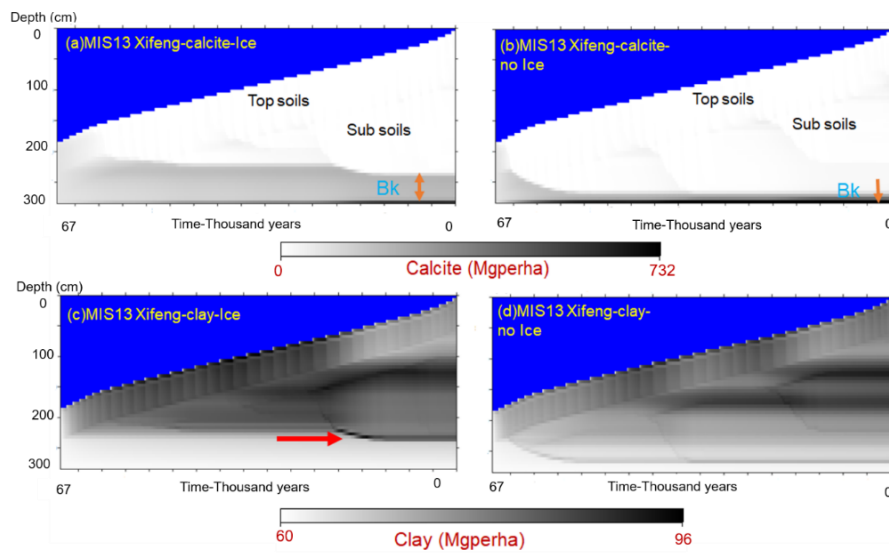


Figure 4-13 Evolution of calcite (top panel) and clay (bottom panel) in Xifeng during MIS13 in ice (OrbGHGIce) and no ice (OrbGHG) experiments. Orange arrows depict the formation of calcic horizons (Bk) and clay migration depths in red.

The simulated Jiuzhoutai paleosol in the NW Loess Plateau shows a very weak pedogenic effect in both scenarios (**Figure 4-14**). This is because the northwest CLP receives low precipitation. The weak pedogenesis in the northwestern CLP has been confirmed by many authors (e.g Ma et al., 2017, Sun et al., 2006a).

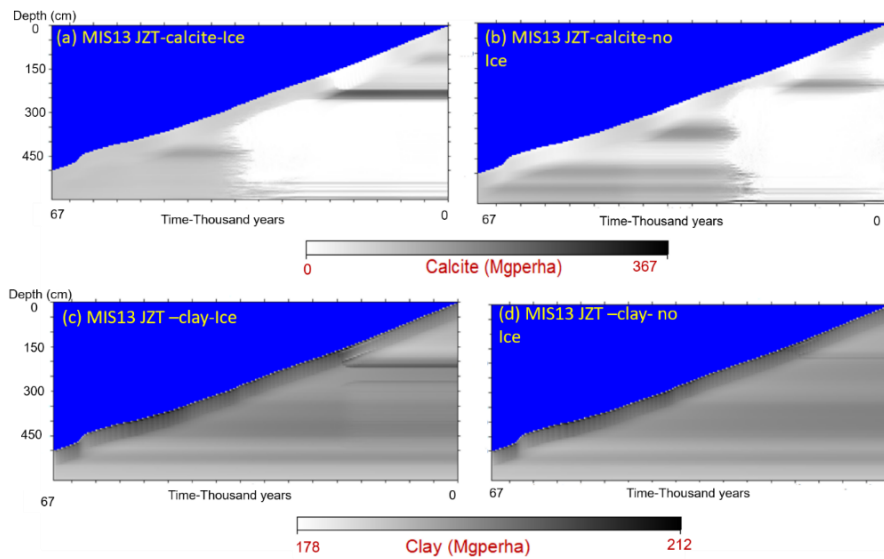


Figure 4-14 Evolution of calcite (top panel) and clay (bottom panel) in Jiuzhoutai during MIS 13 in ice (OrbGHGIce) and no ice (OrbGHG) experiments.

In summary, our results show that ice volume changes in the NH have an indirect impact on the simulated evolution of P, T, soil properties, and the depth pattern of soil properties. The simulated MIS 11 paleosol shows intense leaching of soil components in response to indirect effect of NH ice sheets through its control on precipitation, however with an initial delay of soil development. During MIS 13, the indirect impact of larger ice sheets on soil properties is apparent in the first 39,000 years of MIS 13, where the paleosol shows relatively less decarbonatization and clay migration in response to ice sheets, which is followed by an intense leaching at the end of MIS 13. The delay of soil development during MIS 13 is apparently low compared to MIS 11 in the beginning; however, there are larger ice sheets at the beginning of MIS 11 and MIS 13. MIS 13 shows strong carbonate leaching and clay migration than in MIS 11 interglacial. In both interglacials, the simulated paleosol show indirect response to ice-sheets that gradually declines from the southeast to the northwestern of the CLP, reflecting a minor response to the ice sheet impact and therefore its influence on precipitation over the northwestern CLP is low.

4.3.4 Comparison of simulated and observed S4 and S5-1 paleosols in the southeast CLP

In this section, a data-model comparison is made between the observed MIS 11 and MIS 13 paleosols in the Xi'an region (in the southern CLP) and the simulated Chang'an paleosols in the ice scenario. It has been reported that these two paleosols are the strongest paleosols on the CLP over the last 1Ma (Guo et al., 1998). Nevertheless, it is not appropriate to compare precisely the paleosol horizon sequences (in the field) with the simulation results. It is because SoilGen2 provides only quantitative expressions of soil properties but does not simulate soil horizon sequences. However, our purpose here is to make a general comparison between simulated and observed paleosols.

Previous studies found that the fourth paleosol (S4) in the CLP generally represents Ah-Bt-Ck- horizon sequence (Bronger and Heinkele, 1989), which can also be identified in our simulated S4 paleosols. In later studies, authors (Zhao et al., 2015; 2018) observed sub-horizon sequences of the S4 paleosol in Chang'an county in the southern CLP, Bt (~1.4-1.5m)-Cs-CI (weathered loess of ~1.9 m)-Ck (~0.2-0.3m). The simulated S4 paleosol in Chang'an shows a Bt horizon (~1.0 m) and a Bk horizon (beneath the Bt horizon). We think that the Cs-CI soil layers correspond to the soils below ~2 m in the simulated S4 paleosol (**Figure 4-15**). The above authors indicate that depth to CaCO₃ concretions is 3.3 m in the Chang'an area; this is consistent with the simulation results (~3.4 m). Therefore, we assume that the simulated S4 paleosol (**Figure 4-15**) is roughly comparable to these observed S4 paleosols in the CLP.

The fifth paleosol (S5-1) corresponds to MIS 13 and is a marker paleosol in the CLP (An et al., 1987). According to field surveys, S5-1 formed in Chang'an shows Bt1 and Bt2 horizons (Han et al., 1998), and pedogenic sub-horizons are observed in the S5-1 paleosol in the Chang'an loess section such as Bt- (~1m) with weathered loess layers, Cf(0.6m)-Cs(1.2m)-Cl(0.6m) (Zhao et al., 2014). The simulated S5-1 paleosol shows a thick Bt development in the sub

soils and a CaCO_3 enriched layer (Bk) at the bottom of the simulated profile (**Figure 4-16**). Another study (Huang et al., 2014) reported a strong Bt formation in the S5-1 paleosol and complete decarbonatization in the Weinan loess section. This indicates that CaCO_3 has migrated out of the Bt layer of S5-1 paleosol in the southeast region. The simulated MIS 13 paleosol show a poorly developed calcic horizon in the middle of the S5-1 profile, and most of the CaCO_3 accumulates firmly in the bottom of the profile with high CaCO_3 content varying between 8-55%. In general, the simulated paleosol development reasonably agrees with these findings of the southeastern CLP, where most of the S5-1 paleosol has been completely decarbonatized (Huang et al., 2014; Zhao et al., 2014). Carbonates are highly susceptible to leaching in the high rainfall regions.

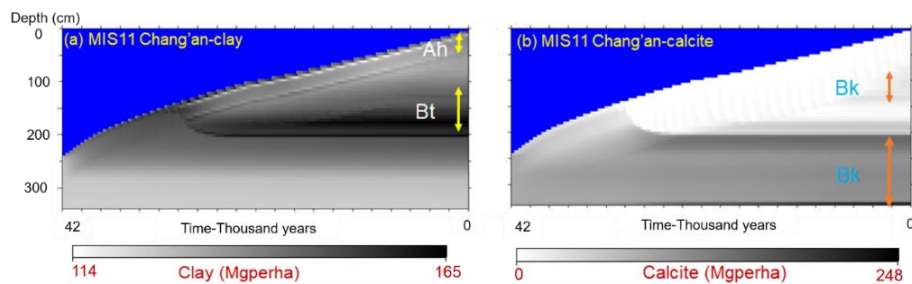


Figure 4-15 The simulated S4 paleosol in Chang'an during MIS 11, evolution of (a) clay, (b) calcite. soil horizons: Bt- clay illuviation, Bk- calcic, Ah- organic mineral top soils.

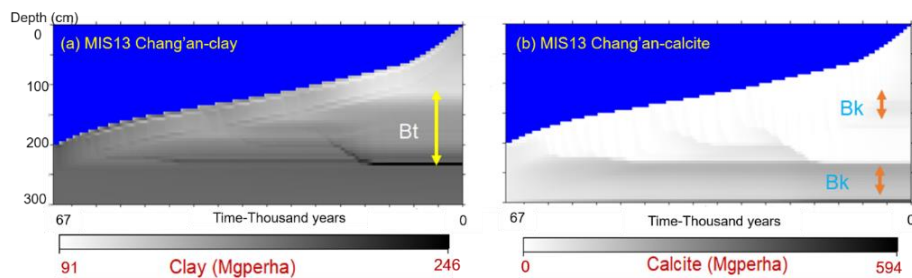


Figure 4-16 The simulated S5-1 paleosol in Chang'an during MIS 13, evolution of (a) clay, (b) calcite. soil horizons: Bt- clay illuviation, Bk- calcic.

4.4. Conclusions

The combined soil-climate model LOVECLIM1.3-SoilGen2 was used to investigate the driving factors of interglacial paleosol formation on the Chinese Loess Plateau and the effect of precession and ice volume on paleosol development.

Sensitivity analyses show that, in MIS 11, in decreasing order, precipitation, dust addition and potential evapotranspiration are sensitive factors for driving changes of calcite in the simulated paleosol; for clay, it is in the order of dust addition, precipitation and potential evapotranspiration. In MIS 13, the order of driving factors for calcite is identical to those of MIS 11, but there is no sensitive individual factor for clay. The combined effects of precipitation and dust addition are the best 2-factor combination. Adding potential evapotranspiration in the MIS 13 paleosol simulation shows a greater sensitivity for clay and calcite than in MIS 11. Therefore, during MIS 13, the leaching of calcite and clay is mostly controlled by precipitation deficit (PP-Evapotranspiration) rather than the precipitation. Overall, the sensitivity analysis revealed that dust addition, precipitation, and potential evapotranspiration are the most sensitive factors for interglacial paleosol development. Reconstruction of these inputs is essential to realistically simulate soil properties developing during an interglacial.

The simulated precipitation peaks and the simulated clay and calcite peaks on the CLP show indirect correspondence with precession minima. Therefore, the simulated paleosols (S1, S2, S3 and S5-1) illustrate an approximate relationship with precession in the four corresponding interglacials MIS 5, MIS7, MIS 9 and MIS 13. However, the relationship is relatively weak in the S4 paleosol due to the small amplitude of precession variation during MIS 11 due to its small eccentricity. We found that the precession minima and the simulated calcite are closely coupled, whereas it is less obvious for the simulated clay, reflecting the slow response time of the slow soil processes (clay migration) to precession. In addition, the simulated clay content in the S1, S2 (to a lesser extent) and S5-1 paleosols show a strong relation with

temperature. Our results are in reasonable agreement with the loess records in the CLP. Overall, the study suggests that precession minima coincides with enhanced monsoonal rainfall and paleosol development over the CLP.

Our model results show that ice sheet changes in the NH could have strong effect on precipitation and temperature on the CLP, in particular at the beginning and the end of the interglacials when ice sheets were large. In general, temperature decreases in response to ice volume increase, but precipitation response is more irregular due to the nonlinear effect of ice sheets on the precipitation in China. The erratic patterns of precipitation changes cause the differences of evolution of paleosol development over time and of soil properties over the depths. In both MIS11 and MIS13, the carbonate leaching and clay migration become greater in response to the smaller ice sheets at the end of the interglacials, but not in the start of the interglacials. During MIS11, paleosol development is retarded nearly by 12 000 years in response to large ice sheets at the beginning of the interglacial. In response to ice sheets, MIS13 shows greater carbonate leaching and clay migration than in MIS11. In both ice and no ice scenarios, soil expressions are gradually declined from the southeast to the northwestern of the CLP. Comparison of our model results with paleosol observations shows qualitative agreement.

Author contributions - Keerthika N. Ranathunga performed the research, data visualization, investigation, interpreting the results and writing of the first draft of the paper. Qiuzhen Yin conceptualized and designed the overall research, provided funding acquisition and reviewed, co-wrote the paper and supervised the research. Peter A. Finke conceptualized the soil modeling experiment, provided the software, reviewed, co-wrote the paper and supervised the research. Zhipeng Wu performed the climate simulations and reviewed the paper.

Acknowledgement

For the climate simulations, computational resources have been provided by the supercomputing facilities of the Université catholique de Louvain (CISM/UCL) and the Consortium des Équipements de Calcul Intensif en Fédération Wallonie Bruxelles (CÉCI) funded by the Fond de la Recherche Scientifique de Belgique (F.R.S.-FNRS) under convention 2.5020.11.

**CHAPTER 5. Soil modeling for Soil Loss
Tolerance estimations: Exploring natural
baselines and long-term variations**

*This chapter has been modified from published manuscript:
Ranathunga, K. N., Finke, P. A., Yin, Q., Verdoodt, A., & Yu, Y. (2021). Soil
modeling for soil loss tolerance estimations: Exploring natural baselines
and long-term variations. Global and Planetary Change, 204, 103548.
doi.org/10.1016/j.gloplacha.2021.103548*

Abstract

Quantification of soil stocks (= soil properties) and ecosystem services (ES) under changing climate need time series of climate and soil data. Here, we propose a new approach combining process-based soil and climate simulations to obtain such time series, and apply it onto a recent interglacial, MIS 5e. We combined the LOVECLIM1.3 climate model and the SoilGen2 soil evolution model to simulate soil development under two scenarios: dust addition plus erosion and erosion-only (both with five erosion rates corresponding to low, natural erosion rates: 0, 0.5, 1.0, 1.5 and 2.0 Mg ha⁻¹ y⁻¹). We quantified five target variables: two soil stocks, Exchangeable Bases (EB) and Soil Organic Carbon (SOC), and three ES: Carbon Sequestration Capacity (CSC), Water Yield (WY) and the ratio of actual over potential evapotranspiration (Ω) at four sites on an aridity gradient on the Chinese Loess Plateau (CLP). We used the obtained time series of these target variables to estimate Soil Loss Tolerance (SLT) threshold values over the full extent of MIS 5e (22 ka). Under increased erosion, EB increases while SOC always declines in both scenarios. In both scenarios, the simulated CSC increases with erosion; contrastingly, the WY decreases with increasing erosion rates. Both CSC, WY and Ω gradually decrease towards the northwest CLP (semi-arid region). For EB and SOC, the determined SLT thresholds are relatively higher in the dust addition than in the erosion-only scenarios, and strictly follow the climate gradient in the CLP. Combined performance index for (1-CSC), WY and Ω , showed that soil ES performance is worse above 1.0 Mg ha⁻¹ y⁻¹. This implies that benchmark levels must be chosen carefully. Our research highlights the potential of using SoilGen2 with LOVECLIM for quantifying soil-based ES and SLT.

Key words: Chinese loess plateau; exchangeable bases; soil organic carbon; carbon sequestration capacity; water yield; Last Interglacial.

5.1 Introduction

Soil is an important non-renewable natural resource and is recognized essential to sustainable development as it renders vast benefits to living beings (Bouma, 2014). These benefits, known as ecosystem services (ES), are classified into four groups: (i) provisioning services (e.g. food, fiber, fuel and fresh water for living beings), (ii) regulating services (e.g. regulating carbon sequestration, erosion control, water purification), (iii) cultural services (e.g. spiritual, religious, educational, recreation and tourism) and (iv) supporting services (e.g. nutrient cycling, habitat reservoir) (Costanza et al., 1997; DeGroot et al., 2002; MEA, 2005).

Dominati et al. (2010) defined the complex relationship between soil and ES by adopting the concept of natural capital. The soil natural capital represents soil stocks (= soil properties expressed on a mass basis) and constitutes the basis for providing soil-based ecosystem goods and services. Soil natural capital is characterized by both inherent (naturally inborn) and manageable properties. Inherent soil properties (e.g. soil depth, slope, texture) are stable properties that are unlikely to change at short-term (but likely at long-term) while manageable soil properties (e.g. soil organic matter, exchangeable bases) are changeable and can be modified through management practices. At long term, we define soil depth as a dynamic soil property, as a variable measure, that is influenced by soil formation factors and environmental conditions. For example, soil erosion decreases soil depth by topsoil removal and, consequently, topsoil organic matter stocks decline.

Soil formation (positive contribution) and degradation (negative contribution) processes underpin the soil natural capital, which subsequently affects the beneficial flows of soil stocks, i.e. the soil-based ES. Many authors have highlighted and agreed that the four groups of ES largely rely on soil (e.g. Bouma, 2014; Daily et al., 1997; Dominati et al., 2014, 2010) and many different soil-based methodologies and frameworks have been initiated (e.g. Calzolari et al., 2016; Fossey et al., 2020; Hewitt et al., 2015; Rutgers et al.,

2012). Adhikari and Hartemink (2016) reviewed extensive literature on the transfer of key soil properties to ES.

Additionally, authors (e.g. Dominati et al., 2010; Greiner et al., 2017) suggest that soil properties are not comprehensively studied in soil-related ES assessments. On the other hand, handling temporal variations of ES must involve dynamically changing soil properties instead of using fixed values (ex: concentration, measurement) collected at one time point. Furthermore, most of the ecosystem studies depend on soil databases, measurements and covering only few years or decades and long-term evolution of ecosystem services and soil stocks (=soil properties) is hardly known due to paucity of legacy data. To better quantify soil-based ES in long-term ES assessments, mathematical modeling of soil development comes as a potential promising alternative (to inventories of soil stocks). It furthermore offers a robust approach to study future ES changes and trends under climate change and human population induced land use and land management change. Process-based, dynamic soil models were highlighted as essential tools in assessing ES (Greiner et al., 2017). Several examples of soil modeling studies have been reported for quantifying ES (see table 2 in Vereecken et al., 2016) and by Lu et al. (2015).

The Chinese Loess Plateau (CLP) is one of the most erodible areas in the world. Our selections were based on ES studies, which describe ecological constraints in the CLP. In the topsoil, loss of soil nutrients and Soil Organic Carbon (SOC) have been widely discussed in response to water erosion (Cai, 2001; Liu et al., 2011; Li et al., 2016b). These soil nutrients (=exchangeable bases, EB), which are commonly regarded and evaluated for understanding the nutrient provision potential for plants in the ES frameworks (DeGroot et al., 2002; MEA, 2005), are included as a soil stock. Carbon Sequestration Capacity (CSC) (together with SOC stocks) and Water Yield (WY) have been intensively assessed in various aspects through different methodologies by various researches in numerous case studies at local, regional and watershed scales, as they are conceived as very important ES in this region vulnerable

to water erosion (Su et al., 2012; 2018; Lu et al., 2015; Lang et al., 2017; Feng et al., 2020; Yin et al., 2020).

Modeled climate time series data are essentially required as input in soil models. As climate plays a dominant role in soil natural capital formation, a clear understanding of how soil-based ES relate to climate dynamics is needed, and this research gap remains to be filled. Climate change likely influences ES, either positively (by developing soil properties) or negatively (by degrading soil properties). To our knowledge, no comprehensive long-term (millennium time scale) study has been conducted in a natural ecosystem with an advanced soil genesis model in combination with a climate model.

Nonetheless, the major external-inputs (e.g. soil erosion and deposition) are equally important to consider. Aeolian dust deposition in the CLP can increase the nutrient content and thickness of the existing surface soils. Deposition of thin layers of dust may contribute positively to the soil development by mixing with the existing soils (Kemp, 2001). Soil erosion is input as external-input during the study.

Regarding soil erosion, to distinguish human-caused accelerated erosion (i.e. rates exceeding soil formation rate) from natural erosion rates in terms of consequences for soil performance, terms like “permissible rates of soil erosion”, “natural erosion levels”, and “Soil Loss Tolerance (SLT)” have been employed (Boardman and Poesen, 2006; Li et al., 2009; Nearing et al., 2017).

Specifically, Verheijen et al. (2009) proposed to define SLT with reference to soil functions. According to the authors, SLT is “any actual soil erosion rate at which a deterioration or loss of one or more soil functions does not occur”—actual soil erosion being “the total amount of soil lost by all recognized erosion types”. Furthermore, the concept of SLT has been extensively applied not only for these on-site impacts but also to prevent off-site consequences by water erosion (e.g. sediment deposition and composition, flood control, water quality) and is being implemented in sustainable soil conservation strategies (Bazzoffi, 2009; Li et al., 2009; DiStefano and Ferro, 2016). In this study, in a natural context and using a pedon-scale model, erosion is considered as an

external-input and therefore common erosion models are not used, which are particularly employed for erosion assessment on arable lands.

Usually, both SLT and ES are studied from an anthropocentric perspective (Bouma, 2014) to evaluate how they fulfill human needs in a sustainable way. However, there are good reasons for evaluating ES and SLT in natural ecosystems with zero human influence: (i) to be set as a benchmark for anthropocentric study in the future use, while (ii) checking if a sensitivity of ES-performance to varying natural erosion rates exists, taking into account climate variability. The above considerations motivated us to study long-term evolution of the soil natural capital in a natural ecosystem by modeling both climate dynamics and soil development under various low (natural) rates of erosion to answer the following questions:

- (i) What are natural fluctuations in the soil EB and SOC stocks and ES?
- (ii) How are these related to natural (low) soil erosion rates?

If soil functioning would be found to have a marked change at certain low erosion rates, then a next question would be:

- (iii) What are SLT values for particular soil functions in natural ecosystems?

To answer the above questions, we combine a mechanistic soil development model, SoilGen2 (Finke and Hutson, 2008; Finke, 2012a) with a climate model of intermediate complexity, LOVECLIM1.3 (Goosse et al., 2010) to estimate how soil EB and SOC stocks and ES fluctuated in MIS 5e.

This leads to the following objectives:

1. To quantify two soil stocks: soil organic carbon (Mg/ha) and exchangeable bases (kmol+/ha) and three ES: water yield (mm), the ratio actual/potential evapotranspiration (Ω) and carbon sequestration capacity (Mg/ha).
2. To assess the effect of various natural (low) erosion rates on soil EB and SOC stocks and ES and thus identify SLT via modeling.
3. To assess the effect of a geographic climate gradient on soil EB and SOC stocks, ES and SLT.

In this study, we focus on the CLP, because soils dating back to past interglacials are well-preserved there, and at present, major erosion problems occur (Shi and Shao, 2000; Feng et al., 2016) that motivate research including the definition of baseline levels of erosion and SLT-estimates. The underlying assumption is that studies based on modeling are an alternative to the more common inventory-based studies on soil natural capital and ES and can additionally be used for prediction and for identification of SLT threshold levels.

5.2 Materials and Methods

5.2.1 Study locations and study periods

We focus on four paleosol sections– from northwest to southeast – Jingyuan, Xifeng, Luochuan and Chang’an in the CLP (**Figure 5-1**). The aridity percentile⁴ of Jingyuan is higher (86.9 %) than that of Xifeng (67.6%), and Luochuan (38.8%) and Chang’an (18.5%), denoting a moister climate at Chang’an. We evaluate the effect of soil erosion in a “natural environment”. Therefore, the last interglacial, MIS 5e (133-111 ka BP), was selected because it is one of the warmest interglacials during the Quaternary and is considered to some degree as an analogue to the future climate (Yin and Berger, 2012). Furthermore, for MIS 5e no assumptions about the (history of) land use have to be made since only natural vegetation occurred.

⁴ The aridity (ratio between average potential evapotranspiration and average precipitation) was mapped by Feng et al. (2004a) and will for each of the four sites be expressed as a percentile.

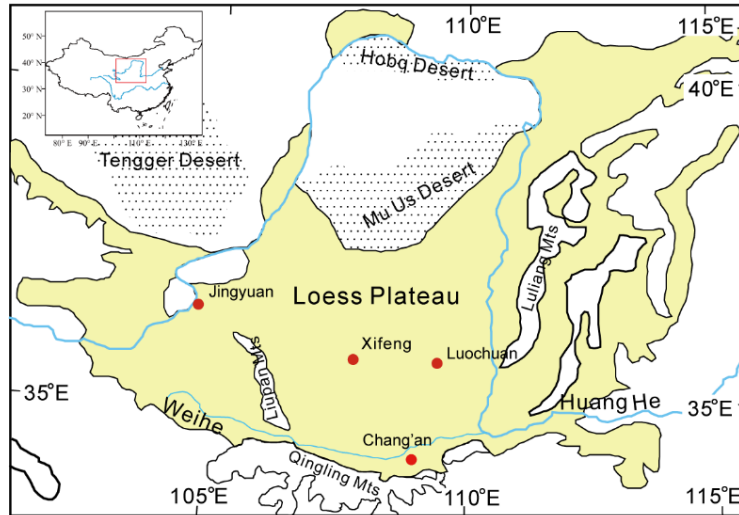


Figure 5-1 Geographic locations, from southeast to northwest Chang'an Luochuan, Xifeng, and Jingyuan in the CLP. Modified after Hao and Guo (2005).

5.2.2 The SoilGen2 model and input data

In order to calculate the soil EB and SOC stocks and ES, the long-term (22 ka) evolution of soil chemical, physical and biological properties and processes were simulated with the SoilGen2 model (Finke and Hutson, 2008; Finke, 2012a). We used the same initial data for the same sites along the southeast-northwest climate gradient earlier simulated by Finke et al. (2017). These data were obtained from a literature survey reported in detail by Finke et al. (2017) and Finke et al. (2021b). Initial mineralogy of the parent material was uniform over four sites. The basic properties of loess that we used in the study are in the Table 5-1 appendix for chapter 5.

The four vegetation types (grass/scrub, deciduous, coniferous, agriculture) in SoilGen2 have unique root distribution patterns and preferences for cation uptake. We applied a maximum rootable depth of 100 cm for both coniferous and deciduous forest, which is the depth of the initial profile and hence is the maximum value that can be given and reasonably its half value of 50 cm is

allocated for grass/scrubs. Bioturbation, was linked to the vegetation type: 8.4 Mg ha⁻¹ y⁻¹ over 40 cm depth for deciduous forest and 16.4 Mg ha⁻¹ y⁻¹ over 45 cm depth for grassland. These values are based on Gobat et al. (1998, p.122).

Aeolian dust deposition and soil loss by water erosion were input as follows: time series data of dust addition or erosion are external-input as events in the soil model. Event data consists of simulation year(s) during which an event occurs and number of compartments (mm) that will be affected by the event.

This dust addition rhythm were based on Guo et al. (2009) and these time series were scaled to site-specific dust deposition rates using spatially distributed total dust addition thickness data for MIS 5e (Lu and Sun, 2000) and are between 10-50 mm/ka in Southeast and Northwest CLP respectively.

The four erosion rates were incorporated through removing compartments (of 50 mm) from the topsoil in the model at time intervals reflecting the erosion rate. Thus, a continuous erosion process is mimicked by regular erosion “events” removing one compartment at a time. The total number of compartments removed at each erosion rate dictates the necessary initial soil depth so that at least 1000 mm of soil profile remains at the end of the simulation. This minimum thickness equivalent to 20 compartments was chosen to ensure numerical stability of the SoilGen2 model. In essence, the timing of soil erosion “events” during MIS 5e is needed as input data in the model. Hereto, it is necessary to calculate how many years it takes to remove one soil compartment. This way, we can introduce soil erosion into the model over the full simulation period. For example, here we calculate the annual soil depth lost and the time interval (years) required to remove a 50 mm (=T) soil compartment for each of the defined erosion rates (Mg ha⁻¹ y⁻¹) as a function of soil Bulk Density (BD) using the following equations **Eq. [5-1]** and **Eq. [5-2]**.

$$\text{Soil depth lost per year (m)} = \frac{\text{Erosion rate} \left(\frac{\text{kg}}{\text{m}^2 \cdot \text{year}} \right)}{\text{Bulk density} \left(\frac{\text{kg}}{\text{dm}^3} \right)} \times 10^{-3}$$

Eq. [5-1]

Years taken to remove $T(m)$ thickness =

$$T \times \frac{\text{Bulk density} \left(\frac{\text{kg}}{\text{dm}^3} \right)}{\text{Erosion rate} \left(\frac{\text{kg}}{\text{m}^2 \cdot \text{year}} \right) \times 10^{-3}}$$

Eq. [5-2]

Table 5-1 shows the relation between the erosion rates ($\text{Mg ha}^{-1} \text{y}^{-1}$), the number of soil compartments removed by erosion over the full duration of MIS 5e, and the necessary total soil profile thickness (m) at the start of simulation and years to remove 0.05 m.

Table 5-1 Description of the soil erosion scenarios implemented in the event file in SoilGen2.

Soil erosion rate ($\text{Mg ha}^{-1} \text{y}^{-1}$)	Number of compartments removed from the soil profile over 22 ka	Total soil thickness removed (m)	Years to remove 0.05m of soil layer
0.5	19	0.95	1150
1.0	38	1.90	575
1.5	57	2.85	383
2.0	76	3.80	287

5.2.3 Climate simulations

The LOVECLIM1.3 simulation covers the time span of 22 ka from 133 to 111 ka BP onto four grid cells covering the entire loess plateau. The ice sheets are fixed to their present-day state, while keeping two main climate forcings: Greenhouse Gas (GHG) concentration (CO_2 , CH_4 and N_2O) and latitudinal and seasonal variation of insolation. Time series of monthly mean temperature

(T), precipitation (P) and potential evapotranspiration (Ep) were input in the SoilGen2.

5.2.4 Soil EB and SOC stocks, Ecosystems and scenario

Two major scenarios were applied: one with dust addition combined with soil erosion and the other with only soil erosion (no dust addition). Twenty runs were simulated for each scenario: five soil erosion rates for four sites for assessing Soil Loss Tolerance (SLT).

5.2.4.1 Soil organic carbon

SoilGen2 simulates the mass of organic carbon (Mg/ha) per five-cm compartment, for each year over the total period. This output is aggregated over the top 30 cm. The topsoil organic carbon stock (SOC) then follows from Eq. [5-3]

$$SOC \left(\frac{Mg}{ha} \right) = \sum_{c=1}^6 (SOC_c) \quad \text{Eq. [5-3]}$$

Where SOC_c indicates simulated mass of Soil Organic Carbon (Mg/ha) per depth of five cm.

5.2.4.2 Exchangeable bases

The exchangeable bases (EB) is defined as the sum of the macronutrients calcium (Ca), magnesium (Mg), potassium (K) and sodium (Na) on the exchange complex. It thus represents that part of the Cation Exchange Capacity (CEC) occupied by exchangeable bases. The CEC is in SoilGen2 a variable of the clay and organic matter content. SoilGen2 aggregates the exchangeable bases for each year over 30 cm as in Eq. [5-4]:

$$EB \left(\frac{kmol+}{ha} \right) = \sum_{c=1}^6 (X Ca_c + X Mg_c + X K_c + X Na_c) * \rho_c \times 0.5$$

Eq. [5-4]

Where EB represents the summation of major exchangeable basic cations, XCa_c , XMg_c , XK_c , and XNa_c in mmol+/kg soil in compartment c (5 cm), ρ_c is

the bulk density (kg/dm³) in this compartment and 0.5 is the conversion factor from mmol+/kg to kmol+/ha, accounting for compartment thickness. The soil bulk density varies in the soil compartment over time, however the model assumes constant volume in each soil compartment during simulations.

5.2.4.3 Organic carbon sequestration capacity

Concerning the carbon sequestration capacity (CSC), as stated by many authors (Six et al., 2002; Stewart et al., 2007; Angers et al., 2011; Feng et al., 2013), the capacity to sequester additional SOC in soils is the difference between the maximum “theoretical” capacity and current SOC level in the soil’s fine particles. Following this view, we use the Hassink (1997) approach to define the maximum carbon-saturation in the simulated soils, and the difference between the amount SOC already present and the maximum in the upper 30 cm in soil was used for CSC estimation.

The maximum carbon storage in a soil is defined here by the carbon saturation level (C_{sat} , g/kg soil). C_{sat} is calculated in each simulation year by using the protocol that has been derived by Hassink (1997):

$$C_{sat} \left(\frac{g}{kg} \right) = 4.09 + 0.37 \times (\% \text{ particles} < 20\mu\text{m}) \quad \text{Eq. [5-5]}$$

Eq. [5-5] describes the total carbon in soil associated with soil particles less than 20 μm , thus the clay and part of the silt fractions, which change due to soil development processes. Then, CSC (Mg/ha) is estimated as follows for the upper 30 cm of soil:

$$CSC \left(\frac{Mg}{ha} \right) = \sum_{c=1}^6 ((C_{sat\ c} \times \rho_c \times 0.5) - SOC_c) \quad \text{Eq. [5-6]}$$

Where, ρ is the bulk density (kg/dm³), which is also a variable. 0.5 is used as unit conversion to Mg/ha per compartment (c) of 0.05 m. SOC_c (Mg/ha) is the soil organic carbon stock in a particular year. CSC (Mg/ha) is calculated through the difference between C_{sat} and SOC in that year.

5.2.4.4 Water yield

In the evaluation of ES, water can perform functions such as either water regulation (e.g. control floods) or water supply (e.g. plant available water content) (Dominati et al., 2010) and these are very strongly linked. Here we consider water yield (WY) the loss of water below the root zone, and the ratio actual/potential evapotranspiration (Ω) to indicate plant water stress. We estimate how much water leaves the soil profile (=drainage), after plant water uptake, surface evaporation and interception evaporation associated with vegetation type. We take as root zone the upper 1m of soil depth, corresponding to the deepest root zone of the possible vegetation types (i.e. that of deciduous forest). We calculated overland flow by considering all non-infiltrating water to be runoff and assumed that both overland flow and drainage below the root zone contribute to basins, rivers and ground water recharge. However, since SoilGen2 is a 1-D model we did not simulate the flowpaths of water lost from the soil profile, as in landscape-scale studies.

Model runs showed that the long-term average surface runoff was less than 1% of the net precipitation for both scenarios (dust+erosion and only erosion) for both the most arid and the least arid plots. The low surface runoff was due to the high (natural) vegetation cover and flat terrain position in the simulated plots as well as the high infiltration capacity of the loess soils relative to the rainfall intensity. Then, annual water yield (=drainage) can simply be calculated as follows:

$$\text{Water Yield (mm)} = P - \sum_{t=0}^{365} \sum_{c=1}^{20} Ea_{tc} \quad \text{Eq. [5-7]}$$

Where P stands for the annual precipitation (mm), (site level precipitation) and Ea_{tc} is the actual evapotranspiration (mm), which is summed over 20 compartments c (1m) and per day t .

Then, to estimate how much water is available for plants (Ω) we use the potential evapotranspiration (E_p) from LOVECLIM1.3 on an annual basis, thus we obtain:

$$\Omega (-) = \frac{\sum_{t=0}^{365} \sum_{c=1}^{20} Ea_{tc}}{Ep} \quad \text{Eq. [5-8]}$$

5.2.4.5 Assessing the soil loss tolerance

Various definitions of SLT have been adopted in the past (Wischmeier and Smith, 1979; Sparovek and De Maria, 2003; Boardman and Poesen, 2006; Li et al., 2009; Alewell et al., 2015; Duan et al., 2017). Given the natural setting in our study, the most appropriate legacy definition of SLT is the soil erosion rate that equals more or less the soil formation rate. Thus, SLTs are usually derived through soil formation rates from bedrock material. However, for specific environments such as loess deposits, parent material for interglacial soil, estimating SLT value is very tricky, because it has no relation to the underlying bedrock. Therefore, we refine this definition by setting the SLT at that rate of erosion above which a deterioration of soil stocks (soil properties) and ES performance occurs. An erosion rate of 2.0 Mg ha⁻¹ y⁻¹ is considered the upper limit of natural erosion rates in the CLP where plateau landscape is assumed and simulated and include 5 erosion rates: no erosion, 0.5, 1.0, 1.5 and 2.0 Mg ha⁻¹ y⁻¹. The selected erosion rates are very small (insignificant) compared to accelerated soil erosion rates. Human-induced accelerated erosion did not occur during MIS 5e, which motivates our choice of erosion rates and our selections accord with natural and geologic erosion rates as reported by Granger et al. (1996), Wilkinson and McElroy (2007), Nearing et al. (2017, in there table 1 shows erosion rates within the range of 0.8–1.9 Mg ha⁻¹ yr⁻¹). Moreover, we assume that these minimum natural erosion rates gradually continue over a very long period (22 ka) (although the model does this pulsewise by removing soil compartments).

We obtain SLT by evaluating how much the EB and SOC stock, over MIS 5e, responds to various erosion rates, and identifying at what erosion rate a marked change occurs (this was identified based on cumulative amount). A marked change is visually identified when the difference of a stock between two adjacent erosion rates is clearly larger than the difference between two other adjacent erosion rates, e.g. the difference between rates 1.5-2.0 is larger than that between 1.0 and 1.5 Mg ha⁻¹ y⁻¹. Potentially, each individual soil EB

and SOC stock and ecosystem service may lead to a different SLT. Therefore, we propose to combine performance indicator based on the three quantified ES as follows:

1. For each ES (CSC, WY, Ω), calculated using Eq. [5-6], [5-7] or [5-8], we obtain a performance indicator PI for each erosion rate e at a site s in one of both scenarios by dividing the calculated ES by the maximum ES over the 5 erosion rates for this site:

$$PI_{ES,e,s} (-) = \frac{ES_{e,s}}{\max ES_{e=0, 0.5, 1, 1.5, 2.0}} \quad \text{Eq. [5-9]}$$

2. A combined performance indicator CPI for each erosion rate, site and scenario is calculated by multiplication:

$$CPI_{e,s} (-) = PI_{(1-CSC),e,s} \times PI_{WY,e,s} \times PI_{\Omega,e,s} \quad \text{Eq. [5-10]}$$

5.3. Results and discussion

5.3.1. Spatio-temporal trends in simulated climate and vegetation

Downscaled climate data (P and T) representative for the four sites are given in **Figure 5-2**. In **Figure 5-2**, year zero indicates the end of the interglacial. The simulated climatic data capture the climatic gradient that prevails on the plateau during the entire Quaternary (Feng et al., 2004a). Chang'an in the southeast receives the highest precipitation (on average 915 mm) whereas northwest located Jingyuan is characterized by the most strongly expressed semi-arid conditions, with the lowest precipitation (on average 330 mm) (**Figure 5-2a**). All four sites show a much wetter first half of the interglacial and a dryer second half. The variation of precipitation follows well the variation of the boreal summer insolation which depends strongly on the climatic precession and is the main controlling factor of the East Asian precipitation (Yin et al., 2009). The high precipitation in the first half of the simulation period corresponds to a time of high summer insolation, and the low precipitation in the second half of the simulation period corresponds to low summer insolation.

The precipitation reaches a minimum about 18,000 years from the start of the interglacial and increases again after. This is because summer insolation reaches a minimum about 18,000 years from the start of the interglacial and increases after. This change in climate forcing has been well captured in the climate model. The annual mean temperature increases from Jingyuan to Chang'an, the 1000-year moving average ranging roughly from 6°C to 14°C (**Figure 5-2b**). The highest mean temperatures occur during the second half of the interglacial at all sites.

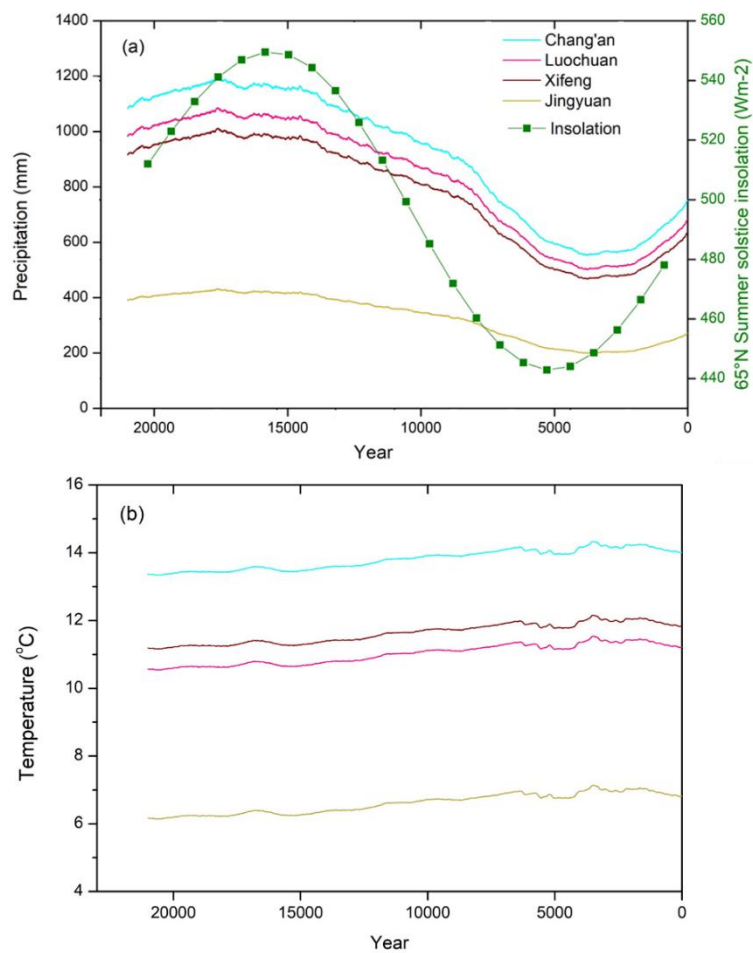


Figure 5-2 A 1000-year moving average applied to the simulated climatic data for the MIS 5e (duration 22000 years, x axis) at the four locations: annual mean (a) precipitation (mm) and (b) temperature (°C). Green dotted line indicates the summer insolation during MIS 5e.

Vegetation types (output at coarse scale of LOVECLIM1.3) respond to the degree of aridity (Ep/P) at each particular site, and thus regional scale vegetation types differ along the climatic transect as well, both in space and time. During MIS 5e, deciduous forest is found in 96%, 85% and 61% of the years in Chang'an (wettest site), Luochuan, and Xifeng respectively. During the drier periods at each of these sites, grass/scrub vegetation is found. Jingyuan (driest site) by contrast predominantly has grass/scrub vegetation in 87% of the years, and deciduous forest in the less frequently occurring wetter periods.

5.3.2 Soil EB and SOC stocks evolution and SLT

5.3.2.1 Assessment of exchangeable bases

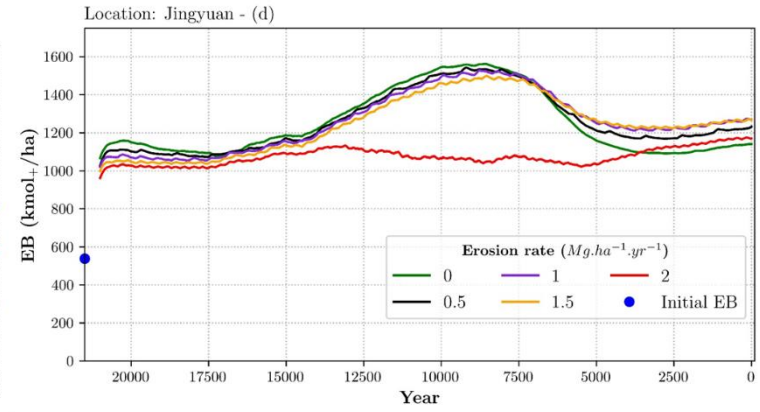
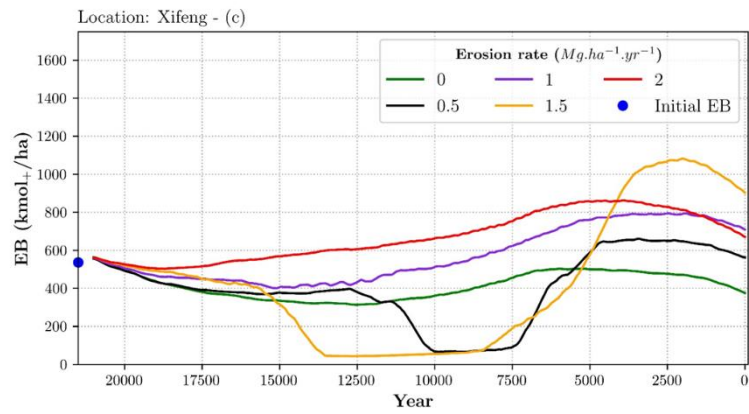
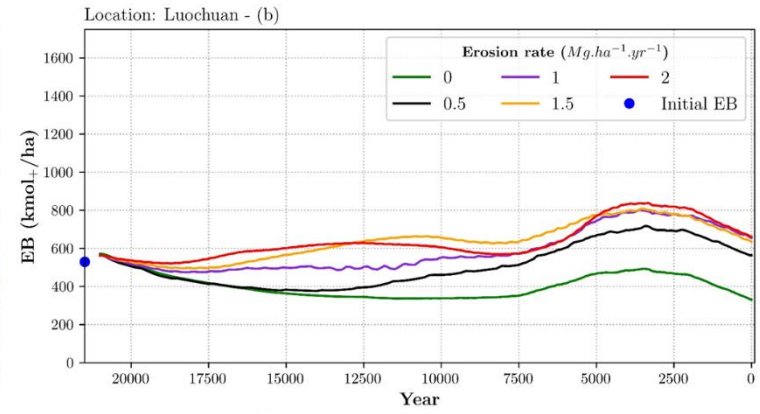
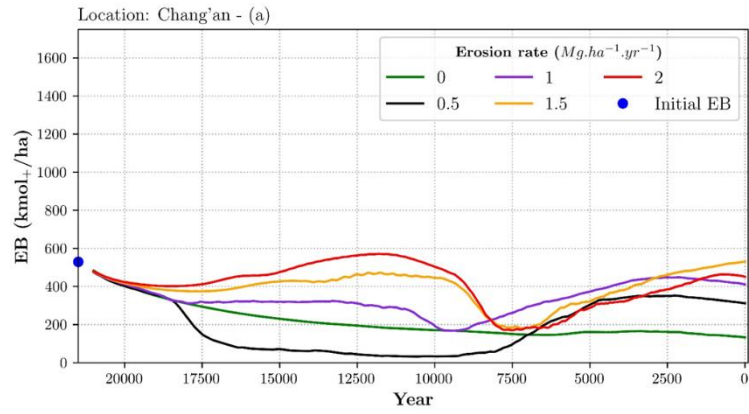
Figure 5-3 presents the evolution of the absolute amounts of EB. For all the sites in both scenarios, the evolution of EB stock, for the duration of MIS 5e, can be explained by simulated soil profile distributions of calcite and total exchangeable bases, which are similar. As the CLP soils developed in calcite-rich loess parent material and calcite-rich added dust, the simulated EB were dominated by calcium ions in the soils. Also the initial exchangeable Ca^{+2} dominated the exchangeable bases (**Table A5-1 in appendix for chapter 5**). For all the sites (**Figure 5-3**) in both scenarios, the calculated EB increases with erosion at the end of the interglacial (rightmost).

The evolution of EB fluctuated depending on the total amount of base ions in the top soils, and a large decrease of bases can be related to loss of calcite. When soil erosion depletes calcite in the soils, the EB decreases (whiter areas), and if the top soil contains a calcite rich layer, the EB increases (darker areas).

In erosion only scenario (location-Chang'an in **Figure 5-3a**), an erosion rate of $0.5 \text{ Mg ha}^{-1} \text{ y}^{-1}$ depletes the initial soils exchangeable bases because the litter layer is removed, which is a source of basic cations, and thus the base cation nutrient pump by the vegetation is weakened. The nutrient pump is not weakened at zero erosion. Simulated exchangeable bases (**Figure 5-4a**) and calcite profile distributions (see also **Figure 5-4b**) show very low bases in the

top soils early in the time series (whiter areas in **Figure 5-4a, b**). At erosion rates above $0.5 \text{ Mg ha}^{-1} \text{ y}^{-1}$, the calcite-rich layer is exposed by erosion in Chang'an (for example at $2.0 \text{ Mg ha}^{-1} \text{ y}^{-1}$ **Figure 5-4c, d**), and this leads to higher EB (**Figure 5-3a**).

In Xifeng (**Figure 5-3c**), EB during part of the interglacial is less than that at zero erosion for rates of $0.5 \text{ Mg ha}^{-1} \text{ y}^{-1}$ (**Figure 5-5a, b**), and $1.5 \text{ Mg ha}^{-1} \text{ y}^{-1}$ (**Figure 5-5c, d**). The weakened nutrient pump (removal of litter layer containing cations) and the depths of removal and accumulation of calcite are influencing the EB (**Figure 5-5**), but not in a straightforward way because of interacting processes. However, at the end of the interglacial (rightmost), the net effect is that increasing erosion rates increase the EB, as in Chang'an, but values of EB at Xifeng are higher because the drier climate leads to shallower calcite accumulation and thus easier exposure by erosion (**Figure 5-5e, f**). In Jingyuan (**Figure 5-3d**), most of the EB are higher in the middle of the interglacial, while the EB lowers at $2.0 \text{ Mg ha}^{-1} \text{ y}^{-1}$ due to erosion in the top soils (**Figure 5-6a, b**).



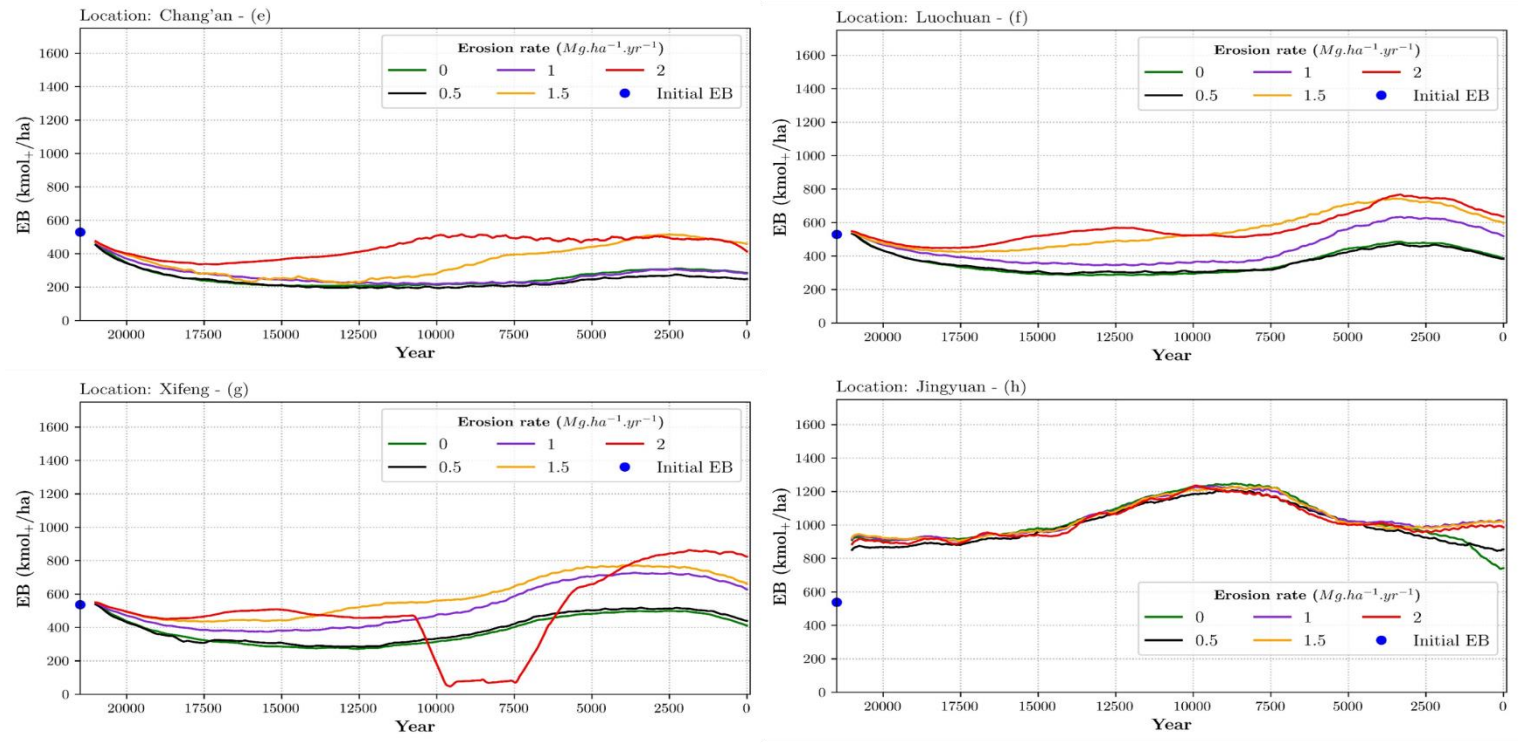


Figure 5-3 Effect of natural erosion rates on EB evolution, in erosion-only (a, b, c, d) and dust addition plus erosion scenario (e, f, g, h). X-axis is simulation year and y-axis is scaled to 1600 kmol₊/ha. A blue dot at the y-axis represents initial EB value determined by the parent material at the start of simulation. Colored lines denote different rates of erosion.

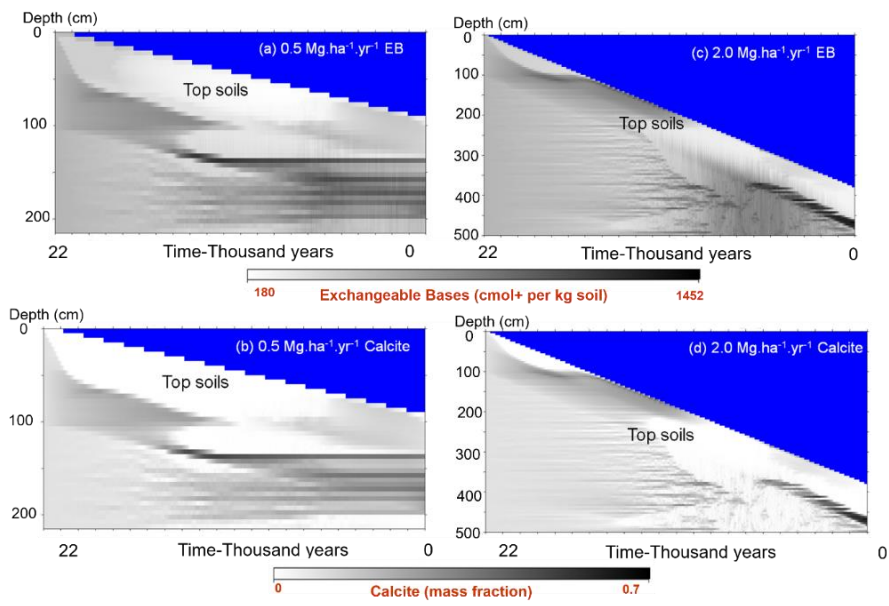


Figure 5-4 Comparison of simulated exchangeable bases and calcite distribution for soils in Chang'an in erosion-only scenario.

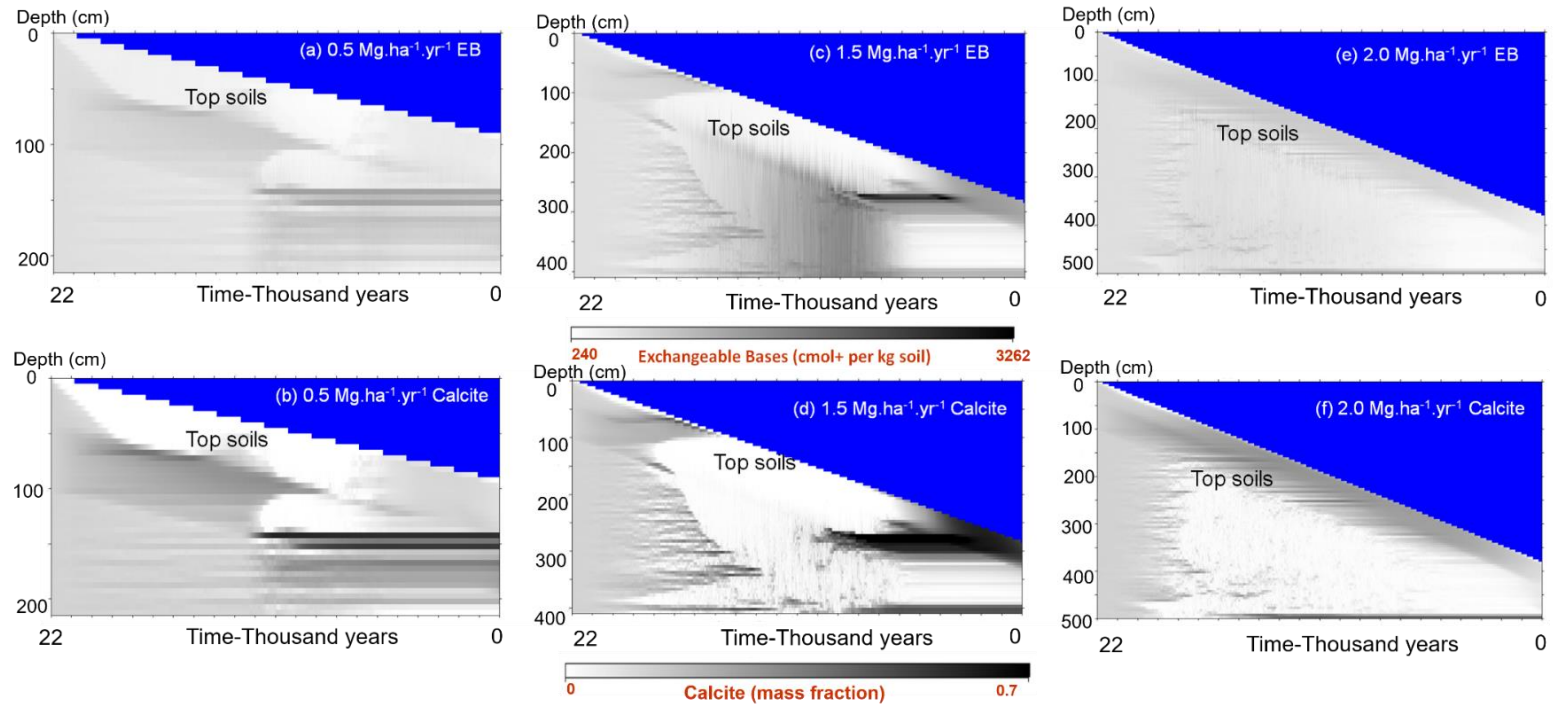


Figure 5-5 Comparison of simulated exchangeable bases and calcite distribution for soils in Xifeng in erosion-only scenario.

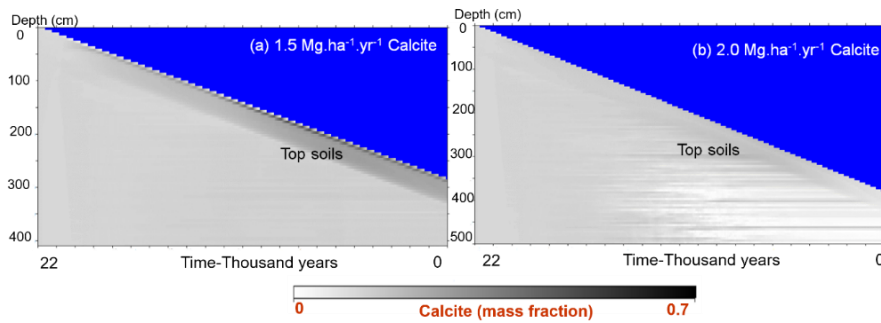


Figure 5-6 Comparison of simulated calcite distribution between 1.5 and 2.0 $\text{Mg ha}^{-1} \text{ yr}^{-1}$ for soils in Jingyuan in erosion-only scenario.

Similarly, in the dust addition plus erosion scenario, the EB and calcite distribution together explain both the decrease and increase of EB in Xifeng at $2.0 \text{ Mg ha}^{-1} \text{ yr}^{-1}$ (**Figure 5-3g** and **Figure 5-7 a, b**). As mentioned before, in Jingyuan (**Figure 5-3h**), EB increases due to reaching calcite rich top soil layers at 1.5 and $2 \text{ Mg ha}^{-1} \text{ yr}^{-1}$ erosion at the end of the interglacial (**Figure 5-8 a, b**). At Jingyuan a little change of EB was observed over time and for different erosion rates in the first 20 ka (**Figure 5-3h**).

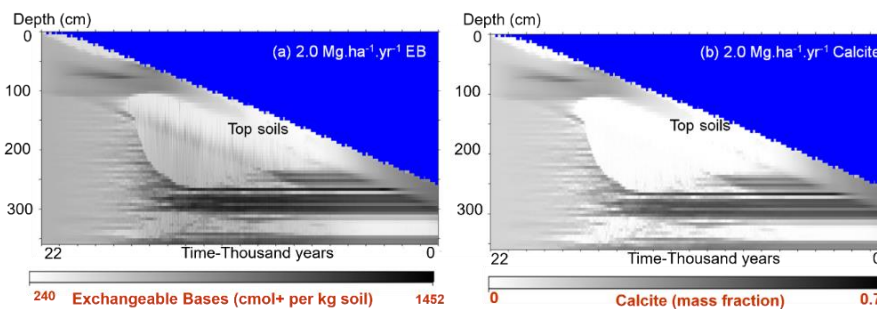


Figure 5-7 Comparison of simulated exchangeable bases and calcite distribution for soils in Xifeng in dust addition plus erosion scenario.

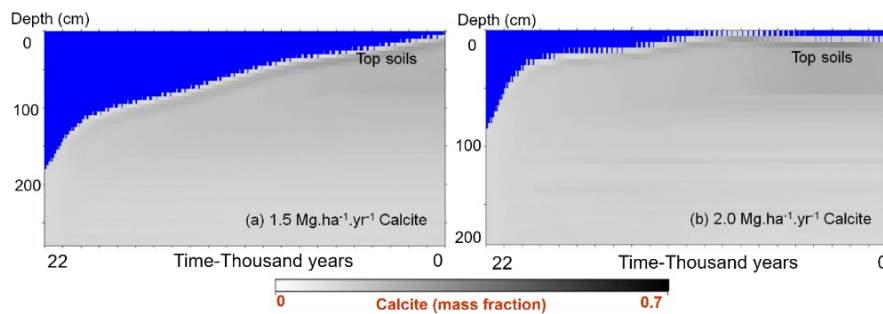


Figure 5-8 Comparison of simulated calcite distribution between 1.5 and 2.0 $\text{Mg. ha}^{-1} \cdot \text{yr}^{-1}$ for soils in Jingyuan in dust addition plus erosion scenario.

These findings suggest that depending on the initial amounts of bases, calcite contents in the parent material and in the added dust and the intensity of calcite, leaching and clay migration processes in different locations together regulate exchangeable bases in the studied soils. The EB decreases from Jingyuan to Chang'an by following the climate gradient in the CLP. In general, the lowest EB was found at the moist Chang'an due to leaching of base cations from the surface soil and the highest EB is found at Jingyuan because of less leaching and intense loess accumulation.

Overall, our findings suggest that increasing erosion rates have a positive effect on exchangeable bases within the context of chosen natural erosion rates in the CLP soils. **Table 5-2** represents rates of erosion with respect to EB, where major differences occur (increasing /decreasing) along the climatic gradient for each case (=SLT). In general, at the three sites with the most expressed summer monsoon (e.g. Chang'an, Luochuan and slightly in Xifeng), the SLT indicates the erosion rate above which EB increases due to reaching calcite-rich soil layers and at the most arid site (Jingyuan), the SLT indicates the erosion rate above which the EB decreases (or no effect of erosion).

Table 5-2 SLT values for EB for four locations.

Exchangeable Bases	Chang'an	Luochuan	Xifeng	Jingyuan
	soil loss tolerance values (Mg ha ⁻¹ y ⁻¹)			
Dust addition plus Erosion	Above 1.0	Above 0.5	Above 0.5	No effect
Erosion only	Above 0.5	Above 0	Above 1.0-1.5	Above 1.5

5.3.2.2 Assessment of soil organic carbon

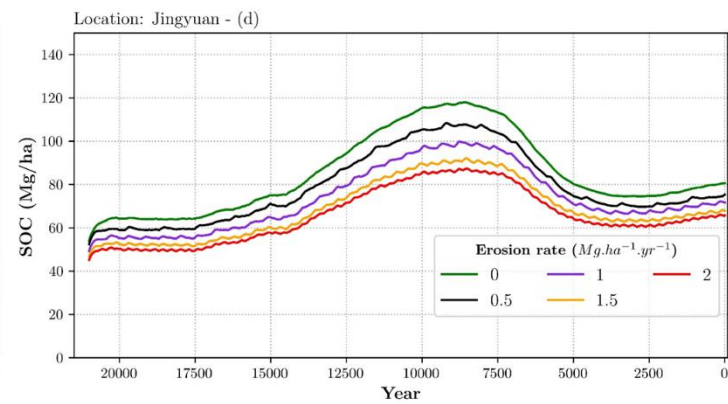
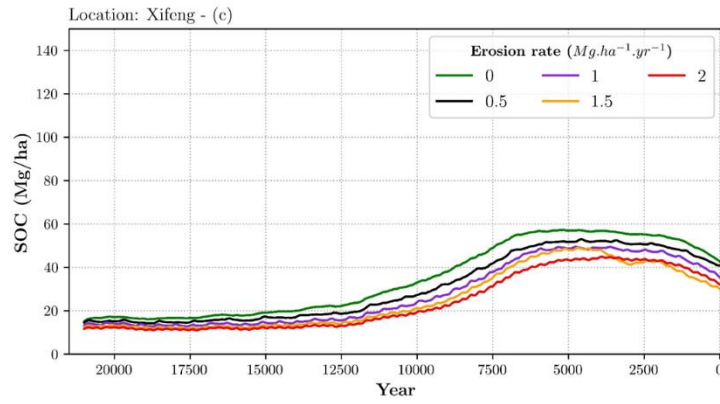
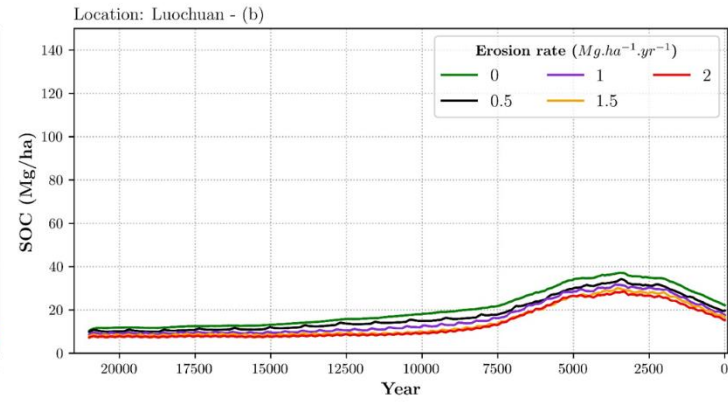
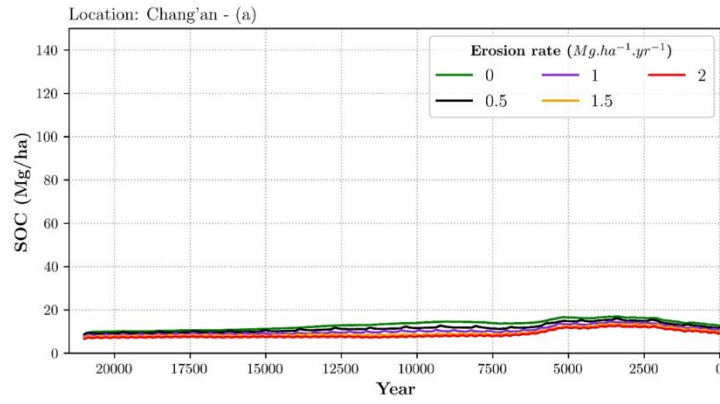
Figure 5-9 presents the evolution of the absolute amounts of SOC. These SOC indicate a decrease of SOC at increasing erosion rate in the erosion-only (**Figure 5-9a, b, c and d**). In the dust addition plus erosion scenario (**Figure 5-9e, f, g and h**), where the SOC-evolution pattern is ambiguous due to combined effects of both erosion and dust deposition, where dust deposition gradually buries the litter layer which then becomes incorporated in the soil.

The observed pulses in **Figure 5-9** are due to both dust addition and soil erosion processes defined in the model. At an annual scale, dust addition first leads to a lower OC in the new top layer and buries the old top layer plus the litter layer below. Erosion removes the top layer and the litter layer and thus depletes SOC. Depicted as a moving average, these pulses are somewhat dampened. The simulated patterns of the effect of dust deposition and erosion on OC are presented in **Figure A5-5 in appendix for chapter 5**.

In addition, less SOC is a result of strong SOC decomposition at moist and warm locations such as Chang'an and Luochuan. Therefore, considering the location effect, the calculated SOC is minimal at Chang'an, due to high decomposition rates and the effect of the erosion rate is minimal (**Table 5-3**). A high amount of SOC was modeled at Jingyuan, because of low decay rates in a cold and dry climate. However, on the other hand, precipitation is the variable that limits plant biomass production in the semi-arid northwestern CLP (Xu et al., 2007) such as Jingyuan in this study. Therefore, the simulated

amounts of SOC in Jingyuan is probably high. Differences in plant biomass production varied, according to the downscaled LOVECLIM-simulations, in Jingyuan (average 4.0 Mg C ha⁻¹ y⁻¹, grass/scrub vegetation) and Chang'an (average 7.0 C Mg ha⁻¹ y⁻¹, forest vegetation) and these influence the amount of SOC in the soil.

However, it is important to notice that the quantified Net Primary Production (NPP) varies with the different vegetation types and climate gradient in the studied sites as mentioned in **section 5.3.1**. In both scenarios, the increase of SOC between nearly 12500 and 5000 years (Jingyuan) and the last 7500 years of MIS 5e (Luochuan and Xifeng) is due to the dominance of grass/scrub vegetation in this period.



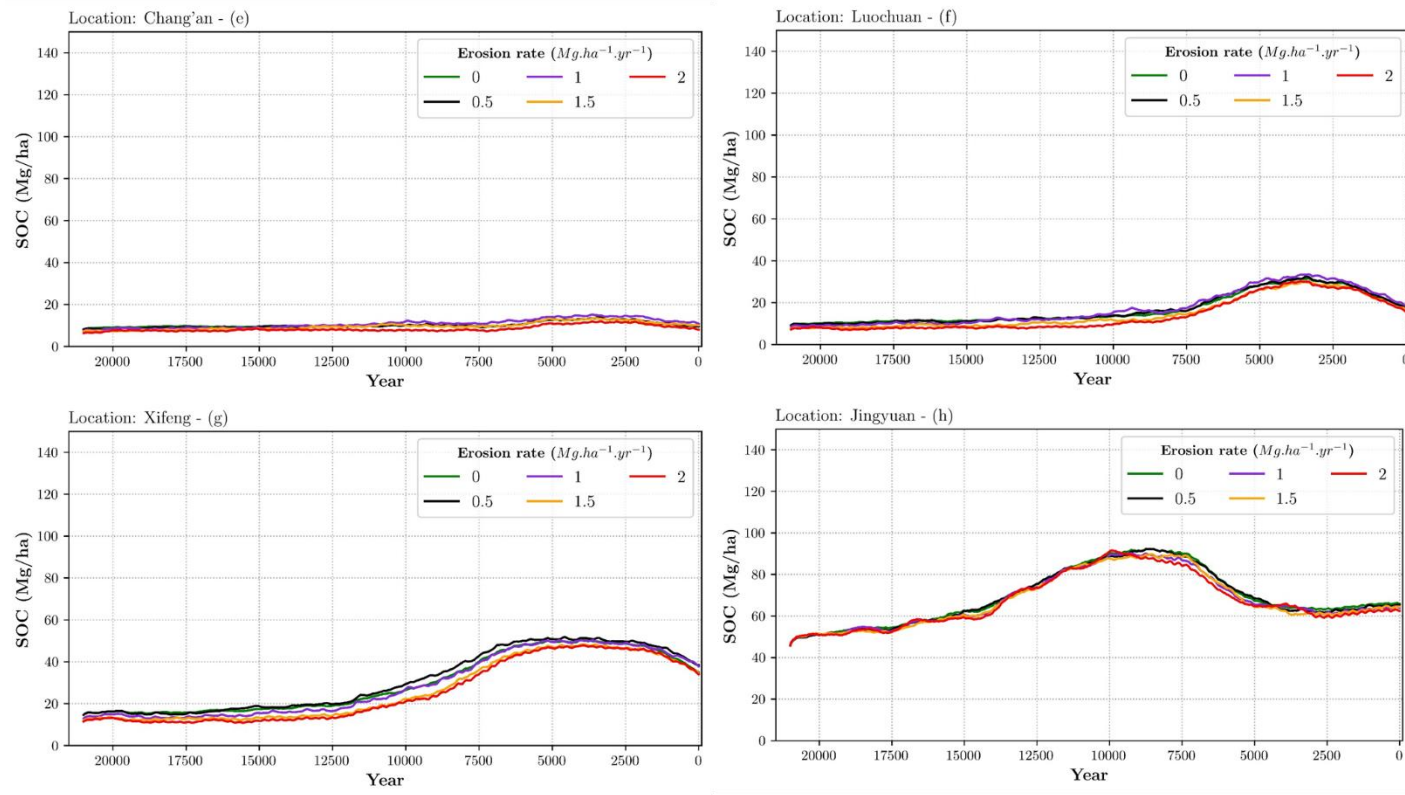


Figure 5-9 Effect of natural erosion rates on SOC evolution, in erosion-only (a, b, c, d) and dust addition plus erosion scenario (e, f, g, h). X-axis is simulation year and y-axis is scaled to 140 Mg/ha. Colored lines denote different rates of erosion.

The SLT levels obtained for SOC along the climatic gradient are given in **Table 5-3**. In the dust deposition plus erosion scenario erosion rates above 1.0 Mg ha⁻¹ y⁻¹ lead to reduced SOC. On the other hand, every rate of erosion above 0 Mg ha⁻¹ y⁻¹ in the erosion-only scenario has a negative effect on SOC as all the lines are clearly below the zero erosion rate (green line).

Table 5-3 SLT values for SOC for four locations.

SOC	Chang'an	Luochuan	Xifeng	Jingyuan
	soil loss tolerance values (Mg ha ⁻¹ y ⁻¹)			
	SOC decreases at			
Dust addition plus Erosion	Minimal effect	Above 1.0	Above 1.0	No effect
Erosion only	Above 0	Above 0	Above 0	Above 0

Table 5-2 and 5-3 data are based on cumulative EB and SOC stocks, which are presented in the **Figures A5-1, A5-2, A5-3, and A5-4 in appendix for chapter 5**. Because absolute EB and SOC stocks show huge variations, making assessment of SLT difficult. As a conclusion, it can be stated that the temporal scale at which the SLT is assessed is influencing the uncertainty of the assessment.

5.3.3 Soil ES evolution and SLT

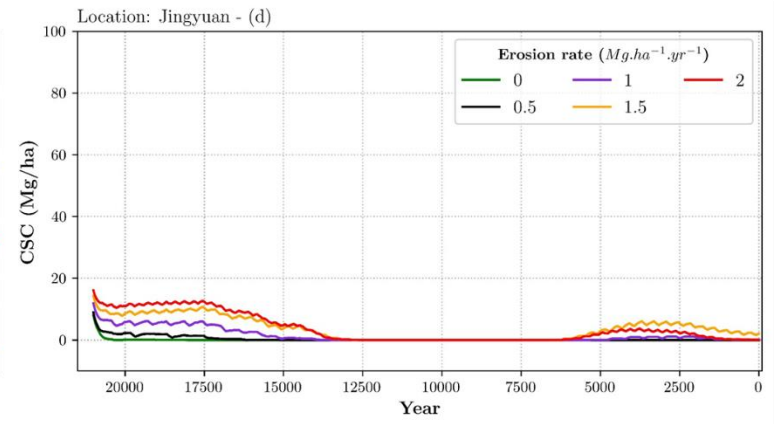
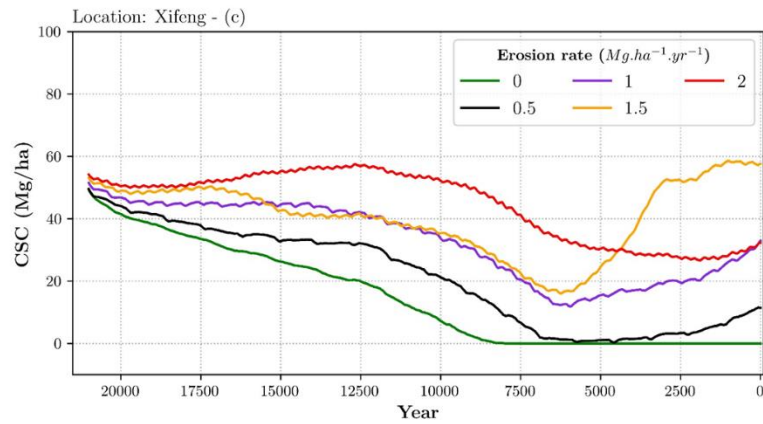
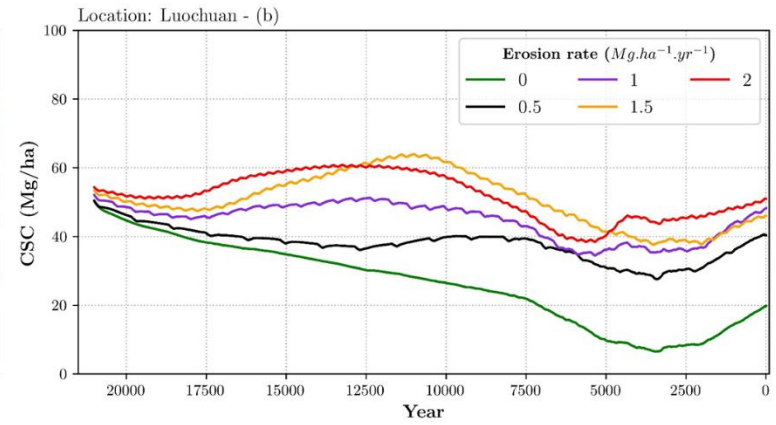
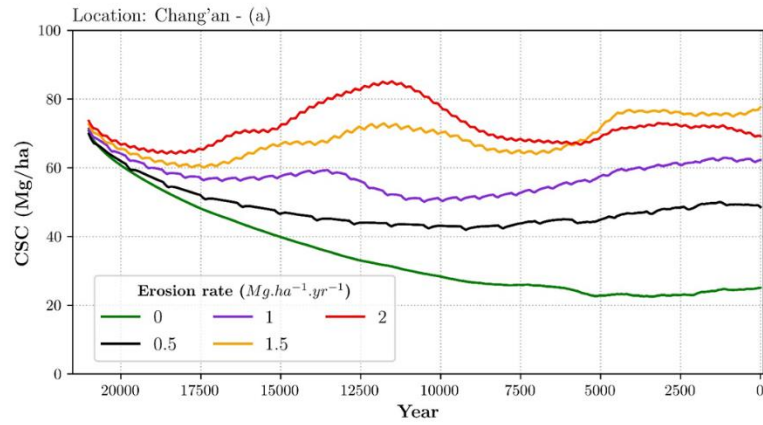
5.3.3.1 Assessment of organic carbon sequestration capacity

Figure 5-10 illustrates the evolution of the absolute amounts of CSC. In both scenarios, CSC increases at increasing rates of erosion. It is reasonable because soil erosion removes soil organic matter and provides the capacity to bind extra carbon in the remaining topsoil layers.

The reason for higher CSC in Xifeng (**Figure 5-10c**) at 1.5 Mg ha⁻¹ y⁻¹ in the last 5000 years of MIS 5e is due to stronger decreasing SOC in the topsoils compared to 2.0 Mg ha⁻¹ y⁻¹ (**Figure 5-11**). This may perhaps be due to textural variations, which also affect CSC calculations (**Eq.5-5**). In general, if the soil has high organic carbon content, CSC is low. Possibly, the dominance

of grass/scrub vegetation and high OC in topsoils in Jingyuan shows zero CSC nearly between 12500 and 5000 years (**Figure 5-10 d, h**) and in Xifeng nearly in the last 7500 years of MIS 5e (**Figure 5-10 c, g**). It should be noted that our CSC only applies to the upper 30 cm and that the effect of off-site burial of SOC is not considered. In both scenarios (**Figure 5-10**), the CSC is decreasing from Chang'an, Luochuan, Xifeng to Jingyuan.

CSC differs between scenarios: lines in the erosion-only scenario (**Figure 5-10 a, b, c and d**) are further apart than in the dust addition+erosion scenario (**Figure 5-10 e, f, g and h**), indicating larger fluctuations of the quantity of CSC. The dust particles bind soil organic carbon due to (i) their fine texture (<20 μm ; Hassink,1997) and (ii) binding on metal surfaces (e.g. Fe-oxides; Doetterl et al., 2018) in the added dust. In the present study, only the effect of the texture of the dust is included. The simulated SOC variations combined with the texture changes will determine the CSC fluctuations. Hence, the CSC graphs (**Figure 5-10**) resemble the SOC graphs (**Figure 5-9**). Hence, in the dust+erosion scenario, the maximum carbon saturation value is changed according to soil texture changes, due to erosion of soil compartments, physical weathering and clay migration to deeper layers. Therefore, dust addition reduces the effect of erosion.



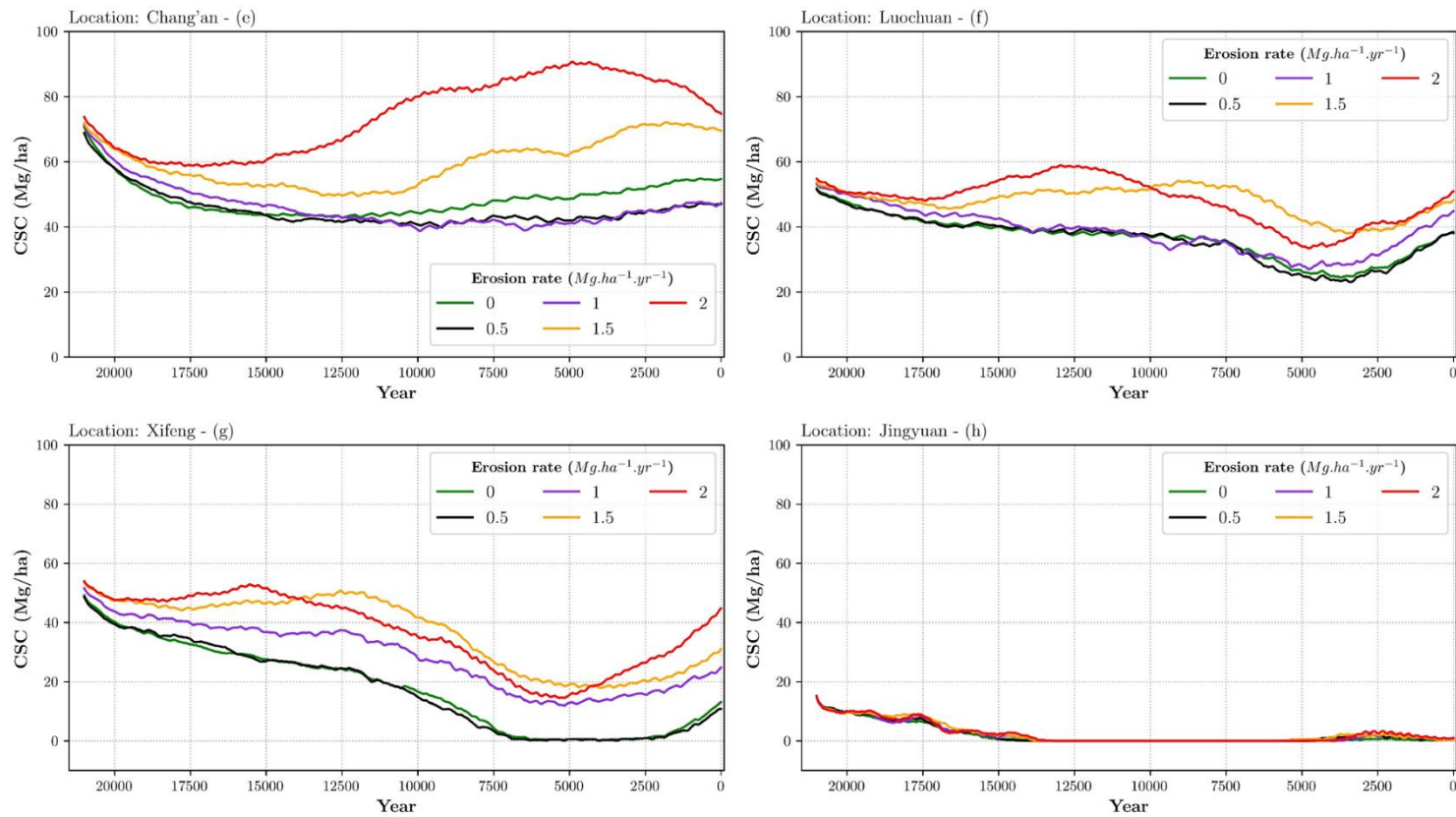


Figure 5-10 Effect of natural erosion rates on CSC evolution in erosion-only (a, b, c, d) and dust addition plus erosion scenario (e, f, g, h). X-axis is simulation year and y-axis is scaled to 100 Mg/ha. Colored lines denote different rates of erosion.

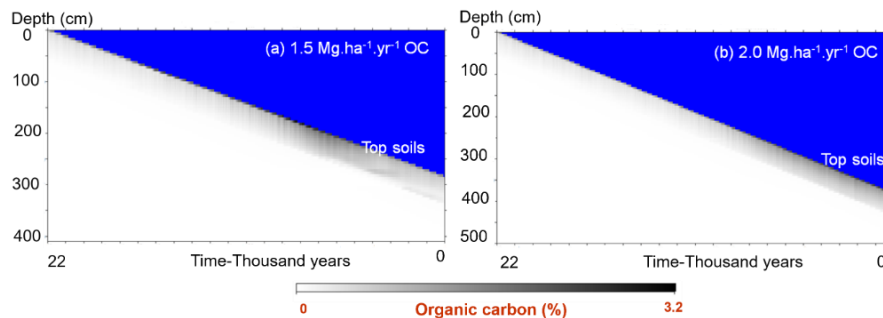


Figure 5-11 Evolution of organic carbon at 1.5 and 2.0 Mg. ha⁻¹. yr⁻¹ at Xifeng in only-erosion scenario. The calculated CSC differences at Xifeng is explained by these simulated OC at 1.5 and 2.0 Mg. ha⁻¹. yr⁻¹.

5.3.3.2 Assessment of water yield and ratio actual/potential evapotranspiration (Ω)

The most important effect of erosion on WY (**Figure 5-13**) is that every rate of erosion above zero reduces the WY (=drainage) in both scenarios, and mostly relates to higher erosion rates: when the zone of export in soil is removed by erosion, a Bt horizon (clay-rich) exposes (**Figure 5-14**). Therefore, we can assume that plant roots enter into the Bt horizon and enhance water uptake from the Bt, where more plant available water is present due to the higher clay content. As a result, there is less leaching of water and WY becomes low. In general, it should be noted that WY lowers towards the semi-arid sites because of low precipitation, and there is no important effect of different erosion rates on water yield at Jingyuan (**Figure 5-13 d and h**). Therefore, precipitation will restrict the WY in more arid (Jingyuan) relative to the moist locations (e.g. Chang'an) where soil properties (e.g. clay content) can play a role in determining the WY.

The impact of erosion rates on WY-evolution is less pronounced in the dust addition+erosion scenario (**Figure 5-13 e, f, g and h**) than in the erosion-only scenario (a strong reduction of water yield) (**Figure 5-13 a, b, c and d**). This may be due to the addition of dust containing fine materials which improves water retention, compensating topsoils removed by water erosion. **Figure 5-13** shows overlapping lines near the end of the simulated interglacial

(rightmost); this is due to the lower annual average precipitation simulated (Figure 5-2a). This suggests that the amount of precipitation largely determines the WY at the different erosion rates studied.

The ratio of actual over potential evapotranspiration, Ω , informs on how well water demand by vegetation is supplied by available soil water, and thus indicates if biomass production is stressed by soil water shortage. WY and Ω are not strictly inversely related, because not all soil water in the rooted zone is available for plants, and zero WY does not necessarily mean that plant water need is satisfied. The calculated Ω between erosion rates is not much differed between scenarios. We therefore illustrate Ω from two extreme climates from locations: Chang'an and Jingyuan (Figure 5-12).

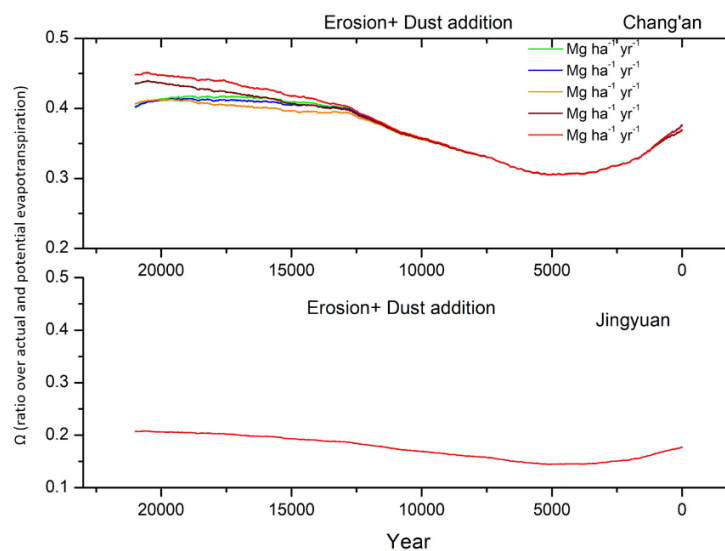
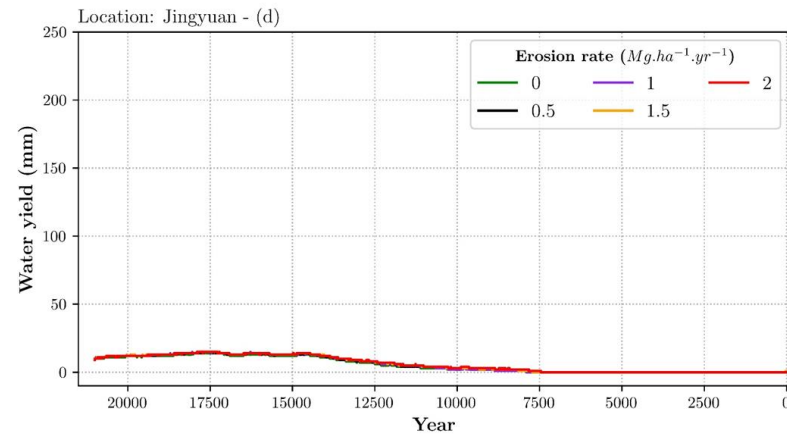
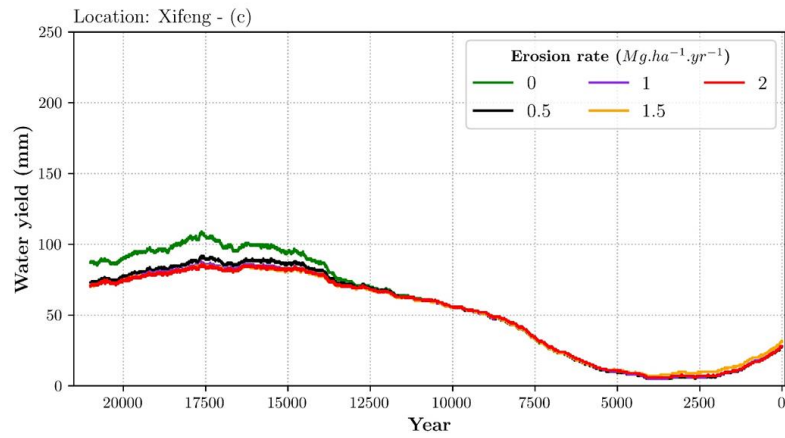
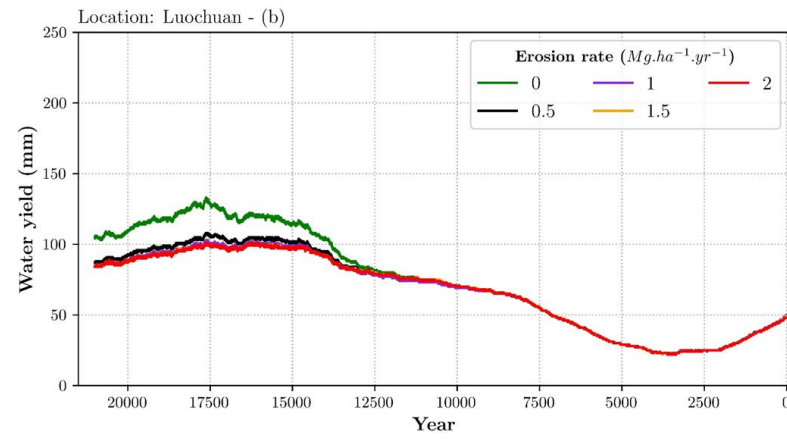
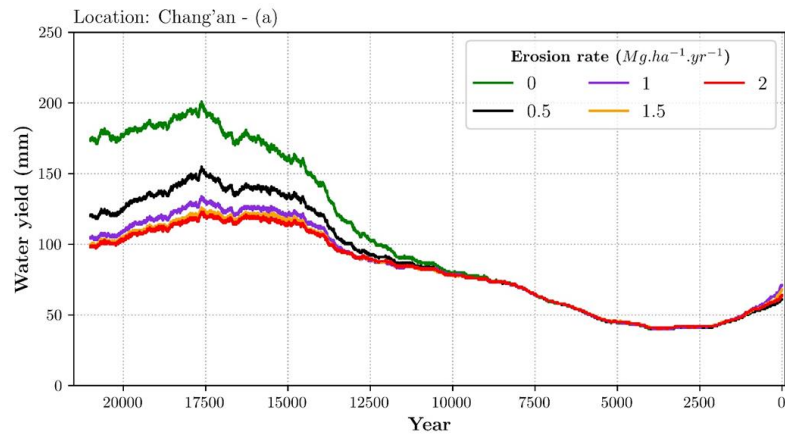


Figure 5-12 The ratio of actual over potential evapotranspiration, Ω , in Chang'an and Jingyuan in erosion+ dust addition scenario



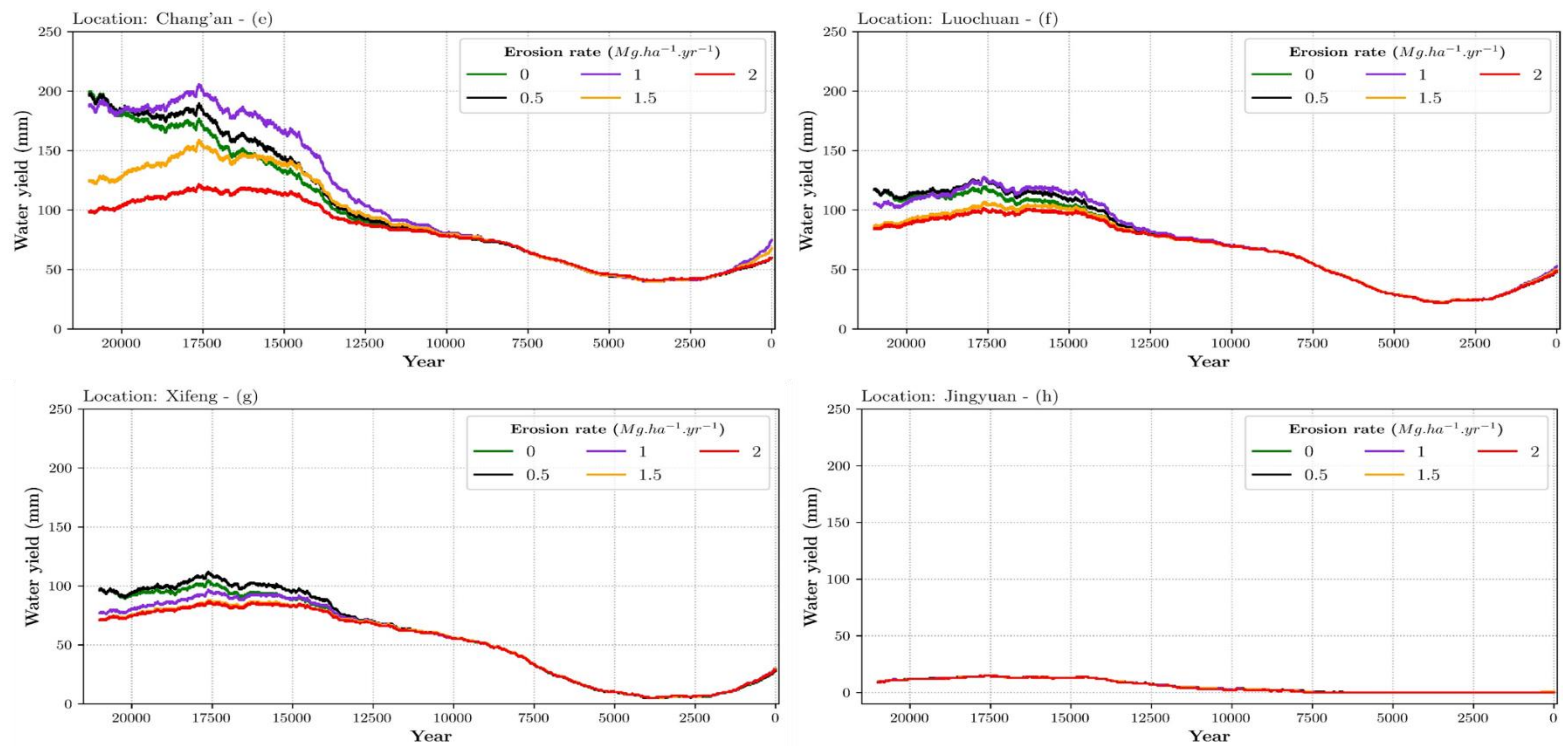


Figure 5-13 Effect of natural erosion rates on WY evolution, in erosion-only (a, b, c, d) and dust addition plus erosion scenario (e, f, g, h). X-axis is simulation year and y-axis is scaled to 250 mm. Colored lines denote different rates of erosion.

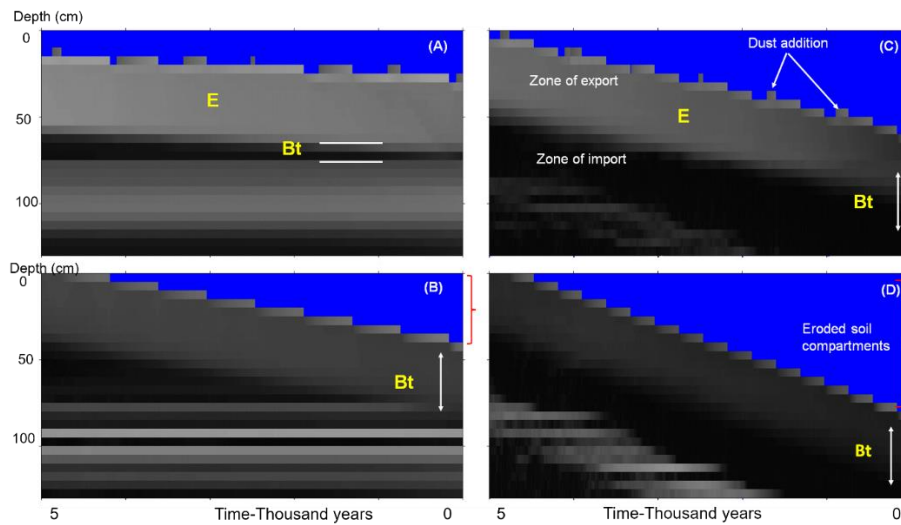


Figure 5-14 Clay content evolution over last 5 ka of MIS 5e. Zero is the last year of simulation in x axis; y axis is soil profile depth. Formation of Bt and E horizons is depicted by yellow, in dust addition plus erosion (upper), and erosion only (lower) in Chang'an; A, B ; $1.0 \text{ Mg ha}^{-1} \text{ y}^{-1}$ and C, D ; $2.0 \text{ Mg ha}^{-1} \text{ y}^{-1}$. Note that the Bt forms near the surface at C and D. Gray scale ranges from 0 to 42 mass % of clay. Blue stands for the atmosphere.

5.3.4 Combining performance indices for ecosystem services

The combined performance indices for ES were calculated for the two scenarios at the five erosion rates by applying Eq [5-9] for the ES: CSC, WY and Ω and then multiplying these indices using Eq [5-10]. The result in Figure 5-15 shows higher erosion rates ($1.5 - 2.0 \text{ Mg ha}^{-1} \text{ y}^{-1}$) influence the studied ecosystem services negatively, while lower erosion rates ($0.5 - 1.0 \text{ Mg ha}^{-1} \text{ y}^{-1}$) do not show a large negative impact. Like identified for the ES: CSC and WY in preceding sections, dust addition reduces the effect of erosion on ES at lower erosion rates. The ES performance is approximately constant in the dust addition plus erosion scenario (Figure 5-15a), whereas it is much more prominent in the erosion-only scenario (Figure 5-15b). For both scenarios, combined ES performance indicator showed a negative performance above $1.0 \text{ Mg ha}^{-1} \text{ y}^{-1}$.

Figure 5-15b shows that the combined index is higher in erosion-only scenario than in the dust addition plus erosion scenario (**Figure 5-15a**) especially at lower erosion rates. The difference in the combined index is mainly due to the individual effect of the evolution of CSC, WY and Ω , which reflect the combined effect of soil forming factors, erosion and dust addition. For example, surprisingly, Jingyuan, shows a high index in erosion-only scenario (**Figure 5-15b**), due to its higher amount of SOC at lower erosion rates, compared to the other sites, while it is much lower in the dust addition plus erosion scenario (**Figure 5-15a**). These differences are attributed to simulated SOC and therefore CSC in soils. Erosion-only scenarios suggest a better soil ES performance at more arid sites at low erosion rates than at the two moist sites. However, focusing simply on erosion may overlook the relevance of knowing the correct plant biomass productivity and the relation between aridity and dust deposition.

Considering the simulated soil development and climate change under this study, we propose sites located near deserts would be considerably influenced by dust addition (e.g. Jingyuan) relative to the moister sites. Therefore, we stress that dust deposition and its composition are also important factors of SOC, CSC and SLT estimations.

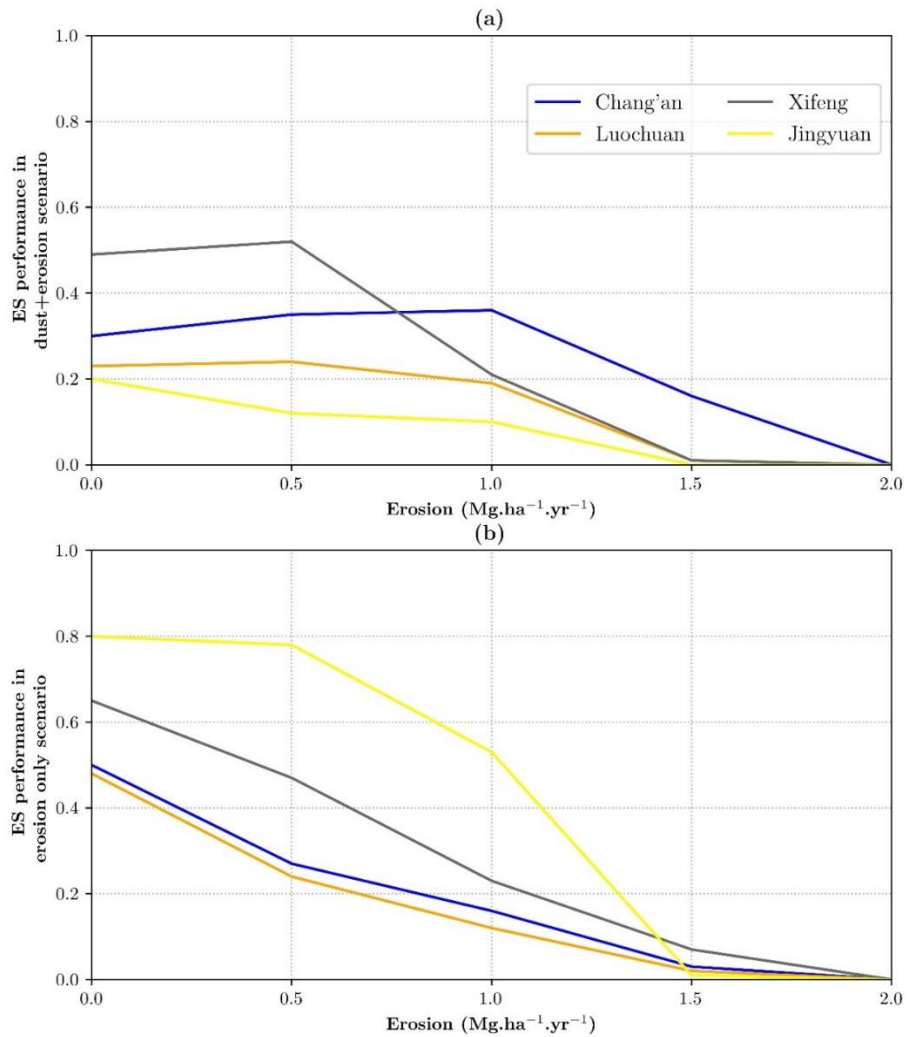


Figure 5-15 Combined performance indices for three simulated ecosystem services (1-CSC, WY and Ω per scenario) (a) dust+erosion and (b) erosion-only and per erosion rate for the simulation locations.

5.3.5 Concept of SLT under erosion/dust accumulation scenarios and semi-arid climate

Linking with the objectives, the variability in soil EB and SOC stocks and ES-performance was shown (Figures 5-3, 5-9, 5-10, 5-13, 5-15) and causes were identified (Figures 5-4, 5-5, 5-6, 5-7, 5-8, 5-11 and 5-14). Our simulation-

based SLT and combined ES-performance indices confirm a difference between the two scenarios, where the erosion-only scenario shows wider differences in the combined index over lower erosion rates. In contrast, the differences are minor and approximately constant in the dust addition plus erosion scenario. Because of dust addition, for soil EB and SOC stocks, dust addition plus erosion scenario shows slightly higher SLT than erosion-only scenario. Our results show a clear sensitivity of the soil model outputs to different climate evolutions along the aridity transect, which allows for comparative scenario studies like we performed. Combined climate-soil evolution modeling is key to enabling such analyses. Based on the concept of SLT, at the low “natural” erosion rates under the semi-arid climate in this study, soil-based ES showed a negative performance above $1.0 \text{ Mg ha}^{-1} \text{ y}^{-1}$, even though some stocks (SOC) respond negatively and (EB) respond positively above this rate. We studied all the soil EB and SOC stocks and ES solely to evaluate how those evolve under natural vegetations. Thus, evaluating soil quality based on these indices from an agricultural productivity perspective is beyond the scope of this study, and it must be noted as well that the study concerns MIS 5e. Finally, the SLT at various erosion rates are estimated for a semi-arid, monsoon-type climate evolution. The found SLT are therefore bound to these climates.

Off-site effects of erosion may negatively affect water bodies and also change soil depth at accumulation locations. However, the studied erosion rates are low and would not produce a lot of colluvium, and the 1-D soil model does not allow to calculate mass redistribution over a landscape. For these reasons, we did not include erosion modeling nor discussed off-site problems. The only way that we see to include off-site effects, is to add a separate series of scenarios of colluviation, which would probably be an enrichment to the study but is also not easily done. We did not include this, also because off-site effects are of impact under agricultural land use but much less under natural vegetation as in MIS 5e.

Our results showed climate is an important driver in SLT quantifications. Therefore, time series of climate data are required to understand the “soil

change” for a given location. Understanding “soil change” is vital in determining the soil status for supplying soil stocks (soil properties) and ES, which change under different climatic conditions (precipitation, temperature). Therefore, it is increasingly necessary to integrate soil changes with other components (hydrosphere, lithosphere, atmosphere, and biosphere) of the Earth system to obtain a better understanding of soil processes, ES, and globally concerning matters such as SLT. Therefore, we propose that soil-climate modeling approaches provide a better framework that can fully capture the role of soils in a coupled system.

5.4 Conclusions

In this study, we test a new modeling approach for estimating selected soil EB and SOC stocks and ES and assessing possible SLT in four locations on the CLP over 22 ka. We show the importance of mechanistic soil modeling for quantifying ES as the initial step for assessing ES. We stress that mathematical modeling is a better option for assessment of soil stocks (soil properties) and ES than common inventory-based studies, for a number of reasons: (i) stocks (soil properties) and ES can be quantified; (ii) past, present and future situations can be quantified; (iii) effects of scenarios of the forcing factors (e.g. climate, erosion) can be studied; (iv) while extrapolation of data inventory based assessments is risky, extrapolations using mechanistic instruments are less risky. Because physical laws like the conservation of mass, potential-driven water and solute flow constrain the results even when boundary conditions become extreme (e.g. high rainfall), while empirical relations are risky to be applied outside their domain.

The main findings are:

- (i) Two soil stocks, EB and SOC, respond differently to increased erosion. Whereas SOC decreases when erosion occurs, usually EB increases with erosion in both scenarios, in response to huge variations in calcium-rich horizons that become part of the topsoil over the modeling period.

- (ii) Three ecosystem services, CSC, WY and Ω respond differently to increased erosion. SLT, as assessed by the combined ES performance indicator, showed a negative performance above 1.0 Mg ha⁻¹ y⁻¹. This SLT-threshold is bound to the studied (semi-arid, monsoon) climate evolution.
- (iii) SLT benchmark levels should be chosen carefully based on analysis of the effect of natural erosion rates.
- (iv) Dust deposition may obscure the effect of erosion in ES performance, however, it must be studied further.

Author contribution

Keerthika N. Ranathunga performed the research by simulating soil, integrating data, visualizing and interpreting the results and writing the paper. Peter A. Finke conceptualized the overall research and did part of the soil simulations and provided the software, reviewed the paper and supervised the research. Qiuzhen Yin provided the climate data for soil simulations, funding acquisition and reviewed, and supervised the research. Ann Verdoodt conceptualized the research experiment on soil erosion rates. Yanyan Yu provided soil data for soil simulations and reviewed the paper.

CHAPTER 6. Conclusions

In this dissertation, we aimed to understand the paleoclimate-to-paleosols relations in the Chinese Loess Plateau using dynamic soil-climate models. As discussed in the introduction, no model considers the dynamic interactions between climate evolution and soil paleosol development in comprising soil processes and co-evolution of different soil characteristics. We overcame this limitation by combining a soil and a climate model, SoilGen2-LOVECLIM1.3, to simulate the paleo(soil) evolution on a long time scale (several thousands of years). The objectives of this thesis were to (1) calibrate the SoilGen2 model, (2) apply the soil-climate model to assess the relative contributions of climate, vegetation, and dust addition and the indirect effects of forcing factors acting on paleosols, e.g. precession and ice sheets, and (3) demonstrate the application of the SoilGen2 model to assess the soil EB and SOC stocks and soil ecosystem services under defined natural rates of erosion. The major conclusions are summarized hereunder.

6.1 The SoilGen2 model calibration on the Chinese Loess Plateau

The first objective is presented in chapter 3 of this thesis that aims at calibrating the SoilGen2 model for different soil process parameters. The calibration process included three major soil process formulations: decarbonatization, clay migration, and soil organic carbon cycling, represented by various process parameters. Previous studies (Yu et al., 2013; Finke et al., 2015) identified that the SoilGen2 model output is most sensitive to the process parameters of these three processes. Due to the high computational demand of the model, calibration was done on a parameter by parameter basis, grading from the most sensitive process parameter to less sensitive parameters. The simulated soil properties such as contents of organic carbon, clay, and calcite were confronted with measurements, and the best-calibrated values were obtained by calculating the dissimilarity between both. The calibration results mainly were in the range of literature values. **Table 6-1** summarizes the calibrated parameters and best-calibrated values.

Table 6-1 SoilGen2 calibrated process parameters and associated optimal values.

	Process parameter with units	Optimal value
(i)	Dissolution constant of calcite ($\log_{10} k_{so}$)	-9.0
(ii)	Interception evaporation fraction (-) for grass/shrubs/agriculture	0.03
(iii)	Thickness of the ectorganic layer (mm)	0.5
(iv)	Pressure head (hPa) at which macropores empty	-18
(v)	Filter coefficient for clay (-)	0.5
(vi)	Particle splitting probability and soil temperature change $^{\circ}\text{C}$ / hour	2.163×10^{-6} 0.95
(vii)	Decomposition rate (yr^{-1}) of humus	0.0025
(viii)	Ratio of ectorganic/endorganic litter (-)	60/40
(ix)	Decomposition rate of (yr^{-1}) of resistant plant material	0.02
(x)	Partitioning coefficient CO_2 / (BIO+HUM) (-)	2.1

Soil modelers acknowledge that model uncertainty would still remain after calibration due to uncertain model boundary conditions during soil development. To explore this, we evaluated the effect of ten reconstructed dust addition rhythms on the quality of the calibration during the Holocene. Results showed a strong sensitivity between the dust addition rhythms and the studied soil properties, in decreasing order, calcite>soil organic carbon>clay content >CEC by 73.59%, 8.52%, 2.01%, and 0.16%, respectively. The conclusion was therefore drawn that the quality of the SoilGen2-simulated paleosol properties is sensitive to various uncertain dust addition patterns during the Holocene and can be improved by defining correct initial and boundary conditions during simulations.

6.2 The response of calcite and clay content in paleosol to interglacial climate, vegetation and dust addition, precession and ice volume

In chapter 4, our results showed that precipitation, dust addition, potential evapotranspiration, in decreasing order, had the largest influence on the depth redistribution of soil properties (mass of calcite) in MIS 11 and MIS 13. The

simulated clay content was influenced in decreasing order by dust addition, precipitation and potential evapotranspiration for MIS 11. In MIS 13, there was no single factor the most important for clay but a combination of factors (the best 2-factor combination was precipitation and dust addition) and potential evapotranspiration had a considerable impact when compared to that in MIS 11. The conclusion was therefore drawn that precipitation, dust and evapotranspiration are the major driving factors on paleosols in the CLP, but their relative importance varies between soil properties and between interglacials.

For the second specific objective, we tested the impact of precession on paleosol properties (fraction of mass change in calcite and clay relative to initial mass) during MIS 5, MIS 7, MIS 9, MIS 11 and MIS 13 in Chang'an. Our results showed an indirect role of precession on paleosol development through the simulated precipitation and temperature. The simulated S1, S2, S3 and S5-1 paleosols showed clear precession footprints, whereas weak precession footprints were detected in the S4 paleosol. Overall, the calcite peaks approached the peaks of precession and precipitation, while the clay peaks also matched to a lesser degree. Besides precipitation, there was a good correlation between the simulated clay content and the mean annual temperature during MIS 5, MIS 7 and MIS 13. The precession footprint in the simulated paleosols was partly similar to loess records in the Western CLP. In conclusion, the simulated paleosols showed a delayed response due to indirect forcing of precession variability, which varied between interglacials and between soil properties (calcite and clay).

We set up two experiments with ice (OrbGHGIce) and without ice sheets (OrbGHG) to examine the paleosol response to indirect effect of ice sheet-induced climate changes in two interglacials, MIS 11 and MIS 13 in Jiuzhoutai, Xifeng, and Chang'an. As expected, the simulated annual mean precipitation and temperature during MIS 11 and MIS 13 responded to ice sheet changes in the NH. In response to ice sheets through its control on precipitation and temperature, the simulated paleosols showed stronger decarbonatization and clay migration at the end of MIS 11 and MIS 13, but not at the beginning of

these interglacials. Compared to MIS 11, these processes were much more substantial in MIS 13. In response to ice sheets and therefore its control on interglacial climate variability, paleosols expressions gradually weakened from southeast to northwest on the Loess Plateau. In conclusion, the results demonstrated the large and indirect impact of ice sheets on soil processes, carbonate leaching and clay migration in the CLP, where paleosol show indirect response to ice sheets variations during MIS 11 and MIS 13 interglacials.

6.3 Effect of soil-climate evolution on soil stocks and soil ecosystem services under defined erosion rates

Finally, in chapter 5, the SoilGen2 model was applied (i) to understand how the two soil stocks: Exchangeable Bases (EB) and Soil Organic Carbon (SOC), and three soil-based ecosystem services: Carbon Sequestration Capacity (CSC), Water Yield (WY) and the ratio of actual over potential evapotranspiration (Ω) vary under natural soil erosion rates; (ii) to quantify the loess soil tolerance values of these particular soil stocks and soil ecosystems services. Our hypothesis was that process-based soil-climate models could better assess soil stocks and - ecosystem services than most inventory-based studies because models describe temporal variation of target properties and not just the final stage.

We tested the hypothesis on the recent paleosol formed in the loess of China during the last interglacial, MIS 5e. Two scenarios were defined: (i) to assess the integrated effect of dust addition plus erosion on soil- stocks and ecosystem services, and (ii) to assess the effect of erosion-only on soil- stocks and ecosystem services (both scenarios comprising five erosion rates corresponding to low, natural erosion rates: 0, 0.5, 1.0, 1.5 and 2.0 Mg ha⁻¹ y⁻¹). Our results showed that in calcium-rich top soils, EB usually increased with increased erosion rates in both scenarios. The SOC decreased in response to increased erosion in both scenarios. For EB and SOC, the determined SLT thresholds were relatively larger in the dust addition scenario than in the erosion-only scenario and strictly followed the climate gradient in the CLP. In

both scenarios, three ecosystem services, CSC, WY and Ω evolved differently: the simulated CSC increased with increased erosion; contrastingly, the WY decreased with increasing erosion rates. Both CSC, WY, and Ω gradually decreased towards the northwest CLP. The estimated soil loss tolerance values for the combined ES performance indicator showed a negative soil ES performance above $1.0 \text{ Mg ha}^{-1} \text{ y}^{-1}$. The obtained SLT is particularly important in the studied semi-arid climates at the low “natural” erosion rates in this study. Overall, the SLT values for soil stocks and for the combined ES performance indicator confirmed that dust addition might compensate for the effect of erosion on ES performance. In conclusion, results from this study demonstrated the necessity to carefully choose SLT benchmark rates in a natural context in order to assess the impact of human-induced erosion on soil stocks and ecosystem services.

Author contribution- This chapter was written by KN Ranathunga.

CHAPTER 7. Limitations, recommendations and perspectives

7.1 Paleosol evolution modeling - Scientific limitations

Three major limitations were identified during the study. 1. Input loess data limitation, 2. Soil- and climate model limitations, limitations in their coupling, lack of soil-climate feedback and scale problem, 3. Simulation limitation, including run time limitation and the lack of post-deposition/after-burial processes.

7.1.1 Input data

One of the largest limitations in modeling studies is that almost all mechanistic models may require a large amount of input data that is ultimately used to drive simulations (Sauer et al., 2012; Vereecken et al., 2016).

In order to reduce the uncertainties of paleosol simulations, full-scale extensive information on cl, o, r, p, t (soil- forming factors) data is needed thereby allowing to run a “full-CLORPT” soil formation model (Finke, 2012b). In paleosol modeling, the SoilGen2 soil formation model was run in “reconstruction mode” (Finke, 2012b) and therefore, it required extensive environmental data from the past. Part of these data, for example, the paleoclimate data (precipitation, temperature, potential evapotranspiration) and paleo vegetation data of the interglacials were simulated by LOVECLIM1.3 (these were described in previous chapters) which itself also has uncertainty and bias. These climate data then become input into the soil model. However, finding data for dust deposition rhythms and associated dust/loess composition (e.g. texture, mineralogy) of both underlying loess parent material and added dust were the main challenges in this study. Typically, C-horizon properties correspond to the soil parent material, which is found to be the unweathered loess material at the bottom of a paleosol profile, and is used as the initial condition of the paleosols to be simulated. Similarly, as paleosols surface accretes by the addition of dust during interglacials in the CLP, dust parent material properties are also important. In addition, chapter 3 showed that the uncertainty of dust deposition patterns directly influenced the accuracy of the model output; therefore, another limitation is finding age-depth models for reconstructing dust deposition

patterns for every interglacial. Therefore, uncertain dust deposition (distribution/ composition) during the interglacial could partly hinder the quality of the simulation results in the study. Collecting initial loess and dust data in the field and associated laboratory analysis is the most difficult and time-consuming process in modeling paleosols. Therefore, data are often rare with reasonable resolution (e.g. number of sampling points in a paleosol section) for middle to late Pleistocene loess layers. For instance, obtaining actual dust addition rates and dust chemical composition is very elusive for paleosol simulations because these measured data are not often published and/or relatively rare for every location, in some cases almost entirely lacking, especially for periods older than the Holocene. Thus, one of the difficulties in this study is to obtain realistic dust/loess input data. The initial input data for soil models can be collected from various sources (as we did): measurements (lab, field), literature sources and model boundary conditions can be derived from paleoclimate model simulations, proxy records, and historical records, which may be imprecise and result in uncertainty (Finke et al., 2021a).

Long-term duration of paleosol formation, erroneous input data, uncertain soil forming initial and boundary conditions in SoilGen2 will significantly influence SoilGen2 results (Finke et al., 2015; Keyvanshokouhi et al., 2016) and can partly explain the model deviation from measured data (e.g. during calibration). In the context of paleosol modeling, Retallack (1998) also stated that obtaining precise input data is the largest limitation in mathematical soil formation models. In SoilGen2, therefore, more realistic input data will likely improve reconstruction of the paleosols.

7.1.2 Climate and soil model limitations

Limitations related to models in the study can be listed as (i) soil and (ii) climate model limitations, (iii) lack of soil-climate feedback and (iv) issues in coupling in between models (scaling issues).

(i) The Soil model limitations

First, the soil model limitations, which are mainly due to the model process coverage, are discussed below. According to Minasny et al. (2015), SoilGen2

is one of the pedon scale models with the widest process coverage. Even though SoilGen2 is a heavy run time model, we demonstrated that it encompasses sufficient processes to simulate the paleosol development in the study. However, a certain number of processes and features are not yet implemented in the current model version and could be added improved in the future. They are related to (1) clay new-formation, (2) vegetation development mechanisms, (3) soil volume changes (e.g. due to bioturbation, weathering, clay migration, tillage practices), and (4) redox processes (allowing among others a better reconstruction of the distribution of Fe).

(1) Addition of new-formation of clay minerals in SoilGen2

Clay migration is one of the main processes in soil formation, and clay content (and its vertical redistribution) represents the strength of soil formation. In SoilGen2, the clay content is mainly controlled by bioturbation, clay migration and physical weathering, and the latter two are directly a function of climate. In addition, a relation exists between organic carbon and clay content and the Cation Exchange Capacity (CEC). Moreover, clay mineralogy influences the magnitude of clay migration in SoilGen2. For example, formation of 2:1 clay minerals will increase clay migration; their weathering and formation of 1:1 clay minerals may reduce clay migration. Therefore, such a process should be added in SoilGen2 based on the process of chemical weathering (primary and secondary minerals), which is already in SoilGen2. The improvement of the new formation of clay minerals in SoilGen2 weathering module has been designed and studied by (Opolot, 2016). Nevertheless, this functionality also strongly improves the application of the SoilGen2 model in various settings, not only in loess soils but also in andosols, ferralsols, acrisols, lixisols with different primary and secondary minerals.

(2) Vegetation development in SoilGen2

In SoilGen2, a relation between mean annual temperature and precipitation is used to calculate the annual plant biomass input (NPP) (Miami model, Lieth, 1975). As far as organic matter mineralization and their decay rates are concerned, the input of plant litter is important as a function of climate,

vegetation, and land use. In SoilGen2, the evolution of soil properties and vegetation development are connected only through annual litter input and plant uptake of cations. The effect of the evolving soil properties (e.g. pH, soil moisture) on the vegetation development is not considered yet. Therefore, an interactive mechanism between the soil and vegetation growth needs to be incorporated as a function of climate. For example, one could focus on implementing plant development module of global vegetation models like LPJ (Sitch et al., 2003) into SoilGen2. Such an implementation will improve the model ability to simulate the effect of climate and land use changes on both soil and vegetation development evolution (e.g. vegetation development over the aridity gradient in the Loess Plateau).

(3) Improving soil volume changes in SoilGen2

Most mechanistic and all soil evolution models assume a constant soil volume in each soil compartment over time (Sollins and Gregg, 2017). Likewise, SoilGen2 assumes constant soil volume over time, and therefore bulk density and porosity may not be accurately simulated by SoilGen2. The simulation (in-)accuracy of these soil properties can also be partly attributed to the bulk density measurements in the CLP-paleosols and loess layers, which are often rare and may result from post-depositional compaction due to overburden with the above layers. Nevertheless, the consequences of such simplification on model outputs are not negligible when the soil is influenced by (de) calcification, clay migration, weathering, bioturbation, tillage practices as well as dust addition and associated bulk density changes over the soil forming duration (Keyvanshokouhi et al., 2016; Sollins and Gregg, 2017). Moreover, the combination of texture, bulk density and SOC does influence the h-theta-K relations in SoilGen. For example, Keyvanshokouhi et al. (2016) found that the SoilGen2 model underestimates the soil bulk density when the constant volume is considered (especially on the upper part of the soil profile). Additionally, soil volume changes and associated structural changes should be added in SoilGen2 to simulate the effect of soil structure on OC dynamics (e.g. physical SOC protection in soil micropores, organic matter decomposition rates) especially for simulating recent Holocene soils under

agriculture. Moreover, soil structure related soil porosity distribution needs to be implemented to calculate soil hydraulic properties and content of water at different soil depths, which affect transport of soil components (e.g. calcite, clay). Such a process definition will improve the model ability to simulate paleoclimate-paleosol relations in the dust addition.

(4) Absence of redox processes

In addition, redox process description is absent in the current version of SoilGen2. In the CLP, profile distribution of secondary Fe oxides or oxyhydroxides iron content in paleosol profiles are considered as a proxy for the degree of soil development through magnetic susceptibility measurement, which is triggered by different iron containing minerals, e.g. ferrimagnetic minerals such as goethite, hematite, lepidocrocite, maghemite, ferrihydrite. Those secondary minerals containing Fe are important in magnetic susceptibility measurement in paleosols, during interglacials. The fate of secondary Fe oxides minerals are not simulated by SoilGen2. However, some iron (Fe^{+2}) bearing primary minerals such as Augite (Pyroxene) (FeSiO_3) and Fayalite (Olivine) (Fe_2SiO_4) can be defined in SoilGen2, but the vertical redistribution (mainly of Fe^{+2} , released by weathering) is not simulated. Nevertheless, not only Fe^{+2} (mobile) containing minerals but also minerals comprising both Fe^{+2} and Fe^{+3} (immobile) will determine the magnetic susceptibility in paleosols. In the future, to use Fe content as a proxy for soil development, first we need to improve the model to add the formation of secondary minerals from the primary iron minerals, that can be compared with the magnetic susceptibility measurement. Second, the movement of secondary iron minerals should be incorporated to represent the profile distribution of Fe. These issues become a limitation when comparing the simulated vertical distribution of iron by SoilGen2 with magnetic susceptibility measurements in paleosols on the CLP.

Overall, the mismatch between the SoilGen2 simulated soil properties and measurements (chapter 3) can partly be attributed to the aforementioned limitations.

(ii) The climate model limitations

Regarding the LOVECLIM1.3 climate simulations, bias exists in its present-day simulation on the CLP. It is known that application of similar bias of 1971-2000 to the LOVECLIM simulated geological periods (MIS 5, 7, 9, 11, 13) is inescapable, because there is no other approach to correct the climate model output. However, these biases are strong particularly in mid- and low-latitudes and can be propagated along simulations over long periods. In addition, there may be uncertainties due to low resolution of the LOVECLIM1.3 simulated climate data in the CLP. These issues would be the case if one would apply proxy records to deduce paleoclimate information, with associated uncertainties in climate model simulations and can be partly avoided through multi-model ensemble models. However, using quantitative climate data simulated by models is better than using qualitative data from paleoclimate reconstructions by proxies. Moreover, quantitative reconstructions of monthly climate fields that are required by SoilGen2 are rare.

(iii) Lack of soil-climate feedback

In the attempt of modeling soil processes under climate change, it is of utmost importance that we simulate soil-climate feedback. However, due to limited understanding in this regard, we may fail to accurately represent soil-climate feedback.

The effect of soil-climate on vegetation development and feedbacks among them are not captured in SoilGen2. First, it requires adding a vegetation module in SoilGen2 that can incorporate the effect of climate on both vegetation development and associated biomass production. The vegetation-related parameters, in turn, act on organic carbon dynamics, which in turn affects soil mineral content and then soil bulk density changes and associated hydraulic properties (e.g. soil moisture content). In SoilGen2, feedback mechanisms exist between soil organic carbon cycle dynamics and soil mineralogical composition: CO₂ produced by mineralization affects the carbonate equilibria and may thus lead to a change in the dissolution/precipitation of calcite, which then may affect soil pH and then

affect the chemical weathering of minerals. To simulate the paleo(soil) evolution, the impact of climate on soil and associated feedbacks and interactions among them becomes crucial. Moreover, the feedback mechanisms that exist between soil organic carbon cycle dynamics and other soil properties such as soil moisture and temperature (as decay rate modifiers), processes involved in organic carbon distribution (e.g. water and heat flow, tillage, bioturbation) are considered in SoilGen2. However, capturing these feedback and interactions between soil-climate is important for reconstructing recent soils and projecting SOC stocks in agricultural soils and it will further enhance the sensitivity and applicability of the SoilGen2 model to soil-climate modeling studies. Nevertheless, feedbacks between soil-plant-climate are indispensable when simulating climate change and soil ecosystem services (e.g. water yield). In addition, a number of additional climate-plant-soil feedbacks will be interesting to consider in the future such as the impact of changing vegetation on albedo, on evapotranspiration, on litter composition, on the biogeochemical element cycling, on element biolifting (inorganic nutrient uptake by plants as a result of chemical weathering of rocks) as a function of rooting depth.

(iv) Issues of scale

The SoilGen2 and LOVECLIM1.3 model components cannot be directly connected because of scale issues: the spatial support is vastly different. The resolution of LOVECLIM1.3 is low (5.6° latitude*longitude) for simulating soil development at the pedon scale ($1 \times 1 \text{ m}^2$). So it is necessary to bring both models to a same spatial support; this is done via spatial downscaling. The downscaling method was based on a statistical relationship between climate parameters of the whole Loess Plateau and local site level climate parameters based on maps. In downscaling, the LOVECLIM1.3 model output (monthly annual mean temperature, precipitation, potential evapotranspiration at 5.6°) is transferred to soil model input at $1 \times 1 \text{ m}^2$ (described in chapter 2). A direct coupling can be done when the climate model operates at a greater resolution (Roberts et al., 2020), whereas in our case temporal support must be similar inside models when downscaling. We chose for a coupling based on monthly

averages of P, Ep and T, which are downscaled inside the soil model (**Figure 2-5**).

7.1.3 Simulation limitations

(i) Run time

One of the technical limitations of the current version of the SoilGen2 model is its run time. At present, SoilGen2 takes about 16 days of run time for a 60-compartment (300cm) soil profile for 67 000 years of soil formation using high-performance computers, which nevertheless reduces the runtime hours compared to old-version computers. Minasny et al. (2015) explained that high computational demand depends on the number of processes that the model can simulate, mainly because of introducing water, heat, gas and solute flow and soil chemistry models like SoilGen2, are computationally expensive. Therefore, sensitivity analysis and model calibration require simple methods in terms of computing time of paleosol simulation in SoilGen2 (e.g. Yu et al., 2013), which restricts the application of multiple-run calibration methods. Nevertheless, the issue of heavy run time will be solved with advancing technology and computing power.

(ii) Lack of post-deposition/after-burial processes

Post-depositional processes usually include surface mixing and pedogenesis process (Sun et al., 2010) that may influence the field-observed paleosol properties. The model considers the post-depositional weathering process characterized by e.g. carbonate leaching and mobility of elements, but not the formation of in-situ formation of clay and magnetic minerals. Surface mixing of loess will not be accurately mimicked without knowing the accurate variations (high/low) of sedimentation rates between sites. Thus we think, the depth of surface mixing of loess (due to low vegetation cover) can be partially mimicked through the bioturbation process during simulation. For example, because of local sedimentation rate variations and dramatic phases of very rapid sedimentation like in the western part of the CLP, compared to the southern part of the CLP, the thickness of the surface mixing layer can be different between sites. Meanwhile, since the paleosols are simulated only in

the defined interglacial periods, some of the post-burial effects (e.g. increasing bulk density of top of the paleosols) that we observe in the field soil cannot be mimicked in the simulations. The absence of potential post-depositional alterations might influence the discrepancies between the simulated and observed paleosols in this study. Nevertheless, post-deposition processes also affect the precise dating of loess and paleosols in the CLP. These discrepancies might influence soil expressions between sites in the Loess Plateau as well as between the simulated and observed paleosols.

7.2 Recommendations for future research

In modeling studies, there is no flawless model. Box (1976) once stated, "all models are wrong, but some are useful". Thus, models need to be used in such a way that their potential is fully exploited to discriminate between scenarios. Based on the results and conclusions obtained, following future studies can be carried out.

7.2.1 Future perspectives on model calibration and paleosol simulations

Regarding soil model calibration, the calibration usually compares the simulated soil properties at the end of the simulation period and measurements of the present status of soil profiles. In other words, we only have the current status of soil for verifying the calibrated models output variables. Due to the longer temporal scale of calibration (more than 17 ka in Holocene in this study), soil process parameters may not be sensitive to the simulated and measured soil properties, and therefore calibration process becomes uncertain. In order to avoid relying only on the final state for model calibration, the soil model can be calibrated for several shorter timescales (Sauer, 2010), where soil properties developed in the same parent material change more strongly (chronosequences) than in longer timescales.

It should be noted that even after calibration, models are not free from errors and uncertainties. In order to minimize errors, models should undergo an assessment of the accuracy of model output variables. There is a possibility

to test the model accuracy in locally measured Holocene soils (for testing the accuracy of the calibration results in chapter 3). Therefore, simulation data should be compared to field measured soil properties (e.g. clay content, organic carbon content, soil pH, CEC and calcite content) obtained at the simulation locations, checking the accuracy of the calibration results in chapter 3. Moreover, these accuracy tests can be focused on faster soil processes such as SOC dynamics in soils. Similarly, measured paleosol data of Middle to Late Pleistocene paleosols (chapter 4) in the CLP can be used to assess the influence of model uncertainty on identified phase-similarities between precession footprint and soil response and check on the identified lags.

7.2.2 Future perspectives on soil-based ecosystem services

Soils play a key role in various ecosystem services. In this thesis, we emphasized how soil process-based modeling (pedogenic modeling) can contribute to the long-term dynamics of soil stocks and ecosystem services in the CLP. As far as potential applications of the modeling approach for SLT are concerned, a possible future study is understanding SLT in a managed land-use context. SLT would be calculated for higher, man-induced erosion rates. An extension of this study towards higher erosion rates might be useful to identify tipping points, erosion rates that will result in long-term loss of performance when exceeded. For the future application of the present study in an Anthropocene perspective, appropriate (shorter) time-scales need to be chosen, especially when simulations are linked to field studies. The natural (e.g. climate, erosion, and deposition) and human intervention (e.g. land-use types, agricultural practices: tillage, irrigation, fertilization) factors must be assessed in the modeling. Therefore, a future study should satisfy time series data needs in a managed land-use context.

Author contribution

This chapter was designed and written by KN Ranathunga. Peter Finke and Qiuzhen Yin had a great contribution through providing extra materials for further referencing, reviewing and correcting the flow of this chapter.

Appendix for chapter 2

Table A2-1 latitudes and longitudes of the selected sections in the study and its locations in the CLP (below)

LOCATION	LATITUDE (N)	LONGITUDE (E)
CHANG'AN	34.10	109.58
LUOCHUAN	35.80	109.40
WEINAN	34.30	109.50
CHANGWU	35.23	107.78
XIFENG	35.80	107.60
JINGYUAN	36.35	104.60
LANZHOU (JZT)	35.46	103.50
TAOYU	35.20	107.76
CHENJIAGOU	34.28	107.62

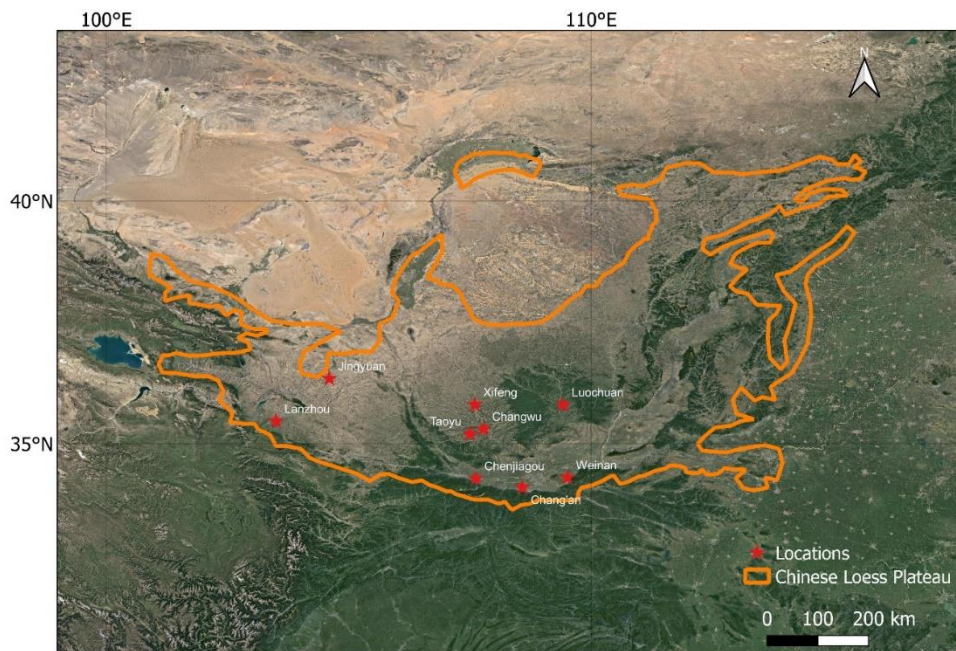


Figure A2-1 Simulation locations in the CLP referenced in the thesis.

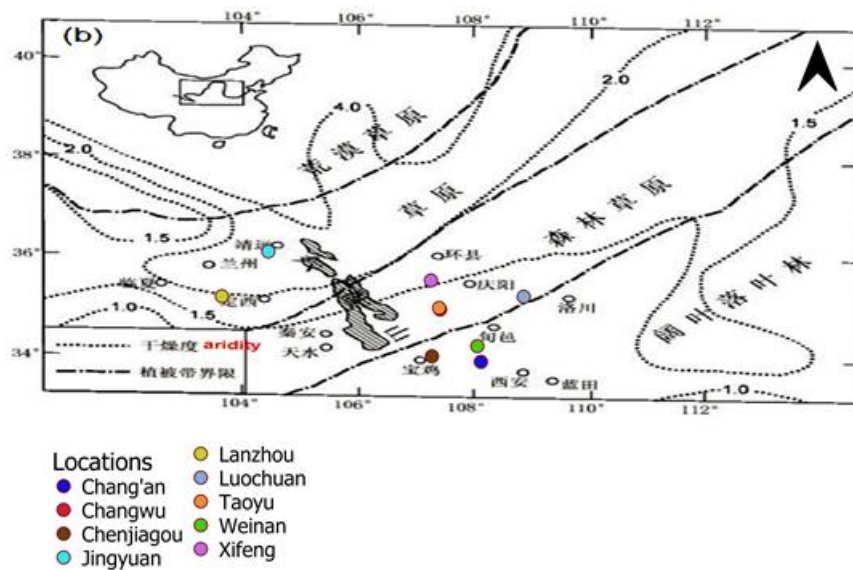


Figure A2-2 Simulation locations and the aridity of the CLP Feng et al. (2004a)

Table A2-2. Seventeen Minerals used in the SoilGen2 model. Minerals such as Calcite, Gypsum and Gibbsite can precipitate but all other minerals weather and release ions into the soil solution.

Name of the mineral	Unit
Gypsum	Mass fraction
Calcite	Mass fraction
Gibbsite $Al(OH)_3$	Mass fraction
Albite $NaAlSi_3O_8$	Mass fraction
K-feldspar $KAlSi_3O_8$	Mass fraction
Muscovite $KAl_3Si_3O_{10}(OH)_2$	Mass fraction
Biotite $KMg_{1.5}Fe_{1.5}AlSi_3O_{10}(OH)_2$	Mass fraction
Quartz SiO_2	Mass fraction
Chlorite As Clinocllore $Mg_5Al_2Si_3O_{10}(OH)_8$	Mass fraction
Anorthite $CaAl_2Si_2O_8$	Mass fraction
Fosterite Mg_2SiO_4	Mass fraction
Augite As Orthoferrosilite $FeSiO_3$	Mass fraction
Kaolinite $Al_2Si_2O_5(OH)_4$	Mass fraction
Illite $Si_{3.4}O_{10}(OH)_2Mg_{0.02}Al_{2.38}Ca_{0.01}K_{0.44}$	Mass fraction
Montmorillonite Average Composition $Si_4O_{10}(OH)_2Mg_{0.33}Al_{1.67}Ca_{0.04125}Mg_{0.04125}K_{0.0825}Na_{0.0825}$	Mass fraction
Hornblende $Ca_2Mg_4AlSi_6.7AlO_{22.4}$	Mass fraction
Fayalite Fe_2SiO_4	Mass fraction

Appendix for chapter 3

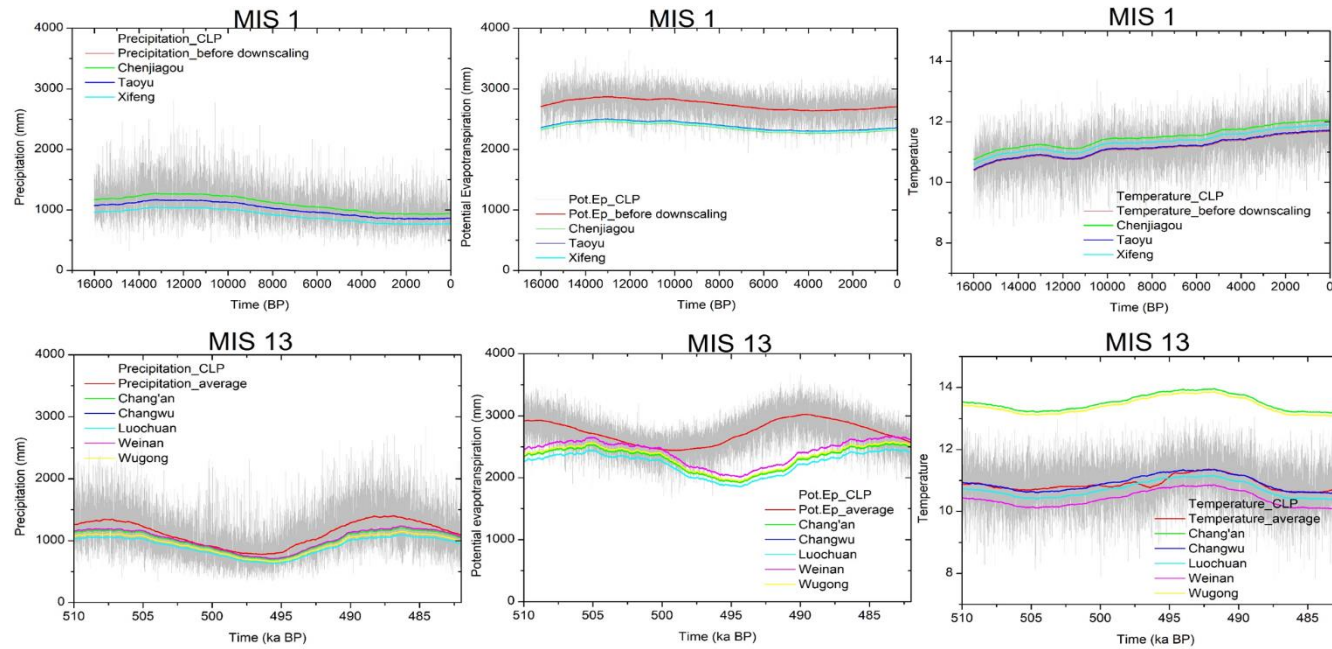


Figure A3-1 The simulated variations of the climate (temperature, precipitation, potential evapotranspiration) during MIS1 (top panel) and MIS13 (bottom panel) over the whole Chinese Loess plateau and point locations. Both yearly total (P, Ep) or mean (T) (grey line) and a 1000-year running mean are shown.

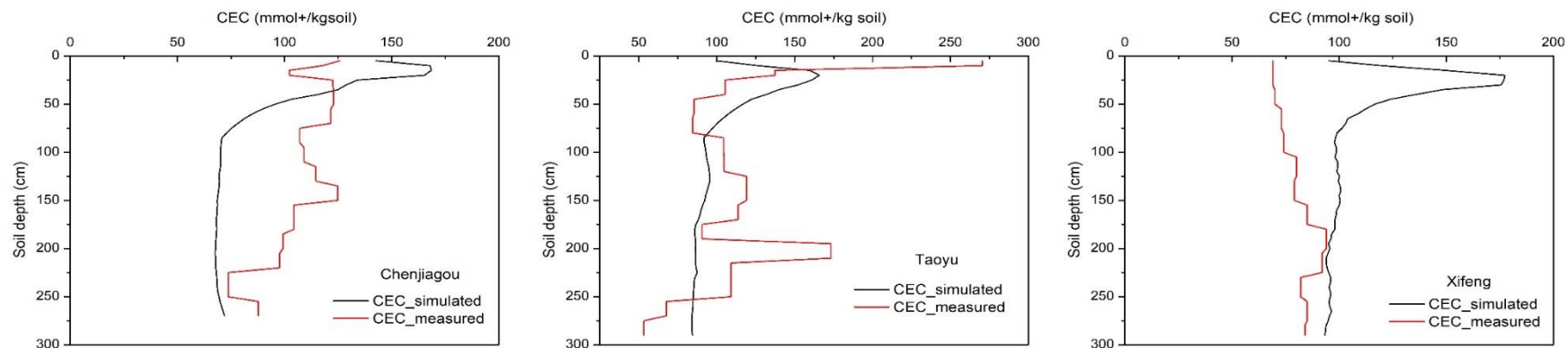


Figure A3-2 Measured and simulated Cation Exchange Capacity (CEC) in Holocene soils.

All the measured soil properties for Holocene soils are presented in Tables A3-1, A3-2, A3-3, A3-4 and A3-5. All the measured soil properties for Holocene soils are presented in Tables A3-1, A3-2, A3-3, A3-4. In there, the OC (potassium dichromate volumetric method), pH (potentiometry) and CEC (equilibrium method, ATC-160 conductivity meter, China) were measured in Analysis and Testing Center, the lab of Institute of Agriculture Environment and Sustainable Development, Chinese Academy of Agriculture Sciences. CaCO_3 (acid base titration method), soil texture (clay, silt and sand) (Mastersizer2000, Japan) bulk density (ring method) were measured in the lab of Institute of Geology and Geophysics, Chinese Academy of Sciences. The data in the Table A3-4 were measured in Soil and Mineralogy lab of Institute of Geology and Geophysics, Chinese Academy of Sciences.

Table A3-1. Dust and soil properties in Chenjiagou in the Holocene.

Dust above soil	OC (%)	CaCO ₃ (%)	Clay (%)	Silt (%)	Sand (%)	CEC*(mmol+/kg soil)	Bulk density (kg/dm ³)	Gypsum* (%)
Lo	0.38	7.94	8.82	86.98	4.20	78.52	1.37	0.1

Top (cm)	Bot (cm)	OC (%)	CaCO ₃ (%)	Clay (%)	Silt (%)	Sand (%)	pH	CEC (mmol+/kg soil)	Bulk density (kg/dm ³)
0	5	1.27	7.43	10.04	86.58	3.38	8.31	125.84	
5	10	0.90	6.84	10.76	85.94	3.30	8.18	117.72	
10	20	0.72	6.64	10.55	86.39	3.06	8.08	102.16	1.37
20	30	0.74	6.91	11.13	85.84	3.03	8.07	122.36	
30	50	0.50	6.62	10.96	86.02	3.02	8.4	122.92	
50	70	0.51	3.48	11.08	85.82	3.11	8.67	121.59	
70	90	0.51	0.00	11.81	85.11	3.08	8.53	107.02	
90	110	0.48	2.41	12.28	85.35	2.36	8.33	109.08	
110	130	0.49	4.39	10.14	87.50	2.36	7.95	114.66	1.52
130	150	0.54	1.61	13.94	84.35	1.71	7.96	124.78	
150	180	0.32	5.46	9.20	87.07	3.73	8.08	104.36	
180	200	0.52	15.96	7.33	88.40	4.28	8.36	99.25	
200	220	0.32	17.18	9.09	86.43	4.48	8.25	97.68	1.51
220	250	0.35	16.44	10.00	86.30	3.70	8.36	73.64	
250	280	0.34	17.64	8.86	86.80	4.34	8.53	87.80	

Dust below soil	OC (%)	CaCO ₃ (%)	Clay (%)	Silt (%)	Sand (%)	CEC (mmol+/kg soil)	Bulk density (kg/dm ³)	Gypsum* (%)
L1	0.38	7.94	8.82	86.98	4.20	89.58	1.37	0.1

*Note that CEC in Lo is incorrect. Bulk densities were kept as the lowest measurements (1.37) and Gypsum (%) is assumed in both Lo and L1.

Table A3-2. Dust and soil properties in Taoyu in the Holocene.

Dust above soil	OC* (%)	CaCO ₃ (%)	Clay (%)	Silt (%)	Sand (%)	CEC* (mmol+/kg soil)	Bulk density* (kg/dm ³)	Gypsum* (%)
Lo	0.001	7.86	8.45	84.05	7.5	74.32	1.15	0.5

Top (cm)	Bot (cm)	OC (%)	CaCO ₃ (%)	Clay (%)	Silt (%)	Sand (%)	pH	CEC (mmol+/kg soil)
0	10	2.30	4.69	8.90	82.64	8.46	7.7	270.32
10	20	0.70	6.45	9.13	88.13	2.74	8.36	137.43
20	40	0.51	5.75	7.63	85.60	6.77	8.4	105.29
40	60	0.46	6.07	7.34	85.27	7.39	8.47	85.38
60	80	0.42	7.85	9.33	82.60	8.08	8.51	84.53
80	100	0.42	7.03	10.32	81.95	7.73	8.52	104.35
100	120	0.44	3.48	9.43	83.47	7.10	8.57	104.71
120	150	0.54	2.98	8.92	84.67	6.41	8.48	119.10
150	170	0.62	4.32	8.13	86.20	5.67	8.54	113.71
170	190	0.54	6.27	8.41	86.02	5.57	8.49	90.65
190	210	0.50	9.77	6.46	86.21	7.33	8.42	173.15
210	230	0.30	14.12	8.43	85.37	6.20	8.61	109.25
230	250	0.34	13.34	9.29	81.79	8.91	8.4	109.06
250	270	0.30	12.74	9.09	82.92	7.99	8.37	67.64
270	280	0.21	13.00	6.97	86.12	6.92	8.68	53.24

Dust below soil	OC (%)	CaCO ₃ (%)	Clay (%)	Silt (%)	Sand (%)	CEC (mmol+/kg soil)	Bulk density* (kg/dm ³)	Gypsum* (%)
L1	0.29	7.86	8.45	84.05	7.5	84.79	1.37	0.5

*Note that CEC and OC (%) in Lo are incorrect. Bulk density and Gypsum (%) are assumed.

Table A3-3. Dust and soil properties in Xifeng in the Holocene.

Dust above soil	OC* (%)	CaCO ₃ (%)	Clay (%)	Silt (%)	Sand (%)	CEC* (mmol+/kg soil)	Bulk density* (kg/dm ³)	Gypsum* (%)
Lo	0.001	3.83	10.66	80.46	8.88	77.30	1.15	0.5

Top (cm)	Bot (cm)	OC (%)	CaCO ₃ (%)	pH	CEC (mmol+/kg soil)
0	15	0.30	5.46	8.6	69
15	30	0.41	4.52	8.5	69
30	50	0.39	3.87	8.6	70
50	75	0.37	3.52	8.8	73
75	100	0.37	2.76	9.1	74
100	125	0.42	2.82	8.3	80
125	150	0.45	1.99	8.2	79
150	175	0.40	1.44	8.2	85
175	200	0.55	2.57	7.9	94
200	225	0.37	2.8	8.1	92
225	250	0.36	4.77	7.7	82
250	275	0.41	3.65	7.8	85
275	300	0.32	4.45	8.0	84
300	350	0.25	5.27	7.9	73
350	400	0.29	5.02	8.1	71
400	450	0.26	6.68	8.5	91
450	500	0.30	4.97	8.4	93

Dust below soil	OC (%)	CaCO ₃ (%)	Clay (%)	Silt (%)	Sand (%)	CEC (mmol+/kg soil)	Bulk density* (kg/dm ³)	Gypsum* (%)
L1	0.27	3.83	10.66	80.46	8.88	88.20	1.37	0.5

*Note that CEC and OC (%) in Lo are incorrect. Bulk density and Gypsum (%) are assumed.

Table A3-4. Mineralogical composition of both deposited dust and parent loess in Holocene soils.

Site	Albite	K-Feldspar	Muscovite	Quartz	Chlorite	Illite	Otherite*
Mass%							
Chenjiagou	16.68	11.18	0.97	45.09	9.02	14.21	2.85
Taoyu	12.67	9.14	1.12	57.00	6.35	11.20	2.52
Xifeng	19.46	5.52	1.67	58.33	5.05	8.30	1.67

*Otherite refers to a user-defined mineral with geochemical composition of silica, iron (Fe⁺²) and oxygen ions.

Table A3-5. Soil texture in Xifeng in the Holocene (Data source. Dr. Hao Lu, Chinese Academy of Sciences, China).

Top(cm)	Bot(cm)	clay%	silt%	sand%
0	10	9.62	79.25	11.13
10	20	9.98	80.00	10.01
20	30	9.25	80.17	10.58
30	40	12.70	78.26	9.04
40	50	10.81	79.13	10.06
50	60	12.76	77.94	9.31
60	70	12.98	77.41	9.61
70	80	12.92	76.83	10.25
80	90	12.87	76.49	10.65
90	100	14.11	74.67	11.22
100	110	13.75	75.21	11.04
110	120	15.74	74.97	9.29
120	130	14.46	75.30	10.24
130	140	14.32	76.09	9.59
140	150	14.00	76.40	9.60
150	160	10.30	76.85	12.85
160	170	13.07	75.31	11.61
170	180	22.81	73.08	4.11
180	190	20.41	75.71	3.87
190	200	18.84	77.30	3.86
200	210	12.77	82.28	4.94
210	220	14.15	80.94	4.91
220	230	19.72	74.69	5.59
230	240	19.78	72.22	8.00
240	250	21.43	72.43	6.15
250	260	15.48	79.31	5.20
260	270	25.22	68.98	5.80
270	280	23.24	71.46	5.30
280	290	17.56	75.55	6.89
290	300	15.39	75.73	8.88
300	310	9.50	79.45	11.05
310	320	10.48	80.96	8.57
320	330	8.28	81.11	10.61
330	340	10.22	81.03	8.75
340	350	10.14	81.76	8.11
350	360	11.18	80.50	8.32

360	370	9.92	81.58	8.49
370	380	11.70	79.89	8.41
380	390	10.73	81.96	7.31
390	400	11.34	80.94	7.73
400	410	10.36	81.40	8.24
410	420	12.33	80.22	7.45
420	430	11.25	80.81	7.94
430	440	11.19	80.45	8.36
440	450	11.08	81.42	7.50
450	460	10.62	81.25	8.13
460	470	12.07	81.24	6.68
470	480	13.14	79.92	6.94
480	490	14.51	79.53	5.96
490	500	12.76	79.99	7.25

Soil data used for MIS13 paleosol simulations are presented in Tables A3-6 and A3-7.

Table A3-6. Properties of parent material and deposited dust during MIS13 used for SoilGen2. Note that except texture data (from the references mentioned) other data are from Finke et al. (2021b).

	Parent material	CaCO ₃ (%)	Clay (%)	Silt (%)	Sand (%)	CEC* (mmol+/kg soil)	Bulk density (kg/dm ³)	Gypsum (%)
Chang'an (Han et al., 1998)	dust	8.0	27.3	72.5	0.2			
	loess	8.0	40.0	59.7	0.3	153.12	1.15	0.15
Changwu (Yin, 2008) Chinese	dust	9.0	14.5	58.5	27.0			
	loess	9.0	14.5	78.5	7.0	153.12	1.15	0.15
Wugong (Huang, 2011)Chinese	dust	10.70	48.0	45.0	7.0			
	loess	10.70	36.0	54.0	10.0	153.12	1.15	0.13
Luochuan (An et al., 1987)	dust	13.0	28.0	68.0	4.0			
	loess	13.0	48.0	40.0	12.0	153.12	1.15	0.15
Weinan (Han et al., 1998)	dust	16.0	35.0	64.6	0.4			
	loess	16.0	35.0	61.0	4.0	153.12	1.15	0.15

*Initial CEC was not corrected for clay and OC content and was kept as identical between locations.

Table A3-7. Mineralogical composition of both deposited dust and parent loess in MIS13 paleosols (Finke et al., 2021b).

Site	Parent material	Albite	K-Feldspar	Muscovite Mass%	Quartz	Chlorite	Anorthite	Kaolinite	Montmorillonite	Hornblende
Changwu	dust	5.29	3.18	23.28	34.60	12.83	2.27	5.88	2.27	1.25
	loess	5.29	3.18	23.28	34.60	12.83	2.27	5.88	2.27	1.25
Chang'an	dust	5.35	3.21	23.53	34.99	12.97	2.29	5.94	2.30	1.27
	loess	5.35	3.21	23.53	34.99	12.97	2.29	5.94	2.30	1.27
Wugong	dust	5.19	3.12	22.84	33.96	12.59	2.23	5.77	2.23	1.23
	loess	5.19	3.12	22.84	33.96	12.59	2.23	5.77	2.23	1.23
Luochuan	dust	5.30	3.19	23.88	32.42	8.14	2.27	5.76	4.69	1.20
	loess	5.30	3.19	23.88	32.42	8.14	2.27	5.76	4.69	1.20
Weinan	dust	8.08	4.86	13.28	30.61	1.74	3.46	2.93	17.01	1.85
	loess	8.08	4.86	13.28	30.61	1.74	3.46	2.93	17.01	1.85

All the mineralogical composition in over and –under lying loess keep as identical.

Tables A3-8 and A3-9 show MIS13 paleosol data from literature.

Table A3-8. Measured clay% in MIS13 paleosol in Chang'an and Weinan.

Top(cm)	Bot(cm)	Clay%	Top(cm)	Bot(cm)	Clay%
Chang'an (Han et al., 1998)			Weinan (Han et al., 1998)		
0	20	27	0	20	31.5
20	40	31	20	40	35
40	60	34.5	40	60	38.5
60	80	37	60	80	42
80	100	39	80	100	44
100	120	41	100	120	43
120	140	44	120	140	41.5
140	160	44.5	140	160	40
160	180	43.5	160	180	38

Table A3-9. Measured clay% in MIS13 paleosol in Luochuan, Wugong and Changwu.

Top(cm) soil	Bot(cm) soil	Clay% in Luochuan	Clay% in Wugong	Clay% in Changwu
		An et al., 1987	Huang, 2011, Chinese	Yin, 2008, Chinese
0	20	20	39	14.5
20	40	26	42	18
40	60	32	45.5	20.5
60	80	36	50	22
80	100	38	52	20
100	120	40	51.5	18.75
120	140	44	50	19
140	160	52	47	20
160	180	50	44	18

Comparison of measured and simulated contents of calcite and organic carbon content (in the Holocene) at the end of calibration. Clay content is confronted to measurements during MIS 13 along the soil profile.

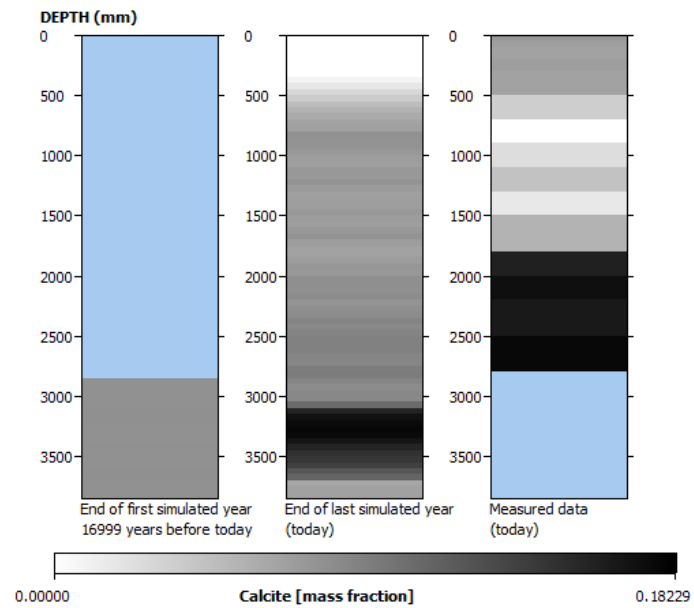


Figure A3-3 Initial (first bar), simulated (middle bar) and measured (last bar) calcite content (mass fractions) in Chenjiagou in the Holocene.

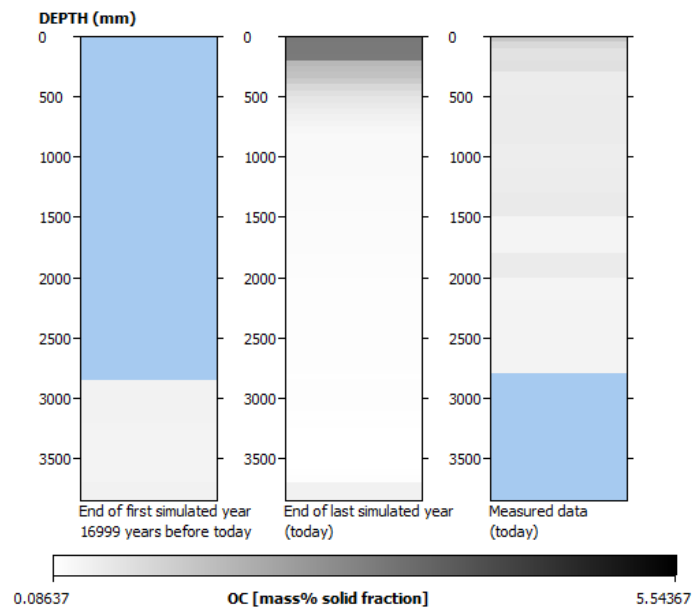


Figure A3-4 Initial (first bar), simulated (middle bar) and measured (last bar) organic carbon content (mass %) in Chenjiagou in the Holocene.

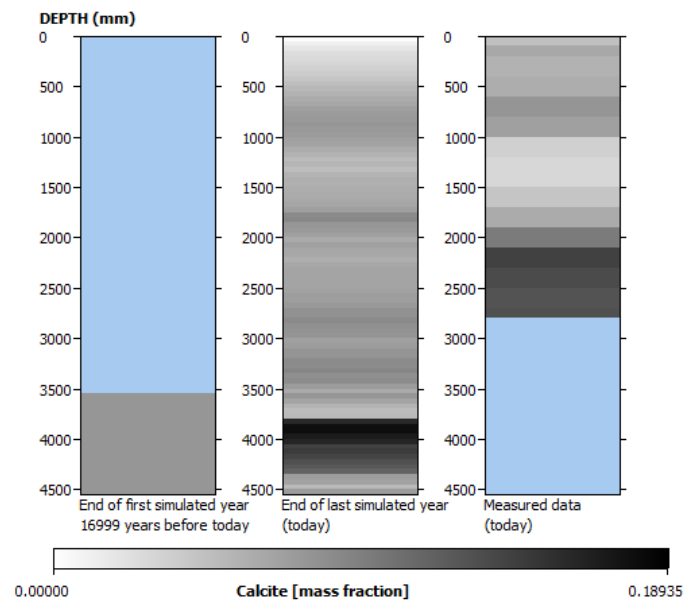


Figure A3-5 Initial (first bar), simulated (middle bar) and measured (last bar) calcite content (mass fractions) in Taoyu in the Holocene.

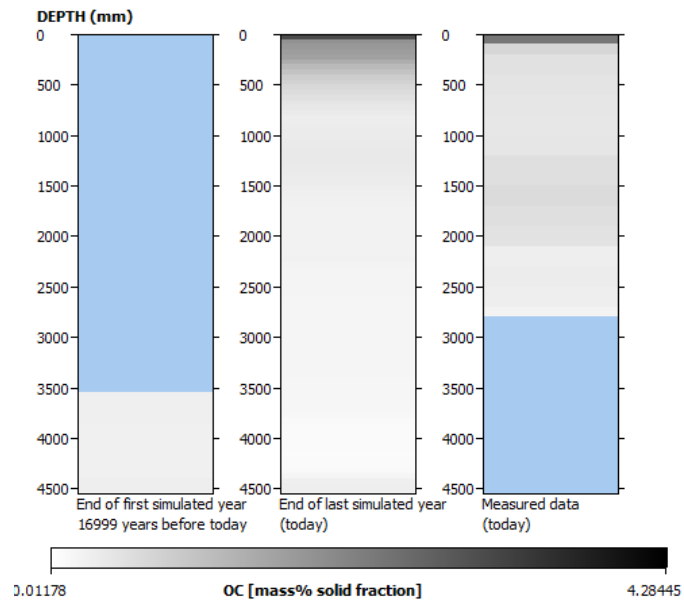


Figure A3-6 Initial (first bar), simulated (middle bar) and measured (last bar) organic carbon content (mass %) in Taoyu in the Holocene.

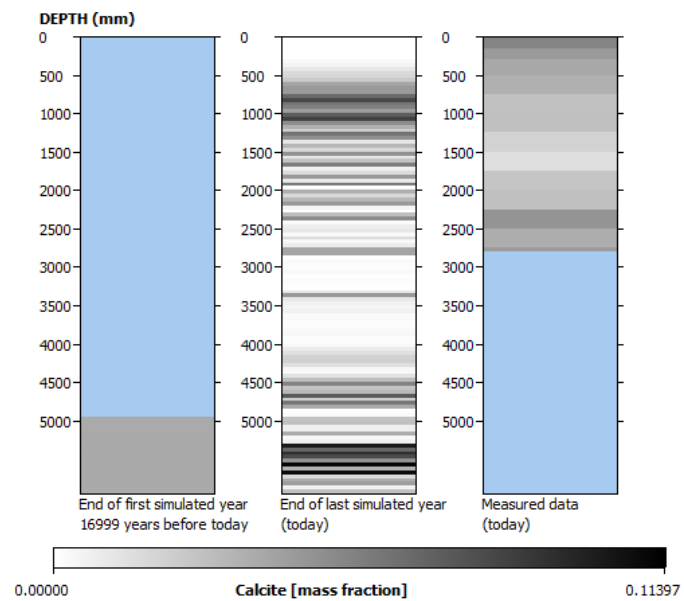


Figure A3-7 Initial (first bar), simulated (middle bar) and measured (last bar) calcite content (mass fractions) in Xifeng in the Holocene.

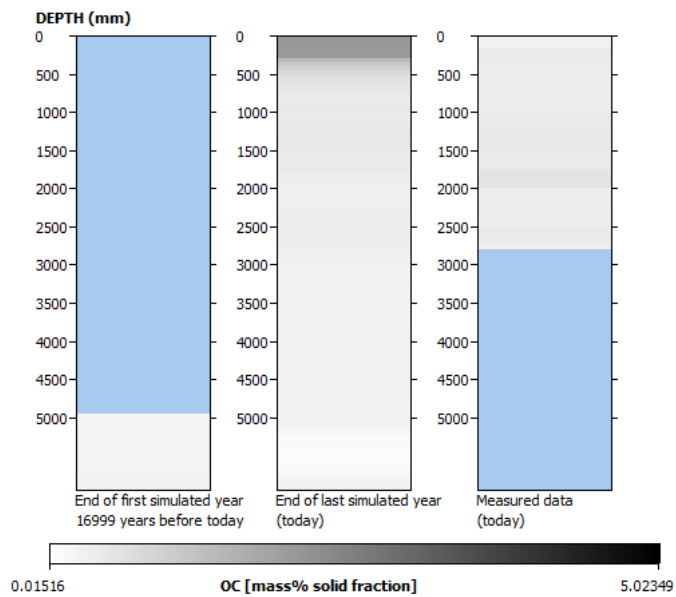


Figure A3-8 Initial (first bar), simulated (middle bar) and measured (last bar) organic carbon content (mass %) in Xifeng in the Holocene.

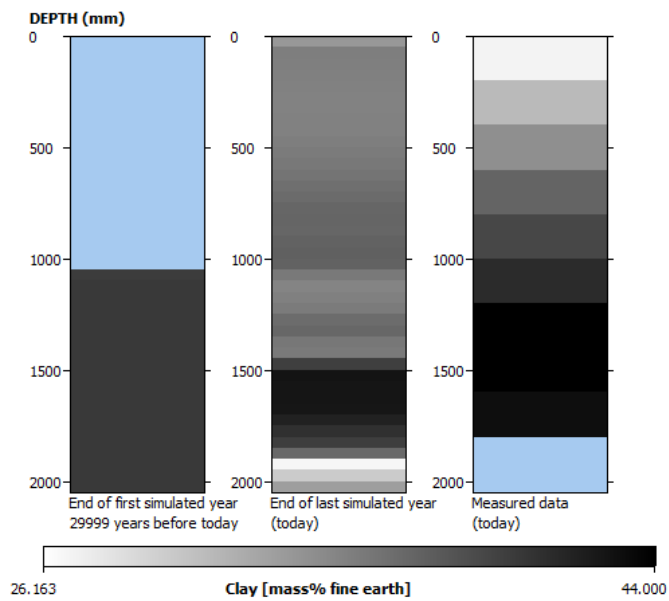


Figure A3-9 Initial (first bar), simulated (middle bar) and measured (last bar) clay content (mass %) in Chang'an in MIS 13.

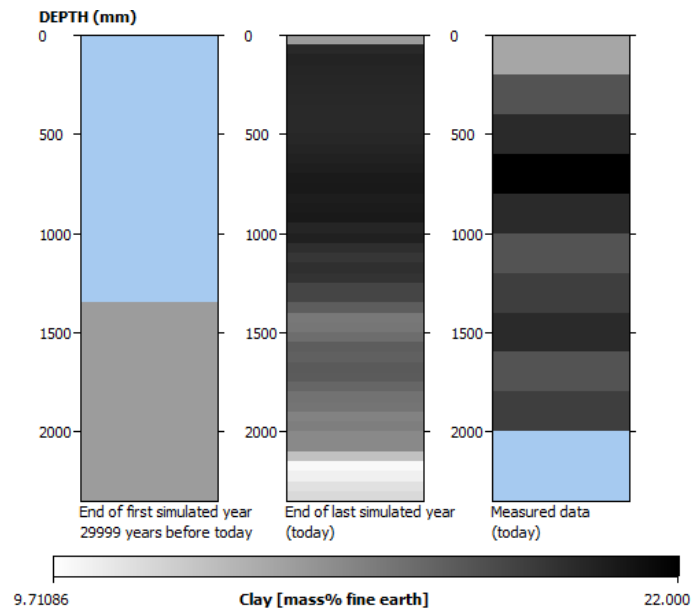


Figure A3-10 Initial (first bar), simulated (middle bar) and measured (last bar) clay content (mass %) in Changwu in MIS 13.

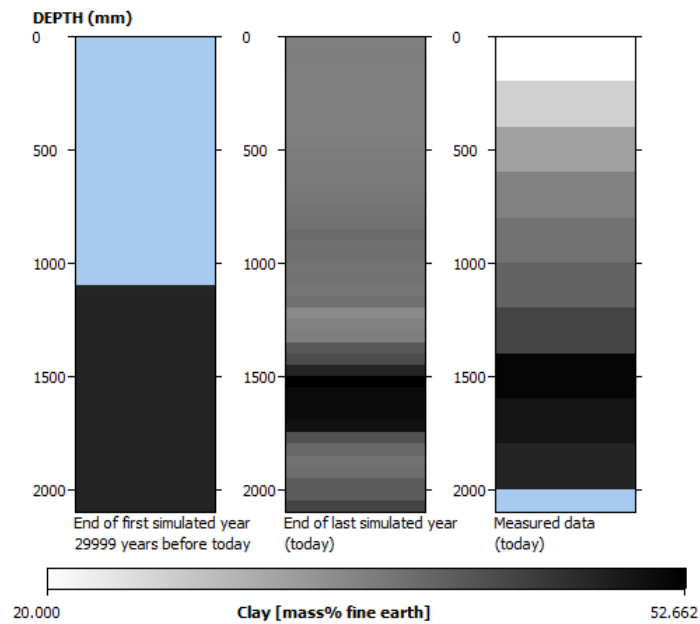


Figure A3-11 Initial (first bar), simulated (middle bar) and measured (last bar) clay content (mass %) in Luochuan in MIS 13.

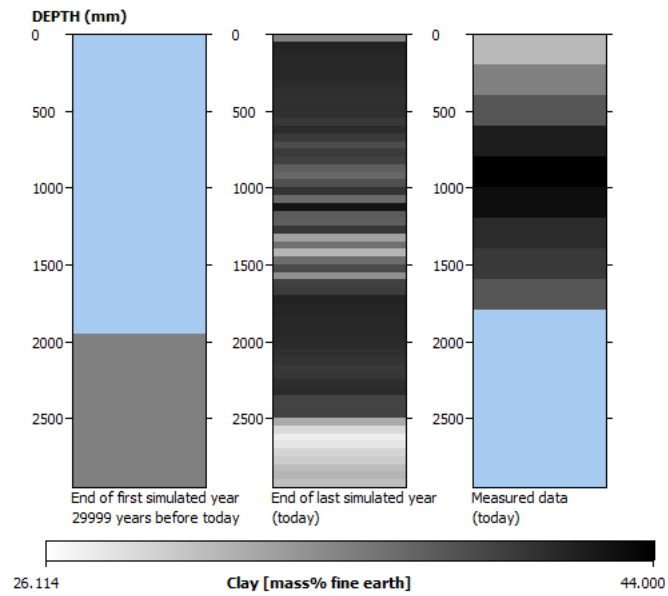


Figure A3-12 Initial (first bar), simulated (middle bar) and measured (last bar) clay content (mass %) in Weinan in MIS 13.

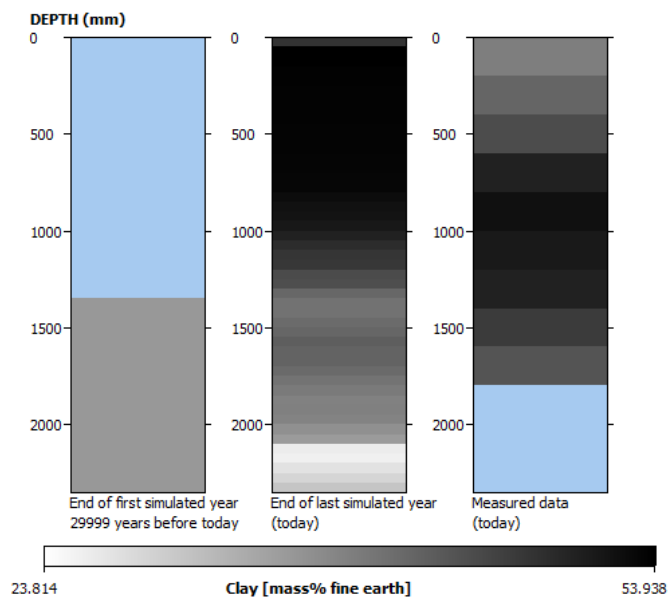


Figure A3-13 Initial (first bar), simulated (middle bar) and measured (last bar) clay content (mass %) in Wugong in MIS 13.

In SoilGen2, the splash detachment rate ($\text{g m}^{-2} \text{h}^{-1}$), D is estimated as follows in Eq. A3-1.

$$D = kd * E * R * (1 - sc) * DCs \quad \text{Eq.A-1}$$

where kd is the soil detachability coefficient (g J^{-1}). E ($\text{J m}^{-2} \text{mm}^{-1}$) is the kinetic energy of the rainfall calculated using the relation from the revised universal soil loss equation (Brown and Foster, 1987). R (mm hour^{-1}) is rainfall intensity and sc is a fraction for accounting for the soil cover or humus profile. DCs is the amount of readily available dispersible particles (g g^{-1} soil) at the surface 1 mm. So, the thickness of the ectorganic layer thickness determines available dispersible clay particles.

In SoilGen2 the dispersible clay transportation via macropores is calculated as follows:

$$fDC = \{1 - (SC/CSC)\} * \theta_{macro} * fVC \quad \text{Eq.A-2}$$

where, fDC is the fraction of dispersed clay, θ_{macro} is the volumetric water fraction ($\text{m}^3 \text{water m}^{-3} \text{soil}$) held in macro-pores. θ_{macro} is tuned via pressure head in macropores, $h\theta_{macro}$ (hPa) near saturation during calibration. The h can be calibrated in the model. SC ($\text{mmolc dm}^{-3} \text{water}$) is the total electrolyte concentration, and CSC ($\text{mmolc dm}^{-3} \text{water}$) is the critical salt concentration, both are computed by the model. fVC is the fraction of clay volume in soil.

Some of the dispersible clay particles are filtered (due to surface roughness) during its transportation via macropores. The amount of filtered clay, F ($\text{g m}^{-3} \text{hour}^{-1}$) can be calibrated via the filter coefficient, n as follows:

$$F = f_{ref} * V_{ref}^n * V^{1-n} * C * \theta \quad \text{Eq.A-3}$$

where, f_{ref} (m^{-1}) is a reference filter coefficient, v_{ref} (m hour^{-1}) is the reference pore-water velocity in macropores at which f_{ref} is measured. V is the current pore water velocity that is simulated by SoilGen2. C is the particle concentration ($\text{g m}^{-3} \text{water}$) and n is an empirical exponent, which was subjected to calibration and we calibrated n .

Finally, production of clay by physical weathering is computed in SoilGen2 as follows:

$$PS = PS_{max} \text{ if } \frac{dT}{dt} > B \quad \text{Eq.A-4}$$

$$\frac{PS_{max} * \frac{dT}{dt}}{B} \text{ if } \frac{dT}{dt} \leq B$$

where, the parameter, PS_{max} is dimensionless and it is the maximal split probability and B is the threshold temperature gradient ($^{\circ}\text{C hour}^{-1}$) over dt where PS reaches its maximum value and T is the temperature. These two parameters are subjected to calibrated (PS and B), where the temperature gradient per soil compartment (5 cm) determines the number of events required to achieve successful splits.

$$E(N) = \frac{m}{PS} \quad \text{Eq.A-5}$$

The number of grains in any particle size class i that is split in dt is then given by the number,

$$S_{i,dt} = \min(k_{i,t-dt}, \frac{K_{i,t-dt}}{E}) \quad \text{Eq.A-6}$$

where $k_{i,t-dt}$ is the number of grains in particle size class at the start of dt , and

$$K_{i,t} = K_{i,t-dt} - a * S_{i,dt} + b * 8 * S_{i-1,dt} \quad \text{Eq.A-7}$$

where $a = 0$ for the clay fraction ($i = 11$) and $a = 1$ else; $b = 0$ for the coarsest sand fraction ($i = 1$) and $b = 1$ else. Thus, B and PS_{max} are subjected to changes during calibration.

Table A3-10. Records of Aeolian activity in the loess plateau employed in this study.

Loess section	Latitude Longitude	Method	Important remarks	Uncertainty of OSL soil ages	Reference
(1) Weinan- southern margin of CLP	34°24' 54.8 109° 33' 44	Quartz OSL (4-11μm)	Continuous dust addition for the last 15ka (average age uncertainty +/-0.335 ka years)	Uncertainty of OSL ages range from 0.01 ka years to 0.96 ka years over the measured soil depths of 310 cm	(Kang et al., 2018)
(2) Yuanbao- north western CLP	35° 38' 23.3"N 103° 08' 50.2" E	OSL, coarse- silt-sized quartz (45-63μm)	Continuous dust deposition from 17ka. (average age uncertainty +/-0.913 ka years)	Uncertainty of OSL ages range from 0.06 ka years to 1.3 ka years over the measured soil depths of 400 cm	(Lai and Wintle, 2006)
(3) Beigouyuan Holocene section- northwest CLP	36° 37' 21.3"N 107° 17' 12.2"E	OSL, coarse- quartz-silt (40-63μm)	A most complete 15ka age record. Age interruption between 10-14ka and the absence of ages in the upper 80 cm due to agriculture.	Sedimentation rates : 9.6 +/-7.6 cm/ky (8-10 ka BP), 4.8+/-2.9cm/ky (14.5-18.5 ka BP) and 40.6+/- 7.5 cm/ky (19.6-18.85 ka BP).	(Stevens et al., 2006)
(4) Yaoxian (YXRL) southern CLP	34° 53'N 108° 45'E	OSL quartz (63-150μm)	Absence of ages between 8-18ka due to erosional hiatus. The last 0.8ka was disordered by human activities.	Uncertainty of OSL age ranges from 0.09 ka years to 0.88 ka years over the measured soil depths of 320 cm	(Zhao et al., 2007)
(5) Luochuan- Heimugou- central CLP	35° 45'N 109° 25'E	Quartz OSL	No major age disturbances were reported in the Holocene soil	Uncertainty of OSL age ranges from 0.02 ka years to 1.1 ka years over the soil depths of 200 cm	(Lu et al., 2007)

(6) Jingbian- desert margin of CLP	37° 29' 58.74"N 108° 54'.2 72"E	Quartz OSL (63- 90µm) K-feldspar pIR-IRSL (90-180µm)	Partly (un)disturbed Holocene section.	Uncertainty of OSL age ranges from 0.06 ka years to 1.4 ka years over the soil depths of 200 cm	(Stevens et al., 2018)
(7) Jingyuan1- north west CLP	36° 21'N 104° 37'E	OSL coarse- quartz (50-80 µm)	Dust deposition rates were high and nearly continuous and therefore weak pedogenesis.	Uncertainty of OSL age ranges from 0.01 ka years to 1.0 ka years over the soil depths of 300 cm	(Sun et al., 2010)
(8) Duowa- western CLP	35° 39'N 102° 38' E	OSL-fine- grains (4-11µm)	Quasi-continuous dust addition in the last 12030 years Agricultural practices (e.g. terrace-making) records after 2.5ka.	Uncertainty of OSL age ranges from 20 years to 1150 years over the soil depths of 420 cm	(Roberts et al., 2001)
(9) Jingyuan2- north west CLP	36. 35°N 104 .6°E	OSL coarse- quartz (50-90µm)	High dust deposition rates with weak pedogenesis.	Error of sedimentation rates range from 0.7 to 7.2 cm/kyr at the Jingyuan2 section. Errors of OSL ages in between 0.2-0.8 ka years	(Sun et al., 2012)
(10) Hani peat-north eastern China	42° 13'N 126° 31'E	¹⁴ C AMS radiocarbon	A 14.5ka record of dust deposition.	8- 6 kyr BP- sedimentation rate 6.3 (+/- 1.3g/m ² yr), and 4.5-2.2 kyr BP 20.7 (+/-4.7 g/yr.yr)	(Pratte et al., 2019)

Table A3-11. A summary of Interception loss (%) of gross rainfall for different vegetation in previous studies.

vegetation type	Interception loss (I) of total rainfall (%) (I/P)	climate	Location	Reference
Forests				
Coniferous	25 - 45%		England	(Calder et al., 2003)
Broad-leaved deciduous	10 - 25%			
major Chinese forests (both coniferous and broad-leaved)	14.7 – 31.8%	semi-arid	China	(Wei et al., 2005)
acacia forests (south-facing)	15.80%	semi-arid	China	(Wang et al., 2012)
acacia forests(north-facing)	22.40%			
<i>Picea crassifolia</i> (Spruce forest)	35.1% (-/+)20.7%	semi-arid	CLP, China	(He et al., 2014)
Mixed forest of broad-leaved forest and <i>Pinus koiensis</i> (Korean pine : coniferous)	22% (2010) 21.9% (2011)	semi-arid	Northeastern China	(Sheng and Cai, 2019)
<i>Pinus tabuliformis</i> (Chinese pine trees)	22.4 (+/-) 7.1%	semi-arid	CLP, China	(Jian et al., 2015)
<i>Robinia pseudoacacia</i> (Black locust : deciduous)	21.1(+/-) 6.7%			
<i>Cyclobalanopsis multinervis</i> , <i>Cyclobalanopsis oxyodon</i> , <i>Fagus engleriana</i> , <i>Quercus serrata</i> (Mixed evergreen and deciduous broadleaved forest)	14.30%	subtropical	Northwest China	(Su et al., 2016)
Evergreen broadleaved forest	11.10%	warm temperate	Southwest China	(Liu et al., 2003)
Evergreen broadleaved and pine forest	24.00%	humid subtropical	Central-south China	(Zhang et al., 2006b)
Grass/Shrubs				
<i>Caragana korshinskii</i> Kom. (Korshinsk peashrub-Shrub)	18.3 (+/-) 5.8%	semi-arid	CLP, China	Jian et al., 2015

<i>Hippophae rhamnoides</i> (Sea buckthorn-spiny deciduous shrub)	28.0(+/-) 7.35%			
<i>Caragana korshinskii</i> Kom (Shrubs)	13.99%	semi-arid	China	(Jian et al., 2014)
<i>Diospyrus texana</i> , <i>Acacia farnesiana</i> , <i>Prosopis laevigata</i> (Shrubs)	27.2%	subhumid, Subtropical	Mexico	(Návar and Bryan, 1990)
tussock grasslands	10% (small rain events) 80% (larger rain events)		Ecuador	(Ochoa-Sánchez et al., 2018)
Agricultural crops				
Farmlands (potato, millet)	4.90%	semi-arid	CLP, China	(Wang et al., 2012)
maize	12.50%	semi-arid	CLP, China	(Zheng et al., 2018)

Appendix for chapter 4

Table A4-1 Mean absolute error (MAE) and Gain in MAE for calcite in other extra sensitivity experiments in MIS11

Experiment Calcite in MIS11	Mean absolute error	Gain in MAE%
Joint- Ex (Temp+Evapo)	46086.04	28.17
Joint -Ex (Temp+Dust)	34673.36	45.96
Joint -Ex (Evapo+Dust)	34430.62	46.33
Joint -Ex (PP+Evapo+Temp)	20364.01	68.26
Joint -Ex (PP+Temp+Dust)	6777.00	89.44

Table A4-2 Mean absolute error (MAE) and Gain in MAE for clay in other extra sensitivity experiments in MIS11

Experiment Clay in MIS11	Mean absolute error	Gain in MAE%
Joint- Ex (Temp+Evapo)	17.39	0.09
Joint -Ex (Temp+Dust)	6.64	61.87
Joint -Ex (Evapo+Dust)	7.01	59.71
Joint -Ex (PP+Evapo+Temp)	21.80	-25.38
Joint -Ex (PP+Temp+Dust)	1.39	92.00

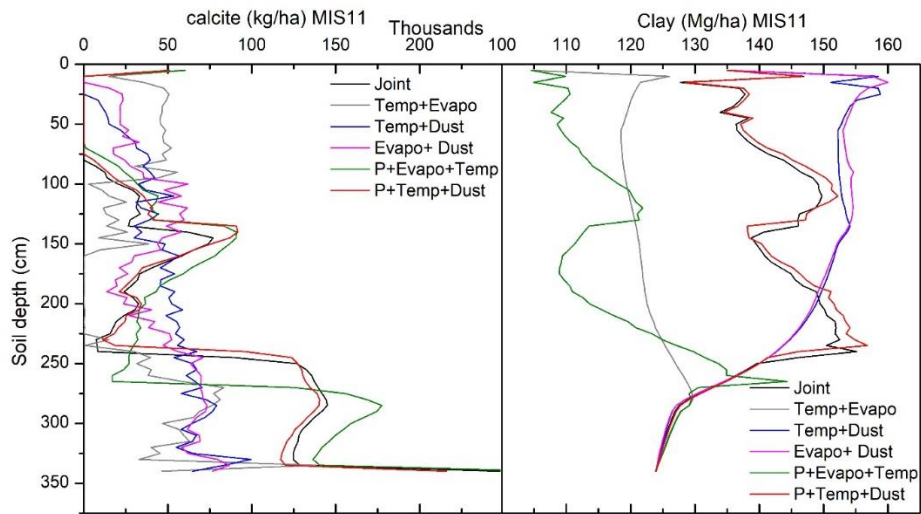


Figure A4-1. Simulated depth distribution of calcite (kg/ha, left) and clay (Mg/ha, right) for MIS11, for the Joint simulation, and parameter combinations with Temperature (Temp), potential evapotranspiration (Evapo) and dust addition (Dust) time series.

Table A4-3 Mean absolute error (MAE) and Gain in MAE for calcite in other extra sensitivity experiments in MIS13

Experiment Calcite in MIS13	Mean absolute error	Gain in MAE%
Joint- Ex (Temp+Evapo)	35636.2	16.80
Joint -Ex (Temp+Dust)	40584.5	5.25
Joint -Ex (Evapo+Dust)	39080.0	8.76
Joint -Ex (PP+Evapo+Temp)	27411.40	36.00
Joint -Ex (PP+Temp+Dust)	18351.00	57.16

Table A4-4 Mean absolute error (MAE) and Gain in MAE for clay in other extra sensitivity experiments in MIS13

Experiment Clay in MIS13	Mean absolute error	Gain in MAE%
Joint- Ex (Temp+Evapo)	13.5	-108.15
Joint -Ex (Temp+Dust)	6.84	-5.23
Joint -Ex (Evapo+Dust)	14.06	-116.31
Joint -Ex (PP+Evapo+Temp)	16.43	-152.70
Joint -Ex (PP+Temp+Dust)	4.72	27.38

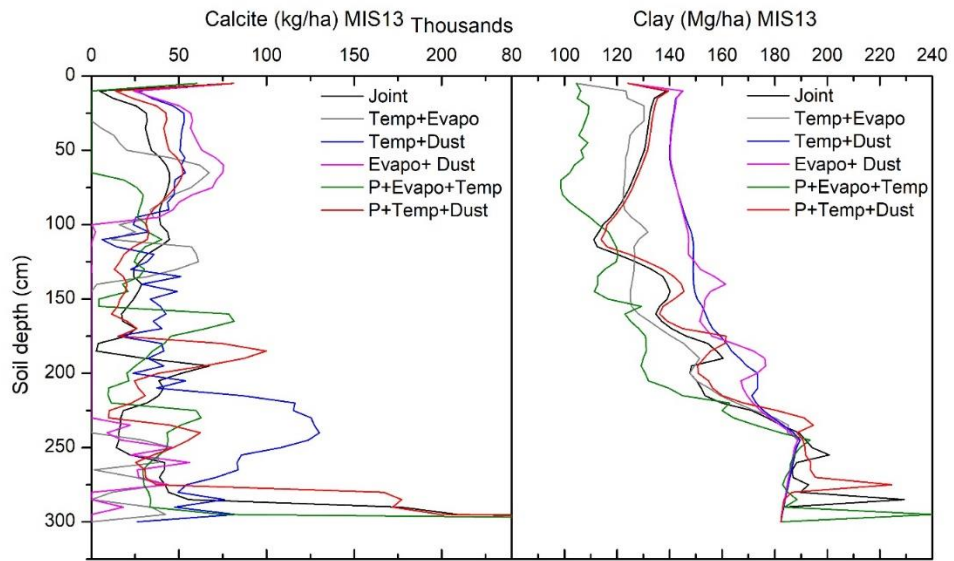


Figure A4-2. Simulated depth distribution of calcite (kg/ha, left) and clay (Mg/ha, right) for MIS 13, for the Joint simulation, and parameter combinations with Temperature (Temp), potential evapotranspiration (Evapo) and dust addition (Dust) time series.

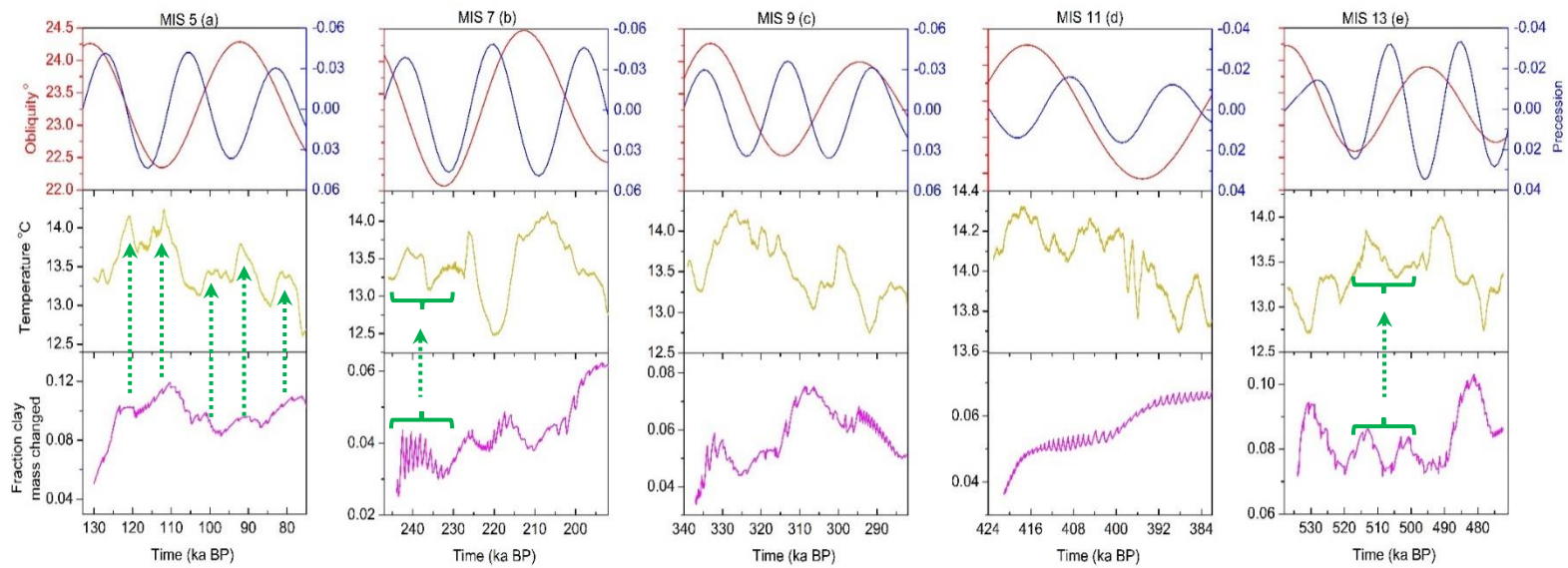


Figure A4-3. Comparison between clay content and annual mean temperature. In each panel, top to bottom obliquity (red) and precession (blue), annual mean temperature (yellow) and the simulated clay content (pink) during MIS 5 (a); MIS 7 (b); MIS 9 (c); MIS 11 (d); MIS 13 (e). Green arrows shows the link between simulated clay and temperature peaks.

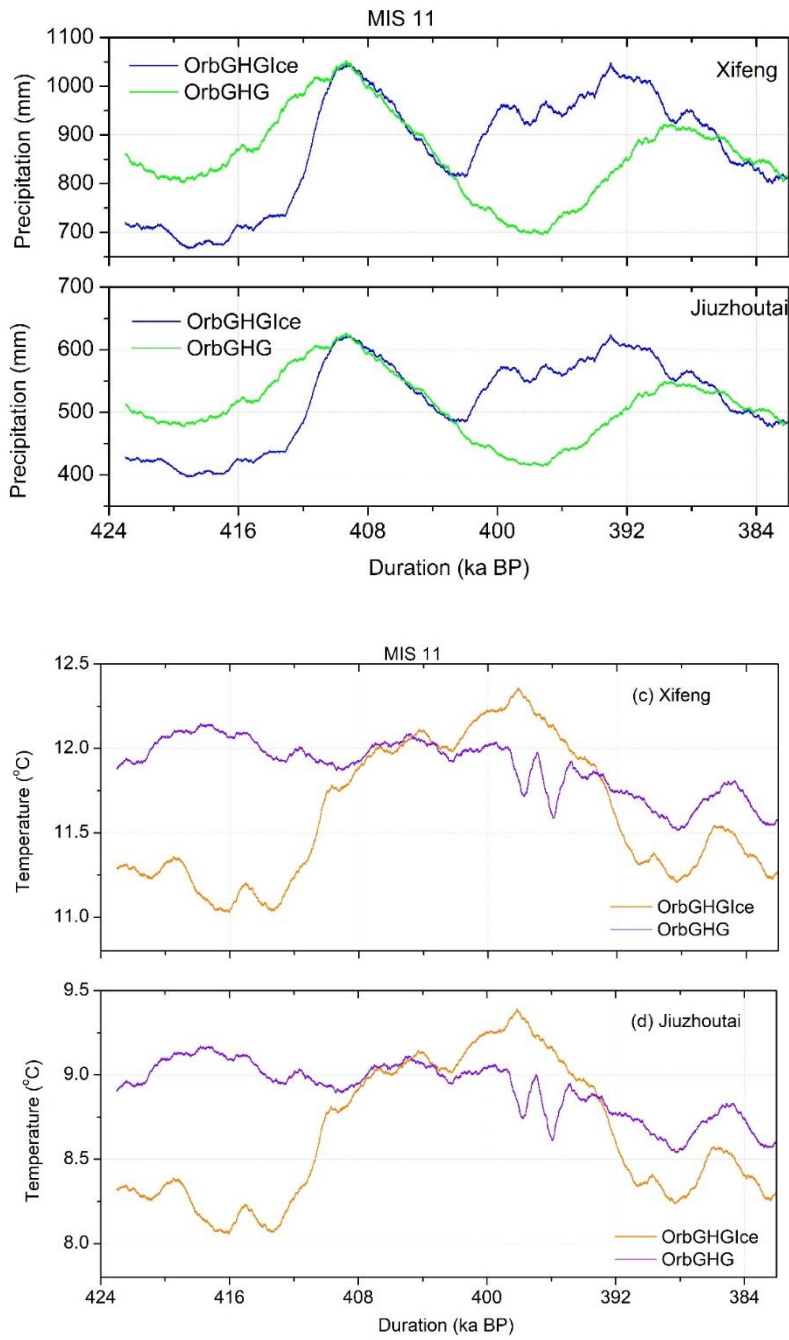


Figure A4-4. The simulated annual mean precipitation, (a) Xifeng, (b) Jiuzhoutai. The simulated annual mean temperature in (c) Xifeng and (d) Jiuzhoutai during MIS 11.

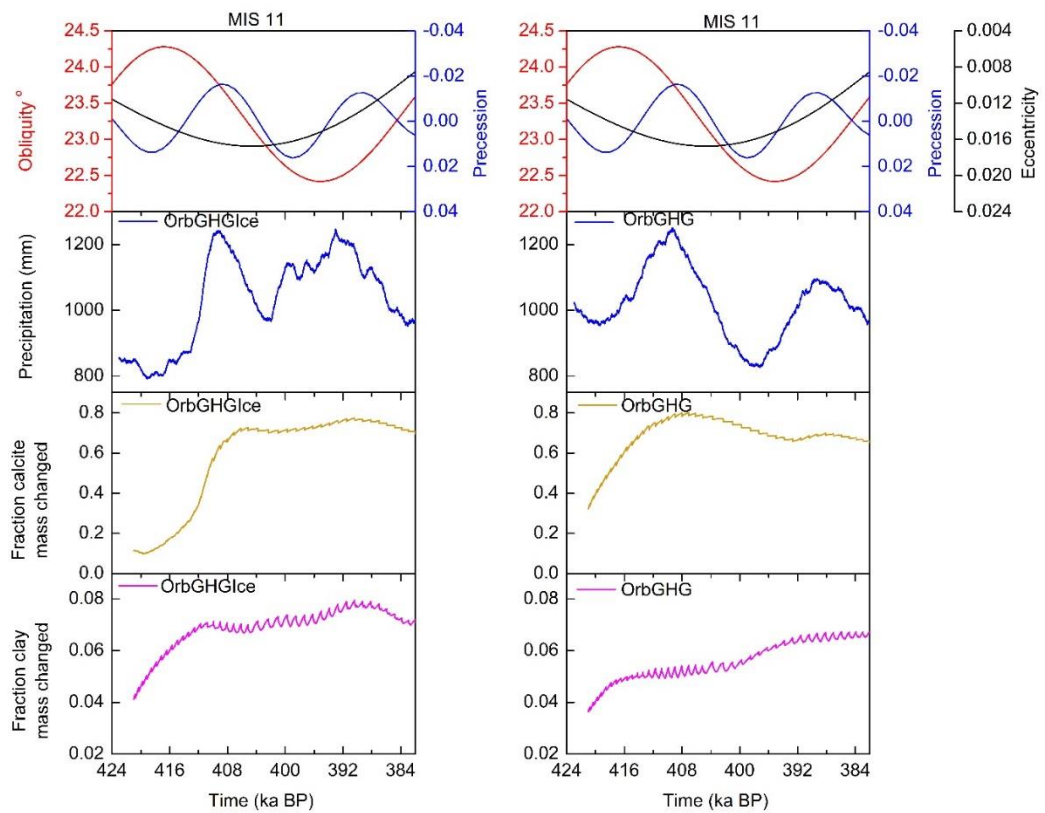


Figure A4-5 Comparison of soil development between the ice scenario (left) and the no ice scenario (right) in Chang'an during MIS 11. In each panel, from top to bottom astronomical parameters, precipitation (blue), calcite (brown) and clay (pink) during MIS11. Note that the variations of profile development of calcite and clay are relatively minor in ice scenario.

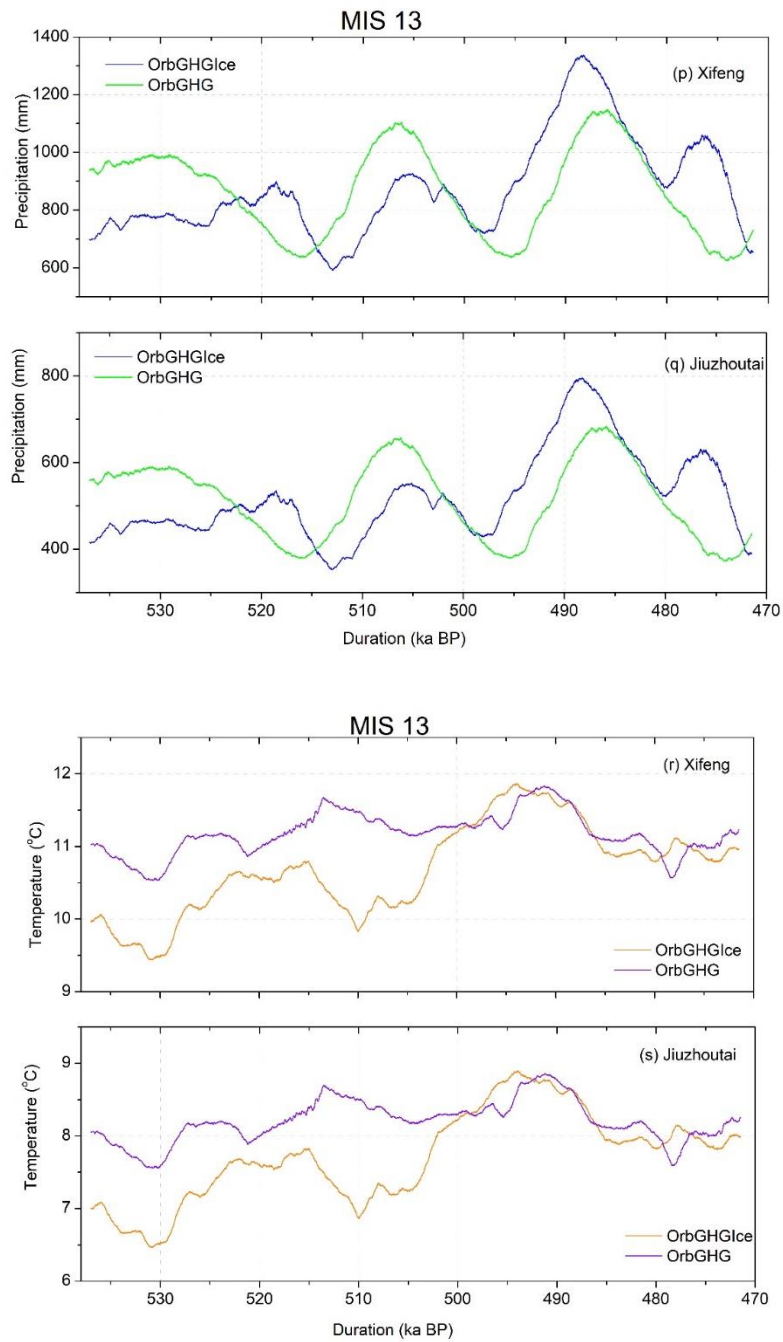


Figure A4-6. The simulated annual mean precipitation, (p) Xifeng, (q) Jiuzhoutai. The simulated annual mean temperature, (r) Xifeng and (s) Jiuzhoutai during MIS 13.

Table A4-5. Initial data for interglacial paleosol simulations in Chang'an, data from Pang and Huang (2006), Zhao, (2005), Jeong et al. (2011), Zhao et al., (2015), Zhao et al. (2018) and from unpublished sources collected by Ms. Shaohua Tian.

Location- Chang'an Southeast CLP								
Interglacial	Parent material	OC%	Sand%	silt%	clay%	Bulk density (kg/dm ³)	CaCO ₃ %	Gypsum%
MIS5	Dust	0.26	12.86	68.7	18	1.26	8.75	0.26
	Loess	0.26	1.56	75	23	1.28	6.3	0.24
MIS7	Dust	0.26	1.56	75	23	1.28	6.3	0.24
	Loess	0.26	0.56	74	25	1.28	15.75	0.25
MIS9	Dust	0.26	0.56	74	25	1.28	15.75	0.25
	Loess	0.26	1.56	77	21	1.28	7.97	0.25
MIS11	Dust	0.26	1.56	77	21	1.28	7.97	0.25
	Loess	0.26	2.56	78	19	1.3	12.5	0.25
MIS13	Dust	0.26	2.56	78	19	1.3	12.5	0.25
	Loess	0.26	1.56	70	28	1.3	6.8	0.25

Table A4-6. Mineral data for interglacial paleosol simulations in Chang'an Geong et al. (2011), Zhao (2005), Zhao et al. (2014), Zhao et al., (2015)

Interglacial	Parent material	Albite	K-Feldspar	Muscovite	Biotite	Quartz	Chlorite	Anorthite	Kaolinite	Illite	Montmorillonite	Hornblende
Mass%												
MIS5	Dust	7.00	4.12	38.34	0.00	27.95	0.36	3.00	0.45	5.13	12.06	1.59
	Loess	7.35	4.65	29.14	0.00	30.02	0.24	3.15	0.72	6.11	16.88	1.73
MIS7	Dust	7.35	4.65	29.14	0.00	30.02	0.24	3.15	0.72	6.11	16.88	1.73
	Loess	6.79	4.15	32.01	0.00	27.41	0.38	2.91	0.69	6.79	17.30	1.57
MIS9	Dust	6.79	4.15	32.01	0.00	27.41	0.38	2.91	0.69	6.79	17.30	1.57
	Loess	12.18	4.29	33.08	0.00	40.45	0.00	5.21	0.00	3.16	0.00	1.63
MIS11	Dust	12.18	4.29	33.08	0.00	40.45	0.00	5.21	0.00	3.16	0.00	1.63
	Loess	11.91	4.40	33.91	0.00	40.12	0.00	5.10	0.00	2.89	0.00	1.67
MIS13	Dust	11.91	4.40	33.91	0.00	40.12	0.00	5.10	0.00	2.89	0.00	1.67
	Loess	12.95	3.98	30.68	0.00	41.39	0.00	5.55	0.00	3.94	0.00	1.51

Table A4-7. Initial and mineral data for interglacial paleosol simulations in Xifeng, and are obtained from (Eden et al., 1994; Zheng et al., 1994; Sun, 2007; Jeong et al., 2011) and from Prof. Qingzhen Hao, and from unpublished sources collected by Ms. Shaohua Tian.

Location- Xifeng								
Interglacial	Parent material	OC%	Sand%	silt%	clay%	Bulk density (kg/dm ³)	CaCO ₃ %	Gypsum%
MIS11	Dust	0.02	4.97	86.07	8.92	1.28	8.41	0.15
	Loess	0.02	5.27	85.56	9.14	1.3	8.64	0.15
MIS13	Dust	0.02	5.27	85.56	9.14	1.3	8.64	0.15
	Loess	0.03	1.69	88.96	9.31	1.3	12	0.15

Interglacial	Parent material	Albite	K-Feldspar	Muscovite	Biotite	Quartz	Chlorite	Anorthite	Kaolinite	Illite	Montmorillonite	Hornblende
Mass%												
MIS11	Dust	9.65	1.53	13.91	0.00	47.39	13.53	4.13	2.00	4.18	1.37	2.32
	Loess	9.42	1.49	16.35	0.00	46.05	13.36	4.04	2.07	4.79	0.56	1.87
MIS13	Dust	9.42	1.49	16.35	0.00	46.05	13.36	4.04	2.07	4.79	0.56	1.87
	Loess	9.56	1.52	14.71	0.00	45.80	15.57	4.10	2.08	4.25	1.03	1.38

Table A4-8. Initial and mineral data for interglacial paleosol simulations in Jiuzhoutai, data obtained from (Zhang et al., 1990; Mahaney et al., 1992; Jeong et al., 2008; Shi et al., 2016; Ye et al., 2018), and from unpublished sources collected by Ms. Shaohua Tian.

Location- Jiuzhoutai								
Interglacial	Parent material	OC%	Sand%	silt%	clay%	Bulk density (kg/dm ³)	CaCO ₃ %	Gypsum%
MIS11	Dust	0.03	0.45	65.1	34.4	1.28	11.41	1
	Loess	0.03	0.45	71.9	27.6	1.3	12	1
MIS13	Dust	0.03	0.45	71.9	27.6	1.3	12	1
	Loess	0.03	1.25	70.2	28.5	1.3	13	1

Interglacial	Parent material	Albite	K-Feldspar	Muscovite	Biotite	Quartz	Chlorite	Anorthite	Kaolinite	Illite	Montmorillonite	Hornblende
Mass%												
MIS11	Dust	10.03	4.76	12.55	0.00	31.97	6.19	4.30	4.47	23.74	0.00	2.00
	Loess	11.07	5.26	13.85	0.00	35.28	2.46	4.74	0.97	20.81	3.39	2.20
MIS13	Dust	11.07	5.26	13.85	0.00	35.28	2.46	4.74	0.97	20.81	3.39	2.20
	Loess	10.93	5.19	13.68	0	34.84	2.96	4.68	1.17	24.34	0	2.18

Appendix for chapter 5

Table A5-1. Initial characteristics of loess and Aeolian dust parent material for each study site (sources are mentioned in Finke et al., 2017)

Site		Clay	Silt	sand	Calcite	Gypsum	Albite	K-Feldspar	Muscovite	Quartz	Chlorite	Anorthite	Kaolinite	Montmorillonite	Hornblende
		mass%													
Jinyuan	Parent material	12.0	73.0	15.0	11.0	0.15	5.17	3.11	22.76	33.84	12.55	2.22	5.75	2.22	1.23
	Dust	12.0	73.0	15.0	14.0	0.15	5.00	3.00	21.99	32.70	12.12	2.14	5.55	2.15	1.18
Chang'an	Parent material	37.2	62.5	0.3	8.00	0.15	5.35	3.21	23.53	34.99	12.97	2.29	5.94	2.3	1.27
	Dust	27.3	72.5	0.2	8.00	0.15	5.35	3.21	23.53	34.99	12.97	2.29	5.94	2.3	1.27
Luochuan	Parent material	14.0	74.0	12.0	13.0	0.2	5.3	3.2	23.9	32.4	8.1	2.3	5.8	4.7	1.2
	Dust	17.0	79.0	4.0	13.0	0.2	5.3	3.2	23.9	32.4	8.1	2.3	5.8	4.7	1.2
Xifeng	Parent material	25.0	53.4	21.6	12.0	0.2	5.2	3.1	22.8	34.0	12.6	2.2	5.8	2.2	1.2
	Dust	25.0	53.4	21.6	12.0	0.2	5.2	3.1	22.8	34.0	12.6	2.2	5.8	2.2	1.2

Table A5-2. Initial soil characteristics of loess and dust parent material for each study site (sources are mentioned in Finke et al., 2017)

Site	CEC (mmol+/kg)	Exchangeable cations (mmol+/kg)			
		Ca ⁺²	Mg ⁺²	Na ⁺	K ⁺
Chang'an	153.12	134.2	16.28	1.32	1.32
Luochuan	153.12	134.2	16.28	1.32	1.32
Xifeng	153.12	134.2	16.28	1.32	1.32
Jingyuan	153.12	134.2	16.28	1.32	1.32

Cumulative exchangeable bases and SOC stocks over 22 ka years (MIS 5e) in four locations. An arrow indicates soil loss tolerance values for each stock (EB and SOC) (for the **Tables 5-2 and 5-3**). There are no arrows if the effect of erosion is negligible on each stocks.

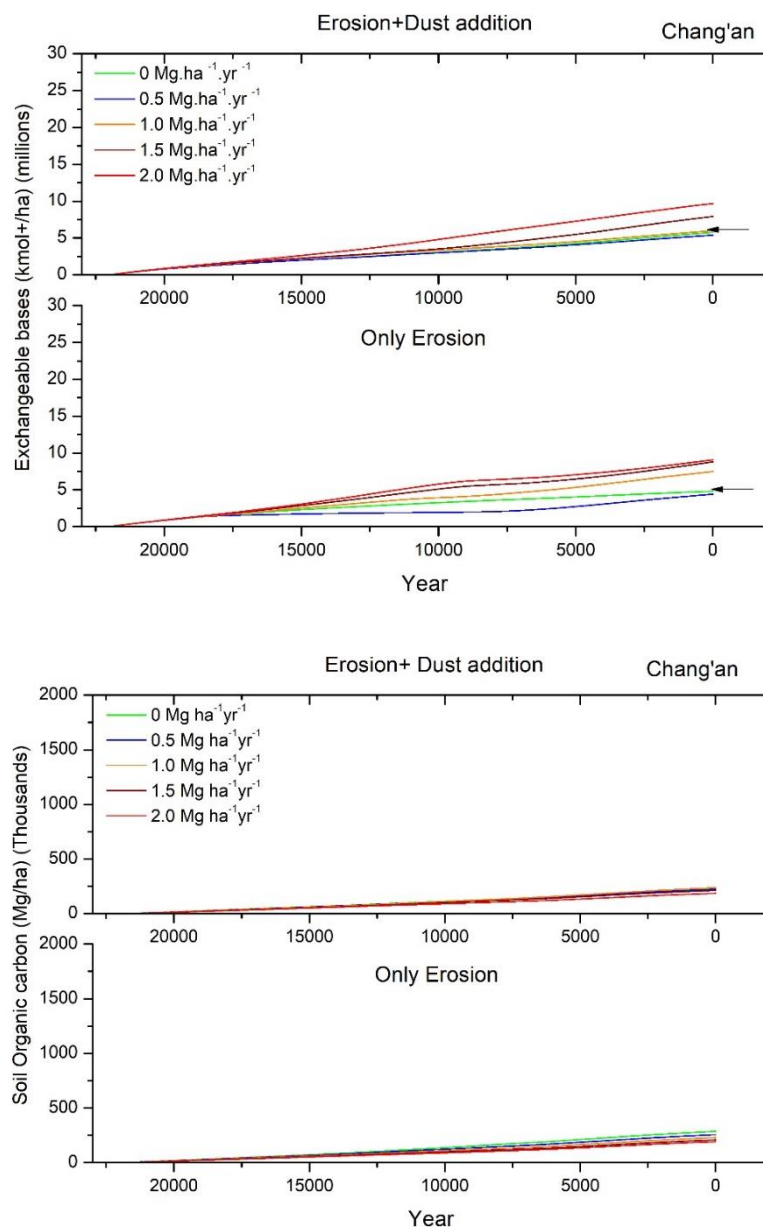


Figure A5-1. Cumulative exchangeable bases and SOC stocks in Chang'an over 22 ka years (MIS 5e).

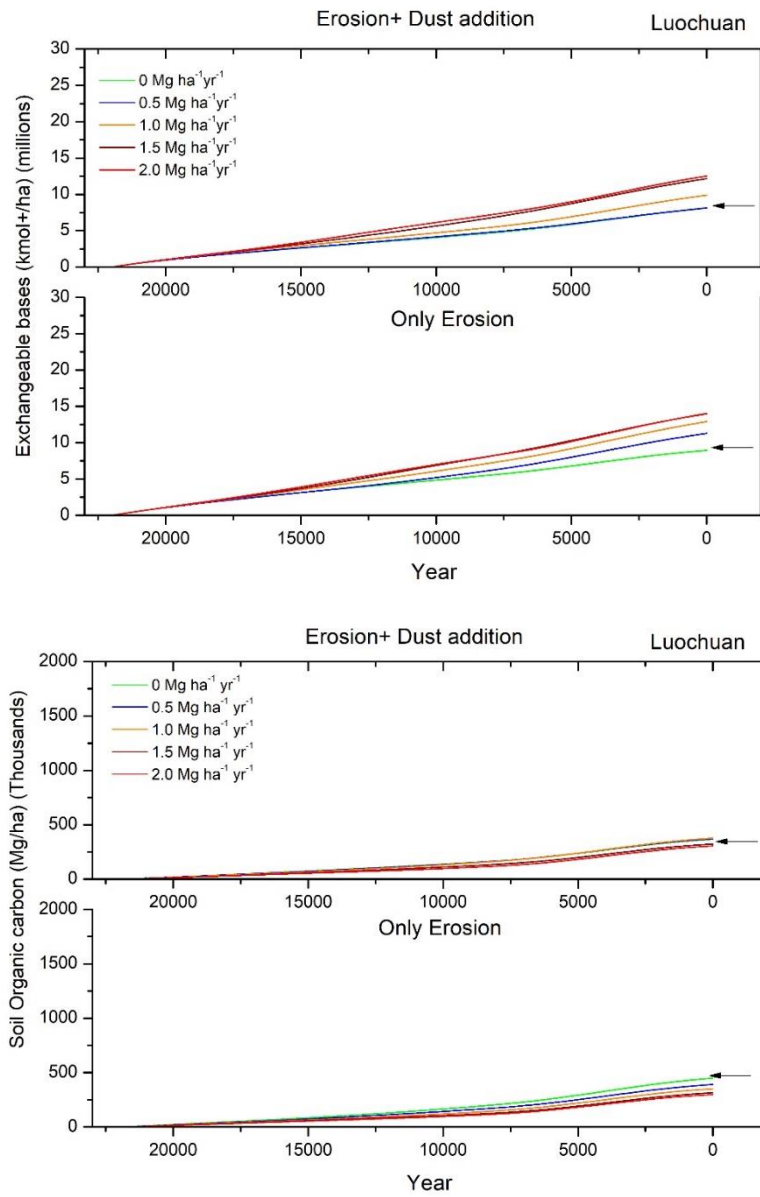


Figure A5-2. Cumulative exchangeable bases and SOC stocks in Luochuan over 22 ka years (MIS 5e).

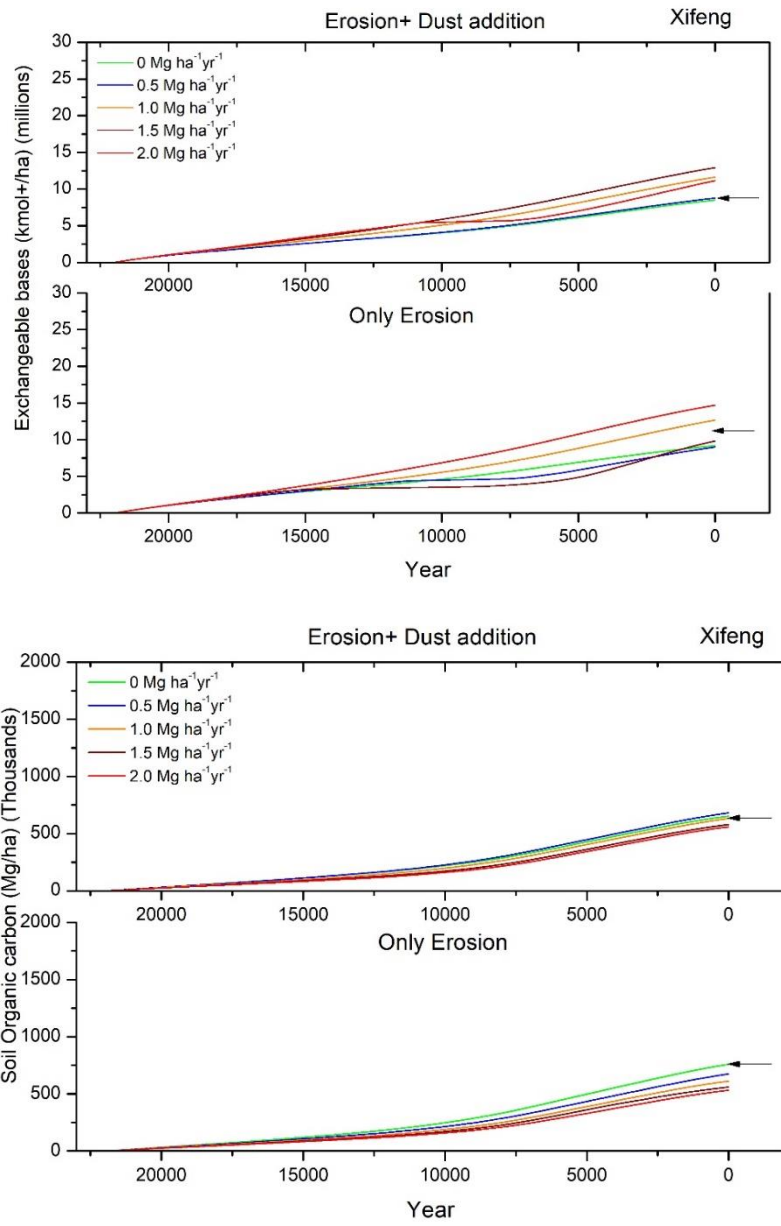


Figure A5-3. Cumulative exchangeable bases and SOC stocks in Xifeng over 22 ka years (MIS 5e).

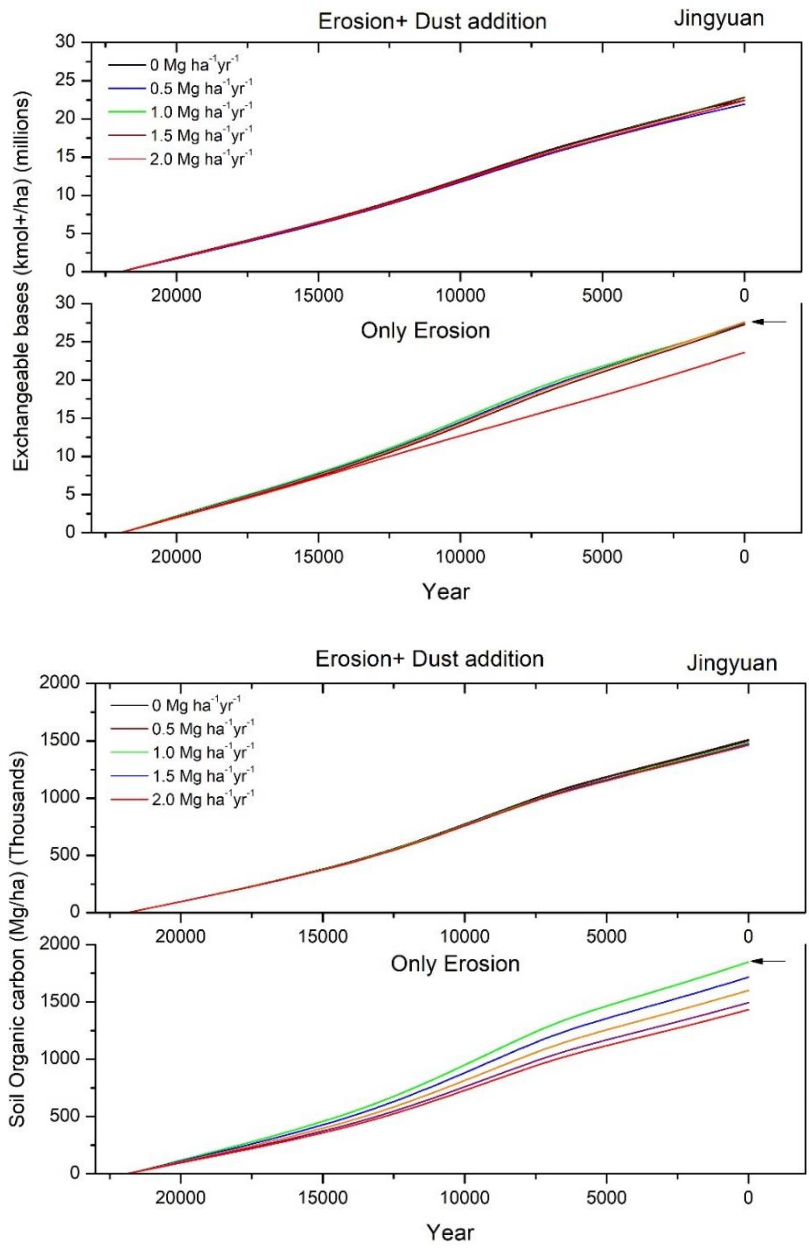


Figure A5-4. Cumulative exchangeable bases and SOC stocks in Xifeng over 22 ka years (MIS 5e).

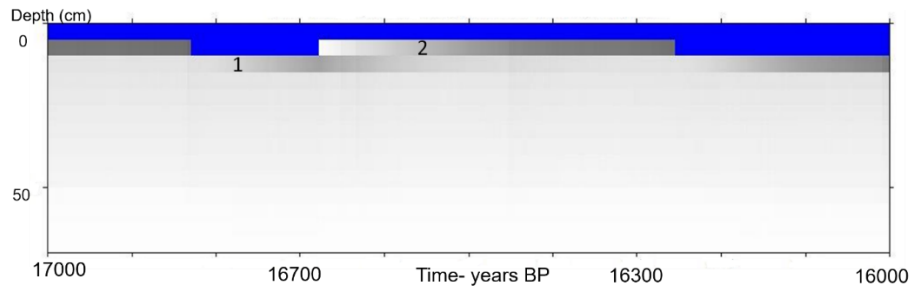


Figure A5-5. The effect of erosion (1) and dust deposition (2) pulses on simulated SOC pattern in SoilGen. Blue denotes air and dark areas in the topsoils show high SOC.

References

- Adhikari, K., Hartemink, A.E., 2016. Linking soils to ecosystem services - A global review. *Geoderma* 262, 101–111. doi:10.1016/j.geoderma.2015.08.009
- Albani, S., Mahowald, N.M., Winckler, G., Anderson, R.F., Bradtmiller, L.I., Delmonte, B., François, R., Goman, M., Heavens, N.G., Hesse, P.P., Hovan, S.A., Kang, S.G., Kohfeld, K.E., Lu, H., Maggi, V., Mason, J.A., Mayewski, P.A., McGee, D., Miao, X., Otto-Bliesner, B.L., Perry, A.T., Pourmand, A., Roberts, H.M., Rosenbloom, N., Stevens, T., Sun, J., 2015. Twelve thousand years of dust: The Holocene global dust cycle constrained by natural archives. *Climate of the Past* 11, 869–903. doi:10.5194/cp-11-869-2015
- Alewell, C., Egli, M., Meusburger, K., 2015. An attempt to estimate tolerable soil erosion rates by matching soil formation with denudation in Alpine grasslands. *Journal of Soils and Sediments* 15, 1383–1399. doi:10.1007/s11368-014-0920-6
- Amundson, R., Richter, D.D., Humphreys, G.S., Jobbágy, E.G., Gaillardet, J., 2007. Coupling between Biota and Earth Materials in the Critical Zone. *Elements* 3, 327–332. doi:10.2113/gselements.3.5.327
- An, Z., 2000. The history and variability of the East Asian paleomonsoon climate. *Quaternary Science Reviews* 19, 171–187. doi:https://doi.org/10.1016/S0277-3791(99)00060-8
- An, Z., Liu, T., Lu, Y., Porter, S.C., Kukla, G., Xihao, W., Yingming, H., 1990. The long-term paleomonsoon variation recorded by the loess-paleosol sequence in Central China. *Quaternary International* 7–8, 91–95. doi:https://doi.org/10.1016/1040-6182(90)90042-3
- An, Z., Kukla, G.J., Porter, S.C., Xiao, J., 1991a. Magnetic susceptibility evidence of monsoon variation on the Loess Plateau of central China during the last 130,000 years. *Quaternary Research* 36, 29–36. doi:10.1016/0033-5894(91)90015-W
- An, Z., Sun, Y., Zhou, W., Liu, W., Qiang, X., Wang, X., Xian, F., Cheng, P., Burr, G.S., 2014. Chinese Loess and the East Asian Monsoon. In: An, Z. (Ed.), *Late Cenozoic Climate Change in Asia*: Springer Netherlands, Dordrecht, pp. 23–143. doi:10.1007/978-94-007-7817-7_2
- An, Z.S., Liu, T., Zhou, Y., Sun, F., Ding, Z., 1987. The paleosol complex S5 in the China Loess Plateau - A record of climatic optimum during the last 1.2 Ma. *GeoJournal* 15, 141–143. doi:10.1007/BF00157939
- An, Z.S., Kukla, G.J., Porter, S.C., Xiao, J.L., 1991b. Late quaternary dust flow on the chinese Loess Plateau. *Catena* 18, 125–132. doi:10.1016/0341-8162(91)90012-M

- Angers, D.A., Arrouays, D., Saby, N.P.A., Walter, C., 2011. Estimating and mapping the carbon saturation deficit of French agricultural topsoils. *Soil Use and Management* 27, 448–452. doi:<https://doi.org/10.1111/j.1475-2743.2011.00366.x>
- Ashley, G.M., 2020. Paleo-Critical Zones, windows into the changing life and landscapes during the Quaternary Period. *Quaternary Research* 96, 53–65. doi:DOI: 10.1017/qua.2020.49
- Bazzoffi, P., 2009. Soil erosion tolerance and water runoff control: Minimum environmental standards. *Regional Environmental Change* 9, 169–179. doi:10.1007/s10113-008-0046-8
- Beck, J.W., Weijian, Z., Cheng, L., Zhenkun, W., Lara, W., Feng, X., Xianghui, K., Zhisheng, A., 2018. A 550,000-year record of East Asian monsoon rainfall from ¹⁰Be in loess. *Science* 360, 877–881. doi:10.1126/science.aam5825
- Berger, A., 1978. Long-Term Variations of Daily Insolation and Quaternary Climatic Changes. *Journal of Atmospheric Sciences* 35, 2362–2367. doi:10.1175/1520-0469(1978)035<2362:LTVODI>2.0.CO;2
- Berger, A., Loutre, M.F., 1991. Insolation values for the climate of the last 10 million years. *Quaternary Science Reviews* 10, 297–317. doi:10.1016/0277-3791(91)90033-Q
- Bethke, C.M., 2007. *Geochemical and Biogeochemical Reaction Modeling*, 2nd ed. Cambridge University Press, Cambridge. doi:DOI: 10.1017/CBO9780511619670
- Beverly, E.J., Lukens, W.E., Stinchcomb, G.E., 2018. Paleopedology as a Tool for Reconstructing Paleoenvironments and Paleoecology BT - Methods in Paleoecology: Reconstructing Cenozoic Terrestrial Environments and Ecological Communities. In: Croft, D.A., Su, D.F., Simpson, S.W. (Eds.), *Methods in Paleoecology*. Springer International Publishing, Cham, pp. 151–183. doi:10.1007/978-3-319-94265-0_9
- Bierkens, M.F.P., Finke, P.A., Willigen, P. de, 2000. *Upscaling and downscaling methods for environmental research*. Dordrecht, Kluwer Academic Publishers.
- Boardman, J., Poesen, J., 2006. Soil Erosion in Europe: Major Processes, Causes and Consequences. In: Boardman, J., Poesen, J. (Eds.), *Soil Erosion in Europe*. John Wiley & Sons, Ltd, Chichester, UK, pp. 477–487. doi:10.1002/0470859202
- Bockheim, J.G., Gennadiyev, A.N., 2000. The role of soil-forming processes in the definition of taxa in Soil Taxonomy and the World Soil Reference Base. *Geoderma* 95, 53–72. doi:[https://doi.org/10.1016/S0016-7061\(99\)00083-X](https://doi.org/10.1016/S0016-7061(99)00083-X)
- Bouma, J., 2014. Soil science contributions towards Sustainable

- Development Goals and their implementation: Linking soil functions with ecosystem services. *Journal of Plant Nutrition and Soil Science* 177, 111–120. doi:10.1002/jpln.201300646
- Box, G.E.P., 1976. Science and Statistics. *Journal of the American Statistical Association* 71, 791–799. doi:10.2307/2286841
- Broadbent, F.E., 2015. Soil organic matter. *Sustainable options in land management* 2, 34–38. doi:10.1002/9780470034590.emrstm1345
- Bronger, A., Heinkele, T., 1989. Micromorphology and genesis of paleosols in the Luochuan loess section, China: Pedostratigraphic and environmental implications. *Geoderma* 45, 123–143. doi:https://doi.org/10.1016/0016-7061(89)90046-3
- Brown, L.C., Foster, G.R., 1987. storm Erosivity Using Idealized Intensity Distributions. *Transactions of the ASABE* 30, 379–386.
- Cai, Q., 2001. Soil erosion and management on the Loess Plateau. *Journal of Geographical Sciences* 11, 53–70. doi:10.1007/BF02837376
- Calder, I.R., Reid, I., Nisbet, T.R., Green, J.C., 2003. Impact of lowland forests in England on water resources: Application of the Hydrological Land Use Change (HYLUC) model. *Water Resources Research* 39. doi:https://doi.org/10.1029/2003WR002042
- Calzolari, C., Ungaro, F., Filippi, N., Guermandi, M., Malucelli, F., Marchi, N., Staffilani, F., Tarocco, P., 2016. A methodological framework to assess the multiple contributions of soils to ecosystem services delivery at regional scale. *Geoderma* 261, 190–203. doi:10.1016/j.geoderma.2015.07.013
- Candy, I., Schreve, D.C., Sherriff, J., Tye, G.J., 2014. Marine Isotope Stage 11: Palaeoclimates, palaeoenvironments and its role as an analogue for the current interglacial. *Earth-Science Reviews* 128, 18–51. doi:https://doi.org/10.1016/j.earscirev.2013.09.006
- Carlyle-Moses, D.E., Gash, J.H.C., 2011. Rainfall interception loss by forest canopies. In: Levia, D., Carlyle-Moses, D., Tanaka, T. (Eds.), *Forest Hydrology and Biogeochemistry, Synthesis of Past Research and Future Directions*. Springer Inc, Dordrecht, pp. 407–423. doi:10.1007/978-94-007-1363-5
- Catt, J.A., 2001. The agricultural importance of loess. *Earth-Science Reviews* 54, 213–229. doi:https://doi.org/10.1016/S0012-8252(01)00049-6
- Chang, C.-P., Wang, Z., Hendon, H., 2006. The Asian winter monsoon. In: Wang, B. (Ed.), *The Asian Monsoon*. Springer Berlin Heidelberg, Berlin, Heidelberg, pp. 89–127. doi:10.1007/3-540-37722-0_3
- Chen, J., Liu, X., Kravchinsky, V.A., 2014. Response of the high-resolution Chinese loess grain size record to the 50°N integrated winter insolation during the last 500,000 years. *Geophysical Research Letters* 41, 6244–

6251. doi:10.1002/2014GL060239

- Cheng, H., Zhang, H., Cai, Y., Shi, Z., Yi, L., Deng, C., Hao, Q., Peng, Y., Sinha, A., Li, H., Zhao, J., Tian, Y., Baker, J.L., Pérez-Mejías, C., 2021. Orbital-scale Asian summer monsoon variations: Paradox and exploration. *Science China Earth Sciences* 64, 529–544. doi:10.1007/s11430-020-9720-y
- Coleman, K., Jenkinson, D.S., 2014. RothC-26.3 - A Model for the turnover of carbon in soil. Model Description and Windows Users Guide (November 1999 issue (modified June 2014)). Harpenden, UK. doi:10.1007/978-3-642-61094-3_17
- Costanza, R., D'Arge, R., Groot, R. De, Farber, S., Grasso, M., Hannon, B., Limburg, K., Naeem, S., O'Neill, R. V., Paruelo, J., Raskin, R.G., Sutton, P., Belt, M. Van Den, 1997. The value of the world's ecosystem services and natural capital. *Nature* 387, 253–260. doi:10.1038/387253a0
- Crockford, R.H., Richardson, D.P., 2000. Partitioning of rainfall into throughfall, stemflow and interception effect of forest type, ground cover and climate. *Hydrological Processes* 14, 2903–2920. doi:10.1002/1099-1085(200011/12)14:16/17<2903::AID-HYP126>3.0.CO;2-6
- Daily, G.C., Matson, P.A., Vitousek, P.M., 1997. Ecosystem services supplied by soil. In: Daily, G. (Ed.), *Nature's Services: Societal Dependence on Natural Ecosystems*. Island press, Washington, DC, pp. 113–132.
- DeGroot, R.S., Wilson, M.A., Boumans, R.M.J., 2002. A typology for the classification, description and valuation of ecosystem functions, goods and services. *Ecological Economics* 41, 393–408. doi:10.1016/S0921-8009(02)00089-7
- DeNovio, N.M., Saiers, J.E., Ryan, J.N., 2004. Colloid Movement in Unsaturated Porous Media: Recent Advances and Future Directions. *Vadose Zone Journal* 3, 338–351. doi:10.2136/vzj2004.0338
- Ding, Z., Yu, Z., Rutter, N.W., Liu, T., 1994. Towards an orbital time scale for chinese loess deposits. *Quaternary Science Reviews* 13, 39–70. doi:https://doi.org/10.1016/0277-3791(94)90124-4
- Ding, Z., Liu, T., Rutter, N.W., Yu, Z., Guo, Z., Zhu, R., 1995. Ice-Volume Forcing of East Asian Winter Monsoon Variations in the Past 800,000 Years. *Quaternary Research* 44, 149–159. doi:DOI: 10.1006/qres.1995.1059
- Ding, Z.L., Xiong, S.F., Sun, J.M., Yang, S.L., Gu, Z.Y., Liu, T.S., 1999. Pedostratigraphy and paleomagnetism of a ~7.0 Ma eolian loess–red clay sequence at Lingtai, Loess Plateau, north-central China and the implications for paleomonsoon evolution. *Palaeogeography, Palaeoclimatology, Palaeoecology* 152, 49–66. doi:https://doi.org/10.1016/S0031-0182(99)00034-6

- Ding, Z.L., Derbyshire, E., Yang, S.L., Yu, Z.W., Xiong, S.F., Liu, T.S., 2002. Stacked 2.6-Ma grain size record from the Chinese loess based on five sections and correlation with the deep-sea $\delta^{18}\text{O}$ record. *Paleoceanography* 17, 5–21. doi:<https://doi.org/10.1029/2001PA000725>
- Ding, Z.L., Derbyshire, E., Yang, S.L., Sun, J.M., Liu, T.S., 2005. Stepwise expansion of desert environment across northern China in the past 3.5 Ma and implications for monsoon evolution. *Earth and Planetary Science Letters* 237, 45–55. doi:<https://doi.org/10.1016/j.epsl.2005.06.036>
- DiStefano, C., Ferro, V., 2016. Establishing soil loss tolerance: An overview. *Journal of Agricultural Engineering* 47, 127–133. doi:[10.4081/jae.2016.560](https://doi.org/10.4081/jae.2016.560)
- Doetterl, S., Berhe, A.A., Arnold, C., Bodé, S., Fiener, P., Finke, P., Fuchslueger, L., Griepentrog, M., Harden, J.W., Nadeu, E., Schnecker, J., Six, J., Trumbore, S., Oost, K. Van, Vogel, C., Boeckx, P., 2018. Links among warming, carbon and microbial dynamics mediated by soil mineral weathering. *Nature Geoscience* 11, 589–593. doi:[10.1038/s41561-018-0168-7](https://doi.org/10.1038/s41561-018-0168-7)
- Dokuchaev, V., 1883. Russian Chernozem. In: *Selected Works of V.V. Dokuchaev. Volume I (Translated in 1967)*. Israel Program for Scientific Translations, Jerusalem.
- Dominati, E., Patterson, M., Mackay, A., 2010. A framework for classifying and quantifying the natural capital and ecosystem services of soils. *Ecological Economics* 69, 1858–1868. doi:[10.1016/j.ecolecon.2010.05.002](https://doi.org/10.1016/j.ecolecon.2010.05.002)
- Dominati, E., Mackay, A., Green, S., Patterson, M., 2014. A soil change-based methodology for the quantification and valuation of ecosystem services from agro-ecosystems: A case study of pastoral agriculture in New Zealand. *Ecological Economics* 100, 119–129. doi:[10.1016/j.ecolecon.2014.02.008](https://doi.org/10.1016/j.ecolecon.2014.02.008)
- Droxler, A.W., Alley, R.B., Howard, W.R., Poore, R.Z., Burckle, L.H., 2003. Unique and exceptionally long interglacial marine isotope stage 11: Window into Earth warm future climate. *Washington DC American Geophysical Union Geophysical Monograph Series* 137, 1–14. doi:[10.1029/137GM01](https://doi.org/10.1029/137GM01)
- Duan, X., Shi, X., Li, Y., Rong, L., Fen, D., 2017. A new method to calculate soil loss tolerance for sustainable soil productivity in farmland. *Agronomy for Sustainable Development* 37. doi:[10.1007/s13593-016-0409-3](https://doi.org/10.1007/s13593-016-0409-3)
- Eden, D.N., Qizhong, W., Hunt, J.L., Whitton, J.S., 1994. Mineralogical and geochemical trends across the Loess Plateau, North China. *CATENA* 21, 73–90. doi:[https://doi.org/10.1016/0341-8162\(94\)90032-9](https://doi.org/10.1016/0341-8162(94)90032-9)
- Evans, M.E., Heller, F., 2001. Magnetism of loess/palaeosol sequences: recent developments. *Earth-Science Reviews* 54, 129–144.

doi:[https://doi.org/10.1016/S0012-8252\(01\)00044-7](https://doi.org/10.1016/S0012-8252(01)00044-7)

- Feng, Q., Zhao, W., Wang, J., Zhang, X., Zhao, M., Zhong, L., Liu, Y., Fang, X., 2016. Effects of Different Land-Use Types on Soil Erosion Under Natural Rainfall in the Loess Plateau, China. *Pedosphere* 26, 243–256. doi:10.1016/S1002-0160(15)60039-X
- Feng, Q., Zhao, W., Hu, X., Liu, Y., Daryanto, S., Cherubini, F., 2020. Trading-off ecosystem services for better ecological restoration: A case study in the Loess Plateau of China. *Journal of Cleaner Production* 257, 120469. doi:10.1016/j.jclepro.2020.120469
- Feng, W., Plante, A.F., Six, J., 2013. Improving estimates of maximal organic carbon stabilization by fine soil particles. *Biogeochemistry* 112, 81–93. doi:10.1007/s10533-011-9679-7
- Feng, Z.-D., Wang, H.B., Olson, C., Pope, G.A., Chen, F.H., Zhang, J.W., An, C.B., 2004a. Chronological discord between the last interglacial paleosol (S1) and its parent material in the Chinese Loess Plateau. *Quaternary International* 117, 17–26. doi:[https://doi.org/10.1016/S1040-6182\(03\)00112-5](https://doi.org/10.1016/S1040-6182(03)00112-5)
- Feng, Z.-D., Wang, H.B., Olson, C.G., 2004b. Pedogenic factors affecting magnetic susceptibility of the last interglacial palaeosol S1 in the Chinese Loess Plateau. *Earth Surface Processes and Landforms* 29, 1389–1402. doi:10.1002/esp.1110
- Finke, P., Opolot, E., Balesdent, J., Berhe, A.A., Boeckx, P., Cornu, S., Harden, J., Hatté, C., Williams, E., Doetterl, S., 2019. Can SOC modelling be improved by accounting for pedogenesis? *Geoderma* 338, 513–524. doi:10.1016/j.geoderma.2018.10.018
- Finke, P.A., 2012a. Modeling the genesis of luvisols as a function of topographic position in loess parent material. *Quaternary International* 265, 3–17. doi:10.1016/j.quaint.2011.10.016
- Finke, P.A., 2012b. On digital soil assessment with models and the Pedometrics agenda. *Geoderma* 171–172, 3–15. doi:10.1016/j.geoderma.2011.01.001
- Finke, P.A., 2020. SOILGEN: A simulation model for soil development in various parent materials. Dept. Environment, Ghent, Belgium.
- Finke, P.A., Hutson, J.L., 2008. Modelling soil genesis in calcareous loess. *Geoderma* 145, 462–479. doi:10.1016/j.geoderma.2008.01.017
- Finke, P.A., Samouëlian, A., Suarez-Bonnet, M., Laroche, B., Cornu, S.S., 2015. Assessing the usage potential of SoilGen2 to predict clay translocation under forest and agricultural land uses. *European Journal of Soil Science* 66, 194–205. doi:10.1111/ejss.12190
- Finke, P.A., Yin, Q.Z., Bernardini, N.J., Yu, Y., 2017. Climate-soil model reveals causes of differences between Marine Isotope Stage 5e and 13

- paleosols. *Geology* 46, 99–102. doi:10.1130/G39301.1
- Finke, P.A., Minasny, B., Temme, A.J.A.M., 2021a. Modeling soil development in a landscape context. In: *Reference Module in Earth Systems and Environmental Sciences*. Elsevier Ltd., pp. 1–12. doi:10.1016/b978-0-12-822974-3.00005-7
- Finke, P.A., Ranathunga Arachchige, K.N., Verdoodt, A., Yu, Y.Y., Yin, Q.Z., 2021b. Unraveling loess records of climate change from the Chinese loess plateau using process-based models. In: Hunt, A., Egli, M., Faybishenko, B. (Eds.), *Hydrogeology, Chemical Weathering and Soil Formation*. AGU Geophysical Monograph Series, pp. 163–175. doi:10.1002/9781119563952.ch8
- Fossey, M., Angers, D., Bustany, C., Cudennec, C., Durand, P., Gascuel-Oudou, C., Jaffrezic, A., Pérès, G., Besse, C., Walter, C., 2020. A Framework to Consider Soil Ecosystem Services in Territorial Planning. *Frontiers in Environmental Science* 8, 1–13. doi:10.3389/fenvs.2020.00028
- Foth, H.D., Ellis, B.G., 1996. *Soil Fertility*, second ed. ed. CRC press, Lewis. doi:https://doi.org/10.1201/9780203739341
- Ganopolski, A., Calov, R., 2011. The role of orbital forcing, carbon dioxide and regolith in 100 kyr glacial cycles. *Climate of the Past* 7, 1415–1425. doi:10.5194/cp-7-1415-2011
- Geißler, C., Kühn, P., Böhnke, M., Bruelheide, H., Shi, X., Scholten, T., 2012. Splash erosion potential under tree canopies in subtropical SE China. *Catena* 91, 85–93. doi:10.1016/j.catena.2010.10.009
- Gobat, J.-M., Aragno, M., Matthey, W., 1998. *Le sol vivant*. Presses polytechniques et universitaires romandes, Lausanne.
- Godderis, Y., Williams, J.Z., Schott, J., Pollard, D., Brantley, S.L., 2010. Time evolution of the mineralogical composition of Mississippi Valley loess over the last 10 kyr: Climate and geochemical modeling. *Geochimica et Cosmochimica Acta* 74, 6357–6374. doi:10.1016/j.gca.2010.08.023
- Gong, D.-Y., Ho, C.-H., 2002. The Siberian High and climate change over middle to high latitude Asia. *Theoretical and Applied Climatology* 72, 1–9. doi:10.1007/s007040200008
- Goosse, H., Brovkin, V., Fichefet, T., Haarsma, R., Huybrechts, P., Jongma, J., Mouchet, A., Selten, F., Barriat, P.Y., Campin, J.M., Deleersnijder, E., Driesschaert, E., Goelzer, H., Janssens, I., Loutre, M.F., Morales Maqueda, M.A., Opsteegh, T., Mathieu, P.P., Munhoven, G., Pettersson, E.J., Renssen, H., Roche, D.M., Schaeffer, M., Tartinville, B., Timmermann, A., Weber, S.L., 2010. Description of the Earth system model of intermediate complexity LOVECLIM version 1.2. *Geoscientific Model Development* 3, 603–633. doi:10.5194/gmd-3-603-2010

- Gower, J.C., 1971. A General Coefficient of Similarity and Some of Its Properties. *Biometrics* 27, 857–871. doi:10.2307/2528823
- Granger, D.E., Kirchner, J.W., Finkel, R., 1996. Spatially Averaged Long-Term Erosion Rates Measured from in Situ-Produced Cosmogenic Nuclides in Alluvial Sediment. *The Journal of Geology* 104, 249–257.
- Greiner, L., Keller, A., Grêt-Regamey, A., Papritz, A., 2017. Soil function assessment: review of methods for quantifying the contributions of soils to ecosystem services. *Land Use Policy* 69, 224–237. doi:10.1016/j.landusepol.2017.06.025
- Guerra, A.J.T., Fullen, M.A., Jorge, M. do C.O., Bezerra, J.F.R., Shokr, M.S., 2017. Slope Processes, Mass Movement and Soil Erosion: A Review. *Pedosphere* 27, 27–41. doi:https://doi.org/10.1016/S1002-0160(17)60294-7
- Guo, Z., Liu, T., Fedoroff, N., Wei, L., Ding, Z., Wu, N., Lu, H., Jiang, W., An, Z., 1998. Climate extremes in Loess of China coupled with the strength of deep-water formation in the North Atlantic. *Global and Planetary Change* 18, 113–128. doi:10.1016/S0921-8181(98)00010-1
- Guo, Z.T., Ding, Z., Liu, D., Liu, T., 1996. Pedosedimentary events in loess of China and Quaternary climatic cycles. *Chinese Science Bulletin* 41, 1189–1193.
- Guo, Z.T., Biscaye, P., Wei, L., Chen, X., Peng, S., Liu, T., 2000. Summer monsoon variations over the last 1.2 Ma from the weathering of loess-soil sequences in China. *Geophysical Research Letters* 27, 1751–1754. doi:10.1029/1999GL008419
- Guo, Z.T., Ruddiman, W.F., Hao, Q.Z., Wu, H.B., Qiao, Y.S., Zhu, R.X., Peng, S.Z., Wei, J.J., Yuan, B.Y., Liu, T.S., 2002. Onset of Asian desertification by 22 Myr ago inferred from loess deposits in China. *Nature* 416, 159–163. doi:10.1038/416159a
- Guo, Z.T., Berger, A., Yin, Q.Z., Qin, L., 2009. Strong asymmetry of hemispheric climates during MIS-13 inferred from correlating China loess and Antarctica ice records. *Climate of the Past* 5, 21–31. doi:10.5194/cp-5-21-2009
- Han, J., Fyfe, W.S., Longstaffe, F.J., 1998. Climatic implications of the S5 Paleosol Complex on the southernmost Chinese Loess Plateau. *Quaternary Research* 50, 21–33. doi:10.1006/qres.1998.1976
- Hao, Q., Guo, Z., 2005. Spatial variations of magnetic susceptibility of Chinese loess for the last 600 kyr: Implications for monsoon evolution. *Journal of Geophysical Research: Solid Earth* 110, 1–10. doi:10.1029/2005JB003765
- Hao, Q., Wang, L., Oldfield, F., Peng, S., Qin, L., Song, Y., Xu, B., Qiao, Y., Bloemendal, J., Guo, Z., 2012. Delayed build-up of Arctic ice sheets

- during 400,000-year minima in insolation variability. *Nature* 490, 393–396. doi:10.1038/nature11493
- Hassink, J., 1997. The capacity of soils to preserve organic C and N by their association with clay and silt particles. *Plant and Soil* 191, 77–87. doi:10.1023/A:1004213929699
- He, W., He, H., Zhu, M., 2015. Calcium Nodules as a Proxy for Quaternary Paleoclimate Change on China's Loess Plateau. *PloS one* 10, e0143928–e0143928. doi:10.1371/journal.pone.0143928
- He, Z.-B., Yang, J.-J., Du, J., Zhao, W.-Z., Liu, H., Chang, X.-X., 2014. Spatial variability of canopy interception in a spruce forest of the semiarid mountain regions of China. *Agricultural and Forest Meteorology* 188, 58–63. doi:https://doi.org/10.1016/j.agrformet.2013.12.008
- Heslop, D., Langereis, C.G., Dekkers, M.J., 2000. A new astronomical timescale for the loess deposits of Northern China. *Earth and Planetary Science Letters* 184, 125–139. doi:PII: S 0 0 1 2 - 8 2 1 X (0 0) 0 0 3 2 4 - 1
- Heslop, D., Dekkers, M.J., Langereis, C.G., 2002. Timing and structure of the mid-Pleistocene transition: records from the loess deposits of northern China. *Palaeogeography, Palaeoclimatology, Palaeoecology* 185, 133–143.
- Hewitt, A., Dominati, E., Webb, T., Cuthill, T., 2015. Soil natural capital quantification by the stock adequacy method. *Geoderma* 241–242, 107–114. doi:10.1016/j.geoderma.2014.11.014
- Holliday, V.T., 2004. *Soils in Archaeological Research*, Soils in Archaeological Research. Oxford University Press. doi:10.1093/oso/9780195149654.001.0001
- Hörmann, G., Branding, A., Clemen, T., Herbst, M., Hinrichs, A., Thamm, F., 1996. Calculation and simulation of wind controlled canopy interception of a beech forest in Northern Germany. *Agricultural and Forest Meteorology* 79, 131–148. doi:10.1016/0168-1923(95)02275-9
- Hu, W., 2007. The distribution map of average rainfall in China (up to 1996): Beijing, National Data Sharing Infrastructure of Earth System Science, scale 1:1,500,000 with grid resolution of 500 m (in Chinese).
- Huang, C., 2011. Clay minerals in loess on the Loess Plateau and its environmental significance. PhD degree thesis, University of Chinese Academy of Sciences, China.
- Huang, C.C., Pang, J., Chen, S., Zhang, Z., 2003. Holocene dust accumulation and the formation of polycyclic cinnamon soils (luvisols) in the Chinese Loess Plateau. *Earth Surface Processes and Landforms* 28, 1259–1270. doi:10.1002/esp.512
- Huang, C.Q., Tan, W.F., Wang, M.K., Koopal, L.K., 2014. Characteristics of

the fifth paleosol complex (S-5) in the southernmost part of the Chinese Loess Plateau and its paleo-environmental significance . *Catena* . doi:10.1016/j.catena.2014.06.009

- Hutson, J.L., Wagenet, R.J., 1992. LEACHM: Leaching, Estimation and Chemistry Model: a Process-based Model of Water and Solute Movement, Transformations, Plant Uptake and Chemical Reactions in the Unsaturated Zone, Continuum Vol.2, Version 3 (Water Resources Institute). Department of Agronomy, Cornell University, Ithaca, NY.
- Ikawa, H., Kourouma, L., 1985. Soil temperature classes in Soil Taxonomy. In: *Soil Taxonomy: Review and Use in the Asian and Pacific Region*. Food and Fert. Tech. Ctr. for the ASPAC Region, Taipei, Taiwan, pp. 121–125.
- Jacobson, R.L., Langmuir, D., 1974. Dissociation constants of calcite and CaHCO_3^+ from 0 to 50°C. *Geochimica et Cosmochimica Acta* 38, 301–318. doi:10.1016/0016-7037(74)90112-4
- Jarvis, N.J., Villholth, K.G., Ulén, B., 1999. Modelling particle mobilization and leaching in macroporous soil. *European Journal of Soil Science* 50, 621–632. doi:10.1046/j.1365-2389.1999.00269.x
- Jenny, H., 1941. *Factors of Soil Formation. A System of Quantitative Pedology*. McGraw-Hill Book Company, New York, London.
- Jeong, G.Y., Hillier, S., Kemp, R.A., 2008. Quantitative bulk and single-particle mineralogy of a thick Chinese loess–paleosol section: implications for loess provenance and weathering. *Quaternary Science Reviews* 27, 1271–1287. doi:https://doi.org/10.1016/j.quascirev.2008.02.006
- Jeong, G.Y., Hillier, S., Kemp, R.A., 2011. Changes in mineralogy of loess–paleosol sections across the Chinese Loess Plateau. *Quaternary Research* 75, 245–255. doi:10.1016/j.yqres.2010.09.001
- Jia, J., Lu, H., Wang, Y., Xia, D., 2018. Variations in the Iron Mineralogy of a Loess Section in Tajikistan During the Mid-Pleistocene and Late Pleistocene: Implications for the Climatic Evolution in Central Asia. *Geochemistry, Geophysics, Geosystems* 19, 1244–1258. doi:10.1002/2017GC007371
- Jian, S., Zhao, C., Fang, S., Yu, K., 2014. Soil water content and water balance simulation of *Caragana korshinskii* Kom. in the semiarid Chinese Loess Plateau. *Journal of Hydrology and Hydromechanics* 62, 89–96. doi:10.2478/johh-2014-0020
- Jian, S., Zhao, C., Fang, S., Yu, K., 2015. Effects of different vegetation restoration on soil water storage and water balance in the Chinese Loess Plateau. *Agricultural and Forest Meteorology* 206, 85–96. doi:10.1016/j.agrformet.2015.03.009
- Kang, S., Wang, X., Lu, Y., 2013. Quartz OSL chronology and dust

accumulation rate changes since the Last Glacial at Weinan on the southeastern Chinese Loess Plateau. *Boreas* 42.

- Kang, S., Wang, X., Roberts, H.M., Duller, G.A.T., Cheng, P., Lu, Y., An, Z., 2018. Late Holocene anti-phase change in the East Asian summer and winter monsoons. *Quaternary Science Reviews* 188, 28–36. doi:<https://doi.org/10.1016/j.quascirev.2018.03.028>
- Kemp, R.A., 2001. Pedogenic modification of loess: Significance for palaeoclimatic reconstructions. *Earth-Science Reviews* 54, 145–156. doi:[10.1016/S0012-8252\(01\)00045-9](https://doi.org/10.1016/S0012-8252(01)00045-9)
- Keyvanshokouhi, S., Cornu, S., Samouëlian, A., Finke, P., 2016. Evaluating SoilGen2 as a tool for projecting soil evolution induced by global change. *Science of the Total Environment* 571, 110–123. doi:[10.1016/j.scitotenv.2016.07.119](https://doi.org/10.1016/j.scitotenv.2016.07.119)
- Klaassen, W., Bosveld, F., Water, E. De, 1998. Water storage and evaporation as constituents of rainfall interception. *Journal of Hydrology* 212–213, 36–50. doi:[10.1016/S0022-1694\(98\)00200-5](https://doi.org/10.1016/S0022-1694(98)00200-5)
- Kohfeld, K.E., Harrison, S.P., 2003. Glacial-interglacial changes in dust deposition on the Chinese Loess Plateau. *Quaternary Science Reviews* 22, 1859–1878. doi:[10.1016/S0277-3791\(03\)00166-5](https://doi.org/10.1016/S0277-3791(03)00166-5)
- Kong, X., Zhou, W., Beck, J.W., Xian, F., Qiang, X., Ao, H., Wu, Z., An, Z., 2020. Loess magnetic susceptibility flux: A new proxy of East Asian monsoon precipitation. *Journal of Asian Earth Sciences* 201, 104489. doi:[10.1016/j.jseaes.2020.104489](https://doi.org/10.1016/j.jseaes.2020.104489)
- Kononova, M.M., 1975. Humus of Virgin and Cultivated Soils. In: Gieseking, J.E. (Ed.), *Soil Components: Vol. 1: Organic Components*. Springer Berlin Heidelberg, pp. 475–526. doi:[10.1007/978-3-642-65915-7_8](https://doi.org/10.1007/978-3-642-65915-7_8)
- Kukla, G., 1987. Loess stratigraphy in central China. *Quaternary Science Reviews* 6, 191–219. doi:[https://doi.org/10.1016/0277-3791\(87\)90004-7](https://doi.org/10.1016/0277-3791(87)90004-7)
- Kukla, G., An, Z., 1989. Loess stratigraphy in Central China. *Palaeogeography, Palaeoclimatology, Palaeoecology* 72, 203–225. doi:[10.1016/0031-0182\(89\)90143-0](https://doi.org/10.1016/0031-0182(89)90143-0)
- Kukla, J., 1970. Correlations between loesses and deep-sea sediments. *Geologiska Föreningen i Stockholm Förhandlingar* 92, 148–180. doi:[10.1080/11035897009453674](https://doi.org/10.1080/11035897009453674)
- Kutzbach, J.E., Liu, X., Liu, Z., Chen, G., 2008. Simulation of the evolutionary response of global summer monsoons to orbital forcing over the past 280,000 years. *Climate Dynamics* 30, 567–579. doi:[10.1007/s00382-007-0308-z](https://doi.org/10.1007/s00382-007-0308-z)
- Kuzyakov, Y., Zamanian, K., 2019. Reviews and syntheses: Agropedogenesis-Humankind as the sixth soil-forming factor and attractors of agricultural soil degradation. *Biogeosciences* 16, 4783–

4803. doi:10.5194/bg-16-4783-2019

- Lai, Z.-P., Wintle, A.G., 2006. Locating the boundary between the Pleistocene and the Holocene in Chinese loess using luminescence. *The Holocene* 16, 893–899. doi:10.1191/0959683606hol980rr
- Lal, R., 2001. Soil degradation by erosion. *Land Degradation & Development* 12, 519–539. doi:https://doi.org/10.1002/ldr.472
- Lang, Y., Song, W., Zhang, Y., 2017. Responses of the water-yield ecosystem service to climate and land use change in Sancha River Basin, China. *Physics and Chemistry of the Earth* 101, 102–111. doi:10.1016/j.pce.2017.06.003
- Laskar, J., 1990. The chaotic motion of the solar system: A numerical estimate of the size of the chaotic zones. *Icarus* 88, 266–291. doi:https://doi.org/10.1016/0019-1035(90)90084-M
- Leopold, M., Völkel, J., Dethier, D., Huber, J., Steffens, M., 2011. Characteristics of a paleosol and its implication for the Critical Zone development, Rocky Mountain Front Range of Colorado, USA. *Applied Geochemistry* 26, S72–S75. doi:https://doi.org/10.1016/j.apgeochem.2011.03.034
- Li, G., Chen, J., Chen, Y., 2013. Primary and secondary carbonate in Chinese loess discriminated by trace element composition. *Geochimica et Cosmochimica Acta* 103, 26–35. doi:10.1016/j.gca.2012.10.049
- Li, J., Song, Z., Ruan, L., Yang, L., Zwieter, L. Van, Hu, Z., He, S., Chenwu, W., Wang, H., 2019. The contribution of Asian dust in the pedogenesis of ultisols in Southeastern China determined by soil grain size. *Journal of Soils and Sediments* 19, 232–240. doi:10.1007/s11368-018-2012-5
- Li, L., Du, S., Wu, L., Liu, G., 2009. An overview of soil loss tolerance. *Catena* 78, 93–99. doi:10.1016/j.catena.2009.03.007
- Li, X., Xiao, Q., Niu, J., Dymond, S., Doorn, N.S. van, Yu, X., Xie, B., Lv, X., Zhang, K., Li, J., 2016a. Process-based rainfall interception by small trees in Northern China: The effect of rainfall traits and crown structure characteristics. *Agricultural and Forest Meteorology* 218–219, 65–73. doi:10.1016/j.agrformet.2015.11.017
- Li, Y., Zhang, W., Aydin, A., Deng, X., 2018. Formation of calcareous nodules in loess–paleosol sequences: Reviews of existing models with a proposed new “per evapotranspiration model.” *Journal of Asian Earth Sciences* 154, 8–16. doi:10.1016/j.jseaes.2017.12.002
- Li, Y., Shi, W., Aydin, A., Beroya-Eitner, M.A., Gao, G., 2020. Loess genesis and worldwide distribution. *Earth-Science Reviews* 201, 102947. doi:https://doi.org/10.1016/j.earscirev.2019.102947
- Li, Y.Y., Shao, M.A., 2006. Change of soil physical properties under long-term natural vegetation restoration in the Loess Plateau of China. *Journal of*

- Arid Environments 64, 77–96. doi:10.1016/j.jaridenv.2005.04.005
- Li, Z., Nie, X., Chang, X., Liu, L., Sun, L., 2016b. Characteristics of soil and organic carbon loss induced by water erosion on the loess plateau in China. *PLoS ONE* 11, 1–13. doi:10.1371/journal.pone.0154591
- Liao, S., 2007. The distribution map of average temperature in China (up to 1996): Beijing, National Data Sharing Infrastructure of Earth System Science, scale 1:1,500,000 with grid resolution of 500 m (in Chinese).
- Lieth, H., 1975. Modeling the Primary Productivity of the World. In: Lieth, H., Whittaker, R.H. (Eds.), *Primary Productivity of the Biosphere*. Springer Berlin Heidelberg, Berlin, Heidelberg, pp. 237–263. doi:10.1007/978-3-642-80913-2_12
- Lin, H., 2011. Three Principles of Soil Change and Pedogenesis in Time and Space. *Soil Science Society of America Journal* 75, 2049–2070. doi:https://doi.org/10.2136/sssaj2011.0130
- Lisiecki, L.E., Raymo, M.E., 2005. A Pliocene-Pleistocene stack of 57 globally distributed benthic δ ¹⁸O records. *Paleoceanography* 20, 1–17. doi:10.1029/2004PA001071
- Liu, T., 1985. *Loess and the Environment*. China Ocean Press, Beijing.
- Liu, T., Ding, Z., 1998. CHINESE LOESS AND THE PALEOMONSOON. *Annual Review of Earth and Planetary Sciences* 26, 111–145. doi:10.1146/annurev.earth.26.1.111
- Liu, W., Fox, J.E.D., Xu, Z., 2003. Nutrient budget of a montane evergreen broad-leaved forest at Ailao Mountain National Nature Reserve, Yunnan, southwest China. *Hydrological Processes* 17, 1119–1134. doi:10.1002/hyp.1184
- Liu, Z., Shao, M., Wang, Y., 2011. Effect of environmental factors on regional soil organic carbon stocks across the Loess Plateau region, China. *Agriculture, Ecosystems and Environment* 142, 184–194. doi:10.1016/j.agee.2011.05.002
- Loutre, M.F., Berger, A., 2003. Marine Isotope Stage 11 as an analogue for the present interglacial. *Global and Planetary Change* 36, 209–217. doi:https://doi.org/10.1016/S0921-8181(02)00186-8
- Lu, H., Sun, D., 2000. Pathways of dust input to the Chinese Loess Plateau during the last glacial and interglacial periods. *Catena* 40, 251–261. doi:10.1016/S0341-8162(00)00090-4
- Lu, H., Liu, X., Zhang, F., An, Z., Dodson, J., 1999. Astronomical calibration of loess–paleosol deposits at Luochuan, central Chinese Loess Plateau. *Palaeogeography, Palaeoclimatology, Palaeoecology* 154, 237–246. doi:https://doi.org/10.1016/S0031-0182(99)00113-3
- Lu, H., Zhang, F., Liu, X., 2003. Patterns and frequencies of the East Asian

- winter monsoon variations during the past million years revealed by wavelet and spectral analyses. *Global and Planetary Change* 35, 67–74. doi:[https://doi.org/10.1016/S0921-8181\(02\)00136-4](https://doi.org/10.1016/S0921-8181(02)00136-4)
- Lu, H., Zhang, F., Liu, X., Duce, R.A., 2004. Periodicities of palaeoclimatic variations recorded by loess-paleosol sequences in China. *Quaternary Science Reviews* 23, 1891–1900. doi:<https://doi.org/10.1016/j.quascirev.2004.06.005>
- Lu, H., Jia, J., Wang, Y., Yin, Q., Xia, D., 2018. The cause of extremely high magnetic susceptibility of the S5S1 paleosol in the central Chinese Loess Plateau. *Quaternary International* 493, 252–257. doi:[10.1016/j.quaint.2018.05.046](https://doi.org/10.1016/j.quaint.2018.05.046)
- Lu, N., Akujärvi, A., Wu, X., Liski, J., Wen, Z., Holmberg, M., Feng, X., Zeng, Y., Fu, B., 2015. Changes in soil carbon stock predicted by a process-based soil carbon model (Yasso07) in the Yanhe watershed of the Loess Plateau. *Landscape Ecology* 30, 399–413. doi:[10.1007/s10980-014-0132-x](https://doi.org/10.1007/s10980-014-0132-x)
- Lu, Y.C., Wang, X.L., Wintle, A.G., 2007. A new OSL chronology for dust accumulation in the last 130,000 yr for the Chinese Loess Plateau. *Quaternary Research* 67, 152–160. doi:<https://doi.org/10.1016/j.yqres.2006.08.003>
- Lyu, A.Q., Yin, Q., Crucifix, M., Sun, Y., 2021. Diverse Regional Sensitivity of Summer Precipitation in East Asia to Ice Volume, CO₂ and Astronomical Forcing. *Geophysical Research Letters* 48, 1–11. doi:[10.1029/2020GL092005](https://doi.org/10.1029/2020GL092005)
- Ma, L., Li, Y., Liu, X., Sun, Y., 2017. Registration of Precession Signal in the Last Interglacial Paleosol (S1) on the Chinese Loess Plateau. *Geochemistry, Geophysics, Geosystems* 18, 3964–3975. doi:<https://doi.org/10.1002/2017GC006964>
- Mahaney, W.C., Hancock, R.G. V., Zhang, L., 1992. Stratigraphy and geochemistry of the Jiuzhoutai loess succession, northwestern China. *Journal of Southeast Asian Earth Sciences* 7, 215–221. doi:[https://doi.org/10.1016/0743-9547\(92\)90001-R](https://doi.org/10.1016/0743-9547(92)90001-R)
- Maher, B.A., 2016. Palaeoclimatic records of the loess/palaeosol sequences of the Chinese Loess Plateau. *Quaternary Science Reviews* 154, 23–84. doi:[10.1016/j.quascirev.2016.08.004](https://doi.org/10.1016/j.quascirev.2016.08.004)
- Maher, B.A., Prospero, J.M., Mackie, D., Gaiero, D., Hesse, P.P., Balkanski, Y., 2010. Global connections between aeolian dust, climate and ocean biogeochemistry at the present day and at the last glacial maximum. *Earth-Science Reviews* 99, 61–97. doi:<https://doi.org/10.1016/j.earscirev.2009.12.001>
- Marin-Spiotta, E., Chaopricha, N.T., Plante, A.F., Diefendorf, A.F., Mueller, C.W., Grandy, A.S., Mason, J.A., 2014. Long-term stabilization of deep

- soil carbon by fire and burial during early Holocene climate change. *Nature Geoscience* 7, 428–432. doi:10.1038/ngeo2169
- MEA, 2005. *Ecosystems and human well-being: Synthesis*. Island press, Washington, DC.
- Meijer, N., Dupont-Nivet, G., Licht, A., Trabucho-Alexandre, J., Bourquin, S., Abels, H.A., 2020. Identifying eolian dust in the geological record. *Earth-Science Reviews* 211. doi:10.1016/j.earscirev.2020.103410
- Meng, X., Liu, L., Miao, X., Zhao, W., Zhang, E., Ji, J., 2021. Significant influence of Northern Hemisphere high latitude climate on appeared precession rhythm of East Asian summer monsoon after Mid-Brunhes Transition interglacials recorded in the Chinese loess. *CATENA* 197, 105002. doi:https://doi.org/10.1016/j.catena.2020.105002
- Minasny, B., McBratney, A.B., 2006. Mechanistic soil–landscape modelling as an approach to developing pedogenetic classifications. *Geoderma* 133, 138–149. doi:https://doi.org/10.1016/j.geoderma.2006.03.042
- Minasny, B., Finke, P., Stockmann, U., Vanwalleghem, T., McBratney, A.B., 2015. Resolving the integral connection between pedogenesis and landscape evolution. *Earth-Science Reviews* 150, 102–120. doi:10.1016/j.earscirev.2015.07.004
- Montanarella, L., Pennock, D.J., McKenzie, N., Badraoui, M., Chude, V., Baptista, I., Mamo, T., Yemefack, M., Singh Aulakh, M., Yagi, K., Young Hong, S., Vijarnsorn, P., Zhang, G.-L., Arrouays, D., Black, H., Krasilnikov, P., Sobocká, J., Alegre, J., Henriquez, C.R., Lourdes Mendonça-Santos, M. de, Taboada, M., Espinosa-Victoria, D., AlShankiti, A., AlaviPanah, S.K., Elsheikh, E.A.E.M., Hempel, J., Camps Arbestain, M., Nachtergaele, F., Vargas, R., 2016. World's soils are under threat. *SOIL* 2, 79–82. doi:10.5194/soil-2-79-2016
- Montgomery, D., 2007. Soil erosion and agricultural sustainability. *Proceedings of the National Academy of Sciences* 104 (33), 13268–13272. doi:10.1073/pnas.0611508104
- Morris, M.D., 1991. Factorial sampling plans for preliminary computational experiments. *Technometrics* 33, 161–174. doi:10.1080/00401706.1991.10484804
- Muhs, D.R., 2013. Loess and its geomorphic, stratigraphic and paleoclimatic significance in the Quaternary. *Reference Module in Earth Systems and Environmental Sciences: Treatise on Geomorphology* 11, 149–183. doi:10.1016/B978-0-12-374739-6.00302-X
- Muri, H., Berger, A., Yin, Q.Z., Karami, M.P., Barriat, P.Y., 2013. The climate of the MIS-13 interglacial according to HadCM3. *Journal of Climate* 26, 9696–9712. doi:10.1175/JCLI-D-12-00520.1
- Návar, J., Bryan, R., 1990. Interception loss and rainfall redistribution by three

- semi-arid growing shrubs in northeastern Mexico. *Journal of Hydrology* 115, 51–63. doi:[https://doi.org/10.1016/0022-1694\(90\)90197-6](https://doi.org/10.1016/0022-1694(90)90197-6)
- Nearing, M.A., Xie, Y., Liu, B., Ye, Y., 2017. Natural and anthropogenic rates of soil erosion. *International Soil and Water Conservation Research* 5, 77–84. doi:[10.1016/j.iswcr.2017.04.001](https://doi.org/10.1016/j.iswcr.2017.04.001)
- Nisbet, T.R., 2005. *Water Use by Trees*. Forestry Commission Information. 65 1–8.
- Nordt, L.C., Driese, S.G., 2013. Application of the Critical Zone Concept to the Deep-Time Sedimentary Record. *The Sedimentary Record* 11, 4–9. doi:[10.2110/sedred.2013.3.4](https://doi.org/10.2110/sedred.2013.3.4)
- NRC, 2001. *Basic research opportunities in Earth science, Basic Research Opportunities in Earth Science*. Washington, DC. doi:<https://doi.org/10.17226/9981>.
- Ochoa-Sánchez, A., Crespo, P., Célleri, R., 2018. Quantification of rainfall interception in the high Andean tussock grasslands. *Ecohydrology* 11, 1–11. doi:[10.1002/eco.1946](https://doi.org/10.1002/eco.1946)
- Opolot, E., 2016. *Modelling soil evolution to assess soil system behaviour under global change*. Ghent University.
- Opolot, E., Yu, Y.Y., Finke, P.A., 2015. Modeling soil genesis at pedon and landscape scales: Achievements and problems. *Quaternary International* 376, 34–46. doi:[10.1016/j.quaint.2014.02.017](https://doi.org/10.1016/j.quaint.2014.02.017)
- Pang, J.L., Huang, C.C., 2006. Mid-Holocene soil formation and the impact of dust input in the middle reaches of the Yellow River, Northern China 171, 552–563. doi:[10.1097/01.ss.0000228040.65023.1b](https://doi.org/10.1097/01.ss.0000228040.65023.1b)
- Pecsi, M., 1990. Loess is not just the accumulation of dust. *Quaternary International* 7–8, 1–21. doi:[10.1016/1040-6182\(90\)90034-2](https://doi.org/10.1016/1040-6182(90)90034-2)
- Peterse, F., Martínez-García, A., Zhou, B., Beets, C.J., Prins, M.A., Zheng, H., Eglinton, T.I., 2014. Molecular records of continental air temperature and monsoon precipitation variability in East Asia spanning the past 130,000 years. *Quaternary Science Reviews* 83, 76–82. doi:<https://doi.org/10.1016/j.quascirev.2013.11.001>
- Poesen, J., 2018. Soil erosion in the Anthropocene: Research needs. *Earth Surface Processes and Landforms* 43, 64–84. doi:<https://doi.org/10.1002/esp.4250>
- Porter, S.C., 2001. Chinese loess record of monsoon climate during the last glacial–interglacial cycle. *Earth-Science Reviews* 54, 115–128. doi:[https://doi.org/10.1016/S0012-8252\(01\)00043-5](https://doi.org/10.1016/S0012-8252(01)00043-5)
- Porter, S.C., An, Z., 1995. Correlation between climate events in the North Atlantic and China during the last glaciation. *Nature* 375, 305–308. doi:[10.1038/375305a0](https://doi.org/10.1038/375305a0)

- Pratte, S., Bao, K., Sapkota, A., Zhang, W., Shen, J., Roux, G. Le, Vleeschouwer, F. De, 2019. 14 kyr of atmospheric mineral dust deposition in north-eastern China: A record of palaeoclimatic and palaeoenvironmental changes in the Chinese dust source regions. *The Holocene* 30, 492–506. doi:10.1177/0959683619892661
- Qiang, X., An, Z., Song, Y., Chang, H., Sun, Y., Liu, W., Ao, H., Dong, J., Fu, C., Wu, F., Lu, F., Cai, Y., Zhou, W., Cao, J., Xu, X., Ai, L., 2011. New eolian red clay sequence on the western Chinese Loess Plateau linked to onset of Asian desertification about 25 Ma ago. *Science China Earth Sciences* 54, 136–144. doi:10.1007/s11430-010-4126-5
- Rasmussen, C., Heckman, K., Wieder, W.R., Keiluweit, M., Lawrence, C.R., Berhe, A.A., Blankinship, J.C., Crow, S.E., Druhan, J.L., Hicks Pries, C.E., Marin-Spiotta, E., Plante, A.F., Schädel, C., Schimel, J.P., Sierra, C.A., Thompson, A., Wagai, R., 2018. Beyond clay: towards an improved set of variables for predicting soil organic matter content. *Biogeochemistry* 137, 297–306. doi:10.1007/s10533-018-0424-3
- Retallack, G.J., 1998. Core concepts of paleopedology. *Quaternary International* 51–52, 203–212. doi:10.1016/S1040-6182(97)00046-3
- Retallack, G.J., 2001. *Soils of the Past: An Introduction to Paleopedology*, Second Edition, 2nd ed. John Wiley & Sons, Inc. doi:10.1002/9780470698716
- Roberts, H.M., Wintle, A.G., Maher, B.A., Hu, M., 2001. Holocene sediment-accumulation rates in the western Loess Plateau, China, and a 2500-year record of agricultural activity, revealed by OSL dating. *The Holocene* 11, 477–483. doi:10.1191/095968301678302913
- Roberts, M.J., Jackson, L.C., Roberts, C.D., Meccia, V., Docquier, D., Koenigk, T., Ortega, P., Moreno-Chamarro, E., Bellucci, A., Coward, A., Drijfhout, S., Exarchou, E., Gutjahr, O., Hewitt, H., Iovino, D., Lohmann, K., Putrasahan, D., Schiemann, R., Seddon, J., Terray, L., Xu, X., Zhang, Q., Chang, P., Yeager, S.G., Castruccio, F.S., Zhang, S., Wu, L., 2020. Sensitivity of the Atlantic Meridional Overturning Circulation to Model Resolution in CMIP6 HighResMIP Simulations and Implications for Future Changes. *Journal of Advances in Modeling Earth Systems* 12, e2019MS002014. doi:https://doi.org/10.1029/2019MS002014
- Roe, G., 2009. On the interpretation of Chinese loess as a paleoclimate indicator. *Quaternary Research* 71, 150–161. doi:DOI: 10.1016/j.yqres.2008.09.004
- Rowley, M.C., Grand, S., Verrecchia, É.P., 2018. Calcium-mediated stabilisation of soil organic carbon. *Biogeochemistry* 137, 27–49. doi:10.1007/s10533-017-0410-1
- Ruhe, R. V., 1956. GEOMORPHIC SURFACES AND THE NATURE OF SOILS. *Soil Science* 82.

- Rutgers, M., Wijnen, H.J. van, Schouten, A.J., Mulder, C., Kuiten, A.M.P., Brussaard, L., Breure, A.M., 2012. A method to assess ecosystem services developed from soil attributes with stakeholders and data of four arable farms. *Science of the Total Environment* 415, 39–48. doi:10.1016/j.scitotenv.2011.04.041
- Rutter, A.J., Morton, A.J., Robins, P.C., 1975. A Predictive Model of Rainfall Interception in Forests. II. Generalization of the Model and Comparison with Observations in Some Coniferous and Hardwood Stands. *The Journal of Applied Ecology* 12, 367–380. doi:10.2307/2401739
- Rutter, N., Ding, Z., Liu, T., 1991. Comparison of isotope stages 1–61 with the Baoji-type pedostratigraphic section of north-central China. *Canadian Journal of Earth Sciences* 28, 985–990. doi:10.1139/e91-089
- Sauer, D., Finke, P., Sørensen, R., Sperstad, R., Schüllli-Maurer, I., Høeg, H., Stahr, K., 2012. Testing a soil development model against southern Norway soil chronosequences. *Quaternary International* 265, 18–31. doi:10.1016/j.quaint.2011.12.018
- Savenije, H.H.G., 2004. The importance of interception and why we should delete the term evapotranspiration from our vocabulary. *Hydrological Processes* 18, 1507–1511. doi:10.1002/hyp.5563
- Schaetzl, R., Thompson, M., 2015. *Soils. soils genesis and geomorphology*, 2nd ed. Cambridge university press.
- Sheldon, N.D., Tabor, N.J., 2009. Quantitative paleoenvironmental and paleoclimatic reconstruction using paleosols. *Earth-Science Reviews* 95, 1–52. doi:10.1016/j.earscirev.2009.03.004
- Sheng, H., Cai, T., 2019. Influence of rainfall on canopy interception in mixed Broad-Leaved-Korean pine forest in Xiaoxing'an Mountains, northeastern China. *Forests* 10, 1–11. doi:10.3390/f10030248
- Shi, F., Yin, Q., Nikolova, I., Berger, A., Ramstein, G., Guo, Z., 2020. Impacts of extremely asymmetrical polar ice sheets on the East Asian summer monsoon during the MIS-13 interglacial. *Quaternary Science Reviews* 230, 106164. doi:https://doi.org/10.1016/j.quascirev.2020.106164
- Shi, H., Shao, M., 2000. Soil and water loss from the Loess Plateau in China. *Journal of Arid Environments* 45, 9–20. doi:10.1006/jare.1999.0618
- Shi, P., Yang, T., Tian, Q., Jiang, S., Fan, Z., Wang, J., 2013. Loess record of climatic changes during MIS 12–10 in the Jingyuan section, northwestern Chinese Loess Plateau. *Quaternary International* 296, 149–159. doi:10.1016/j.quaint.2012.08.2102
- Shi, P., Yang, T., Tian, Q., Li, C., 2016. A warmer but drier Marine Isotope Stage 11 during the past 650 ka as revealed by the thickest loess on the western Chinese Loess Plateau. *Journal of Arid Land* 8, 315–330. doi:10.1007/s40333-016-0123-7

- Shirato, Y., Hakamata, T., Taniyama, I., 2004. Modified rothamsted carbon model for andosols and its validation: changing humus decomposition rate constant with pyrophosphate-extractable Al. *Soil Science and Plant Nutrition* 50, 149–158. doi:10.1080/00380768.2004.10408463
- Sitch, S., Smith, B., Prentice, I.C., Arneth, A., Bondeau, A., Cramer, W., Kaplan, J.O., Levis, S., Lucht, W., Sykes, M.T., Thonicke, K., Venevsky, S., 2003. Evaluation of ecosystem dynamics, plant geography and terrestrial carbon cycling in the LPJ dynamic global vegetation model. *Global Change Biology* 9, 161–185. doi:https://doi.org/10.1046/j.1365-2486.2003.00569.x
- Six, J., Conant, R.T., Paul, E.A., Paustian, K., 2002. Stabilization mechanisms of soil organic matter: Implications for C-saturation of soils. *Plant and Soil* 241, 155–176. doi:10.1023/A:1016125726789
- Smalley, I., O'Hara-Dhand, K., Wint, J., Machalett, B., Jary, Z., Jefferson, I., 2009. Rivers and loess: The significance of long river transportation in the complex event-sequence approach to loess deposit formation. *Quaternary International* 198, 7–18. doi:https://doi.org/10.1016/j.quaint.2008.06.009
- Smalley, I., Marković, S.B., Svirčev, Z., 2011. Loess is [almost totally formed by] the accumulation of dust. *Quaternary International* 240, 4–11. doi:10.1016/j.quaint.2010.07.011
- Soil Survey Staff, 2014. *Keys to soil taxonomy*, 12th ed, Soil Conservation Service. Agriculture, United States Department of Service, Natural Resources Conservation Washington, DC.
- Sollins, P., Gregg, J.W., 2017. Soil organic matter accumulation in relation to changing soil volume, mass, and structure: Concepts and calculations. *Geoderma* 301, 60–71. doi:https://doi.org/10.1016/j.geoderma.2017.04.013
- Sparovek, G., Maria, I.C. De, 2003. Multiperspective analysis of erosion tolerance. *Scientia Agricola* 60, 409–416. doi:10.1590/S0103-90162003000200029
- Stamati, F.E., Nikolaidis, N.P., Schnoor, J.L., 2013. Modeling topsoil carbon sequestration in two contrasting crop production to set-aside conversions with RothC - Calibration issues and uncertainty analysis. *Agriculture, Ecosystems and Environment* 165, 190–200. doi:10.1016/j.agee.2012.11.010
- Stemmer, M., Roth, K., Kandeler, E., 2000. Carbon mineralization and microbial activity in a field site trial used for ¹⁴C turnover experiments over a period of 30 years. *Biology and Fertility of Soils* 31, 294–302. doi:10.1007/s003740050659
- Stevens, T., Armitage, S.J., Lu, H., Thomas, D.S.G., 2006. Sedimentation and diagenesis of Chinese loess: Implications for the preservation of

- continuous, high-resolution climate records. *Geology* 34, 849–852. doi:10.1130/G22472.1
- Stevens, T., Thomas, D.S.G., Armitage, S.J., Lunn, H.R., Lu, H., 2007. Reinterpreting climate proxy records from late Quaternary Chinese loess: A detailed OSL investigation. *Earth-Science Reviews* 80, 111–136. doi:https://doi.org/10.1016/j.earscirev.2006.09.001
- Stevens, T., Buylaert, J.P., Thiel, C., Újvári, G., Yi, S., Murray, A.S., Frechen, M., Lu, H., 2018. Ice-volume-forced erosion of the Chinese Loess Plateau global Quaternary stratotype site. *Nature Communications* 9, 1–12. doi:10.1038/s41467-018-03329-2
- Stewart, C.E., Paustian, K., Conant, R.T., Plante, A.F., Six, J., 2007. Soil carbon saturation: Concept, evidence and evaluation. *Biogeochemistry* 86, 19–31. doi:10.1007/s10533-007-9140-0
- Stockmann, U., 2011. Quantifying pedogenesis processes. PHD thesis. The University of Sydney, New South Wales, Australia.
- Su, C., Fu, B.J., He, C.S., Lü, Y.H., 2012. Variation of ecosystem services and human activities: A case study in the Yanhe Watershed of China. *Acta Oecologica* 44, 46–57. doi:10.1016/j.actao.2011.11.006
- Su, C., Liu, H., Wang, S., 2018. A process-based framework for soil ecosystem services study and management. *Science of the Total Environment* 627, 282–289. doi:10.1016/j.scitotenv.2018.01.244
- Su, L., Zhao, C., Xu, W., Xie, Z., 2016. Modelling interception loss using the revised Gash model: a case study in a mixed evergreen and deciduous broadleaved forest in China. *Ecohydrology* 9, 1580–1589. doi:10.1002/eco.1749
- Sun, 2007. Study on substitute indices of summer monsoon in the Xifeng section and reconstruction of paleoclimate. Master dissertation Hefei University of Technology.
- Sun, A., Guo, Z., Wu, H., Li, Q., Yu, Y., Luo, Y., Jiang, W., Li, X., 2017. Reconstruction of the vegetation distribution of different topographic units of the Chinese Loess Plateau during the Holocene. *Quaternary Science Reviews* 173, 236–247. doi:10.1016/j.quascirev.2017.08.006
- Sun, Y., Clemens, S.C., An, Z., Yu, Z., 2006a. Astronomical timescale and palaeoclimatic implication of stacked 3.6-Myr monsoon records from the Chinese Loess Plateau. *Quaternary Science Reviews* 25, 33–48. doi:https://doi.org/10.1016/j.quascirev.2005.07.005
- Sun, Y., Chen, J., Clemens, S.C., 2006b. East Asian monsoon variability over the last seven glacial cycles recorded by a loess sequence from the northwestern. *Geochemistry, Geophysics, Geosystems* 7–12. doi:10.1029/2006GC001287
- Sun, Y., Wang, X., Liu, Q., Clemens, S.C., 2010. Impacts of post-depositional

- processes on rapid monsoon signals recorded by the last glacial loess deposits of northern China. *Earth and Planetary Science Letters* 289, 171–179. doi:10.1016/j.epsl.2009.10.038
- Sun, Y., Clemens, S.C., Morrill, C., Lin, X., Wang, X., An, Z., 2012. Influence of Atlantic meridional overturning circulation on the East Asian winter monsoon. *Nature Geoscience* 5, 46–49. doi:10.1038/ngeo1326
- Sun, Y., Kutzbach, J., An, Z., Clemens, S., Liu, Z., Liu, W., Liu, X., Shi, Z., Zheng, W., Liang, L., Yan, Y., Li, Y., 2015. Astronomical and glacial forcing of East Asian summer monsoon variability. *Quaternary Science Reviews* 115, 132–142. doi:https://doi.org/10.1016/j.quascirev.2015.03.009
- Sun, Y., Yin, Q., Crucifix, M., Clemens, S.C., Araya-Melo, P., Liu, W., Qiang, X., Liu, Q., Zhao, H., Liang, L., Chen, H., Li, Y., Zhang, L., Dong, G., Li, M., Zhou, W., Berger, A., An, Z., 2019. Diverse manifestations of the mid-Pleistocene climate transition. *Nature Communications* 10, 352. doi:10.1038/s41467-018-08257-9
- Sun, Y., Yan, Y., Nie, J., Li, G., Shi, Z., Qiang, X., Chang, H., An, Z., 2020. Source-to-sink fluctuations of Asian aeolian deposits since the late Oligocene. *Earth-Science Reviews* 200, 102963. doi:https://doi.org/10.1016/j.earscirev.2019.102963
- Sun, Y., Clemens, S.C., Guo, F., Liu, X., Wang, Y., Yan, Y., Liang, L., 2021. High-sedimentation-rate loess records: A new window into understanding orbital- and millennial-scale monsoon variability. *Earth-Science Reviews* 220, 103731. doi:https://doi.org/10.1016/j.earscirev.2021.103731
- Tabor, N.J., Myers, T.S., 2015. Paleosols as indicators of paleoenvironment and paleoclimate. *Annual Review of Earth and Planetary Sciences* 43, 333–361. doi:10.1146/annurev-earth-060614-105355
- Tan, Z.X., Lal, R., Wiebe, K.D., 2005. Global Soil Nutrient Depletion and Yield Reduction. *Journal of Sustainable Agriculture* 26, 123–146. doi:10.1300/J064v26n01_10
- Targulian, V.O., Goryachkin, S. V., 2004. Soil memory: Types of record, carriers, hierarchy and diversity. *Revista Mexicana de Ciencias Geológicas* 21, 1–8.
- Thomas, E.K., Clemens, S.C., Sun, Y., Prell, W.L., Huang, Y., Gao, L., Loomis, S., Chen, G., Liu, Z., 2016. Heterodynes dominate precipitation isotopes in the East Asian monsoon region, reflecting interaction of multiple climate factors. *Earth and Planetary Science Letters* 455, 196–206. doi:10.1016/j.epsl.2016.09.044
- Todorovic, G.R., Stemmer, M., Tatzber, M., Katzlberger, C., Spiegel, H., Zehetner, F., Gerzabek, M.H., 2010. Soil-carbon turnover under different crop management: Evaluation of RothC-model predictions under

- Pannonian climate conditions. *Journal of Plant Nutrition and Soil Science* 173, 662–670. doi:10.1002/jpln.200800311
- Újvári, G., Kok, J.F., Varga, G., Kovács, J., 2016. The physics of wind-blown loess: Implications for grain size proxy interpretations in Quaternary paleoclimate studies. *Earth-Science Reviews* 154, 247–278. doi:https://doi.org/10.1016/j.earscirev.2016.01.006
- VanBreemen, N., Buurman, P., 2002. Soil formation, 2nd ed, *Journal of Chemical Information and Modeling*. Springer Netherlands. doi:10.1007/0-306-48163-4
- Vereecken, H., Vanderborght, J., Schnepf, A., 2014. On the Need to Establish an International Soil Modeling Consortium. In: AGU Fall Meeting Abstracts. Forschungszentrum Jülich, Jülich, Germany), pp. H51C-0618.
- Vereecken, H., Schnepf, A., Hopmans, J.W., Javaux, M., Or, D., Roose, T., Vanderborght, J., Young, M.H., Amelung, W., Aitkenhead, M., Allison, S.D., Assouline, S., Baveye, P., Berli, M., Brüggemann, N., Finke, P., Flury, M., Gaiser, T., Govers, G., Ghezzehei, T., Hallett, P., Hendricks Franssen, H.J., Heppell, J., Horn, R., Huisman, J.A., Jacques, D., Jonard, F., Kollet, S., Lafolie, F., Lamorski, K., Leitner, D., McBratney, A., Minasny, B., Montzka, C., Nowak, W., Pachepsky, Y., Padarian, J., Romano, N., Roth, K., Rothfuss, Y., Rowe, E.C., Schwen, A., Šimůnek, J., Tiktak, A., Dam, J. Van, Zee, S.E.A.T.M. van der, Vogel, H.J., Vrugt, J.A., Wöhling, T., Young, I.M., 2016. Modeling Soil Processes: Review, Key Challenges, and New Perspectives. *Vadose Zone Journal* 15, vzj2015.09.0131. doi:10.2136/vzj2015.09.0131
- Verheijen, F.G.A., Jones, R.J.A., Rickson, R.J., Smith, C.J., 2009. Tolerable versus actual soil erosion rates in Europe. *Earth-Science Reviews* 94, 23–38. doi:10.1016/j.earscirev.2009.02.003
- Vidic, N.J., Lobnik, F., 1997. Rates of soil development of the chronosequence in the Ljubljana Basin, Slovenia. *Geoderma* 76, 35–64. doi:10.1016/S0016-7061(96)00098-5
- Vidic, N.J., Verosub, K.L., Singer, M.J., 2003. The Chinese loess perspective on Marine Isotope Stage 11 as an extreme interglacial. Washington DC American Geophysical Union Geophysical Monograph Series 137, 231–240. doi:10.1029/137GM17
- Wang, L., Wang, S.P., Shao, H.B., Wu, Y.J., Wang, Q.J., 2012. Simulated water balance of forest and farmland in the hill and gully region of the Loess Plateau in China. *Plant Biosystems - An International Journal Dealing with all Aspects of Plant Biology* 146, 226–243. doi:10.1080/11263504.2012.709198
- Wei, X., Liu, S., Zhou, G., Wang, C., 2005. Hydrological processes in major types of Chinese forest. *Hydrological Processes* 19, 63–75. doi:10.1002/hyp.5777

- Wen, M., Cheng, D., Song, J., Zhang, G., Lai, W., Jiang, W., 2018. Impacts of climate change on aridity index and its spatiotemporal variation in the Loess Plateau of China, from 1961 to 2014. *Environmental Earth Sciences* 77, 1–12. doi:DOI:101007/s12665-018-7304-y
- Wilkinson, B.H., McElroy, B.J., 2007. The impact of humans on continental erosion and sedimentation. *Bulletin of the Geological Society of America* 119, 140–156. doi:10.1130/B25899.1
- Wischmeier, W.H., Smith, D.D., 1979. Predicting rainfall-erosion losses from cropland east of the Rocky mountains-Guide for Selection of Practices for Soil and Water Conservation. In: *Agricultural Handbook 282*. U.S Department of Agriculture, Washington.
- Wu, N., Rousseau, D.-D., Liu, T., Lu, H., Zhaoyan, G., Guo, Z., Jiang, W., 2001. Orbital forcing of terrestrial mollusks and climatic changes from the Loess Plateau of China during the past 350 ka. *Journal of Geophysical Research* 106, 20045–20054. doi:10.1029/2001JD900224
- Wu, N., Chen, X., Rousseau, D. -D., Li, F., Pei, Y., Wu, B., 2007. Climatic conditions recorded by terrestrial mollusc assemblages in the Chinese Loess Plateau during marine Oxygen Isotope Stages 12 10. *Quaternary Science Reviews* 26, 1884–1896. doi:10.1016/j.quascirev.2007.04.006
- Wu, Z., Yin, Q., Guo, Z., Berger, A., 2020. Hemisphere differences in response of sea surface temperature and sea ice to precession and obliquity. *Global and Planetary Change* 192, 103223. doi:https://doi.org/10.1016/j.gloplacha.2020.103223
- Xu, B., Shan, L., Li, F., Jiang, J., 2007. Seasonal and spatial root biomass and water use efficiency of four forage legumes in semiarid northwest China. *African Journal of Biotechnology* 6, 2708–2714. doi:10.5897/AJB2007.000-2433
- Ye, X., Zhan-tao, F., Ting-jiang, P., Feng-xia, Y., Li, M., Yu, H., 2018. Preliminary clay mineralogy on the loess-paleosol sequence in the Xijin core, Lanzhou. *Journal of Lanzhou University, Natural science* 54. doi:10.13885/j.issn.0455-2059.2018.01.012
- Yin, G., Wang, X., Zhang, X., Fu, Y., Hao, F., Hu, Q., 2020. InVEST model-based estimation of water yield in North China and its sensitivities to climate variables. *Water (Switzerland)* 12. doi:10.3390/W12061692
- Yin, L., 2008. Research on hydraulic properties of L1-S1 soil layers in loess section of Changwu in Shaanxi province. Master degree thesis, Shaanxi Normal University, China.
- Yin, Q.Z., Berger, A., 2012. Individual contribution of insolation and CO₂ to the interglacial climates of the past 800,000 years. *Climate Dynamics* 38, 709–724. doi:10.1007/s00382-011-1013-5
- Yin, Q.Z., Berger, A., 2015. Interglacial analogues of the Holocene and its

- natural near future. *Quaternary Science Reviews* 120, 28–46. doi:10.1016/j.quascirev.2015.04.008
- Yin, Q.Z., Guo, Z.T., 2008. Strong summer monsoon during the cool MIS-13. *Climate of the Past*, European Geosciences Union (EGU) 4, 29–34. doi:10.5194/cp-4-29-2008
- Yin, Q.Z., Berger, A., Driesschaert, E., Goosse, H., Loutre, M.F., Crucifix, M., 2008. The Eurasian ice sheet reinforces the East Asian summer monsoon during the interglacial 500 000 years ago. *Climate of the Past* 4, 79–90. doi:10.5194/cp-4-79-2008
- Yin, Q.Z., Berger, A., Crucifix, M., 2009. Individual and combined effects of ice sheets and precession on MIS-13 climate. *Climate of the Past* 5, 229–243. doi:10.5194/cp-5-229-2009
- Yin, Q.Z., Wu, Z.P., Berger, A., Goosse, H., Hodell, D., 2021. Insolation triggered abrupt weakening of Atlantic circulation at the end of interglacials. *Science* 373, 1035–1040. doi:10.1126/science.abg1737
- Yu, Y., Wu, H., Finke, P.A., Guo, Z., 2016. Spatial and temporal changes of prehistoric human land use in the Wei River valley, northern China. *Holocene* 26, 1788–1801. doi:10.1177/0959683616645943
- Yu, Y.Y., Finke, P.A., Wu, H.B., Guo, Z.T., 2013. Sensitivity analysis and calibration of a soil carbon model (SoilGen2) in two contrasting loess forest soils. *Geoscientific Model Development* 6, 29–44. doi:10.5194/gmd-6-29-2013
- Zhang, G., Zeng, G.M., Jiang, Y.M., Huang, G.H., Li, J.B., Yao, J.M., Tan, W., Xiang, R., Zhang, X.L., 2006a. Modelling and measurement of two-layer-canopy interception losses in a subtropical evergreen forest of central-south China. *Hydrology and Earth System Sciences* 10, 65–77. doi:10.5194/hess-10-65-2006
- Zhang, G., Zeng, G.M., Jiang, Y.M., Huang, G.H., Li, J.B., Yao, J.M., Tan, W., Xiang, R., Zhang, X.L., 2006b. Modelling and measurement of two-layer-canopy interception losses in a subtropical evergreen forest of central-south China. *Hydrology and Earth System Sciences* 10, 65–77. doi:10.5194/hess-10-65-2006
- Zhang, H., Zhang, L., Zhang, W., 1990. Studies on Carbon and Oxygen Isotopic Geochemical characteristics and Loess sedimentation of Jiuzhoutai Loess profile, Lanzhou. *Journal of Lanzhou University, Natural science* 26, 117–126.
- Zhang, W., Shi, Z., Chen, G., Liu, Y., Niu, J., Ming, Q., Su, H., 2013. Geochemical characteristics and environmental significance of Taledo loess-paleosol sequences of Ili Basin in Central Asia. *Environmental Earth Sciences* 70, 2191–2202.
- Zhang, Z., Li, G., Cai, Y., Liu, Z., An, Z., 2021. Variation of summer

- precipitation $\delta^{18}\text{O}$ on the Chinese Loess Plateau since the last interglacial. *Journal of Quaternary Science* 36, 1214–1220. doi:<https://doi.org/10.1002/jqs.3358>
- Zhao, H., Chen, F.-H., Li, S.-H., Wintle, A.G., Fan, Y.-X., Xia, D.-S., 2007. A record of Holocene climate change in the Guanzhong Basin, China, based on optical dating of a loess-palaeosol sequence. *The Holocene* 17, 1015–1022. doi:[10.1177/0959683607080530](https://doi.org/10.1177/0959683607080530)
- Zhao, J.-B., Luo, X.-Q., Ma, Y.-D., Liu, X.-M., Liu, R., Yue, Y.-L., 2015. The reconstruction of palaeoenvironment during development of the fourth palaeosol in the southern Loess Plateau of China. *Catena* 132, 21–28. doi:[10.1016/j.catena.2015.04.007](https://doi.org/10.1016/j.catena.2015.04.007)
- Zhao, J.-B., Ma, Y.-D., Lui, R., Luo, X.-Q., Shao, T.-J., 2018. Palaeoclimatic and hydrological environments inferred by moisture indexes from the S4 palaeosol section in the Xi'an region, China. *Quaternary International* 493, 127–136. doi:<https://doi.org/10.1016/j.quaint.2018.06.015>
- Zhao, J., 2005. Middle Holocene soil and migration of climatic zones in the Guanzhong Plain of China. *Soil science* 170, 292–299.
- Zhao, J., Cao, J., Jin, Z., Xing, S., Shao, T., 2014. The fifth paleosol layer in the southern part of China's Loess Plateau and its environmental significance. *Quaternary International* 334–335, 189–196. doi:[10.1016/j.quaint.2012.12.044](https://doi.org/10.1016/j.quaint.2012.12.044)
- Zheng, H., Theng, B.K., Whitton, J.S., 1994. Mineral composition of loess-paleosols in the Loess Plateau and its environmental significance. *Geochimica* 23, 113–123. doi:(in Chinese, with English abstract)
- Zheng, J., Fan, J., Zhang, F., Yan, S., Xiang, Y., 2018. Rainfall partitioning into throughfall, stemflow and interception loss by maize canopy on the semi-arid Loess Plateau of China. *Agricultural Water Management* 195, 25–36. doi:[10.1016/j.agwat.2017.09.013](https://doi.org/10.1016/j.agwat.2017.09.013)
- Zhou, J., Fu, B., Gao, G., Lü, Y., Liu, Y., Lü, N., Wang, S., 2016. Effects of precipitation and restoration vegetation on soil erosion in a semi-arid environment in the Loess Plateau, China. *Catena* 137, 1–11. doi:[10.1016/j.catena.2015.08.015](https://doi.org/10.1016/j.catena.2015.08.015)
- Zhu, Y., Jia, X., Qiao, J., Shao, M., 2019. What is the mass of loess in the Loess Plateau of China? *Science Bulletin* 64, 534–539. doi:[10.1016/j.scib.2019.03.021](https://doi.org/10.1016/j.scib.2019.03.021)
- Zwertvaegher, A., Finke, P., Smedt, P. De, Gelorini, V., Meirvenne, M. Van, Bats, M., Reu, J. De, Antrop, M., Bourgeois, J., Maeyer, P. De, Verniers, J., Crombé, P., 2013. Spatio-temporal modeling of soil characteristics for soil-landscape reconstruction. *Geoderma* 207–208, 166–179. doi:[10.1016/j.geoderma.2013.05.013](https://doi.org/10.1016/j.geoderma.2013.05.013)

Curriculum Vitae

Personal information

Last name	Ranathunga Arachchige
First name	Keerthika Nirmani
E-mail	Nirmi.rak@gmail.com
Date of Birth	06-07-1986

Education

2018-2022	Joint PhD student (Reading) between Department of Environment, Faculty of Bioscience Engineering, Ghent University, Belgium and Earth and Life Institute, Faculty of Science Université Catholique de Louvain, Belgium.
2015-2017	Master of science in Physical Land Resources (Soil science option) (magna cum laude) Ghent University, Belgium.
2008-2012	Bachelor in Agricultural Technology and Management (Second Upper), Faculty of Agriculture, University of Peradeniya, Sri Lanka.

Professional Experience

January 2014- August 2015	Environmental Officer, Central Environmental Authority, Ministry of Environmental and Renewable Energy, Sri Lanka
November 2012- July 2013	Academic Instructor, Department of Soil Science, Faculty of Agricultural Technology and Management, University of Peradeniya, Sri Lanka

Awards, grants

Yearly prize of De Boodt-Maselis for Eremology for the best academic performance Msc. in Physical Land Resources (Ghent university, Belgium, 2017)

VLIR-UOS Master degree scholarship for Msc. in Physical Land Resources Ghent university, Belgium (2015-2017)

Government Mahapola Scholarship for Undergraduate studies (Sri Lanka 2008-2012)

Scientific Publications

A1-Journal Articles

Ranathunga, K. N., Finke, P. A., Yin, Q., & Yu, Y. (2022). Calibrating SoilGen2 for interglacial soil evolution in the Chinese Loess Plateau considering soil parameters and the effect of dust addition rhythm. *Quaternary International*, 607, 100-112. doi.org/10.1016/j.quaint.2021.08.019.

Ranathunga, K. N., Finke, P. A., Yin, Q., Verdoodt, A., & Yu, Y. (2021). Soil modeling for soil loss tolerance estimations: Exploring natural baselines and long-term variations. *Global and Planetary Change*, 204, 103548. doi.org/10.1016/j.gloplacha.2021.103548

Article submitted on 5th March 2022

Ranathunga, K. N., Finke, P. A., Yin, Q., & Wu, Z. (2022). Driving factors of interglacial paleosol formation on the Chinese Loess Plateau and the effect of precession and ice sheets” in the journal of *Quaternary Science Reviews*.

Others-Book chapter

Finke, P. A., **Ranathunga, K. N. A.**, Verdoodt, A., Yu, Y., & Yin, Q. (2021) Unraveling loess records of climate change from the Chinese loess plateau using process-based models. In: Hunt, A., Egli, M., Faybishenko, B. (Eds.), *Hydrogeology, Chemical Weathering and Soil Formation*. AGU Geophysical Monograph Series, pp. 163–175. doi:10.1002/9781119563952.ch8

Master Thesis

Niels J F De Baerdemaeker, K. N. A **Ranathunga**, Jana Zinkernagel, Jan Van den Bulcke, Joris Van Acker, H Jochen Schenk, Kathy Steppe. The stability enigma of hydraulic vulnerability curves: addressing the link between hydraulic conductivity and drought-induced embolism". *Tree Physiology*. Volume 39, Issue 10, October 2019, Pages 1646-1664. DOI <https://doi.org/10.1093/treephys/tpz078>

Oral presentations

3rd ISMC Conference 2021– “Advances in Modeling Soil Systems”. Virtual

Keerthika Nirmani Ranathunga; Peter Finke; Yin, Qiuzhen; Yu, Yanyan. Quantifying paleosol development during three interglacial periods in the Chinese Loess Plateau by soil-climate modeling (21 May 2021)

EGU General Assembly 2021, Vienna, Austria, Virtual

Keerthika Nirmani Ranathunga; Peter Finke; Yin, Qiuzhen; Yu, Yanyan. Calibrating SoilGen2 for interglacial soil evolution in the Chinese Loess Plateau considering soil parameters, and the effect of uncertain forcings' (27 April 2021)

Belgium Quaternary Association (BELQUA) -Annual Scientific Workshop 2022, Brussels, Belgium.

Keerthika Nirmani Ranathunga; Peter Finke; Yin, Qiuzhen; Wu Zhipeng. "Modelling the effect of climate, dust deposition and ice sheets on paleosol development on the Chinese Loess Plateau". (29 March 2022)

Monthly TECLIM seminar at Université Catholique de Louvain, 2020

Keerthika Nirmani Ranathunga; Peter Finke; Yin, Qiuzhen; Modelling Interglacial soil formation in Chinese loess plateau (18th May 2020)

EGU General Assembly 2022, Vienna, Austria, Virtual

Keerthika Nirmani Ranathunga; Peter Finke; Yin, Qiuzhen; Wu Zhipeng. "Modelling the relative effect of different climate factors, vegetation and dust deposition on paleosol development on the Chinese Loess Plateau (23 May 2022)

Poster presentations

EGU General Assembly 2019, Vienna, Austria.

Keerthika Nirmani Ranathunga, Peter Finke, Qiuzhen Yin. "Modeling of interglacial paleosol development in the Chinese Loess Plateau" (7-12 April, 2019).

20th Congress of the International Union for Quaternary Research (INQUA), Dublin, Ireland.

Keerthika Nirmani Ranathunga; Peter Finke; Yin, Qiuzhen. "Modeling of interglacial paleosol development in the Chinese Loess Plateau" (24-31 July 2019).

ELI Day -2021, Université Catholique de Louvain, Belgium

Keerthika Nirmani Ranathunga, Peter Finke, Qiuzhen Yin. "Modeling of interglacial paleosol development in the Chinese Loess Plateau (27 May 2021).

24th National Symposium for Applied Biological Sciences, Faculty of Bioscience Engineering, Ghent University, Ghent, Belgium

Keerthika Nirmani Ranathunga, Peter Finke, Qiuzhen Yin. "Modeling of interglacial paleosol development in the Chinese Loess plateau" (4 February 2019).

**Transferable skills, seminars, and trainings attended at
Université Catholique de
Louvain**

- Training session about Open Science, organized by ACELI, at Université Catholique de Louvain (25th Jan. 2021)
- Training session about scientific writing, organized by ACELI, at Université Catholique de Louvain (16th Feb. 2021)
- Training Research Data Management, organized by UCLouvain Libraries' training, at Université Catholique de Louvain (26th April 2022)

**Ghent University:
Transferable skills**

- Doctoral training - Cluster Career management :Job Market for Young Researchers
- Doctoral training - Cluster communication skills : Advanced Academic English: Conference Skills and Advanced Academic English: writing skills
- Doctoral training – Cluster Leadership & Personal efficiency : Personal effectiveness online
- Doctoral training – Cluster Career management :Creative thinking online

Courses taken at Ghent University

- Paleoclimatology (Sep. 2018 – Jan. 2019)

Other

- Participating in seminar and workshop "SOILWORKS 2019" , Soil science society of Belgium (28th January 2019)
 - Field work on the Chinese loess plateau, China (21st April 2019 – 12th May 2019)
-

